

In compliance with the  
Canadian Privacy Legislation  
some supporting forms  
may have been removed from  
this dissertation.

While these forms may be included  
in the document page count,  
their removal does not represent  
any loss of content from the dissertation.



# **Thermodynamics of Polymerization, Dielectric Properties, and a New Orientational Glass**

By

**JINGSONG WANG**

A thesis

Submitted to the School of Graduate Studies

in Partial Fulfilment of the Requirements

for the degree

**Doctor of Philosophy**

McMaster University

© Copyright by JINGSONG WANG, February 2003

Thermodynamics of Polymerization, Dielectric Properties,  
and a New Orientational Glass

*copy*

DOCTOR OF PHILOSOPHY (2003)  
(Materials Science and Engineering)

McMaster University  
Hamilton, Ontario

TITLE: Thermodynamics of Polymerization, Dielectric Properties, and  
a New Orientational Glass

AUTHOR: Jingsong Wang

SUPERVISOR: Professor G. P. Johari

NUMBER OF PAGES: xxiv, 201

# Abstract

Five aspects of disordered solids and polymers have been studied, as follows.

(1). The temperature and pressure modulation effects on structural relaxation have been formulated and simulated. The calculated heat capacity for the modulated conditions shows extra features over that for unmodulated conditions, which may cause misinterpretation of a disordered solid's characteristics.

(2). A new mean field approximation in the lattice-hole model is developed for monodispersed polymer chains. Calculations of the configurational entropy,  $S_{\text{conf}}$  for polydispersed chains, has led to two predictions, (i) a maximum in the plot of configurational heat capacity against the extent of polymerization, and (ii)  $S_{\text{conf}}$  remaining positive at 0 K. Both predictions have been verified by others. The lattice occupancy density contribution to  $S_{\text{conf}}$  has been related to a liquid's viscosity and divergence of the viscosity-pressure plots explained.

(3). From calorimetry and x-ray diffraction studies, a new phase of CuCN, which remains metastable on cooling to 77 K, has been discovered. It shows features characteristic of glasses.  $S_{\text{conf}}$  of this phase has been calculated by using a flexible chain model.

(4). A calorimetric method for determining the transition from mass-controlled to diffusion-controlled reaction kinetics during polymerization has been developed, and verified by experiments. In this transition range, the plot of the reaction rate against the

reciprocal temperature at fixed value of the extent of polymerization deviates from the Arrhenius behavior.

(5). Dielectric studies of linear chain polymerization of a melt in real time, and the polymers ultimately formed have shown that their properties depend upon the thermal history. This is attributed to different molecular level structures, e.g., chains and loops formed under different polymerization conditions.

Altogether these theoretical and experimental studies have a broader consequence for our current understanding of the nature of disordered solids and of their formation from liquids, both molecular and polymeric.

# Acknowledgements

I would like to express my deepest gratitude to Professor G. P. Johari, my supervisor, for his constant support, guidance and patience throughout the whole process of this thesis. Professor Johari has always encouraged me to pursue further in the research.

I would also like to thank Professor M. F. Collins for helping me with the x-ray diffraction studies of cyanides.

I give my thanks to Professor T. Petric and Professor A-C. Shi for their very helpful suggestions to my thesis study.

Special thanks are to Dr. C. Bridge for the technical help in x-ray diffraction experiments. Many thanks to Dr. J. Britten with whom I took the courses that are very useful to my research on x-ray diffraction. I thank Mr. J. G. McAnanama for providing the Labview programs for the GPIB data interface, Dr. D. W. Wasylyshyn for providing some tabulated forms of KWW function, and Dr. T. Kolodiazhnyi for the initial help on the Origin software.

I thank all the faculty and staff in the Department of Materials Science and Engineering for help during my study here.

Thanks to McMaster university and the Department of Materials Science and Engineering for providing me financial supports. I am also grateful for the award of a Bolotkin Scholarship and Ontario Graduate Scholarships in Science and Technology.

I really appreciate the love, care and encourage of my parents-in-law and the sacrifice they have made to support my study, I am in a great debt to them. I am also grateful to my wife for her love and support throughout the course of my studies.

## Table of Contents

<b>Abstract .....</b>	<b>iii</b>
<b>Acknowledgements .....</b>	<b>v</b>
<b>Table of Contents .....</b>	<b>vii</b>
<b>List of Figures .....</b>	<b>xi</b>
<b>List of Tables .....</b>	<b>xxiv</b>
<b>1 Introduction .....</b>	<b>1</b>
<b>2 Temperature and Pressure Modulation Effects on Structural Relaxation of Amorphous Solids .....</b>	<b>6</b>
2.1 INTRODUCTION .....	6
2.2 COMPUTATION OF SINUSOIDAL MODULATION EFFECTS ON PROPERTIES.....	7
2.2.1 Sinusoidal modulation of a variable with time .....	7
2.2.2 A measurable property's second derivative in sinusoidal modulation.....	9
2.2.3 Temperature and pressure modulations without irreversible changes .....	11
2.2.4 Formalism of structural relaxation process.....	16
2.2.5 Modulation during heating.....	28
2.2.6 Square-wave modulation.....	35
2.3 DISCUSSIONS.....	35

2.3.1	Structural relaxation's modification on the net enthalpy and entropy.....	39
2.3.2	The time and temperature dependent heat capacity and $T_g$ .....	40
2.3.3	The effects of square-wave modulation.....	41
2.3.4	The effects of the phase at the start-stage of modulation .....	41
2.3.5	The relaxation time evolution with temperature .....	42
2.3.6	The linear-response, and the physical aspects of the simulations .....	44
2.4	SUMMARY .....	45
<b>3</b>	<b>Lattice Statistics and Thermodynamics during Linear Chain Polymerization</b>	
	<b>and of the Polymer .....</b>	<b>48</b>
3.1	INTRODUCTION .....	48
3.2	THE LATTICE HOLE MODELS AND FLORY-HUGGINS	
	APPROXIMATIONS .....	50
3.3	POLYMER CHAIN STATISTICS IN THE LATTICE HOLE MODELS .....	55
3.3.1	Formalism for a monodispersed polymer .....	55
3.3.2	Formalism for a polydispersed linear chain system .....	61
3.3.3	Configurational entropy and the extent of polymerization .....	66
3.3.4	Configurational heat capacity change during polymerization .....	74
3.4	PRESSURE EFFECTS ON THE LATTICE CHAIN STATISTICS .....	79
3.4.1	Formalism for the effects of pressure on the lattice chain statistics.....	79
3.4.2	The effects of pressure on configurational entropy .....	80
3.4.3	The effects of pressure on configurational heat capacity .....	86
3.4.4	Entropy and heat capacity changes with pressure .....	88

3.4.5	The maximum in the entropy and heat capacity.....	92
3.4.6	The Viscosity of a Polymer System at Different Pressures and Temperatures.....	94
3.5	SUMMARY.....	98
<b>4</b>	<b>Structure and Thermodynamics of a New Orientational Glass, CuCN.....</b>	<b>102</b>
4.1	INTRODUCTION.....	102
4.2	EXPERIMENTAL METHOD.....	104
4.3	STRUCTURAL STUDIES BY X-RAY DIFFRACTION.....	105
4.4	CALORIMETRIC STUDIES.....	109
4.5	CHAIN STATISTICS OF A LINEAR CHAIN IN THE CUCN ORIENTATIONAL GLASS.....	113
4.6	SUMMARY.....	120
<b>5</b>	<b>The Polymerization Reaction Kinetics.....</b>	<b>122</b>
5.1	INTRODUCTION.....	122
5.2	EXPERIMENTAL METHOD.....	124
5.3	RESULTS.....	125
5.4	DISCUSSION.....	129
5.4.1	Effects of the extent of polymerization at a fixed temperature.....	129
5.4.2	Effects of the polymerization temperature at a fixed extent of polymerization.. .....	132

5.4.3	Distinction between the simulated reaction rates for mass- and diffusion-controlled reactions.....	137
5.5	SUMMARY .....	143
<b>6</b>	<b>Dielectric Properties and Polymerization Conditions.....</b>	<b>145</b>
6.1	INTRODUCTION .....	145
6.2	THE DIELECTRIC POLARIZATION AND RELAXATION FORMALISM .	147
6.3	EXPERIMENTAL METHOD .....	151
6.4	RESULTS AND DATA ANALYSIS.....	155
6.5	DISCUSSION .....	172
6.5.1	Dielectric changes during the polymerization process.....	172
6.5.2	Dielectric properties of the polymerized state.....	175
6.6	SUMMARY .....	178
<b>7</b>	<b>Conclusions.....</b>	<b>180</b>
	<b>Appendix A.....</b>	<b>184</b>
	<b>Appendix B.....</b>	<b>188</b>
	<b>Bibliography .....</b>	<b>191</b>
	<b>Nomenclature .....</b>	<b>200</b>

## List of Figures

Figure 2.1: The variation of  $T$  with  $t$  for sinusoidal modulation (solid line) and the consequent change in  $\tau$  (dashed line). (B). The variation of  $P$  with  $t$  for sinusoidal modulation (solid line) and the consequent change in  $\tau$  (dashed line). The horizontal solid lines in A and B represent the mean temperature or pressure,  $T_0$  or  $P_0$  on the left hand side scale, and the relaxation time,  $\tau_0$ , at  $T_0$  or  $P_0$ , on the right hand side scale. The horizontal dotted lined represents  $\langle \tau \rangle$  as labeled. Parameters used for the calculation are given in the text.  
 .....14

Figure 2.2: (A). The plots of  $\phi$  against  $t$  for the  $T$ -modulated and unmodulated conditions. (B). The plots of  $T_f$  against  $t$  for the  $T$ -modulated and unmodulated conditions. (C). The plots of the difference  $\delta\phi$  between the  $\phi$  for the two conditions. (D). The plots of the difference  $\delta T_f$  between the  $T_f$  for the two conditions. The line passing through the oscillating curves for  $\phi_{\text{mod}}$ ,  $\delta\phi$ ,  $\langle T_{f,\text{mod}} \rangle$  and  $\delta T_f$  is the average value in each case. Parameters used for the calculations are given in the text. The data refer to isothermal annealing. ....23

Figure 2.3: (A). The plots of the average value for  $\delta\phi$  against real time for four pairs of  $\beta$  and  $x$ , as noted. (B). Plots of  $\delta T_f$  against real time. Parameters used for the calculation are given in the text .....26

Figure 2.4: (A). The plots of the average value for  $\delta\phi$  against real time for three cases with different values of  $\omega_0$  as noted. The curve labeled  $-\omega_0$  is for the

condition when the phase angle was shifted by  $\pi$ . B. The plots of  $\delta T_f$ , against real time. Parameters used for the calculation are given in the text.....27

Figure 2.5: (A). The plots of  $T_f$ , for the  $T$ -modulated and unmodulated conditions against the temperature during heating of the glass sample at  $4 \text{ K min}^{-1}$ . (B). The plots of the difference,  $\delta T_f$ , between  $\langle T_{f, \text{mod}} \rangle$  and  $T_{f, \text{unmod}}$  against the temperature. Values of  $\beta$  and  $x$  are as noted. The line labeled 1 is the equilibrium line when  $T = T_f$ . Other parameters used for the calculation are given in the text. The horizontal lines are at zero values in each case, with the same vertical scale. The simulation was done for the sine wave function.....31

Figure 2.6: (A). The plots of  $C_p$  for the  $T$ -modulated and unmodulated conditions against the  $T$  during heating of the glass sample at  $4 \text{ K min}^{-1}$ . (B). The plots of the difference,  $\delta C_p$  between the  $C_{p, \text{unmod}}$  and  $\langle C_{p, \text{mod}} \rangle$ . Values of  $\beta$  and  $x$  are as noted. The thick solid lines are the plots of  $\langle C_{p, \text{mod}} \rangle$  and  $\delta C_p$  for  $T$ -modulation in which the phase had been  $\pi$ -shifted at the beginning. Other parameters used for the calculation are given in the text. The horizontal lines are at zero values in each case, with the same vertical scale .....32

Figure 2.7: (A). The plots of  $C_p$  for the  $T$ -modulated and unmodulated conditions against the temperature during heating of the glass sample at  $4 \text{ K min}^{-1}$ . (B). The plots of the difference,  $\delta C_p$  between the  $C_{p, \text{unmod}}$  and  $\langle C_{p, \text{mod}} \rangle$ . Values of  $\beta$  and  $x$  are as noted. Other parameters used are the same as for Fig. 2.5, except that the isothermal structural relaxation time is increased to 4 h. The

horizontal lines are at zero values in each case, with the same vertical scale.

.....33

Figure 2.8: (A). The plots of  $C_p$  for the  $T$ -modulated and unmodulated conditions against the temperature during heating of the glass sample at  $1 \text{ K min}^{-1}$ . (B). The plots of the difference,  $\delta C_p$  between the  $C_{p, \text{unmod}}$  and  $\langle C_{p, \text{mod}} \rangle$ . Values of  $\beta$  and  $x$  are as noted. Other parameters used are the same as for Fig. 2.5, except that the heating rate is decreased to  $1 \text{ K min}^{-1}$ . The horizontal lines are at zero values in each case, with the same vertical scale .....34

Figure 2.9: (A). The plots of  $C_p$  for the  $T$ -modulated and unmodulated conditions against  $T$  during heating of the glass sample at  $4 \text{ K min}^{-1}$ . (B). The plots of the difference,  $\delta C_p$  between the  $C_{p, \text{unmod}}$  and  $\langle C_{p, \text{mod}} \rangle$ . Values of  $\beta$  and  $x$  are as noted. Other parameters used are the same as for Fig. 2.5, except that the frequency of sinusoidal modulation has been increased to  $8\pi/60 \text{ rad s}^{-1}$ . The horizontal lines are at zero values in each case, with the same vertical scale.

.....36

Figure 2.10: (A). The plots of  $T_f$  for the  $T$ -modulated and unmodulated conditions against  $T$  during heating of the glass sample at  $4 \text{ K min}^{-1}$ . The line labeled 1 is the equilibrium line for  $T_f = T$ . (B). The plots of the difference,  $\delta T_f$  between  $\langle T_{f, \text{mod}} \rangle$  and  $T_{f, \text{unmod}}$  against the temperature. Values of  $\beta$  and  $x$  are as noted. Other parameters used for the calculation are given as for Fig. 2.5, except that the modulation is according to a *square-wave*. The horizontal lines are at zero values in each case, with the same vertical scale.....37

Figure 2.11: (A). The plots of  $C_p$  for the  $T$ -modulated and unmodulated conditions against  $T$  during heating of the glass sample at  $4 \text{ K min}^{-1}$ . (B). The plots of the difference,  $\delta C_p$  between the  $C_{p, \text{unmod}}$  and  $\langle C_{p, \text{mod}} \rangle$ . Values of  $\beta$  and  $x$  are as noted. Other parameters used are the same as for Fig. 2.5, except that the  $T$ -modulation is in the form of a square wave and not a sine-wave. The horizontal lines are at zero values in each case, with the same vertical scale.

.....38

Figure 2.12: (A). The plots of  $\tau$  against  $T$  for the  $T$ -modulated and unmodulated conditions during heating of the glass sample at  $4 \text{ K min}^{-1}$ . (B). The plots of the difference,  $\delta\tau$  divided by  $\tau_{\text{unmod}}$ , against  $T$ . Values of  $\beta$  and  $x$  are as noted. The parameters used are the same as for Fig. 2.5, and are given in the text..43

Figure 3.1: Illustration of one configuration of a mono-dispersed polymer system with  $x = 5$  and  $N=10$  on a two dimension  $8 \times 8$  square lattice with  $z = 4$  and  $N_0 = 14$

.....55

Figure 3.2: Illustration of one configuration of a mono-dispersed polymer system on a two dimension  $8 \times 8$  square lattice with  $z = 4$  and  $N_0 = 19$ .....61

Figure 3.3: (A). The five contributions to the configurational entropy of a polymerizing system scaled by the gas constant are plotted against the extent of polymerization at 300 K. The various contributions are indicated by their notations. (B). The corresponding contributions to the configurational heat capacity are plotted against  $\alpha$ .....68

Figure 3.4: (A). The net configurational entropy of a polymerizing system divided by the gas constant at three temperatures is plotted against the extent of polymerization. (B). The corresponding net configurational heat capacity is plotted against  $\alpha$ .....73

Figure 3.5: (A). The five contributions to the configurational entropy for a fixed value of  $\alpha$  ( $= 0.8$ ) in a polymerizing system scaled by the gas constant are plotted against the temperature. The various contributions are indicated by their notations. (B). The corresponding contributions to the configurational heat capacity are plotted against the temperature .....76

Figure 3.6: (A). The net configurational entropy for a fixed value of  $\alpha$  in a polymerizing system scaled by the gas constant are plotted against the temperature. The various contributions are indicated by their notations. (B). The corresponding net configurational heat capacity is plotted against the temperature .....78

Figure 3.7: The contribution to the configurational entropy,  $S^{(\theta,\alpha)}/R$  is plotted against the pressure at a temperature of 300 K. The plots in panels A, B, and C are for the extent of polymerization 0.2, 0.5 and 0.8, respectively. For a fixed  $z$ , the magnitudes of the other three contributions,  $S^{(mix)}/R$ ,  $S^{(z,\alpha)}/R$ ,  $S^{(\alpha)}/R$  which depend only on  $\alpha$ , and the magnitude of  $S^{(f,\alpha z)}/R$ , which depends on both  $T$  and  $\alpha$  but not on  $P$ , are noted in each panel.....81

Figure 3.8: The net configurational entropy ( $S/R = S^{(mix)}/R + S^{(z,\alpha)}/R + S^{(\alpha)}/R + S^{(f,\alpha z)}/R + S^{(\theta,\alpha)}/R$ ), as calculated here is plotted against the pressure. The curves are for the extent of polymerization, 0.2, 0.5 and 0.8. The plots in panels A, B, and

C, were calculated at temperatures of 275 K, 300 K and 325 K, respectively

.....83

Figure 3.9: The plots of pressure against temperature for different fixed configurational entropy. The entropy values are indicated. The plots in panels A, B and C are for the extent of polymerization, 0.2, 0.5 and 0.8, respectively.....84

Figure 3.10: The net configurational entropy ( $S/R = S^{(mix)}/R + S^{(z,\alpha)}/R + S^{(\alpha)}/R + S^{(f,\alpha z)}/R + S^{(\theta,\alpha)}/R$ ) surface in the temperature and pressure plane, as calculated for the extent of polymerization, 0.2, 0.5 and 0.8, as indicated.....85

Figure 3.11: The configurational heat capacity ( $= C^{(f,\alpha z)}/R + C^{(\theta,\alpha)}/R$ ), is plotted against the pressure. The curves are for different extents of polymerization, 0.2, 0.5 and 0.8. The plots in Panels A, B, and C were calculated at temperatures of 275 K, 300 K and 325 K, respectively.....87

Figure 3.12: (A).The net configurational entropy,  $S/R (= S^{(mix)}/R + S^{(z,\alpha)}/R + S^{(\alpha)}/R + S^{(f,\alpha z)}/R + S^{(\theta,\alpha)}/R)$  is plotted against the extent of polymerization occurring at three pressures, 0.1 MPa, 10 MPa and 100 MPa, and at a fixed temperature of 300 K, as indicated. (B). The configurational heat capacity ( $= C^{(f,\alpha z)}/R + C^{(\theta,\alpha)}/R$ ) is plotted against the extent of polymerization for the corresponding  $P$  and  $T$  conditions.....93

Figure 3.13: The calculated  $R/[TS^{(\theta,\alpha)}]$  which is proportional to  $\ln(\eta/\eta_0)$ , is plotted against  $1000/T$ . The curves are for  $P = 500, 400, 300, 200, 100, 50$  Mpa. The plots in Panels A, B, and C were calculated for different extents of polymerization, 0.2, 0.5 and 0.8, respectively.....96

Figure 3.14: The calculated  $R/[TS^{(\theta,\alpha)}]$  which is proportional to  $\ln(\eta/\eta_0)$ , is plotted against pressure. The curves are for  $T = 550, 500, 450, 400, 350, 300, 250$  K. The plots in Panels A, B, and C were calculated for different extents of polymerization, 0.2, 0.5 and 0.8, respectively.....97

Figure 4.1: Powder x-ray diffraction patterns of, (A) the as-received CuCN measured at ~ 298 K, (B) the lines and their relative intensities for the reputed structure in the orthorhombic unit cell for suggested monoclinic structure from JCPDS 1-492, (C) the lines and their relative intensities for the orthorhombic structure from JCPDS 9-152 and (D) the new phase of CuCN obtained after heating to 593 K in an argon environment and thereafter cooling to 298 K.....106

Figure 4.2: Results of the Rietveld analysis of the powder x-ray diffraction of CuCN after heating to 593 K in an argon environment and thereafter cooling to 298 K. The circle symbols represent the powder x-ray diffraction data and the solid line going through the symbols represents the Rietveld fitting results. The dashed line is the difference between the diffraction data and the fitting results. The dashed line was shifted vertically by -1000 for better illustration. Insert is the unit cell of CuCN structure, with the positions of Cu indicated by large circles, those of C by small filled circles and those of N by small empty circles .....108

Figure 4.3: (A). The differential scanning calorimetry thermogram of CuCN obtained by heating at 30 K/min heating rate is shown by curve (1), and that of the structurally transformed sample which had been cooled to 77 K and then

heated is shown by curve (2). (B). The enlarged parts of curves (1) and (2) in Fig. 4.3(A) show the sigmoid shape  $C_p$ -increase for the original CuCN and of its new phase ..... 110

Figure 4.4: The differential scanning calorimetry thermogram of CuCN sample obtained by heating at a rate of 30 K/min. is shown by curves for the conditions of, (1) without annealing, (2). annealed at 318.2 K for 30 min. (3). annealed at 323.2 K for 30 min. (4). annealed at 328.2 K for 30 min. The dotted line for each curve indicates the baseline for each scan if there is no glass transition ..... 112

Figure 4.5: The normalized heat capacity  $C_{p,n}$  plotted against the temperature. The circles denote the data from the DSC measurement and the solid line is the best fit to the data obtained by using Eqs.(2.26) - (2.29) ..... 114

Figure 4.6: (A). The calculated relaxation time  $\tau(t)$  plotted against temperature during the heating at 30 K/min. (B). The calculated fictive temperature  $T_f$  is plotted against the temperature during the heating at 30 K/min. The solid line is for the calculated  $T_f$  and the dashed straight line for  $T_f = T$  ..... 115

Figure 4.7: (A). The illustration of orientations of CN groups in the cell structure with R3m space group of the new CuCN phase. (B). The projection of the Cu atoms on a-b plane. The dashed line indicate the projections of the three possible orientation directions of the CN groups departing from each axis along c direction ..... 116

Figure 4.8: (A). The calculated orientational contribution to the configurational entropy divided by gas constant for the orientational disorder in the linear chains

modeled for the arrangement of CN group is plotted against the temperature.

(B). The corresponding contribution to the configurational heat capacity divided by gas constant is plotted against the temperature .....119

Figure 5.1: The chemical structures of *p*-aminodicyclohexyl methane (PACM) and diglycidyl ether of bisphenol-A(DGEBA), and the four steps of polymerization reactions which forms polymer network in the 1:2 ratio PACM and DGEBA mixture .....126

Figure 5.2: (A) The rate of enthalpy release measured during polymerization of the stoichiometric PACM-DGEBA mixture at five fixed temperatures, as indicated, is plotted against the polymerization time. (B) The extent of polymerization,  $\alpha$ , of the stoichiometric PACM-DGEBA mixture at the indicated temperatures is plotted against the polymerization time ..... 128

Figure 5.3: The logarithmic value of  $[\ln(d\alpha/dt/(1-\alpha))]$  for the stoichiometric PACM-DGEBA mixture is plotted against the extent of polymerization  $\alpha$  at five fixed temperatures, as indicated .....131

Figure 5.4: The logarithmic value of the reaction rate coefficient,  $k$ , for the stoichiometric PACM-DGEBA mixture at different extents of polymerization,  $\alpha$ , is plotted against the reciprocal temperature. The value of  $\alpha$  for each plot is indicated by the symbols.....135

Figure 5.5: (A). The calculated  $\alpha$  for mass-controlled and diffusion-controlled reactions is plotted against the logarithmic reaction time. (B). The corresponding  $d\alpha/dt$  values for a mass controlled and diffusion controlled reaction are plotted

against the logarithmic reaction time. (C). The ratio of corresponding calculated  $(d\alpha_{diff}/dt)/(d\alpha_{mass}/dt)$  values are plotted against the logarithmic reaction time. In (A) and (B), curve 1 refers to the mass-controlled, and curve 2 to the diffusion-controlled reaction kinetics ..... 141

Figure 5.6: (A). The calculated  $d\alpha/dt$  for mass-controlled and diffusion-controlled reactions is plotted against the extent of polymerization  $\alpha$ . Curve 1 refers to the mass-controlled, and 2 to the diffusion-controlled reaction kinetics. (B). The ratio of corresponding calculated  $(d\alpha_{diff}/dt)/(d\alpha_{mass}/dt)$  values is plotted against the extent of polymerization  $\alpha$ ..... 142

Figure 6.1: The chemical structures of aniline (AN) and Resorcinal diglycidyl ether (RDGE), and the first three steps of polymerization reaction which forms linear polymer chain in the 1:1 AN and RDGE mixture..... 153

Figure 6.2: The spectra of  $\epsilon'$  and  $\epsilon''$  measured during the course of polymerization for AN-RDGE mixture at 303.2 K. The symbols correspond to different  $t_{poly}$  (ks) as: (■) 0.20, (●) 24.3, (▲) 50.3, (+) 65.2, (▼) 75.2, (×) 85.2, (◆) 95.1, (\*) 105.2, (□) 115.1, (○)125.0, (Δ) 150.1, (▽) 260.3..... 156

Figure 6.3: The spectra of  $\epsilon'$  and  $\epsilon''$  measured during the course of polymerization for AN-RDGE mixture at 313.2 K. The symbols correspond to different  $t_{poly}$  (ks) as: (■) 1.0, (●) 10.0, (▲) 20.0, (+) 30.0, (▼) 39.9, (×) 49.9, (◆) 59.9, (\*) 72.9, (□) 85.7..... 157

Figure 6.4: The spectra of  $\varepsilon'$  and  $\varepsilon''$  measured during the course of polymerization for AN-RDGE mixture at 323.2 K. The symbols correspond to different  $t_{\text{poly}}$  (ks) as: (■) 5.0, (●) 10.0, (▲) 15.0, (+) 20.0, (▼) 25.0, (×) 30.0, (◆) 35.0, (\*) 40.0, (□) 45.0, (○)50.0, (Δ) 55.0 .....158

Figure 6.5: The spectra of  $\varepsilon'$  and  $\varepsilon''$  measured during the course of polymerization for AN-RDGE mixture at 333.2 K. The symbols correspond to different  $t_{\text{poly}}$  (ks) as: (■) 5.0, (●) 10.0, (▲) 15.0, (+) 20.0, (▼) 25.0, (×) 29.9, (◆) 35.1, (\*) 40.0, (□) 48.0, (○)57.9, (Δ) 66.9 .....159

Figure 6.6: The spectra of  $\varepsilon'$  and  $\varepsilon''$  measured during the course of polymerization for AN-RDGE mixture at 343.2 K. The symbols correspond to different  $t_{\text{poly}}$  (ks) as: (■) 1.01, (●) 2.03, (▲) 3.05, (+) 4.07, (▼) 4.94, (×) 7.55, (◆) 10.0, (\*) 15.1, (□) 57.8.....160

Figure 6.7: The logarithmic dc conductivity  $\log(\sigma_0)$  is plotted against  $\log(t_{\text{poly}})$  during the polymerization of AN-RDGE mixture. The symbols correspond to different  $T_{\text{poly}}$  (K) as: (Δ) 303.2, (○)313.2, (▼) 323.2, (□) 333.2, (◇) 343.2 .....162

Figure 6.8: A typical fitting of dielectric spectra  $\varepsilon'_{\text{dip}}$  and  $\varepsilon''_{\text{dip}}$  with KWW model for AN-RDGE mixture polymerizing at 303.2 K and at  $t_{\text{poly}}$  of 94.3 ks: (A).  $\varepsilon'_{\text{dip}}$  and (B).  $\varepsilon''_{\text{dip}}$ . They are plotted against frequency  $f$  in logarithmic scale. (C). the Cole-Cole plot of  $\varepsilon''_{\text{dip}}$  against  $\varepsilon'_{\text{dip}}$ . The symbols correspond to data obtained and the solid lines are the fitting results with KWW relaxation function ....164

Figure 6.9: The parameters obtained by fitting the dielectric spectra  $\varepsilon'_{\text{dip}}$  and  $\varepsilon''_{\text{dip}}$  with KWW relaxation function for AN-RDGE mixture measured during polymerization: (A). non-exponential parameter  $\beta$ , (B). logarithmic average relaxation time  $\log\langle\tau\rangle$ . These are plotted against  $\log(t_{\text{poly}})$  during polymerization for AN-RDGE mixture. The symbols correspond to different  $T_{\text{poly}}$  (K) as: ( $\Delta$ ) 303.2, ( $\circ$ )313.2, ( $\nabla$ ) 323.2, ( $\blacksquare$ ) 333.2, ( $\diamond$ ) 343.2 ..... 166

Figure 6.10: The parameters obtained by fitting the dielectric spectra  $\varepsilon'_{\text{dip}}$  and  $\varepsilon''_{\text{dip}}$  with KWW relaxation function for AN-RDGE mixture measured during polymerization: (A).  $\varepsilon_s$ , (B).  $\varepsilon_\infty$  and (C).  $\Delta\varepsilon$ . They are plotted against  $\log(t_{\text{poly}})$  during polymerization for AN-RDGE mixture. The symbols correspond to different  $T_{\text{poly}}$  (K) as: ( $\Delta$ ) 303.2, ( $\circ$ )313.2, ( $\nabla$ ) 323.2, ( $\blacksquare$ ) 333.2, ( $\diamond$ ) 343.2 ..... 167

Figure 6.11: The spectra of  $\varepsilon'$  and  $\varepsilon''$  measured during cooling from 400 K to 300 K for AN-RDGE mixture polymerized at 333.2 K for 60 ks and post-polymerized at 400.2 K for 60 ks. The symbols correspond to different temperature (K) as: ( $\blacksquare$ )399.7, ( $\circ$ )389.3, ( $\Delta$ )379.6, ( $\diamond$ )369.3, (+)360.1, ( $\times$ )355.5, (\*)350.5, ( $\nabla$ )345.1, ( $\blacksquare$ )340.5, ( $\bullet$ )329.9, ( $\blacktriangle$ )320.1, ( $\blacklozenge$ )310.0, ( $\nabla$ )306.7 ..... 168

Figure 6.12: The logarithmic dc conductivity  $\log(\sigma_0)$  plotted against  $1000/T$  for AN-RDGE mixture measured during cooling from post polymerization temperature to 300 K. The symbols correspond to different polymerization history as: ( $\Delta$ ) $T_{\text{poly}} = 303.2$  K,  $t_{\text{poly}} = 260$  ks,  $T_{\text{post}} = 400.2$  K,  $t_{\text{post}} = 60$  ks,

(○) $T_{\text{poly}} = 313.2$  K,  $t_{\text{poly}} = 86$  ks,  $T_{\text{post}} = 400.2$  K,  $t_{\text{post}} = 60$  ks, (▽) $T_{\text{poly}} = 323.2$  K,  $t_{\text{poly}} = 60$  ks,  $T_{\text{post}} = 373.2$  K,  $t_{\text{post}} = 60$  ks, (◻) $T_{\text{poly}} = 333.2$  K,  $t_{\text{poly}} = 60$  ks,  $T_{\text{post}} = 400.2$  K,  $t_{\text{post}} = 60$  ks, (◇) $T_{\text{poly}} = 343.2$  K,  $t_{\text{poly}} = 60$  ks,  $T_{\text{post}} = 373.2$  K,  $t_{\text{post}} = 60$  ks.....169

Figure 6.13: The parameters obtained by fitting the dielectric spectra  $\epsilon'_{\text{dip}}$  and  $\epsilon''_{\text{dip}}$  with KWW relaxation for AN-RDGE mixture measured during cooling from post polymerization temperature to 300 K: (A). non-exponential parameter  $\beta$ , (B). logarithmic average relaxation time  $\log\langle\tau\rangle$ . They are plotted against  $1000/T$ .

The symbols correspond to different polymerization history as: (Δ) $T_{\text{poly}} = 303.2$  K,  $t_{\text{poly}} = 260$  ks,  $T_{\text{post}} = 400.2$  K,  $t_{\text{post}} = 60$  ks, (○) $T_{\text{poly}} = 313.2$  K,  $t_{\text{poly}} = 86$  ks,  $T_{\text{post}} = 400.2$  K,  $t_{\text{post}} = 60$  ks, (▽) $T_{\text{poly}} = 323.2$  K,  $t_{\text{poly}} = 60$  ks,  $T_{\text{post}} = 373.2$  K,  $t_{\text{post}} = 60$  ks, (◻) $T_{\text{poly}} = 333.2$  K,  $t_{\text{poly}} = 60$  ks,  $T_{\text{post}} = 400.2$  K,  $t_{\text{post}} = 60$  ks, (◇) $T_{\text{poly}} = 343.2$  K,  $t_{\text{poly}} = 60$  ks,  $T_{\text{post}} = 373.2$  K,  $t_{\text{post}} = 60$  ks.....170

Figure 6.14: The parameters obtained by fitting the dielectric spectra  $\epsilon'_{\text{dip}}$  and  $\epsilon''_{\text{dip}}$  with KWW relaxation function for AN-RDGE mixture measured during cooling from post polymerization temperature to 300 K: (A).  $\epsilon_s$ , (B).  $\epsilon_\infty$  and (C).  $\Delta\epsilon$ . They are plotted against  $1000/T$ . The symbols correspond to different polymerization history as:

(Δ) $T_{\text{poly}} = 303.2$  K,  $t_{\text{poly}} = 260$  ks,  $T_{\text{post}} = 400.2$  K,  $t_{\text{post}} = 60$  ks, (○) $T_{\text{poly}} = 313.2$  K,  $t_{\text{poly}} = 86$  ks,  $T_{\text{post}} = 400.2$  K,  $t_{\text{post}} = 60$  ks, (▽) $T_{\text{poly}} = 323.2$  K,  $t_{\text{poly}} = 60$  ks,  $T_{\text{post}} = 373.2$  K,  $t_{\text{post}} = 60$  ks, (◻) $T_{\text{poly}} = 333.2$  K,  $t_{\text{poly}} = 60$  ks,  $T_{\text{post}} = 400.2$  K,  $t_{\text{post}} = 60$  ks, (◇) $T_{\text{poly}} = 343.2$  K,  $t_{\text{poly}} = 60$  ks,  $T_{\text{post}} = 373.2$  K,  $t_{\text{post}} = 60$  ks.....171

## List of Tables

Table 6.1: The polymerization conditions for AN-RDGE mixture.....	155
---	-----

# Chapter 1

## Introduction

Amorphous solids are states of frozen-in disordered structure. On heating they either transform to a liquid in a continuous manner or crystallize. These are distinguished from crystals which have a long range of order of both molecular positions and orientations, and which melt sharply at a certain temperature. Experimentally, a glass, which is one type of amorphous solid, is produced by cooling a liquid at a certain rate to a temperature where it becomes rigid on the time-scale of one's observations. During this cooling, its self-diffusion coefficient, entropy, and volume decrease continuously until a temperature is reached when the self-diffusion becomes too slow, and the number of available configurations of the liquid does not change during the time period allowed by the cooling rate. The configurational contribution to the entropy and volume cease and their rates of decrease with temperature become less. At this temperature, the viscosity of glass is typically  $10^{13.6}$  Poise, and the molecular relaxation time of the order of  $10^3$  seconds. At this temperature, the liquid is vitrified and seen as a glass, a dynamically frozen-in liquid, and this temperature has been called the vitrification temperature. When a glass is heated the temperature at which its viscosity decreases to  $10^{13.6}$  Poise, and the configurational contributions begin to increase is called the glass transition or glass-softening

temperature. At this temperature, the heat capacity and thermal expansion coefficient increase.

Unlike the perfectly crystalline state and liquid state, an amorphous solid is not in a thermodynamic equilibrium. At a fixed temperature and pressure, all physical properties of a glass change continuously with time. At a fixed temperature, the rate of changes decrease with time and with increase in the temperature, the total magnitude of the change and the rate of change with time increase. This spontaneous change in the properties of a glass with time is known as the structural relaxation. After a certain time, the rate of change in properties becomes too small or too slow to be detectable in the usual observation period, even though the structural relaxation continues.

The disorder in a solid may be canonical, i.e., both orientational and positional, or only positional. Canonical disorder occurs in all glasses. It has been found that in certain plastic crystals, with long range order of molecular positions, there is no long-range order of molecular orientations. These crystals also behave like a glass but only in their thermodynamics and self-diffusion coefficients. In these cases availability of different configurations contributes to the entropy and enthalpy, and therefore these crystals have also been called the glassy crystals. They show the same structural relaxation as glasses.

A liquid can also be vitrified under isothermal conditions by chemical reactions. When its molecules undergo chemical reactions to form an addition product whose size grows spontaneously. The liquid's volume, entropy and enthalpy decrease and the viscosity increases at a fixed temperature until a time when its viscosity has been increased to  $10^{13.6}$  Poise. This has been called the vitrification time. After this time the

liquid becomes rigid, and shows the characteristic features of a glass, but with occurrences of further chemical reactions.

This thesis is aimed at modifying our concepts of thermodynamics and molecular kinetics of the glassy state by performing both theoretical and experimental studies. Although the various topics studied and experiments performed may seem discrete, they form a common theme in the broader aspects of disordered state of liquids and solids, both molecular and polymeric. Prediction of the theories presented here have been verified by others and results of experiments have been used to test the merits of the theories proposed by others. Thus the thesis has a bearing on our fundamental understanding of the nature of disorder. Introduction to each subject covered in the chapters of this thesis and references to the literature are provided as required.

This thesis is divided into seven chapters. Each chapter contains a review of the subject. The next chapter provides a computer-simulation study of the modulation effects on the properties of amorphous solids. The relaxation function and relaxation time were calculated for the temperature and pressure modulation conditions during structural relaxation at a fixed average temperature, and pressure. Here, the temperature modulation effects on normalized heat capacity during a heating process at a fixed rate were also calculated. It is shown that temperature modulation have serious consequences for the observed thermodynamic properties.

In Chapter 3, a new mean field approximation is provided for a monodispersed polymer chain system, and a mathematical procedure is developed for its use in a polydispersed polymer chain system by using the lattice hole model. Thus the

configurational entropy and heat capacity changes during polymerization at different temperature and pressure have been determined at different extents of polymerization. Finally the configurational entropy theory has been used to relate the configurational entropy of a chain polymer system to its viscosity. This calculation is used to explain the diverging curves of viscosity as the temperature is decreased at a fixed pressure and the pressure is increased at a fixed temperature.

In Chapter 4, a structural and thermodynamic study of an orientational glass is provided, and a statistical model similar to the lattice-hole model used in Chapter 3 was developed to calculate the configurational changes of CuCN orientational glass with temperature.

Kinetics of polymerization reaction leading to vitrification is described in Chapter 5. It also provides a new method of determining the change in the reaction kinetics from mass controlled to the diffusion controlled, which ultimately leads to vitrification. The reaction kinetics rate changes of these two different types of reaction have been mathematically described and distinguished in computational simulation.

In Chapter 6, changes in the dielectric relaxation spectra during isothermal polymerization of a linear chain polymer are reported. The dc conductivity, relaxation time, stretched exponential parameter and dielectric properties during polymerization are determined and discussed. The character also provides the changes in the dielectric spectra during cooling after post-polymerization, and discusses the difference in the dielectric properties of fully polymerized samples obtained after subjecting to different thermal histories.

Finally, the conclusions of the thesis are given in Chapter 7.

Because of the rapid emergence of studies in this area, part of the work described in this thesis was submitted for publications on scientific journals. The resulting publications are listed below:

1. G. P. Johari, M. Beiner, C. Macdonald, J. Wang, "The glass-softening temperature range and non-Arrhenius dynamics: the case of vitrified water", *J. Non-Cryst. Solids*, **278**, 58(2000).
2. J. Wang and G. P. Johari, "Effects of sinusoidal temperature and pressure modulation on the structural relaxation of amorphous solids", *J. Non-Cryst. Solids*, **281**, 91(2000).
3. J. Wang and G. P. Johari, "Chain statistics and the changes in the entropy and heat capacity during melt polymerization", *J. Chem. Phys.*, **116**, 2310(2002).
4. J. Wang, M. F. Collins and G. P. Johari, "CuCN: An orientational glass", *Phys. Rev. B.*, **65**, 180103(2002).
5. J. Wang and G. P. Johari, "The gradual transition from mass-controlled to diffusion-controlled kinetics during melt polymerization", *J. Chem. Phys.*, **117**, 9897(2002).

## Chapter 2

# Temperature and Pressure Modulation Effects on Structural Relaxation of Amorphous Solids

### 2.1 Introduction

One of the characteristic feature of an amorphous solid is that its physical properties change monotonically with time,  $t$ , when it is kept at a fixed temperature,  $T$ , and pressure,  $P$ . The phenomenon is known as isothermal structural relaxation or physical aging [Moynihan *et. al.* (1976), Kovacs *et. al.* (1977), Ngai, *et. al.* (1986), Scherer (1986), Johari (1987), Donth (1992), Matsuoka (1992), Hodge (1994), (1995) and (1997)]. At a molecular level, structural relaxation is a consequence of self-diffusion, which brings spontaneously the solid's molecular structure to a lower energy and usually higher density state. Heating increases the molecular diffusion coefficient,  $D$ , and consequently increases the rate of structural relaxation  $k$ , or decreases the structural relaxation time,  $\tau$ , ( $\tau = 1/k$ ). Cooling decreases  $D$  and  $k$  and increases  $\tau$ . The magnitude of  $D$  decreases non-linearly with decrease in the temperature  $T$  at constant pressure, and, in its simplest form, which is the Arrhenius equation,  $D$  is given by,  $D \sim \exp(-E/RT)$ , where  $E$  is the activation energy and  $R$  is the gas constant. Also, the magnitude of  $D$  decreases non-linearly with increase in the pressure  $P$ , at constant temperature. These variations are relevant to both

the theoretical aspects of non-linear, nonexponential, and irreversible phenomena, and for the development of commercial equipment (i.e., Perkin-Elmer, TA Instruments) used for studying thermodynamic changes by modulated calorimetry.

As propagation of sound waves occurs by sinusoidal adiabatic compression and decompression, and is seen as equivalent to a sinusoidal pressure oscillation, the study of pressure modulation effects are also of theoretical and practical significance. Reference to the paper published on this subject is: J. Wang and G. P. Johari, *J. Non-Cryst. Solids*, 281, 91(2000).

## **2.2 Computation of Sinusoidal Modulation Effects on Properties**

Properties of a glass change spontaneously with time and this change is affected by change in  $P$  and in  $T$ . Therefore, when measurements are made by using a sinusoidal variation of  $T$  with  $t$  and of  $P$  with  $t$ , not only would the properties change spontaneously with time, but the rate of their change would also vary according to the temperature and the pressure at any instant during the sinusoidal cycle. We first formulate and analyze the effects of sinusoidal modulation of  $T$  or  $P$ , and then compute the variation of several properties of a glass caused by the sinusoidal modulation of  $T$  or  $P$ . We then compare the changes against the case without modulation.

### **2.2.1 Sinusoidal modulation of a variable with time**

First we consider the effects in general terms, namely, how sinusoidal modulation of a variable,  $y$ , effects an intrinsic property,  $\rho$ , of a material. When the change of  $y$  with macroscopic time,  $t$ , is much slower than the response time of the material's property, the

measured value of  $\rho$  is the “equilibrium value”. For a sinusoidal variation in  $y$  with a mean value  $y_0$ , a modulation amplitude  $\Delta y$  at angular frequency  $\omega_0$ ,  $y(t)$  is given by,

$$y(t) = y_0 + \Delta y \sin(\omega_0 t) \quad (2.1)$$

As  $y$  is varied sinusoidally about  $y_0$ , three cases may arise. (i) If  $\rho$  varies linearly with  $y$  then the net change in  $\rho$  would be sinusoidal, provided no spontaneous change occurs in these properties. (ii) If  $\rho$  varies nonlinearly with  $y$ , as for a material’s thermodynamic properties, such as volume,  $V$ , enthalpy,  $H$ , entropy,  $S$ , heat capacity,  $C_p$ , the net change in  $\rho$  would be cyclical, not sinusoidal, as do the kinetic properties,  $\tau$  and  $D$ , and other physical properties, such as viscosity  $\eta$ , permittivity, phonon frequency etc. (iii) If  $\rho$  changes spontaneously with  $t$ , the net change in  $\rho$  would not be sinusoidal but rather cyclical.

To elaborate, if the temperature of a glass is changed sinusoidally, its properties would change with time,  $t$ , and the temperature,  $T$ , in a reversible manner. The reason is that when  $T$  is varied sinusoidally with  $t$ ,  $D$  would become time dependent and vary cyclically with  $t$ . Because of the non-linear dependence of  $D$  on  $T$ , the maximum increase in  $D$  that would occur at the maximum temperature of the sinusoidal cycle would be more than the maximum decrease in  $D$  that would occur at the minimum temperature of the sinusoidal cycle. Consequently, the effective  $D$  would be more than the value of  $D(T_0)$ , i.e.,  $D$  at the mean temperature,  $T_0$ , of the sinusoidal oscillation. The effective magnitude of  $D$  would correspond to an average temperature higher than  $T_0$ . The structural relaxation rate,  $k$ , would vary in the same manner as  $D$ , and  $\tau$  would vary in an inverse proportion to  $k$ .

The rate at which the physical properties of a glass change with  $t$  depends upon the magnitude of  $D$  at that  $t$  and  $T$ , i.e.,  $D = D(t, T(t))$ . Therefore, if  $D$  of a material did not spontaneously change with  $t$ , i.e.,  $D(t, T(t)) = D(T(t))$ , there would be a net change in its measured physical property after one cycle of sinusoidal  $T$ -modulation which would result from the effective  $D$  being greater than  $D(T_0)$ . The net change in the physical property resulting from diffusion would accumulate with both the time and the amplitude of the  $T$ -modulation. During a given time period, the change observed on temperature modulation would be different from the change observed without temperature modulation on keeping the sample at a temperature  $T_0$ , with the magnitude of  $D$  being  $D(T_0)$ .

### 2.2.2 A measurable property's second derivative in sinusoidal modulation

We first formulate the effect of sinusoidal modulation of a quantity,  $y$  ( $T$  or  $P$ ), on an intrinsic property  $\rho$  of an amorphous material. Generally speaking,  $\rho$  is found to change nonlinearly with change in  $y$ . Therefore, the net change in  $\rho$  at any instant during a phase in the upper part of the sinusoidal cycle would not be equal and opposite to the net change in  $\rho$  at the corresponding reverse phase during the lower part of the cycle. Thus the oscillation of  $\rho$  would become asymmetric about  $y_0$ , and consequently, its average value,  $\langle \rho \rangle$ , would not be equal to the value of  $\rho(y = y_0)$ . As the oscillation of  $\rho$  would be asymmetric, the magnitude of  $\langle \rho \rangle$  would correspond to the new value of  $y$ , or  $\langle y \rangle$ , which would be shifted from  $y_0$  by an amount,  $\delta y = \langle y \rangle - y_0$ . The magnitude of  $\rho$  during the modulation may be given by the Taylor expansion,

$$\rho(y) = \rho_0 + \left( \frac{d\rho}{dy} \right)_{y=y_0} (y - y_0) + \left( \frac{d^2\rho}{dy^2} \right)_{y=y_0} \frac{(y - y_0)^2}{2!} + \dots \quad (2.2)$$

On substituting for  $y$  from Eq. (2.1), we obtain,

$$\rho(y) = \rho_0 + \left( \frac{d\rho}{dy} \right)_{y=y_0} \Delta y \sin \omega_0 t + \left( \frac{d^2\rho}{dy^2} \right)_{y=y_0} \left( \frac{\Delta y}{2} \right)^2 \sin^2 \omega_0 t + \dots \quad (2.3)$$

The average  $\rho$  over the modulation period of one cycle is then given by,

$$\langle \rho \rangle (t) = \frac{1}{t_0} \int_{-(t_0/2)}^{+(t_0/2)} \rho(t') dt' \quad (2.4)$$

where  $t_0 (= 2\pi/\omega_0)$  refers to the modulation period. On substituting Eq. (2.3) in Eq. (2.4) and integrating over the indicated limits, the odd-order terms of  $\sin(\omega_0 t)$  are found to be zero, and Eq. (2.4) becomes,

$$\langle \rho \rangle = \rho_0 + \left( \frac{d^2\rho}{dy^2} \right)_{y=y_0} \left( \frac{\Delta y^2}{4} \right) + \left( \frac{d^4\rho}{dy^4} \right)_{y=y_0} \left( \frac{\Delta y^4}{64} \right) + \dots \quad (2.5)$$

The difference between  $\langle \rho \rangle$  observed on modulation and  $\rho_0$  observed without modulation is given by,

$$\langle \rho \rangle - \rho_0 = \left( \frac{d^2\rho}{dy^2} \right)_{y=y_0} \left( \frac{\Delta y^2}{4} \right) + \left( \frac{d^4\rho}{dy^4} \right)_{y=y_0} \left( \frac{\Delta y^4}{64} \right) + \dots \quad (2.6)$$

According to Eq. (2.6), when the modulation amplitude is small, the fourth and higher even-order terms in RHS of Eq. (2.6) can be neglected. Therefore,

$$\langle \rho \rangle - \rho_0 = \left( \frac{d^2\rho}{dy^2} \right)_{y=y_0} \left( \frac{\Delta y^2}{4} \right) + \dots \quad (2.7)$$

Thus the difference,  $[\langle \rho \rangle - \rho_0]$ , would be either positive or negative depending only on the sign of the term  $(d^2\rho/dy^2)$  at  $y = y_0$ .

It is known that for entropy, volume and self diffusion coefficient ( $S$ ,  $V$  and  $D$ )  $d\rho/dT > 0$ , and for viscosity and relaxation time ( $\eta$  and  $\tau$ ),  $d\rho/dT < 0$ . Moreover,  $(d^2\rho/dT^2)$  is positive for the  $S$ ,  $V$ ,  $D$ ,  $\eta$ , and  $\tau$ , irrespective of whether  $(d\rho/dT)$  is negative or positive. For  $S$ ,  $V$  and  $D$ ,  $d\rho/dP < 0$  and for  $\eta$  and  $\tau$ ,  $d\rho/dP > 0$ , and  $(d^2\rho/dP^2)$  is positive for all the above-given quantities. Thus, for the properties,  $S$ ,  $V$ ,  $D$ ,  $\eta$  and  $\tau$ , the sinusoidal modulation of either  $T$  or  $P$  would result in a higher averaged magnitude  $\langle\rho\rangle$  in comparison with  $\rho_0$  obtained without modulation.

The magnitude of  $\delta y$  would vary with the type of variable  $y$  (i.e.,  $T$  or  $P$ ), the magnitude of  $\Delta y$  and the manner in which  $\rho$  changes with  $y$ , i.e.,  $d\rho/dy$ . When  $y$  is chosen to be  $T$  and the property  $\rho$  is such that  $(d\rho/dy)$  is positive, as for  $S$ ,  $D$  and  $V$ ,  $\langle y \rangle$  would exceed  $y_0$ . Similarly, when  $\rho$  is chosen such that  $(d\rho/dy)$  is negative, as for the variation of  $\tau$  and  $\eta$  with  $T$ ,  $\langle\rho\rangle$  would still be greater than  $\rho_0$  at  $y_0$ , but  $\langle y \rangle$  would be less than  $y_0$ . When  $y$  represents  $P$ , whose effect is normally opposite to that of  $T$ ,  $\langle\rho\rangle$  would also exceed  $\rho_0$  and  $\langle y \rangle$  would be less than  $y_0$  for  $S$ ,  $D$  and  $V$  and more than  $y_0$  for  $\tau$  and  $\eta$ .

### 2.2.3 Temperature and pressure modulations without irreversible changes

The above-given general description may now be made specific for the sinusoidal modulation of the variable  $T$  or  $P$  by using the relaxation time  $\tau$ , as a diffusion related, intrinsic property of a material. We may express the variation of  $\tau$  with  $T$  in its simplest form, by the Arrhenius equation,

$$\tau = \tau_{\infty} \exp\left[\frac{E_A}{RT}\right] \quad (2.8)$$

where  $\tau_\infty$  is the magnitude of  $\tau$  at a formally infinite temperature,  $E_A$  is the Arrhenius energy and  $R$  the gas constant.

A sinusoidal variation of  $T$  ( $= T_0 + \Delta T \sin \omega_0 t$ ) would produce a variation of  $\tau$ , according to,

$$\tau(t) = \tau_\infty \exp \left[ \frac{E_A}{R(T_0 + \Delta T \sin \omega_0 t)} \right] \quad (2.9)$$

As described in Section 2.2.2 for a general case, during each sinusoidal cycle,  $\langle \tau \rangle$  would not correspond to  $\tau$  at  $T_0$ . Instead it would correspond to a temperature ( $T_0 + \delta T$ ), and its average magnitude would be given by:

$$\langle \tau \rangle (t) = \frac{1}{t_0} \int_{t-(t_0/2)}^{t+(t_0/2)} \tau(t') dt' \quad (2.10)$$

where  $t$  refers to the time at which the observation is made and  $t_0$  ( $= 2\pi/\omega_0$ ) is the  $T$ -modulation period.

The corresponding equation for sinusoidal pressure variation at a constant temperature is given by,

$$\tau = \tau(P=0) \exp \left[ \frac{\Delta V^*}{RT} P \right] \quad (2.11)$$

where  $\tau(P=0)$  is the magnitude of  $\tau$  at zero pressure,  $\Delta V^*$  the volume of activation, and  $R$  the gas constant. For a sinusoidal variation of  $P$ ,

$$P(t) = P_0 + \Delta P \sin(\omega_0 t) \quad (2.12)$$

On combining Eqs. (2.11) and (2.12),

$$\tau(t) = \tau(P = 0) \exp \left[ \frac{\Delta V^*}{RT} (P_0 + \Delta P \sin \omega_0 t) \right] \quad (2.13)$$

Therefore during a sinusoidal  $P$ -cycle,  $\langle \tau \rangle$  would not correspond to  $\tau$  at  $P_0$ . Instead, it would correspond to  $(P_0 + \delta P)$ , and its average magnitude at  $t$  would be given by:

$$\langle \tau \rangle (t) = \frac{1}{t_0} \int_{t-t_0/2}^{t+t_0/2} \tau(t') dt' \quad (2.14)$$

where  $t_0 (= 2\pi/\omega_0)$  is the  $P$ -modulation period.

For simulating these effects, we use  $\tau_\infty = 10^{-14}$  s, the phonon vibration time scale,  $E_A = 500$  kJ/mol and  $T_0 = 200$  K and calculate the variation of  $\tau$  with  $t$  for both the unmodulated and modulated conditions. For the latter, we use  $\Delta T$  of 1.5 K (as recommended by TA instruments) and  $\omega_0$  of  $2\pi \times 10^{-2}$  rad s<sup>-1</sup> (or  $f = 10$  mHz). The calculated value of  $\tau$  is plotted against  $t$  on the ordinate scale on RHS in Fig. 2.1(A). For the modulated condition, it is shown by the dashed line, and for the unmodulated condition, it is shown by the solid horizontal line. The corresponding sinusoidal variation of temperature is shown by the solid line. The calculated  $\langle \tau \rangle$  is also plotted against  $t$  as a dotted line in Fig. 2.1(A) for the modulated condition.

The values of  $\tau$  were calculated for sinusoidal variation of  $P$  by using  $P_0 = 500$  bar,  $\tau(P = 0) = 1$  s,  $\Delta V = 100$  ml mol<sup>-1</sup>,  $\omega_0 = 2\pi \times 10^{-2}$  rad s<sup>-1</sup> ( $f = 10$  mHz) and  $\Delta P = 100$  bar. These values are plotted against  $t$  in Fig. 2.1(B) with the ordinate shown on the right hand side. For the modulated condition, the corresponding plot is shown by the dashed line, and for the unmodulated condition, it is shown by the solid horizontal line. Here the

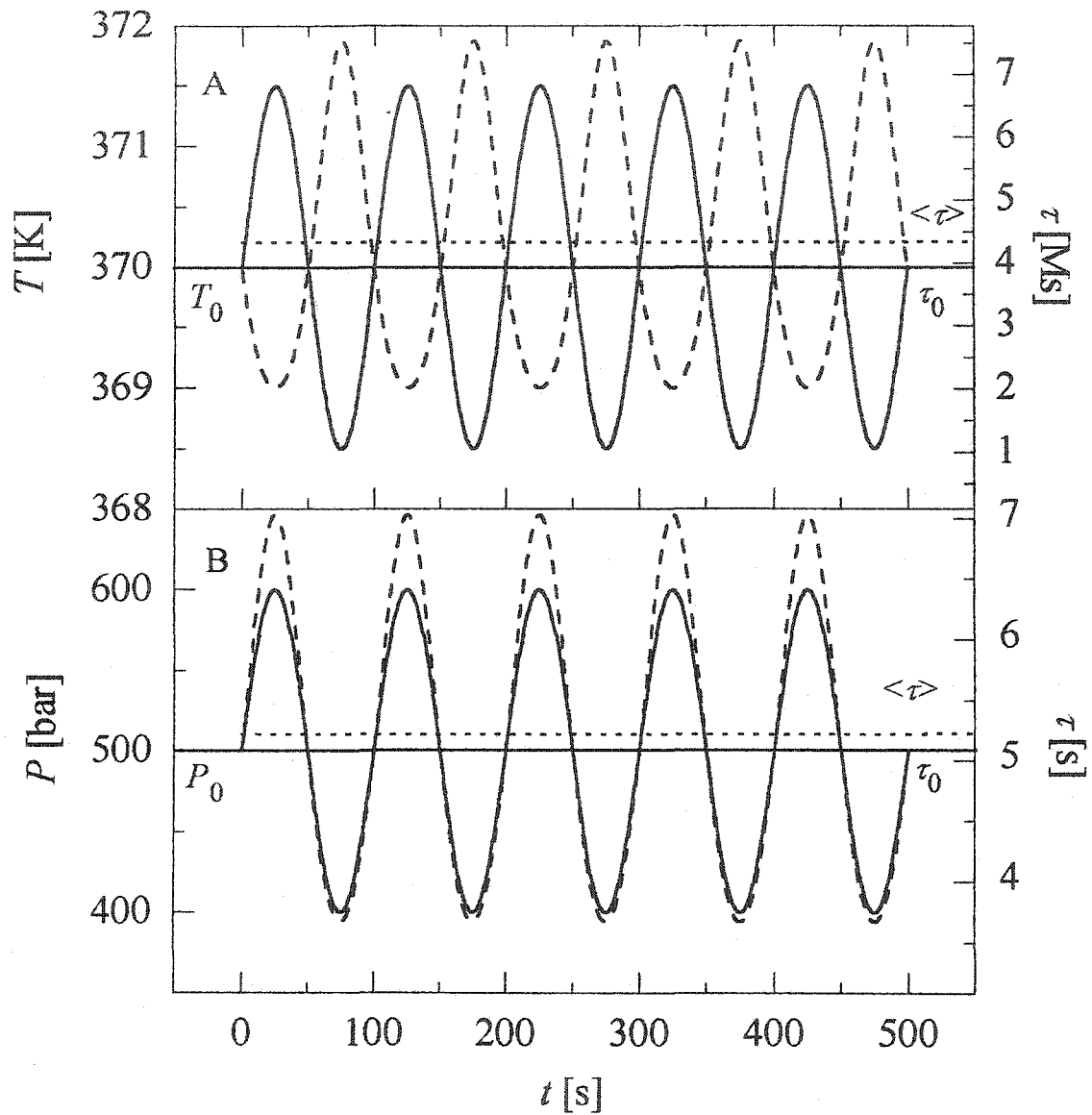


Fig. 2.1. (A). The variation of  $T$  with  $t$  for sinusoidal modulation (solid line) and the consequent change in  $\tau$  (dashed line). (B). The variation of  $P$  with  $t$  for sinusoidal modulation (solid line) and the consequent change in  $\tau$  (dashed line). The horizontal solid lines in A and B represent the mean temperature or pressure,  $T_0$  or  $P_0$  on the left hand side scale, and the relaxation time,  $\tau_0$ , at  $T_0$  or  $P_0$ , on the right hand side scale. The horizontal dotted lined represents  $\langle \tau \rangle$  as labeled. Parameters used for the calculation are given in the text.

corresponding sinusoidal variation in  $P$  and modulated  $\langle \tau \rangle$  are shown by the solid line and the horizontal dotted line.

At the outset of this chapter, we had mentioned that modulation would change the rate of a property's spontaneous change with time if the property itself changed nonlinearly with  $T$  or  $P$ . Mathematical treatment of this observation should be general, and here we illustrate it for the diffusion rate,  $k$  ( $= 1/\tau$ ), which varies with  $T$  in an Arrhenius manner:

$$k = k_0 \exp(-E_A/RT) \quad (2.15)$$

where  $E_A$  is the activation energy. The difference between the average value of  $\langle k \rangle$  and  $k$  both at  $T_0$  may be obtained by combining Eqs. (2.7) and (2.8),

$$\langle k \rangle - k_0 = \left( \frac{d^2 k}{dT^2} \right)_{T=T_0} \frac{(\Delta T)^2}{4} \quad (2.16)$$

$$\text{or, } \langle k \rangle - k_0 = \frac{(\Delta T)^2 k_0 E_A}{4RT_0^3} \left( \frac{E_A}{RT_0} - 2 \right) e^{-\frac{E_A}{RT_0}} \quad (2.17)$$

where all notations are as described before. For the usual condition,  $E_A/RT_0 > 2$ , in Eq. (2.17), the LHS term ( $\langle k \rangle - k_0$ ) is positive. Accordingly, ( $\langle k \rangle - k_0$ ) would increase linearly with  $(\Delta T)^2$  for a given  $E_A$  and  $T_0$ . Its value would be much more sensitive to the term  $\exp(-E_A/RT_0)$  than to the cubic term in  $T_0$  in Eq. (2.17).

Similarly, for pressure modulation,

$$k = k_0 \exp(-\Delta V^* P/RT) \quad (2.18)$$

$$\text{or, } \langle k \rangle - k_0 = \left( \frac{d^2 k}{dP^2} \right)_{P=P_0} \frac{(\Delta P)^2}{4} = \frac{(\Delta P)^2 k_0}{4} \left( \frac{\Delta V^*}{RT} \right) e^{-\frac{\Delta V^*}{RT}}, \quad (2.19)$$

i.e., that the average rate of the process on  $P$ -modulation would be greater than its rate in the unmodulated conditions, and this difference may be calculated from the knowledge of  $\Delta V^*$  and  $k_0$ .

From the above analysis, we find that the modulation of either  $T$  or  $P$  would increase the average values of both the relaxation time  $\tau$  and the relaxation rate  $k$ , even though  $\tau$  and  $k$  are inversely related by  $\tau = 1/k$ . To summarize, the difference between a physical property  $\rho$  in the case of sinusoidal modulation of variable  $y$  and in the case of non-modulation,  $[\langle \rho \rangle - \rho_0]$ , is determined by the second derivative of  $\rho$  with respect to the variable  $y$ ,  $(d^2 \rho / dy^2)$ , multiplied by  $(\Delta y)^2 / 4$ , which is a quarter of the modulation intensity. When  $(d^2 \rho / dy^2)$  is positive, as for most cases, sinusoidal modulation of  $y$  would increase the average  $\langle \rho \rangle$  value from the unmodulated  $\rho_0$  value, and this increase can be calculated from the dependence of  $(d^2 \rho / dy^2)$  on the variable  $y$ .

#### 2.2.4 Formalism of structural relaxation process

During the structural relaxation process of an amorphous solid at a fixed  $T$  and  $P$ , the magnitude of a physical property,  $\rho$ , such as,  $H$ ,  $S$ ,  $V$  and  $D$ , decreases monotonically with  $t$  [Moynihan *et al.* (1976), Hodge (1994), (1995) and (1997)]. The value of  $\rho(t)$  would approach a constant  $\rho_\infty$  as  $t$  approaches  $\infty$ , i.e., at a formally infinite time. For convenience, we define a normalized relaxation function  $\phi(t)$  for the property  $\rho$  by,

$$\phi(t) \equiv \frac{\rho(t)}{\rho_\infty} \quad (2.20)$$

It is recognized that for molecular dynamics of a liquid and glass,  $\phi(t)$  is written in terms of linear stretched exponential relaxation in macroscopic time  $t$ , as originally given by Gardon and Narayanaswamy (1970) and Narayanaswamy (1971):

$$\phi(t)|_{t \rightarrow t'} = \exp \left[ - \left( \frac{t}{\tau(t \rightarrow t')} \right)^\beta \right], \quad (2.21)$$

where  $\tau$  is now defined as the characteristic structural relaxation time and  $\beta$  is an empirical parameter with value between zero and one. More generally, by using the Narayanaswamy reduced time variable [Narayanaswamy (1971)], as

$$\xi(t) = \int_0^t \frac{dt'}{\tau(t')}, \quad (2.22)$$

the nonlinear form of the stretched exponential relaxation function can be written [Tool (1946), Gardon and Narayanaswamy (1970), Narayanaswamy (1971), Moynihan *et. al.* (1976), Hodge (1994), (1995) and (1997)]:

$$\phi(t) = \exp \left[ - \xi(t)^\beta \right] = \exp \left\{ - \left[ \int_0^t \frac{dt'}{\tau(t')} \right]^\beta \right\} \quad (2.23)$$

The magnitude of  $\beta$  determines both the rate of change in a physical property, e.g.,  $S$ ,  $H$ ,  $V$ , the index of refraction at a given instant, and the shape of their plots against  $t$ . The physical properties of an amorphous solid are described also by its fictive temperature,  $T_f$ ,

which is defined as the temperature at which the material would correspond to its internal equilibrium state [Tool (1946), Gardon and Narayanaswamy (1970), Narayanaswamy (1971), Moynihan *et. al.* (1976), Hodge (1994), (1995) and (1997)]. By incorporating the Boltzmann time-temperature superposition principle [Boltzmann (1876), Hopkinson (1877), Curie (1888)],  $T_f$  can be calculated from:

$$T_f = T_1 + \int_{T_1}^T dT' \left\{ 1 - \exp \left[ - \left( \int_{T'}^T \frac{dT''}{q(T'')\tau(T'')} \right)^\beta \right] \right\} \quad (2.24)$$

where  $T_1$  is the temperature from which cooling of the equilibrium liquid begins, and  $q$  is the cooling or the heating rate ( $q = dT/dt$ ). The change in  $\tau$  with  $t$  is related to the change in  $\tau$  with  $T_f$  at a fixed  $T$  is described by an equation [Narayanaswamy (1971), Moynihan *et. al.* (1976), Kovacs *et. al.* (1977), Ngai *et. al.* (1986), Scherer (1986), Donth (1992), Matsuoka (1992), Hodge (1994), (1995) and (1997)],

$$\tau = A \exp \left[ \frac{x\Delta h^*}{RT} + \frac{(1-x)\Delta h^*}{RT_f} \right] \quad (2.25)$$

where  $A$  is the pre-exponential term with units of time, which is found to be much less than the characteristic time for the phonon modes [Moynihan *et. al.* (1976), Hodge (1994), (1995) and (1997)],  $x$  is the non-linearity parameter, whose magnitude is between zero and one,  $\Delta h^*$  is the effective activation energy,  $R$  the gas constant and  $T$  is the fixed temperature. (Note that non-linearity here refers to a departure from the Arrhenius equation, for which  $x = 1$ .) According to Eq. (2.25),  $\tau$  of an amorphous solid increases on its structural relaxation with time, as  $T_f$  decreases with  $t$ .

During cooling from an equilibrium liquid state, the fictive temperature,  $T_f$ ,  $D$ ,  $H$ ,  $S$  and  $V$  of a glass forming system decrease continuously until a temperature is reached when the diffusion becomes too slow to contribute to the energy and volume change in the time period allowed by the cooling rate. At this temperature, the liquid is said to be vitrified and is seen as a glass. Further cooling of a glass does not decrease its  $T_f$ . This  $T$ -invariant value of  $T_f$  of the vitrified state is denoted by  $T_f(0)$ , which is the fictive temperature at the end of its cooling process (or the beginning of its isothermal relaxation).

When kept at a  $T$  below the vitrification temperature, a glass undergoes structural relaxation which may be studied either at a fixed  $T$  or with increasing  $T$ , by heating at a fixed rate. At a fixed  $T$ , spontaneous structural relaxation decreases  $T_f$  of a glass monotonically with  $t$  at a rate that itself decreases with decrease in  $T_f$ , as for a self-retarding process. Glassy state of a given material structurally relaxes faster when it has been produced by rapid cooling and its  $T_f(0)$  is high, than when it has been produced by slow cooling and its  $T_f(0)$  is low. On heating at a certain rate, structural relaxation is affected by both  $t$  and  $T$ . As  $t$  increases, structural relaxation rate decreases at a fixed  $T$ , and as  $T$  is increased at a (mathematically) fixed  $t$ , the relaxation rate increases according to Eq.(2.25), because  $T_f$  decreases. Thus the rate of decrease of  $T_f$  is reduced as  $t$  increases and is increased as  $T$  increases. The net change in  $T_f$  is determined by the partial cancellation of the two effects, which in turn is determined by the heating rate.

Simon and McKenna (1997) have also done simulations for modulated differential calorimetry in glass forming liquids kept at a fixed mean temperature. In their

calculations, they used  $x = 1$  in Eq. (2.25) and calculated the dynamic heat capacity  $C_p'$  and  $C_p''$ . The agreement of their calculations with experimental data seemed reasonable for glycerol [Birge and Nagel (1985), Birge (1986)] and for poly(vinyl acetate) [Beiner *et al.* (1996)]. No calculations for heating a glass sample, as is done in scanning calorimetry was attempted by them, possibly because of the complications in the calculations.

For computation of  $\tau$  from Eqs. (2.23) - (2.25), it is required that cooling and heating be done in consecutive, step-wise changes,  $\Delta T_j$  for  $T$ , after a certain time,  $\Delta t_k$  for  $t$ . On including the  $\Delta T_j$  and  $\Delta t_k$  steps for cooling and heating processes, we may write,

$$\phi_n(t) = \exp \left[ - \left( \sum_{k=0}^n \frac{\Delta t_k}{\tau_k} \right)^\beta \right] \quad (2.26)$$

$$\tau_n = A \exp \left[ \frac{x\Delta h}{RT_n} + \frac{(1-x)\Delta h}{RT_{f,n-1}} \right] \quad (2.27)$$

$$T_{f,n} = T_1 + \sum_{j=1}^n \Delta T_j \left\{ 1 - \exp \left[ - \left( \sum_{k=j}^n \frac{\Delta t_k}{\tau_k} \right)^\beta \right] \right\} \quad (2.28)$$

where  $n$  is all inclusive number of steps in the cooling, isothermally keeping a glass and thereafter in the heating procedures. For procedures in which isothermal relaxation occurs,  $\frac{\Delta T_k}{q_k \tau_k}$  in Eq. (2.28) becomes equal to  $\frac{\Delta t_k}{\tau_k}$ . The computational accuracy increases as the magnitude of  $\Delta T_j$  and  $\Delta t_k$  in Eq. (2.28) is reduced but the total time for the computation also increases. As a compromise between the accuracy and the time required for computation, we have used:  $\Delta T_j \sim 0.1 - 0.2$  K for cooling, and  $1/64$  K (15.625 mK) for

heating, with  $\Delta t_k$  of  $t_0/16 - t_0/256$  for  $T$ -modulation. The integration needed for these calculations and the related procedure have been generally accepted as valid and appropriate [Moynihan *et. al.* (1976), Pascheto *et. al.* (1994), Hodge (1994), (1995) and (1997)]. We used Turbo Pascal Software to write programs for our calculations. For the calculation of one curve, the typical running time on a Pentium II personal computer ranged from half an hour to 12 hours depended on the parameters.

For the unmodulated condition, Eqs. (2.23) and (2.24) yield the decrease in  $\phi$  and  $T_f$  with  $t$ . When  $T$  is modulated,  $\phi$  and  $T_f$  change with  $t$  also for the reason that  $T$  in the exponential term of Eq. (2.24) changes according to  $\Delta T \sin \omega_0 t$ , producing a cyclically change in  $T_f$ , which is superimposed on the monotonic decrease of  $T_f$  with  $t$ . Thus  $\phi$  and  $T_f$  change with  $t$  at a fixed  $T_0$  for the unmodulated condition, but change with  $t$  at an average  $\langle T \rangle$  for the  $T$ -modulated condition.

For computing the changes due to structural relaxation isothermally, a liquid may be cooled rapidly from its equilibrium state at a high temperature to a nonequilibrium metastable state of a glass. During the cooling, its molecular dynamics remains much faster than the modulation period, and therefore the liquid remains at equilibrium at both extremes,  $T_{\max}$  and  $T_{\min}$ , of the modulation cycle. For this purpose, the cooling rate itself should remain much faster than  $\omega_0$ , as long as  $T \gg T_g$ . Thus the effect of modulation during cooling is insignificant. When the temperature is in the vitrification range, the effects become significant and need to be included in the formalism. These effects may then be computed either without  $T$ -modulation, or with  $T$ -modulation using a selected value of  $\Delta T$ .

As a thermodynamic or optical property is usually directly related to  $T_f$  [Narayanaswamy (1971)], the calculations require only that  $T_f$  be determined, which may then be related to those properties. We use several cooling rates, and different values of  $T_0$  to calculate the decrease in  $T_f$  with  $t$ . Since the fictive temperature and the relaxation function in a modulation condition vary with the time during a cycle, only average value of  $T_{f,mod}$  and  $\phi_{mod}$  can be determined. This average values of  $\langle T_{f,mod} \rangle$  and  $\langle \phi_{mod} \rangle$  was calculated from Eq. (2.4) where  $\langle \rho \rangle(t)$  representing  $\langle T_{f,mod} \rangle(t)$  and  $\langle \phi_{mod} \rangle(t)$ . As an example, the material may be cooled from the equilibrium state at 470 K to the non-equilibrium state at 370 K at  $720 \text{ K min}^{-1}$  in  $\Delta T_j$  steps of 0.1 K, and decrease in  $T_f$  may be determined during the cooling. The system under computation was kept at  $T_0$  of 370 K and its  $\phi$  and  $T_f$  computed with changing  $t$  using Eqs. (2.23)- (2.25), initially for the simplest condition,  $\beta = 1$ , and  $x = 1$ , and with  $\ln A = -150$  and  $\Delta h^* = 590 \text{ kJ mol}^{-1}$ . The calculated values of  $\phi$  and  $T_f$  for different conditions are plotted against  $t$  in Figs. 2.2(A) and 2.2(B), respectively. For the  $T$ -modulated case, we use,  $\Delta T = 2.5 \text{ K}$  and  $\omega_0 = \pi \text{ mrad s}^{-1}$  for cooling the sample at  $720 \text{ K min}^{-1}$ , from 470 K to 370 K in  $\Delta T_j$  steps of 0.1 K. The sample is then kept at  $T_0$  of 370 K, with  $\Delta T$  and  $\omega_0$  for  $T$ -modulation the same as during the cooling described above and its  $\phi_{mod}(t)$  and  $T_{f,mod}(t)$  were calculated by using the same values of  $\beta$ ,  $x$ ,  $\ln A$  and  $\Delta h^*$  as for the unmodulated condition. These  $\phi_{mod}(t)$  and  $T_{f,mod}(t)$  values are also plotted against  $t$  in Fig. 2.2(A) and 2.2(B). The difference between the  $\phi$  values for the unmodulated and modulated conditions,  $\delta\phi = \phi_{unmod} - \langle \phi_{mod} \rangle$ , is plotted against  $t$  in Fig. 2.2(C) and that between the  $T_f$  values,  $\delta T_f = T_{f,unmod} - \langle T_{f,mod} \rangle$  against  $t$

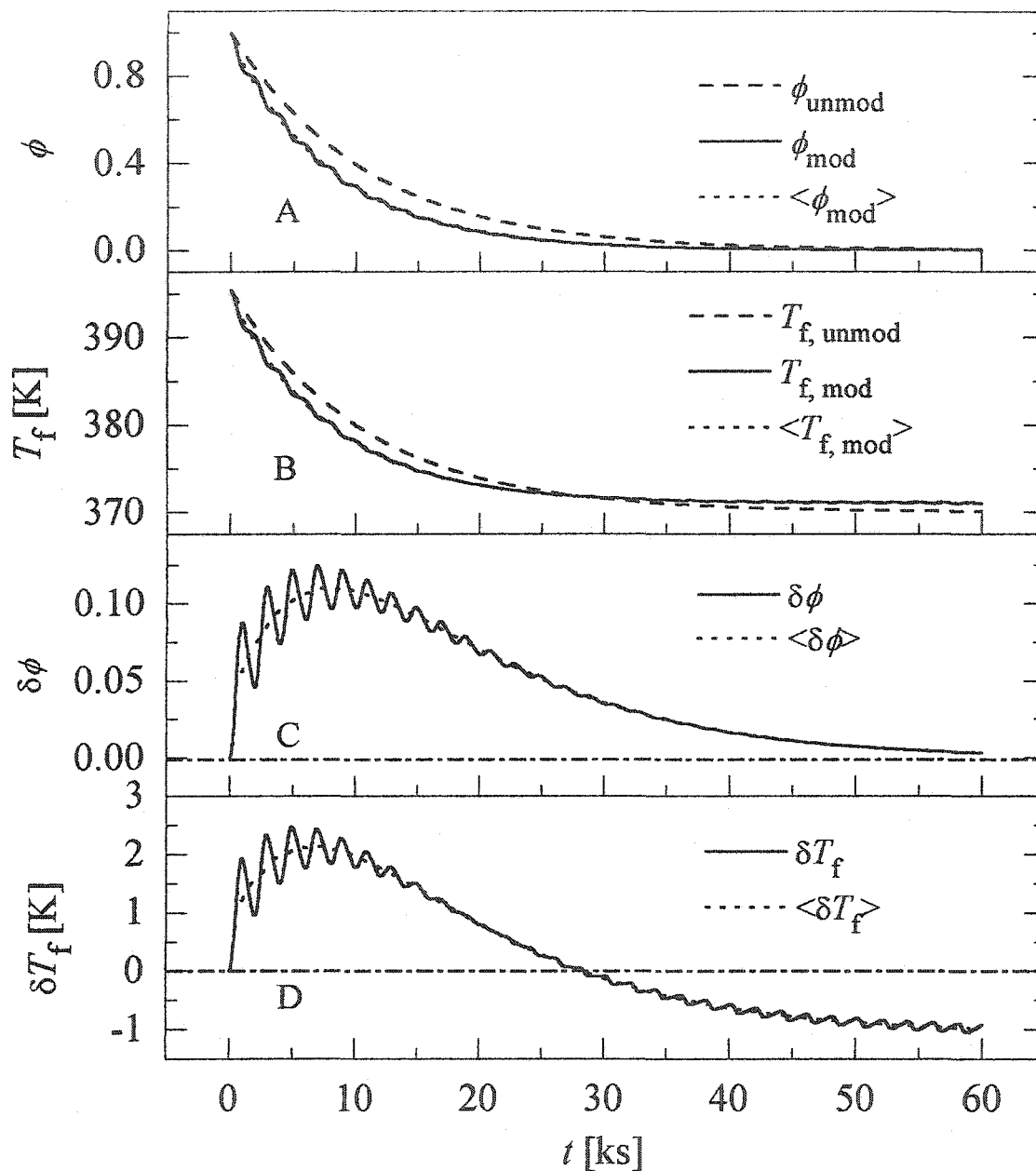


Fig. 2.2. (A). The plots of  $\phi$  against  $t$  for the  $T$ -modulated and unmodulated conditions. (B). The plots of  $T_f$  against  $t$  for the  $T$ -modulated and unmodulated conditions. (C). The plots of the difference  $\delta\phi$  between the  $\phi$  for the two conditions. (D). The plots of the difference  $\delta T_f$  between the  $T_f$  for the two conditions. The line passing through the oscillating curves for  $\phi_{\text{mod}}$ ,  $\delta\phi$ ,  $\langle T_{f, \text{mod}} \rangle$  and  $\delta T_f$  is the average value in each case. Parameters used for the calculations are given in the text. The data refer to isothermal annealing.

in Fig. 2.2(D). These show that  $\phi_{\text{unmod}}$  and  $T_{f,\text{unmod}}$  are, as expected, decreasing functions of  $t$ , but while  $\phi_{\text{mod}}$  and  $T_{f,\text{mod}}$  remain an overall decreasing function, the decrease is superposed on another effect, which causes local oscillations in its slope in the plots against  $t$ . Values of  $\langle\phi_{\text{mod}}\rangle$ ,  $\langle T_{f,\text{mod}}\rangle$ ,  $\langle\delta\phi\rangle$  and  $\langle\delta T_f\rangle$  were also determined and these are plotted against  $t$  in Fig. 2.2(A) to 2.2(D). The curves show that  $\langle\phi_{\text{mod}}\rangle$  decreases faster than  $\phi$ , and that  $\langle T_{f,\text{mod}}\rangle$  decreases faster than  $T_{f,\text{unmod}}$  initially and then decreases slowly. This produces the appearance of a cross-over in their curves at a certain time,  $t_x$ . The oscillation envelope of  $\langle\phi_{\text{mod}}\rangle$  is initially large, and tends to vanish as  $t \rightarrow \infty$ . Similarly, the oscillation envelope of  $T_{f,\text{mod}}$  is initially large, decreases up to a certain time  $t_x$ , and thereafter increases and becomes constant as  $t \rightarrow \infty$ .

The observation in Fig. 2.2(B) that  $T_{f,\text{mod}}$  remains higher than  $T_{f,\text{unmod}}$  as  $t \rightarrow \infty$  seems surprising at first sight, and needs to be explained. The increase in  $T$  to  $T_{\text{max}}$  value during the modulation brings the sample to a high  $T_f$ -state where its structural relaxation is faster than at  $T_0$ , and therefore  $T_f$  decreases more rapidly at  $T_{\text{max}}$  than at  $T_0$ . The temperature decrease to  $T_{\text{min}}$  correspondingly causes  $T_f$  to decrease more slowly at  $T_{\text{min}}$  than at  $T_0$ . Thus after one modulation, the sample is left with a  $T_f$  lower than the  $T_f$  without modulation at the same  $t$ . When  $t$  has increased such that, the sample is close to the equilibrium state, an increase in  $T$  of the sinusoidal cycle to  $T_{\text{max}}$  causes it to cross the equilibrium line. Here  $T_f$  now increases with  $t$  instead of decreasing with  $t$ . A decrease to  $T_{\text{min}}$  of the cycle returns it to the condition where  $T_f$  still decreases. Since structural relaxation is faster at  $T_{\text{max}}$  than at  $T_{\text{min}}$ , the net effect is that  $\langle T_{f,\text{mod}}\rangle$  becomes equal to  $T_{f,\text{unmod}}$ . When the sample is closer still to the equilibrium state,  $\langle T_{f,\text{mod}}\rangle$  exceeds  $T_{f,\text{unmod}}$ ,

and remain so as  $t \rightarrow \infty$ . The difference at  $t \rightarrow \infty$  is expected to be  $(\Delta T)^2 [d^2 T_f / dT^2] / 4$  at  $T = T_0$  according to Eq. (2.7), and to vary with the activation energy of the relaxation. The plots of  $\phi$ ,  $T_f$ ,  $\delta\phi$  and  $\delta T_f$  obtained from the above calculations in Fig. 2.2 show the results for the following two conditions, (i)  $\phi$  is a simple exponential, or  $\beta = 1$  in Eq. (2.22), and (ii)  $\tau$  varies in an Arrhenius manner, or  $x = 1$  in Eq. (2.24), and not additionally with  $T_f$ .

We now perform calculations for the condition when  $\phi$  is a stretched-exponential function, i.e.,  $0 < \beta \leq 1$  in Eqs.(2.23-2.24), and further that  $\tau$  varies additionally with  $T_f$ , i.e.,  $0 < x \leq 1$ . For this purpose, we choose  $\ln A = -150$  and  $\Delta h^* = 590 \text{ kJ mol}^{-1}$ , as in the preceding calculations, and use three conditions, (i)  $\beta = 1$  and  $x = 0.5$ , (ii)  $\beta = 0.5$  and  $x = 0.5$ , and (iii)  $\beta = 0.5$  and  $x = 1$ . The calculated  $\langle \delta\phi \rangle$  values for these conditions are plotted against  $t$  in Fig. 2.3(A) and of  $\langle \delta T_f \rangle$  in Fig. 2.3(B). The plots show that the peak in  $\langle \delta\phi \rangle$ , which appears at  $t$  of  $\sim 7$  ks, shifts to a shorter  $t$  of  $\sim 1$  ks and its height decreases from 0.11 to 0.06 when  $\beta$  is decreased from 1 to 0.5. The effect of decreasing  $x$  or increasing non-linearity is qualitatively similar to a decrease in  $\beta$ , but is enhanced when  $\beta$  is decreased. The cross-over time,  $T_x$ , of  $\langle \delta T_f \rangle$  increases when  $\beta$  is decreased at a constant  $x$ . It increases also when  $x$  is decreased at a constant  $\beta$ . Thus, in principle, a set of  $\beta$  and  $x$  pairs may be found for which  $T_x$  would remain constant.

Next, we consider the effects of a change in the modulation frequency  $\omega_0$  on  $T_f$ . For that purpose, we use  $\omega_0$  values as  $2\pi/30$ ,  $10\pi/30$  and  $20\pi/30 \text{ rad s}^{-1}$ ,  $\beta = 1$ ,  $x = 1$ ,  $\ln A = -150$  and  $\Delta h^* = 590 \text{ kJ mol}^{-1}$  as before, and calculate  $\langle \delta\phi \rangle$  and  $\langle \delta T_f \rangle$ . These are plotted against time in Fig. 2.4(A) and 2.4(B), respectively, which shows that the height

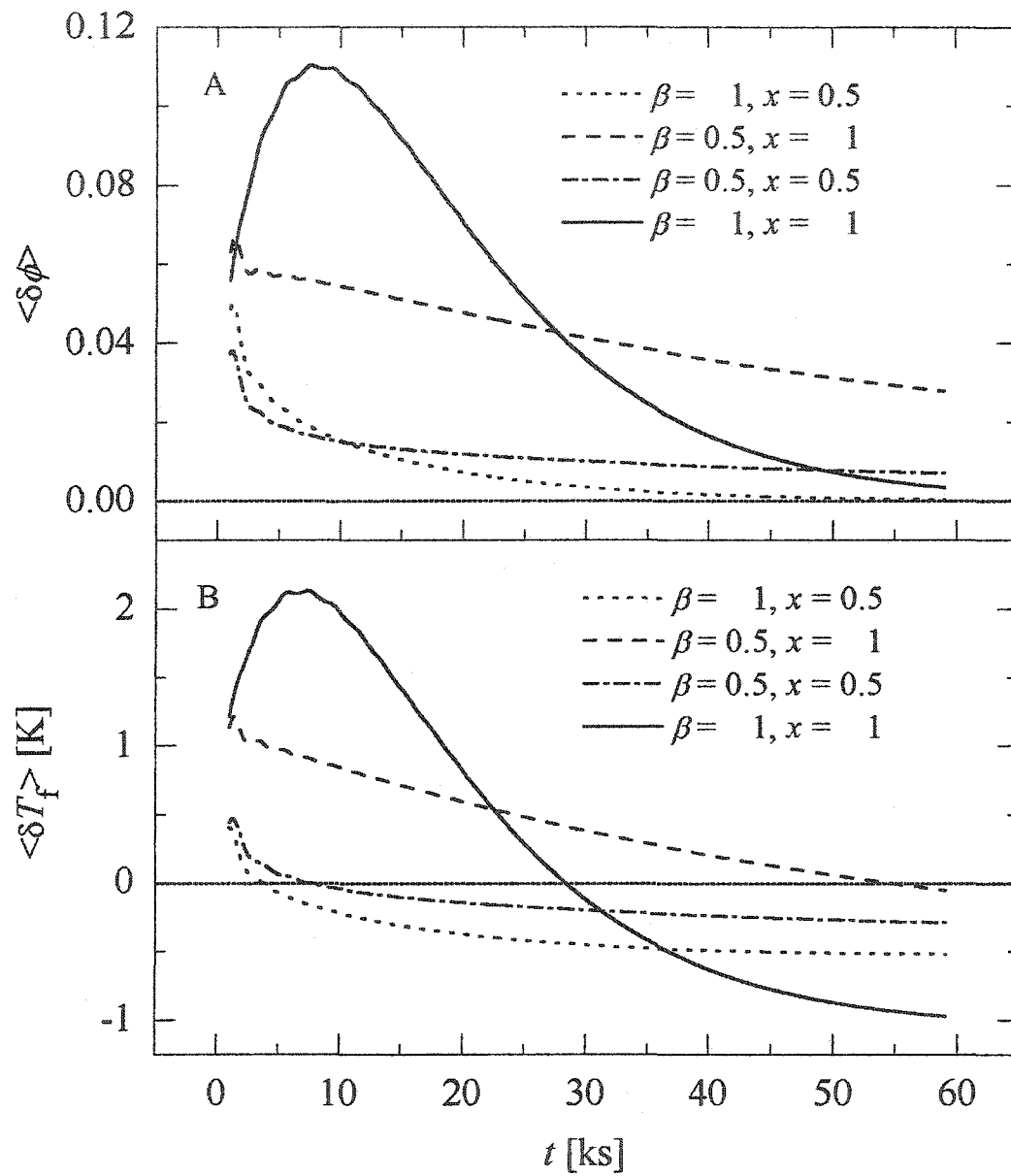


Fig. 2.3. (A). The plots of the average value for  $\delta\phi$  against real time for four pairs of  $\beta$  and  $x$ , as noted. (B). Plots of  $\delta T_f$  against real time. Parameters used for the calculation are given in the text.

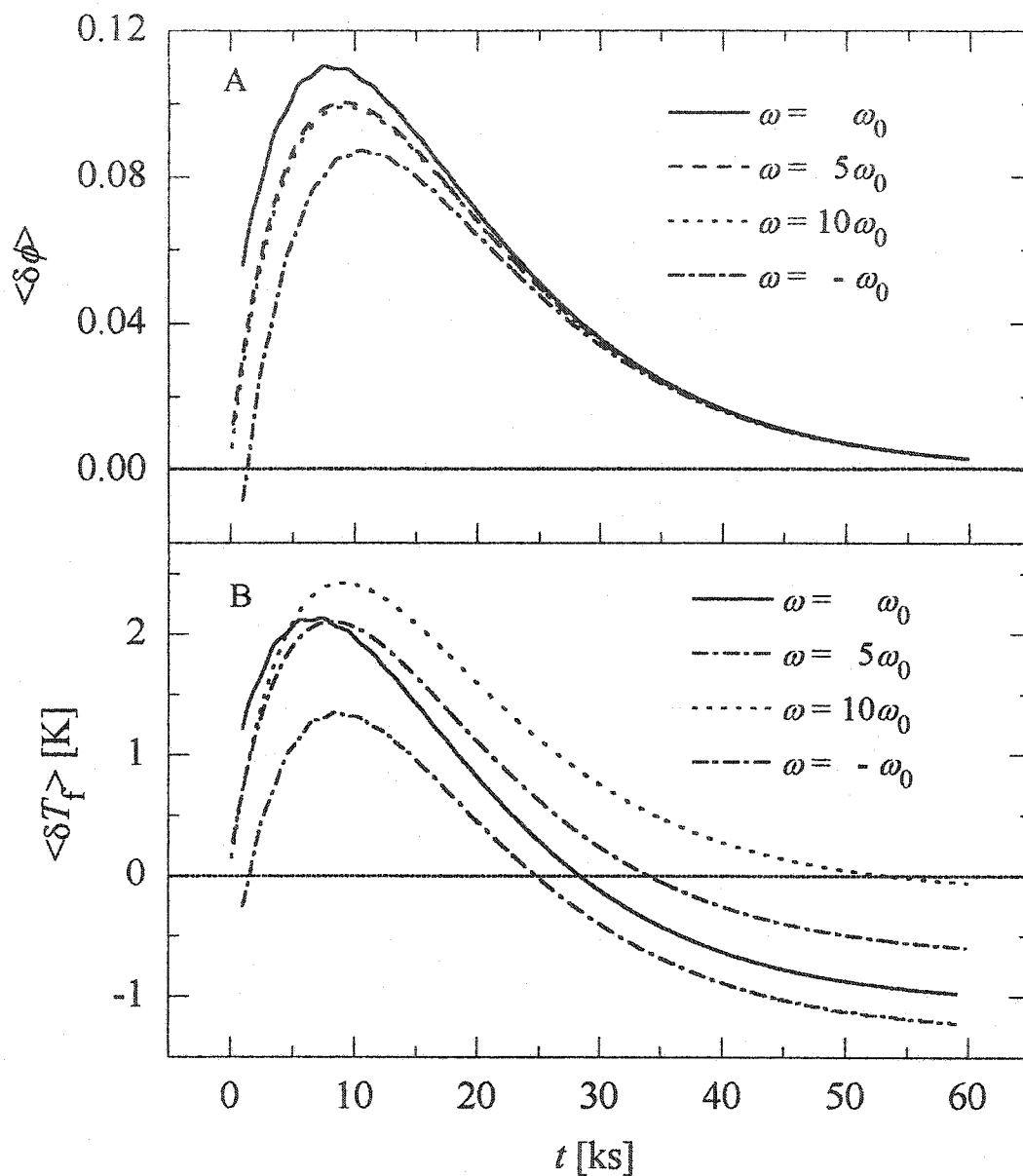


Fig. 2.4. (A). The plots of the average value for  $\delta\phi$  against real time for three cases with different values of  $\omega_0$  as noted. The curve labeled  $-\omega_0$  is for the condition when the phase angle was shifted by  $\pi$ . (B). The plots of  $\delta T_f$  against real time. Parameters used for the calculation are given in the text.

of the peak in  $\langle \delta\phi \rangle$  decreases on increasing the modulation frequency and the crossover time  $t_x$  of  $\langle \delta T_f \rangle$ , which is shown by the crossing of the zero-line, shifts to longer time.

The above-given calculations are based on the conditions that  $T = T_0$  at  $t = 0$ , or that  $T$  increases towards  $T_{\max}$  of the sinusoidal cycle as the structural relaxation begins from  $T_f(0)$ . Another condition of interest is when  $T$  decreases towards  $T_{\min}$  of the sinusoidal cycle as the structural relaxation begins from  $T_f(0)$ , i.e. the phase angle is shifted by  $\pi$ , or equivalently  $\omega_0$  becomes  $-\omega_0$ . For this condition, we may write  $\Delta T \sin(\omega_0 t + \pi)$  in place of  $\Delta T \sin(\omega_0 t)$  for the  $\pi$ -shifted phase starting at  $T = T_0$  and calculate the values of  $\langle \delta\phi \rangle$  and  $\langle \delta T_f \rangle$  starting from  $T_f(0)$ . These values are also plotted in Fig. 2.4(A) and 2.4(B). The plots show that up to a macroscopic time,  $t = \pi/\omega_0$ ,  $\langle \delta\phi \rangle$  remains negative and thereafter becomes positive. The position of the peak in  $\langle \delta\phi \rangle$  is shifted to the right and its height decreases in comparison with the height of the peak for unshifted phase conditions. This produces two crossover points in the corresponding plot of  $\langle \delta T_f \rangle$  in the case of the  $\pi$ -shifted phase angle. The second cross-over point,  $t_{x,2}$ , which appears after the  $\langle \delta T_f \rangle$  peak in Fig. 2.4(B), corresponds to the cross-over point  $t_x$  in the normal phase conditions, and its magnitude is less than that of  $t_x$ .

### 2.2.5 Modulation during heating

When an amorphous solid is heated at a certain rate, its structural relaxation time changes in two ways, (i) it increases with  $t$  as the sample approaches its equilibrium state, and this increase occurs at a higher rate when  $T$  increases, and (ii) it decreases as  $T$  increases. A combination of these effects is expressed by Eq. (2.28), with  $0 < x \leq 1$ . For this purpose,

the quantity determined experimentally is the specific heat,  $C_p$ . Since  $T_f$  is directly related to the enthalpy or energy, its derivative with respect to  $T$  yields normalized  $C_p$  [Moynihan *et. al.* (1976), Pascheto *et. al.* (1994), Hodge (1994), (1995) and (1997)]. The calculations however yield  $C_p$  values normalized by the difference between the  $C_p$  at the two extreme temperatures of the glass softening range. The normalized  $C_p$  is then compared against the normalized value of the measured  $C_p$ . Henceforth, we drop the notation for normalized, and write  $C_{p,n}$  for the  $n$ th step of calculations,

$$C_{p,n} = \frac{dT_f}{dT} = \frac{T_{f,n} - T_{f,n-1}}{T_n - T_{n-1}} \quad (2.29)$$

For simulating the  $C_p$  values during the heating of a glass, we use  $\ln A = -355.7$ ,  $\Delta h^* = 1147.4 \text{ kJ mol}^{-1}$ , which is the same values as used for a typical polymer, polymethyl methacrylate [Hodge (1994), (1995) and (1997)]. We also use several values of  $\beta$  and  $x$ . The simulation was begun by cooling the equilibrium liquid from 400 K to  $T_0$  of 375 K at  $20 \text{ K min}^{-1}$ , using the computational steps of 0.2 K in  $T$ . The sample in the simulation was kept at 375 K for 1 h in the unmodulated condition and heated to 400 K at  $4 \text{ K min}^{-1}$  in the unmodulated condition using the computational  $T$ -steps of 1/64 K. The procedure was repeated for cooling to 375 K, and the sample was then kept at 375 K for 1 h with  $T$ -modulation using  $\Delta T = 0.637 \text{ K}$ , and  $\omega_0 = 2\pi/60 \text{ rad s}^{-1}$ . It was finally heated from 375 K to 400 K at  $4 \text{ K min}^{-1}$  with the same  $T$ -modulation as at 375 K and using the computational steps of 1/64 K. The calculations were performed for four pairs of  $\beta$  and  $x$  values, (i)  $\beta = 1.0$ ,  $x = 1$ , (ii)  $\beta = 0.5$ ,  $x = 1$ , (iii)  $\beta = 1$ ,  $x = 0.5$ , and (iv)  $\beta = 0.5$ ,  $x = 0.5$ . For each pair, this yields two curves against the temperature, one curve for  $T_{f,\text{unmod}}$  and

the second for  $\langle T_{f,mod} \rangle$  (calculated by averaging  $T_{f,mod}$  using Eq. (2.4)), which are shown in Fig. 2.5(A). The difference,  $\delta T_f (= \langle T_{f,mod} \rangle - T_{f,unmod})$ , between each set of the two curves in Fig. 2.5(A) is plotted against  $T$  in Fig. 2.5(B).

Both  $\langle C_{p, mod} \rangle$  and  $C_{p, unmod}$  were calculated by differentiating the values of  $\langle T_{f,mod} \rangle$  and  $T_{f,unmod}$ , provided in the curves of Fig. 2.5(A) with respect to  $T$ . These are plotted against  $T$  in Fig. 2.6(A) and the difference,  $\delta C_p (= C_{p, unmod} - \langle C_{p, mod} \rangle)$  is plotted against  $T$  in Fig. 2.6(B). To examine the effect of the phase angle at the start of the modulation,  $\langle C_{p, mod} \rangle$  and  $\delta C_p$  were calculated for the condition of modulation with a  $\pi$ -phase shift, or equivalently  $\omega_0 = -2\pi/60 \text{ rad s}^{-1}$ . These values are plotted in thick solid line in Figs. 2.6(A) and 2.6(B). To examine the effects of increase in the annealing period, the calculations were repeated with the same parameters, and the annealing period was increased from 1 h to 4 h. The plots of the calculated  $C_{p, unmod}$  and  $\langle C_{p, mod} \rangle$  and  $\delta C_p$  are shown in Figs. 2.7(A) and 2.7(B). Both  $C_{p, unmod}$  and  $\langle C_{p, mod} \rangle$  also change with change in the cooling rate, heating rate, and the magnitudes of  $\ln A$  and  $\Delta h^*$ , and  $\langle C_{p, mod} \rangle$  further varies with the modulation frequency and  $\Delta T$ . Clearly, there would be virtually an infinite number of shapes of the curves that may be generated to show these variations. But,  $\ln A$ ,  $\Delta h^*$ ,  $\beta$  and  $x$  are unique for a given liquid and glass, and when the cooling rate of the liquid and the amplitude of  $T$ -modulation are kept fixed, effects of a variation of only two quantities need be shown here, (i) variation of the heating rate and (ii) variation of the modulation frequency. For that purpose, we recalculate  $C_{p, unmod}$  and  $\langle C_{p, mod} \rangle$  by using the same parameters as used for curves in Fig. 2.6(A), but decrease the heating rate from  $4 \text{ K min}^{-1}$  to  $1 \text{ K min}^{-1}$ . The curves obtained are shown in Fig. 2.8(A) and 2.8(B). In the

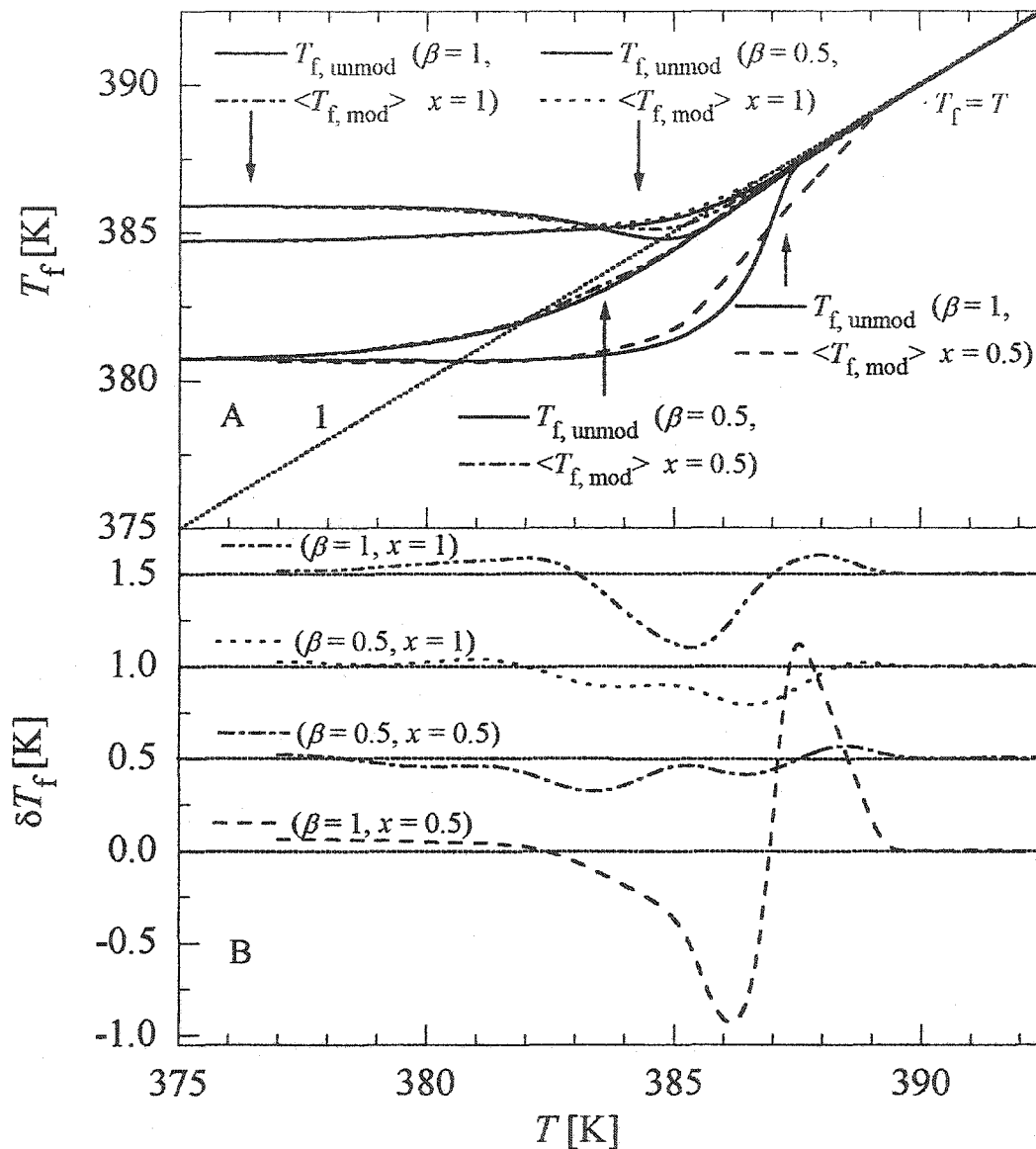


Fig. 2.5. (A). The plots of  $T_f$ , for the  $T$ -modulated and unmodulated conditions against the temperature during heating of the glass sample at  $4 \text{ K min}^{-1}$ . (B). The plots of the difference,  $\delta T_f$ , between  $\langle T_{f, \text{mod}} \rangle$  and  $T_{f, \text{unmod}}$  against the temperature. Values of  $\beta$  and  $x$  are as noted. The line labeled 1 is the equilibrium line when  $T = T_f$ . Other parameters used for the calculation are given in the text. The horizontal lines are at zero values in each case, with the same vertical scale. The simulation was done for the sine wave function.

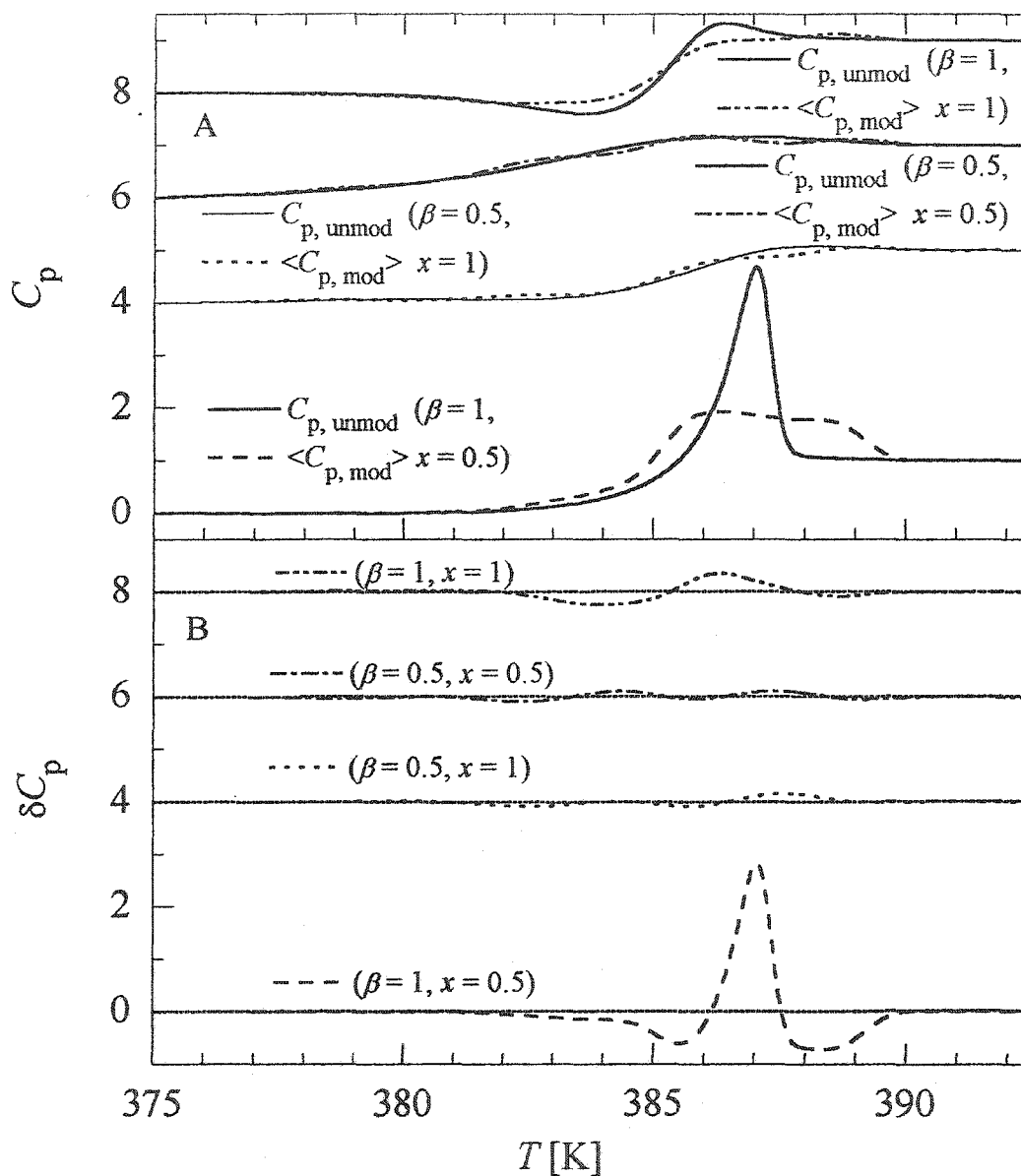


Fig. 2.6. (A). The plots of  $C_p$  for the  $T$ -modulated and unmodulated conditions against the  $T$  during heating of the glass sample at  $4 \text{ K min}^{-1}$ . (B). The plots of the difference,  $\delta C_p$  between the  $C_{p, \text{unmod}}$  and  $\langle C_{p, \text{mod}} \rangle$ . Values of  $\beta$  and  $x$  are as noted. The thick solid lines are the plots of  $\langle C_{p, \text{mod}} \rangle$  and  $\delta C_p$  for  $T$ -modulation in which the phase had been  $\pi$ -shifted at the beginning. Other parameters used for the calculation are given in the text. The horizontal lines are at zero values in each case, with the same vertical scale.

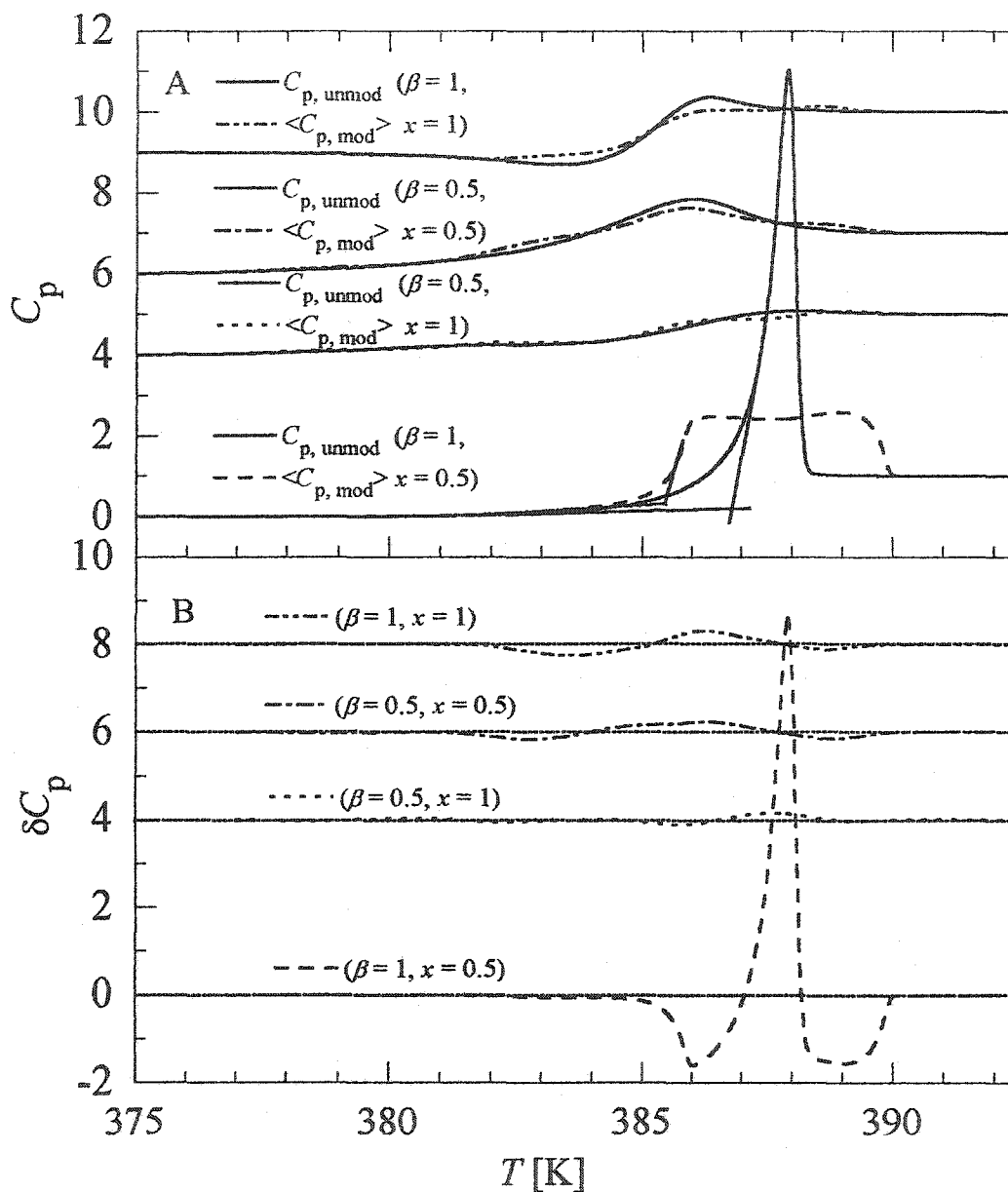


Fig. 2.7. (A). The plots of  $C_p$  for the  $T$ -modulated and unmodulated conditions against the temperature during heating of the glass sample at  $4 \text{ K min}^{-1}$ . (B). The plots of the difference,  $\delta C_p$  between the  $C_{p, \text{unmod}}$  and  $\langle C_{p, \text{mod}} \rangle$ . Values of  $\beta$  and  $x$  are as noted. Other parameters used are the same as for Fig. 2.5, except that the isothermal structural relaxation time is increased to 4 h. The horizontal lines are at zero values in each case, with the same vertical scale.

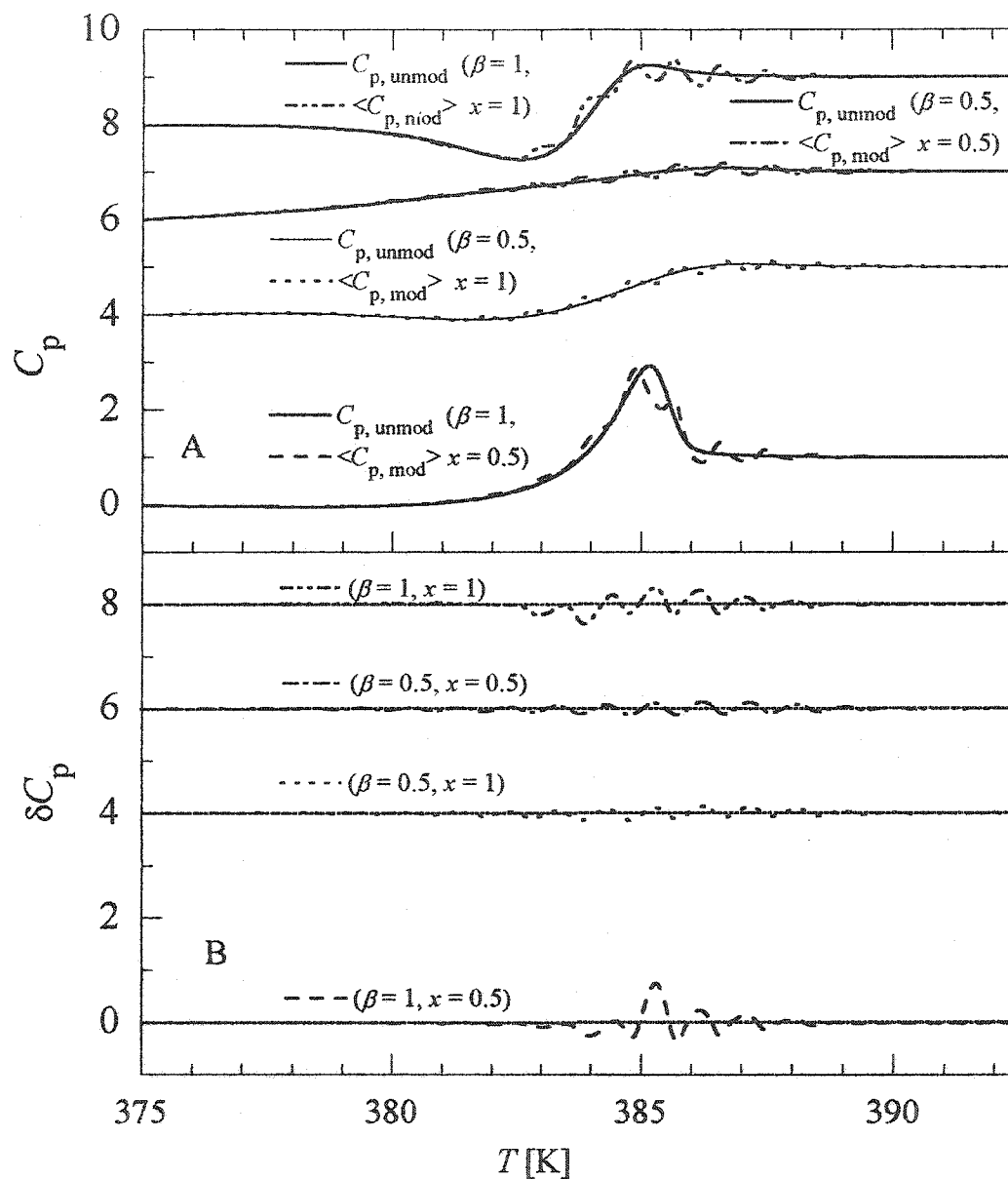


Fig. 2.8. (A). The plots of  $C_p$  for the  $T$ -modulated and unmodulated conditions against the temperature during heating of the glass sample at  $1 \text{ K min}^{-1}$ . (B). The plots of the difference,  $\delta C_p$  between the  $C_{p, \text{unmod}}$  and  $\langle C_{p, \text{mod}} \rangle$ . Values of  $\beta$  and  $x$  are as noted. Other parameters used are the same as for Fig. 2.5, except that the heating rate is decreased to  $1 \text{ K min}^{-1}$ . The horizontal lines are at zero values in each case, with the same vertical scale.

second calculation, we increase  $\omega_0$  from  $2\pi/60$  rad  $s^{-1}$  to  $8\pi/60$  rad  $s^{-1}$  and obtain the curves shown in Figs. 2.9(A) and 2.9(B).

### 2.2.6 Square-wave modulation

Finally, we determine the effect of the change in the shape of the modulation curve on  $T_f$ ,  $\delta T_f$ ,  $C_{p, \text{unmod}}$  and  $\langle C_{p, \text{mod}} \rangle$ . For that purpose the  $T$ -modulation was changed from a sinusoidal wave to a square wave of the same frequency while keeping other conditions the same as in Figs. 2.5 and 2.6, and the quantities of  $T_{f, \text{unmod}}$ ,  $\langle T_{f, \text{mod}} \rangle$  and  $\delta T_f$ ,  $C_{p, \text{unmod}}$ ,  $\langle C_{p, \text{mod}} \rangle$  and  $\delta C_p$  were recalculated. These values are plotted against the temperature in Figs. 2.10 and 2.11. (Note that Fig. 2.10 was obtained by the square wave modulation and Fig. 2.5 by the sine wave modulation, the plots in these two figures differ in details, although they may look similar.).

## 2.3 Discussion

First, we examine whether the results of  $T$ -modulation described above are consistent with the precepts of thermodynamic. To do so, we use the preceding method to determine the net heat evolved for both the modulated and the unmodulated conditions. This was done for structural relaxation at a fixed temperature and thereafter for structural relaxation during the heating to a temperature above the glass softening range. It is required by the first law of thermodynamics that the  $C_p dT$  integral between two temperatures, one for the glass and second for the equilibrium liquid, be identical, irrespective of the values of  $\Delta T$ ,  $\omega_0$ ,  $\beta$ ,  $x$ ,  $\ln A$ ,  $\Delta h^*$ , cooling rate or heating rates, and the

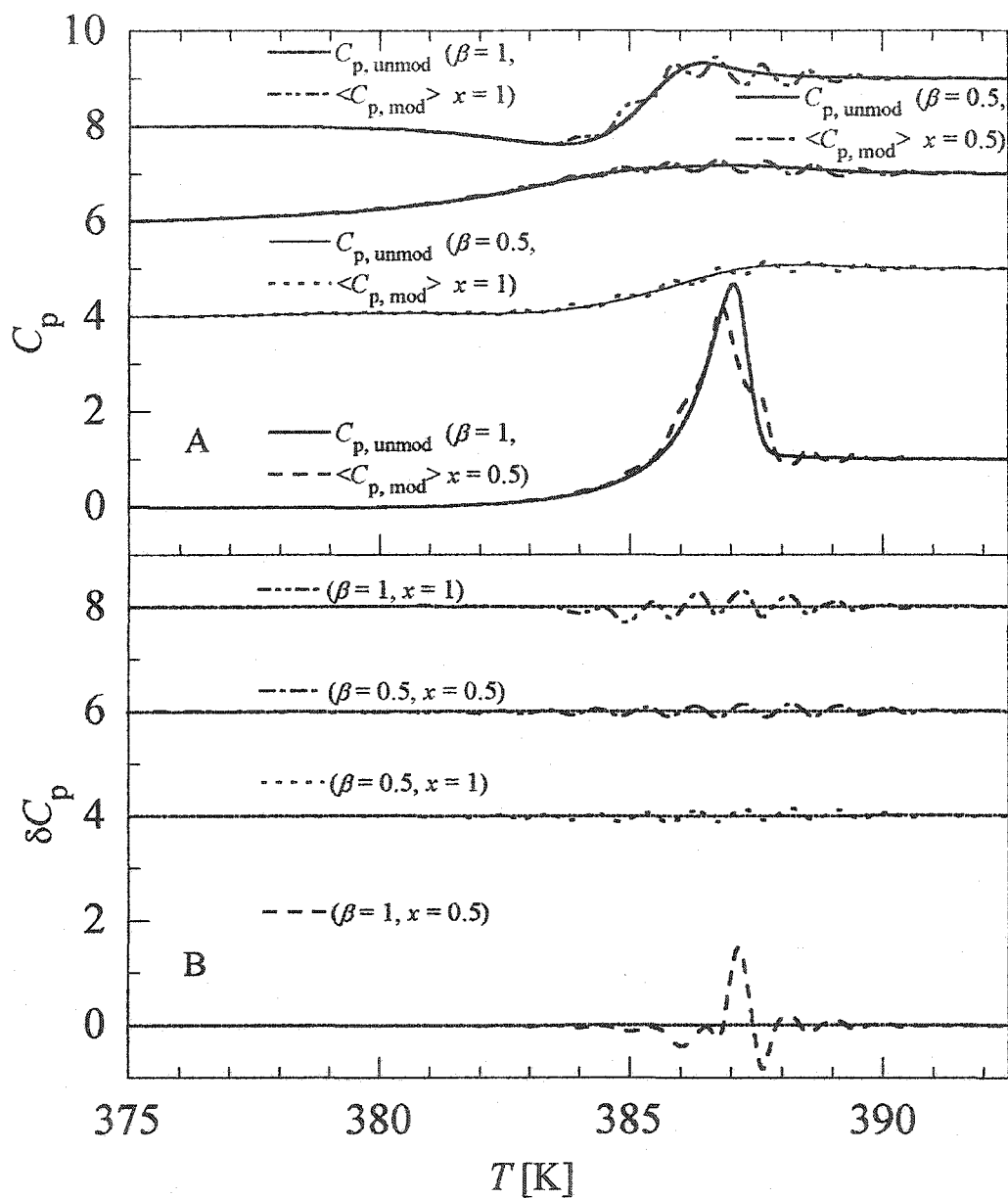


Fig. 2.9. (A). The plots of  $C_p$  for the  $T$ -modulated and unmodulated conditions against  $T$  during heating of the glass sample at  $4 \text{ K min}^{-1}$ . (B). The plots of the difference,  $\delta C_p$  between the  $C_{p, \text{unmod}}$  and  $\langle C_{p, \text{mod}} \rangle$ . Values of  $\beta$  and  $x$  are as noted. Other parameters used are the same as for Fig. 2.5, except that the frequency of sinusoidal modulation has been increased to  $8\pi/60 \text{ rad s}^{-1}$ . The horizontal lines are at zero values in each case, with the same vertical scale.

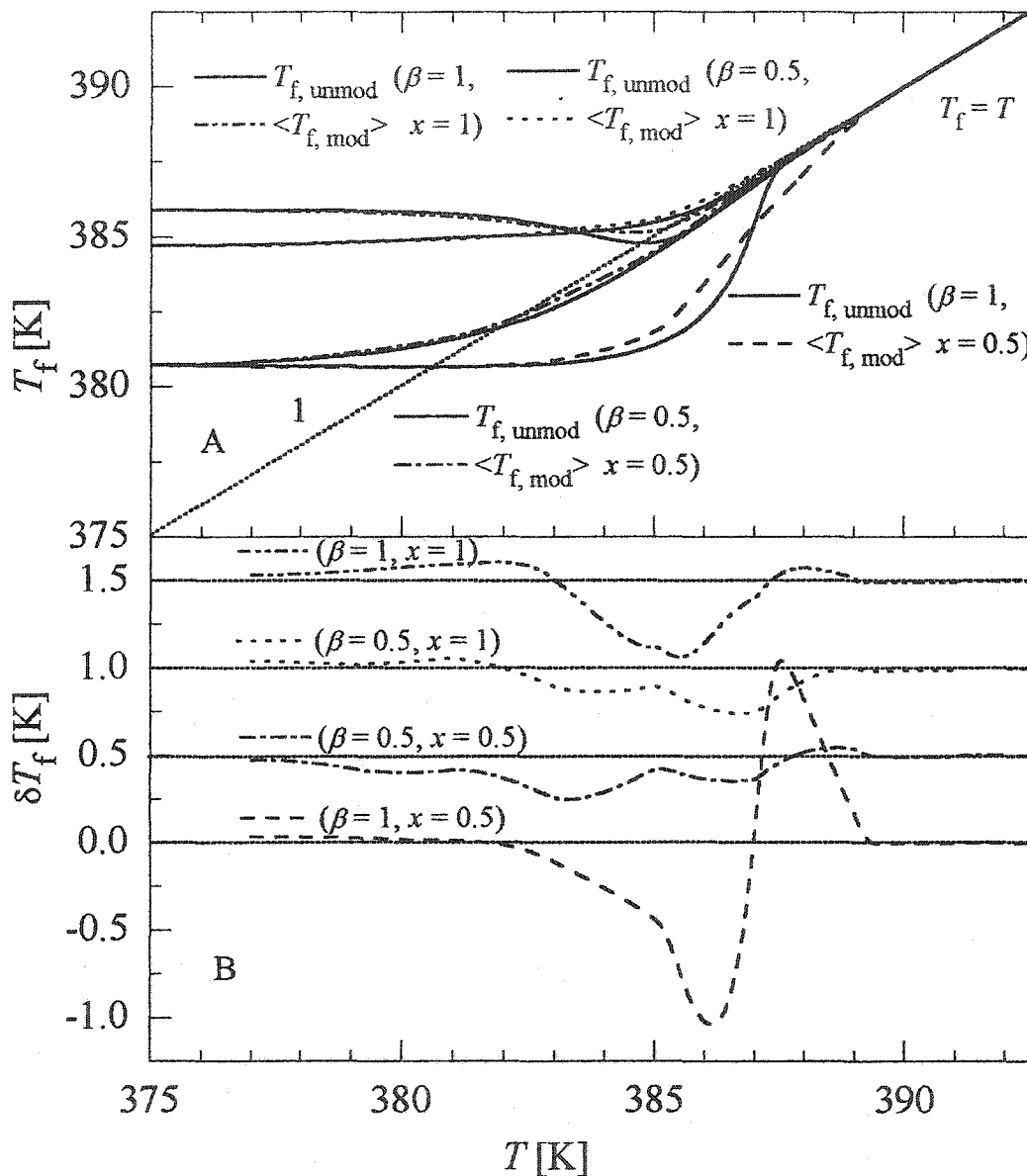


Fig. 2.10. (A). The plots of  $T_f$  for the  $T$ -modulated and unmodulated conditions against  $T$  during heating of the glass sample at  $4 \text{ K min}^{-1}$ . The line labeled 1 is the equilibrium line for  $T_f = T$ . (B). The plots of the difference,  $\delta T_f$ , between  $\langle T_{f, \text{mod}} \rangle$  and  $T_{f, \text{unmod}}$  against the temperature. Values of  $\beta$  and  $x$  are as noted. Other parameters used for the calculation are given as for Fig. 2.5, except that the modulation is according to a *square-wave*. The horizontal lines are at zero values in each case, with the same vertical scale.

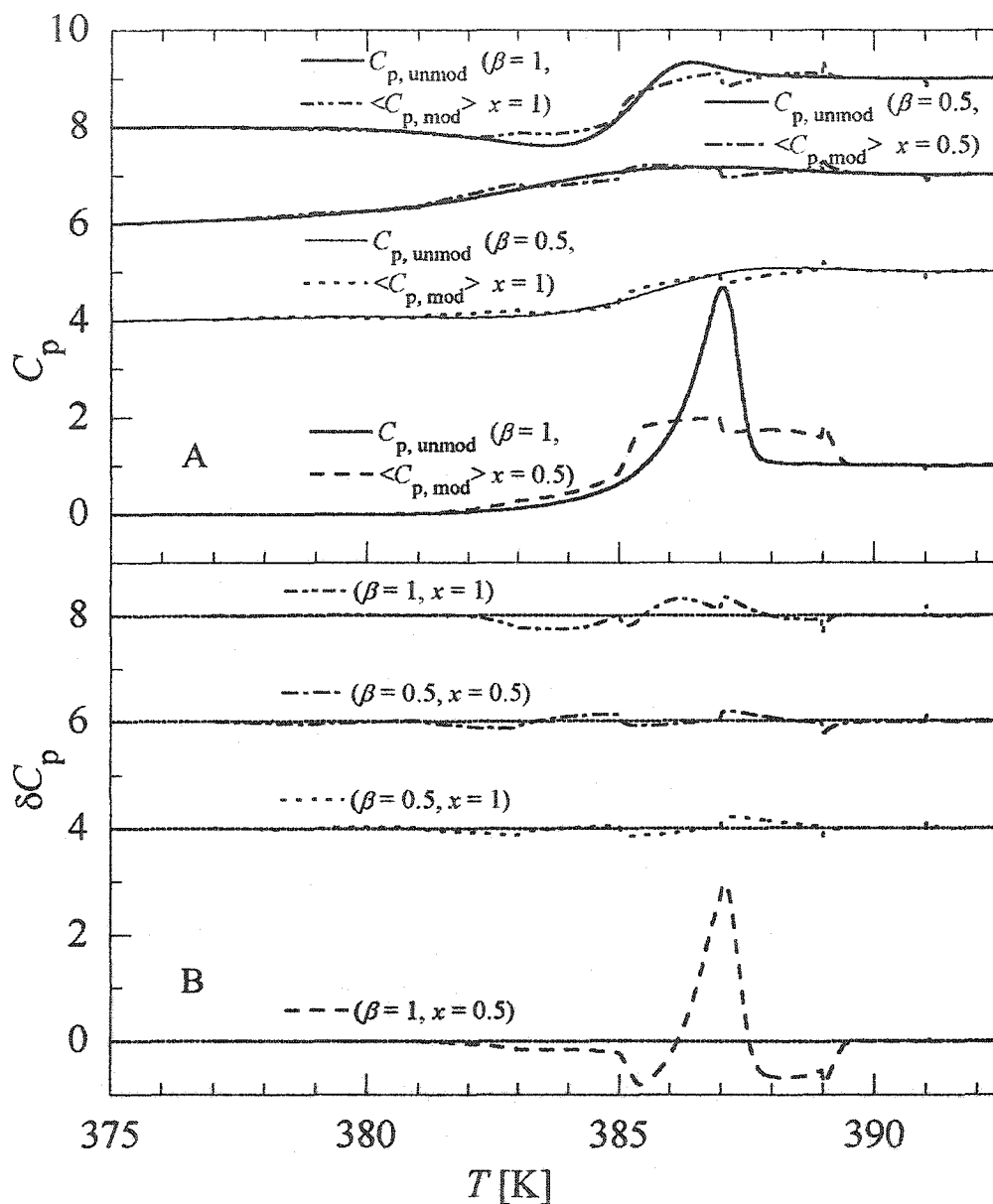


Fig. 2.11. (A). The plots of  $C_p$  for the  $T$ -modulated and unmodulated conditions against  $T$  during heating of the glass sample at  $4 \text{ K min}^{-1}$ . (B). The plots of the difference,  $\delta C_p$  between the  $C_{p, \text{unmod}}$  and  $\langle C_{p, \text{mod}} \rangle$ . Values of  $\beta$  and  $x$  are as noted. Other parameters used are the same as for Fig. 2.5, except that the  $T$ -modulation is in the form of a square wave and not a sine-wave. The horizontal lines are at zero values in each case, with the same vertical scale.

time for isothermal structural relaxation. This was tested by numerical integration of the  $C_p$  against  $T$  plots shown in Figs. 2.6 - 2.11, and several more sets of data not shown here. The difference between the  $C_p dT$  integrals for the various conditions was found to be less than 0.04%, which is due to the errors in the averaging procedures and the method of integration (multiple Simpson rule) used here. Therefore, we conclude that the calculations given here are thermodynamically consistent internally. As most of the physical aspects have already been described here, we only discuss the modifications in the physical properties resulting from  $T$ -modulation in the following six sections.

### 2.3.1 Structural relaxation's modification on the net enthalpy and entropy

The ultimate  $T_f$  for the unmodulated condition is the temperature at which the glass is isothermally kept. The first effect of modulation during isothermal structural relaxation is that the effective  $T_f$  is raised above the isothermal or mean temperature,  $T_0$ , after the cross-over time,  $t_x$ , in Figs. 2.2-2.4, has been reached. Since enthalpy, entropy and volume decrease as  $T_f$  decreases and the elastic modulus, refractive index, and phonon frequencies increase, this means that the first set of properties would be higher for the modulated condition and the second set of properties lower. This would appear as a lesser than expected loss in the magnitude of the first set of properties and gain in the second set of properties in a structural relaxation experiment. The discrepancy in the properties would correspond to an increase in the temperature by  $\delta T_f$ . As  $\delta T_f$  itself approaches the magnitude of  $\Delta T$  as  $t \rightarrow \infty$ , the discrepancy observed ultimately would correspond to the difference between the magnitudes of the property at  $T_0$  and at  $T_0 + T_{\max}$ . This appears to be a natural consequence of a non-linear change in the property with change in  $T$ .

### 2.3.2 The time and temperature dependent heat capacity and $T_g$

Figures 2.6(A) - 2.10(A) clearly show that extra features in  $C_p$  appear when  $T$  is modulated during the heating of a glass. When  $\beta = 1$ , and  $x = 1$ , the modulation produce a second sigmoid-like feature before the equilibrium state of the liquid is reached, as is seen in Fig. 2.6(A). This feature persists even after the glass has been structurally relaxed isothermally for a longer period of time prior to the heating (see Fig. 2.7(A)). The decrease in the heating rate from 4 to 1 K min<sup>-1</sup> tends to reduce this feature, as seen in Fig. 2.8(A), as does an increase in  $\omega_0$  in Fig. 2.9(A), where the shape of the curve is not smooth but is defined by wave whose further averaging would reveal the curve. A decrease in the magnitude of either  $\beta$  or  $x$  or both, from unity, changes the shape of the feature but more for the modulated condition than for the unmodulated. The maximum change is found when  $x$  is reduced and  $\beta$  is kept fixed. This is seen in the plot calculated for the case,  $\beta = 1$ ,  $x = 0.5$  and seen in Figs. 2.6(A) and 2.7(A). Here  $T$ -modulation produces the appearance of a second peak at high temperatures, which is only partially merged with the initial sigmoid-shape rise. Its magnitude decreases with decrease in the heating rate and with increase in  $\omega_0$ , as seen in Figs. 2.8(A) and 2.9(A), respectively, where the curves apparently require further averaging for smoothing.

The glass softening temperature,  $T_g$ , is usually determined from the intersection temperature of two straight lines, (i) the tangent to the point of inflection on the sigmoid-shape endotherm, and (ii) the extrapolated line from  $C_p$  of the glass [Moynihan *et. al.* (1976), Kovacs *et. al.* (1977), Ngai, *et. al.* (1986), Scherer (1986), Donth (1992),

Mastuoka (1992), Hodge (1994), (1995) and (1997)]. As the endothermic features change on  $T$ -modulation, it is clear that  $T_g$  determined from the  $T$ -modulated experiment would be different from that determined from the unmodulated experiment. This is shown by the lines drawn on the curve for  $\beta = 1$ ,  $x = 0.5$ , in Fig. 2.7(A), and which yields a lower  $T_g$  for the  $T$ -modulated heating than for unmodulated heating. More significantly, the extra features observed on  $T$ -modulation may lead to a misinterpretation of the dynamics of the glass and supercooled liquids.

### 2.3.3 The effects of square-wave modulation

When  $T$ -modulation is done by using a square-wave instead of a sine-wave, the effects observed become more prominent, because the glass stays at its  $T_{\max}$  and  $T_{\min}$  for a longer duration than it does in the sinusoidal modulation. Also, instead of the smooth curves which is observed for sinusoidal modulation for the same heating rate and  $\omega_0$ , abrupt changes in  $C_p$  appear at the time (and temperature during heating at a fixed rate) when  $T$  in the square-wave suddenly increases or suddenly decreases. So, although the features become less smooth, the increase in the magnitude of the effect clearly shows that the modulation effects are substantial.

### 2.3.4 The effects of the phase at the start-stage of modulation

When the phase angle at the start of the sinusoidal modulation was shifted by  $\pi$ , the extra feature of  $\langle C_{p, \text{mod}} \rangle$  caused by modulation showed a shift for all the four cases, as seen in Fig. 2.6(A). It is evident that in comparison with the results for the condition when the phase angle is zero at the start of the modulation, the  $\pi$ -shift in the phase has a lesser

effect when  $\beta = 0.5$ , and  $x$  is either 0.5 or 1. The effect is more when  $\beta = 1$  and  $x$  is either 0.5 or 1. The difference,  $\delta C_p$ , also shifts and becomes opposite in sign to that of zero phase at the start for the condition when  $\beta = 0.5$  and  $x$  is either 0.5 or 1. It shifts by a relatively small amount when  $\beta = 1$  and  $x$  is either 0.5 or 1. These conditions are more evident in the region where the effects of glass softening overwhelm the modulation effects when  $\beta = 1$  and  $x$  is either 0.5 or 1. So the phase of the sinusoidal oscillation for the modulation also determines the shape of the  $C_p$  against  $T$  curve. When  $\beta = 1$  and  $x = 1$ ,  $\langle C_{p, \text{mod}} \rangle$  with zero phase at the beginning of modulation has qualitatively similar features to the unmodulated condition. This similarity is lost when the phase is  $\pi$ -shifted. This may be useful in determining the optimum modulation results when changes of  $\Delta T$  and  $\omega_0$  are undesirable.

### 2.3.5 The relaxation time evolution with temperature

We now consider how the  $t$ -, and  $T$ -dependent structural relaxation time,  $\tau$ , evolves when the glass is heated at a fixed rate. To illustrate, we select the conditions used for the simulations described already in Figs. 2.5 and 2.6, and the same four pairs of  $\beta$  and  $x$ . The calculated  $\tau$  for the  $T$ -modulated and unmodulated conditions are plotted against  $T$  in Fig. 2.12(A), and the ratio,  $(\delta \tau / \tau_{\text{unmod}})$ , is plotted in Fig. 2.12(B). The values of  $\tau$  differ most for the unmodulated and modulated pair, when  $\beta = 1$ ,  $x = 0.5$  and less when  $0 < \beta < 1$ ,  $x = 1$  or  $\beta = 0.5$ ,  $x = 0.5$ . The difference may reach values as high as a factor of 7.2 in the glass softening region.

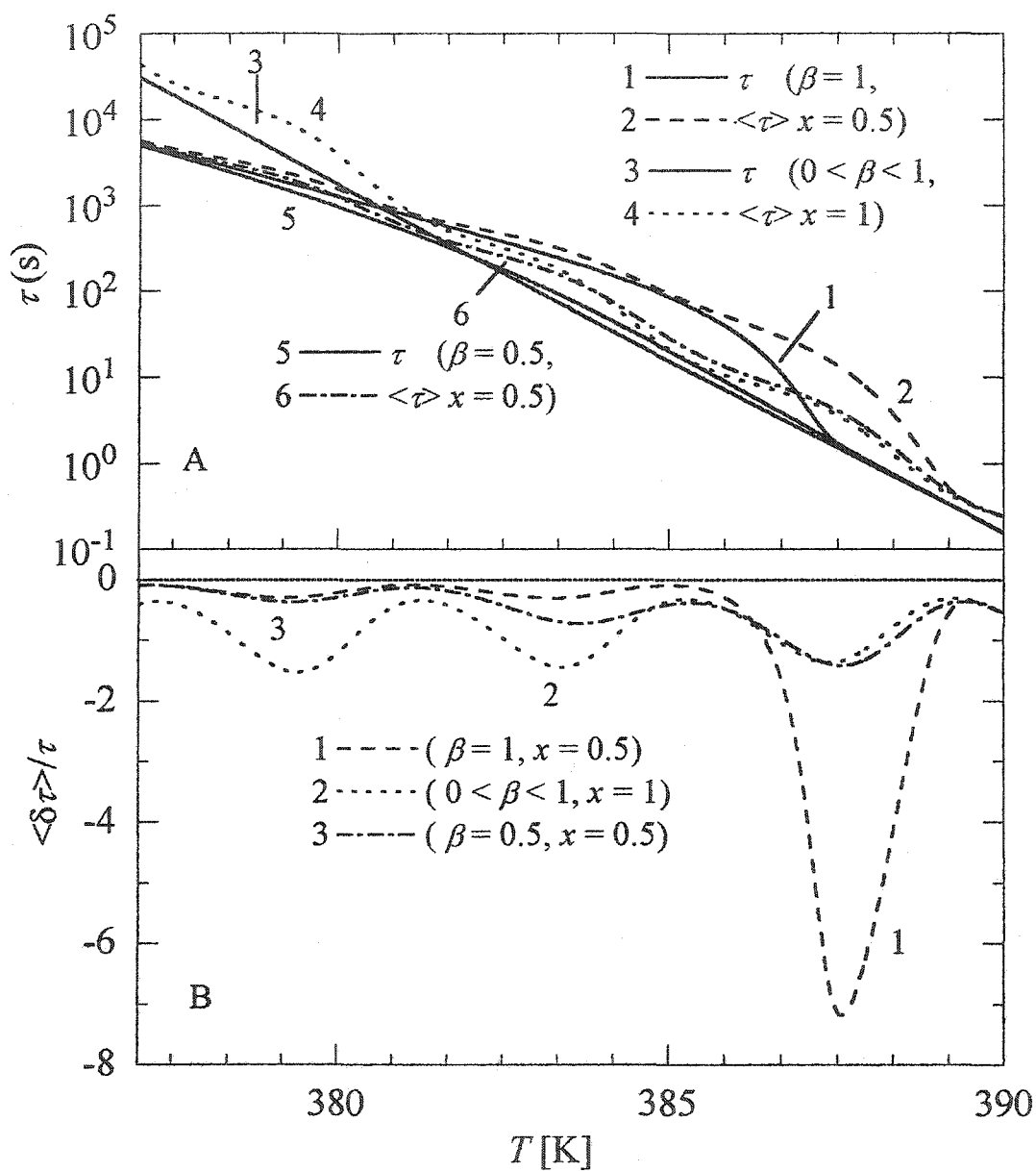


Fig. 2.12. (A). The plots of  $\tau$  against  $T$  for the  $T$ -modulated and unmodulated conditions during heating of the glass sample at  $4 \text{ K min}^{-1}$ . (B). The plots of the difference,  $\delta\tau$  divided by  $\tau_{\text{unmod}}$ , against  $T$ . Values of  $\beta$  and  $x$  are as noted. The parameters used are the same as for Fig. 2.5, and are given in the text.

### 2.3.6 The linear-response, and the physical aspects of the simulations

There is currently an ongoing discussion on the limitations of the linear response theory's [Landau and Lifshitz (1980)] application for relaxation phenomenon. This is described in the papers of Jeong and Moon (1995), Schawe and Theobald (1998), Baur and Wunderlich (1998), and Simon and McKenna (1997) and (2000), particularly for those processes that lead to configurational freezing on vitrification of liquids. These limitations are of course as valid for dielectric and mechanical responses as they are for thermal responses. In such cases, the magnitude of the sinusoidal variation of the electrical field, strain and temperature is kept small enough to minimize the non-linear effects, but they do not entirely vanish. In particular these effects in a calorimetric experiment significantly increase two important properties, (i) the amplitude of the heat capacity change at  $T_g$ , and (ii) the fraction of higher harmonics in the periodic heat flow.

It is to be noted that [Schawe and Theobald (1998)] have found that the upper limit for the modulation amplitude of 1.5 K is within the linear response for the dynamic heat capacity measurements of polystyrene. The amplitude of 1.5 K used in the simulation for isothermal annealing here is the same. The amplitude of 0.637 K used in the simulation here during heating is less than half of that. Therefore, effects from the non-linear response in  $\Delta T$  have been ignored in our calculations, and this is consistent with the recommendation for modulated scanning calorimetry that  $\Delta T$  be equal to the ratio of the heating rate to the modulation period, which is 0.637 K, as used here. Moreover, the experimental accuracy available with the commercial equipment is unable to detect non-linear response up to  $\Delta T < 2$  K, which is  $\sim 1.4$  K more than the  $\Delta T$  used

here. The advantages of pressure modulation are yet to be recognized, but it seems that the non-linear effects in sinusoidal pressure experiments would be considerably less, and more tractable than in the temperature modulation.

Finally we discuss the physical implications of the results. It is evident from our discussion that, (i) changes in the modulation period and modulation amplitude have a large effect on the apparent heat capacity and the calorimetric signal, and (ii) the magnitude of the molecular dynamics-controlling properties calculated from such experiments may be used to test the theories of the liquid's molecular dynamics itself. Such experimental investigations have not been possible so far, although the effects of modulation on chemical reaction processes have been tested [Johari *et. al.* (1999)]. Also, since a pressure-increase has an opposite effect on the molecular dynamic properties of a liquid and glass than the temperature-increase, the combined modulation of the two would provide us a way of maintaining conditions at which the molecular relaxation time would not change in a modulation cycle, thus revealing the change in the static properties corresponding to the equilibrium and the molecular relaxed states. It is hoped that this study would stimulate interests in new experiments in the currently wide-spread use of modulated calorimetry and ultrasonics.

## 2.4 Summary

Mathematical simulation and numerical computation of the temperature modulation effects on the structure relaxation process during structural relaxation and heating show that the modulation has substantial effects on the observed enthalpy decrease and heat

capacity change with time and temperature. The effect of pressure modulation, as in an ultrasonic experiment, is similar. The shape of the heat capacity against temperature curve and the glass softening endotherm are remarkably changed by the modulation, as is the shape of the enthalpy curve with time. This is the consequence of the nonlinear response of a material's diffusion or structural relaxation rate on the temperature, and not necessarily from the stretched-exponential and non-linear relaxation characteristics, whose changes have been used for describing the structural relaxation of a glass. The latter two features add to the changes already caused by the sinusoidal modulation. These effects are important in the interpretation of the data obtained by the currently developing techniques of sinusoidal temperature-modulation and in the use of ultrasonic waves in studying the spinodal decomposition.

The effect is fundamental to all processes in which temperature, pressure or concentration may be sinusoidally modulated. Therefore, it has significance for our current efforts in incorporating temperature-modulation in calorimetry [Schawe (1995), Alig (1997), Beiner *et. al.* (1998), Kahle *et. al.* (1999)], and studying the frequency-dependent specific heat [Birge and Nagel (1988), Dixon and Nagel (1988), Birge *et. al.* (1986), Brittmann *et. al.* (1994)] and thermal conductivity [Brittmann *et. al.* (1994)]. In addition to its use in monitoring irreversible processes by using ultrasonic waves and in studying the spinodal decomposition in a liquid [Brittmann *et. al.* (1994)], the temperature- and pressure- modulation may provide significance information on the second-order phase transformation, particularly at the critical point of a liquid [Mayer *et. al.* (1997), Brittmann *et. al.* (1981)], for which formalisms are available (see citations in

Brittmann *et. al.* (1984)]) in terms of dynamic scaling [Mayer *et. al.* (1997), Bhattacharya and Ferrel (1981)].

## Chapter 3

# Lattice Statistics and Thermodynamics during Linear Chain Polymerization and of the Polymer

### 3.1 Introduction

There are several phenomenological theories for vitrification of liquids. These theories have also been used for the vitrification of polymer melts. Amongst these the free volume theory [Turnbull and Cohen (1961) and (1971), Grest and Cohen (1981)] relates the viscosity of a liquid to its free volume and the entropy theory [Adam and Gibbs (1965)] relates the viscosity to the configurational entropy. For the vitrification of polymer melts a general form of statistical thermodynamic treatment has also been used. This treatment, is based on the description of the partition function originally given by Mayer and Göppert-Mayer (1940), and the quasi-lattice model [Meyer (1939)], and on a mean-field approach provided by Bragg and Williams (1934).

In this mean-field approach, it had been considered that there is, (i) a multiplicity of possible configurations within a given volume and internal energy of a system, and, (ii) molecular interactions are limited only to the near-neighbors. The quasi lattice model of Meyer (1939) combined with the mean field approximation is referred to as the lattice-

hole model, and this model has been used for describing polymers chains statistics by Flory (1941), (1942) and (1956). Flory had originally developed this model for a polymer solution (1941, 1942). The mean field approximation was later modified by Huggins (1942). The lattice-hole model for a polymer solution which uses the Huggins mean field approximation has been generally called the Flory-Huggins model and the mean-field approximation is generally referred to as the Flory-Huggins approximation.

Flory (1956) had calculated the Gibbs free energy of a polymer dissolved in a solvent for a special case of polymer chains of equal length (mono-dispersed case) and varying covalent bond stiffness distributed on the polymer chains. Based on Flory's model, Gibbs and DiMarzio (1958) and DiMarzio and Gibbs (1958, 1959) extended the calculation to pure polymers in order to determine the variation of the configurational entropy,  $S_{\text{conf}}$ , of a polymer with temperature, i.e., the decrease in  $S_{\text{conf}}$  on cooling a polymer melt. Both the Flory's original formalism and the subsequent calculations by Gibbs and DiMarzio (1958) for  $S_{\text{conf}}$ , have been critically examined on fundamental grounds by Gujrati (1980), Gujrati and Goldstein (1981), Milchev (1983), and Wittmann (1991). Also, Flory's lattice hole model has been extended and modified several times by Gutzow (1962), Milchev and Gutzow (1982), Gutzow and Schmelzer (1995), and Petroff *et. al.* (1996). Wittmann (1991) has discussed this subject and distinguished these models on the basis of his view of the mean field approximations. In a monograph on the vitreous state, Gutzow and Schmelzer (1995) have reviewed the history of the lattice-hole models. Here we first consider the development of these models and their limitations and weaknesses, and identify the need for a better mean field approximation. We finally

propose a new mean-field approximation and use it for developing thermodynamics of the irreversible growth of a polymer chain as occurs during the polymerization process. These are provided in the subsequent section. In a section thereafter we would consider its application to the process of linear-chain polymerization. In the subsequent Chapter we will use our mean field approximation for quasi one-dimensional chains in an orientationally-disordered crystal. This study has been published in a paper, J. Wang and G. P. Johari, *J. Chem. Phys.*, 116, 2310(2002).

### 3.2 The Lattice Hole Model and the Flory-Huggins Approximations

Flory's original model (1941, 1942, 1956) had been developed for semi-flexible polymer chains of identical lengths dispersed in a solvent. In this model, each lattice site was occupied by either one repeat unit (monomer) of the polymer or by one molecule of the solvent. The co-ordination number of the repeat unit,  $z$ , was kept the same as that of each site on the lattice, and this number  $z$  was defined as the connectivity of the sites on the lattice. Thus the quantity  $z$  is 4 for both a two dimensional square lattice and three dimensional tetrahedral lattice, 6 for a three dimensional simple cubic lattice, 8 for a bcc lattice, and 12 for an fcc lattice and an hcp lattice. The covalent bonds between two repeat units of a polymer chain were seen to be either flexible or non-flexible (or rigid). The overall covalent bond flexibility,  $f$ , of the polymer system was defined as the ratio of the total number of flexible covalent bonds to the total number of covalent bonds.

The exact mathematical solution to polymer chain statistics requires the use of graph theory for determining the number of configurations obtained by random, self-avoiding walks (SAW). Kasteleyn (1962, 1967) has provided an exact solution of SAW

problem for the simplest case of a closed-packed collection of dimers without monomers, holes or flexible bonds. For a slightly less simple case, it is generally found that mathematical complexity becomes too high to allow an explicit solution [Kasteleyn (1962, 1967)]. Because of the lack of explicit solution of SAW models, mean field approximations have continued to be used.

Flory showed that when the flexibility of a polymer chain  $f$  exceeds a critical value of  $\approx 0.63$  ( $= 1 - e^{-1}$ ), a disorder-order transition occurs in the state of a polymer. In a later treatment of the Flory model (1956), Gibbs and DiMarzio (1958) interpreted the sites occupied by the solvent molecules as empty sites or holes, and therefore modified the expressions for an effective coordination number,  $z$ . Unlike Flory (1956), Gibbs and DiMarzio (1958) incorporated a temperature-dependent population of holes in their model for polymer chain statistics. The hole population was determined by the strength of interaction between the polymer's repeat unit and the hole. The resulting model thus had a feature which allowed for the generally known finite compressibility of a polymer melt, and a decrease in its compressibility with decreasing temperature. Gibbs and DiMarzio (1958) found that the value of  $S_{\text{conf}}$  thus calculated for a polymer system containing chains and holes decreased and appeared to become negative below a certain temperature. This was seen by them as a confirmation of the Kauzmann extrapolation of the entropy of molecular liquids towards the entropy of a crystal [Kauzmann (1948)]. How this  $S_{\text{conf}}$  would vary with temperature if the free energy calculations are redone in the Flory-Huggins approximations and how modifying some of the concepts of embedding the repeat units on lattice sites would change these calculations has been

already reported by others [Gutzow (1962), Gujrati (1980), Gujrati and Goldstein (1981), Milchev and Gutzow (1982), Milchev (1983), Wittmann (1991), Petroff *et. al.* (1996)] and in a monograph by Gutzow and Schmelzer (1995). These papers and the monograph may be consulted for details.

Gibbs and DiMarzio (1958) deduced that  $S_{\text{conf}}$  of polymer chains would decrease to zero at a temperature,  $T_2$ . This temperature was found to be 80% to 90 % of a polymer's glass softening temperature,  $T_g$ . They concluded that an equilibrium liquid on cooling would undergo a second order phase transformation of Ehrenfest type at  $T_2$ . In order to examine the arrangements of a single polymer chain on a square lattice, Gujrati and Goldstein (1981) used the random walks description and incorporated Kasteleyn's [(1962), (1967)] results of self-avoiding random walk on the so-called Manhattan lattice, i.e., a special square lattice. From their detailed analysis, they concluded that the Gibbs-DiMarzio's conclusion (1958) is not derivable from the Huggins approximate solution (1942) to Flory's model (1941, 1942), and that even an approximate calculation does not lead to a negative value of configurational entropy at a finite temperature. This seems to remove the basis for the inference of a second order phase transformation at  $T_2$ , as deduced by Gibbs and DiMarzio (1958) and Gibbs (1960). By using Hamilton walks on a honeycomb lattice, Gordon *et. al.* (1976) also showed that the Flory-Huggins approximate estimate of Hamilton walks is a gross underestimate. The inference for  $S_{\text{conf}}$  becoming zero at  $T > 0$  K was also examined by Gutzow (1962, 1972, 1977) and Gutzow and coworkers [Milchev and Gutzow (1982), Gutzow and Schmelzer (1995), Petroff *et. al.* (1996)]. Milchev (1983) provided a new argument on the manner of chain-packing in

a monodispersed system, and concluded that  $S_{\text{conf}}$  of a polymer would not become zero at  $T_2$ . Rather, it would approach zero only at 0 K. He also showed that for an infinitely long polymer chain in the Gibbs-DiMarzio formalism (1958),  $S_{\text{conf}}$  was underestimated by an exact value of the gas constant  $R$  ( $= 8.314 \text{ J/mol K}$ ). Therefore,  $S_{\text{conf}}$  of an infinitely long polymer chain, with no holes on the lattice sites and no flexible bonds, should be equal to  $R$  at  $T_2$ , and not zero, as had been deduced earlier by Gibbs and DiMarzio (1958), DiMarzio and Gibbs (1958, 1959), and Gibbs (1960).

Based on the lattice-hole theory, Sanchez and Lacombe (1976) have developed a theory for liquids. They have derived an equation of state for a pure liquid, which is a mono-disperse system. Lacombe and Sanchez (1976) also developed a theory for mixtures of liquids which is a poly-disperse system. In the calculations of the partition functions in both papers, they used the limit approximation that  $z$  approaches infinity, as in the Guggenheim (1944, 1966) model, although this limit seems formally implausible. The result obtained by using this large  $z$  limit is equivalent to the result obtained in the Flory-Huggins approximations [Sanchez and Lacombe (1976)].

We adapt the basic concepts of the lattice-hole model, examine its limitations, and propose a new mean-field approximation to obtain a more accurate description of the polymer chain statistics. We then use our formalism to describe how  $S_{\text{conf}}$  would vary when polymerization reactions occurring spontaneously in a liquid increase the size of the species from molecular size to a distribution of polymer chains of increasing average length. From this modified version, we calculate the consequent change in the heat capacity and the decrease in the entropy to an equilibrium value at a constant

temperature. In this consideration, thermal energy for any given distribution of chain lengths continues to maintain a finite population of holes until 0 K is reached on cooling. At 0 K, this population vanishes. As a result of a distribution of chain lengths,  $S_{\text{conf}}$  remains finite at 0 K. The calculations lead to two new findings: (i) The heat capacity and entropy of a liquid should increase in the beginning of its polymerization. (ii) The zero value for  $S_{\text{conf}}$  would not be reached at  $T = 0$  K for a polydispersed system, because the temperature-independent entropy of mixing of the various chains of different lengths persist at 0 K when polymerization is inhibited. Only for an infinitely long chain polymer would the entropy approach zero at 0 K. This is analogous to the case of a mixture of isotopes of an element (and other crystals that do not demix) whose entropy of mixing in the thermodynamically equilibrium state persists at 0 K. The first finding is consistent with the heat capacity measurement performed earlier [Ferrari *et. al.* (1996)] with the intention of determining the increase in structural relaxation time on a liquid's spontaneous polymerization at a fixed temperature. The second finding is consistent with the inference drawn in earlier studies that the entropy of a liquid in internal equilibrium would approach zero at 0 K [Johari, (2000a), (2000b), (2001a), (2001b)]. The discussion of the model and of the calculated quantities and the implications of the calculations are included in the subsequent section.

We also develop a formalism for the change in the configurational entropy and heat capacity at different pressures at a fixed temperature, at different temperatures at a fixed high pressure and determine the effects of pressure. This is done for different extents of polymerization, thus yielding the surfaces of thermodynamic properties in a

temperature-pressure plane for a given average molecular weight. Finally, we use this formalism for determining how the viscosity of a given polymer would change with change in temperature or pressure.

### 3.3 Polymer Chain Statistics in the Lattice Hole Model

#### 3.3.1 Formalism for a monodispersed polymer

In a monodispersed linear polymer system, every linear polymer chain has the same number of repeat units or monomers, say  $x$ . The length of each polymer chain is also expressed as the number of repeat units  $x$ . When such a system contains  $N$  linear chains, each of length  $x$ , the corresponding lattice contains a total number of  $(xN + N_0)$  sites, where  $N_0$  is the number of sites occupied by the holes, or by the solvent molecules as in Flory's model. In this manner, only one repeat unit is placed on one lattice site. For an example, if  $x = 5$  and  $N = 10$ , the mono-dispersed system expressed on a  $8 \times 8$ , two dimension, square lattice with  $z = 4$  and  $N_0 = 14$  is shown in Fig. 3.1.

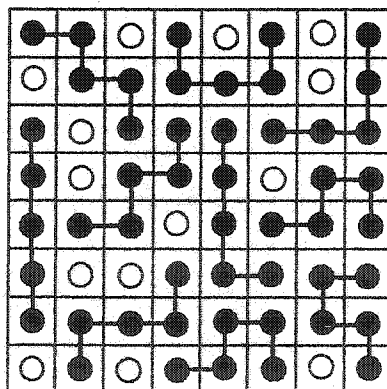


Fig. 3.1. Illustration of one configuration of a mono-dispersed polymer system with  $x = 5$  and  $N = 10$  on a two dimension  $8 \times 8$  square lattice with  $z = 4$  and  $N_0 = 14$ .

The number of configurations available for such an ensemble varies with  $x$ ,  $N$ ,  $N_0$ ,  $z$  and  $f$ , as defined earlier. A comparison of the implications of different approximations used in the various lattice models has been done by Wittmann (1991). He expressed these models in quantitative terms, occasionally by rewriting the equations in notations different from those of the original authors, and then critically examined their weaknesses. In Wittmann's (1991) paper, the number of configurations available, or the number of microstates of a polymer system in lattice-hole theory is given by,

$$\Omega(N, x, N_0, f, z) = \left[ \frac{1}{2^N N!} \prod_{j=1}^N M(j) \prod_{m=1}^{x-1} z(j, m) \right] \left\{ \binom{N(x-2)}{fN(x-2)} \left( \frac{1}{z-1} \right)^{(1-f)N(x-2)} \left( \frac{z-2}{z-1} \right)^{fN(x-2)} \right\} \quad (3.1)$$

where the term  $1/N!$  is a result of the indistinguishability of  $N$  polymer chains and the term  $1/2^N$  is a result of the fact that different sequences in which repeat units are placed to form a chain are taken twice. The term in curly brackets is a binomial distribution function. It represents the probability that out of the  $N(x-2)$  covalent bonds, there are exactly  $fN(x-2)$  flexible bonds of high energy  $\varepsilon$  and  $(1-f)N(x-2)$  rigid bonds of zero energy, i.e., in the ground state. The probability of a covalent bond being flexible is defined by the ratio,  $(z-2)/(z-1)$ . The term,  $M(j)$  in Eq. (3.1) is equal to  $[xN + N_0 - (j-1)x]$ . It represents the number of ways by which the first repeat unit of the  $j$ -th chain may be placed on the lattice after  $(j-1)$  chains have been already embedded in the lattice. The effective coordinate number,  $z(j, m)$ , in Eq. (3.1) is given by  $z(j, m) = z(m)[\gamma(j, m)]$  where the definition of the term  $[\gamma(j, m)]$  has been different in the different models,  $z(m)$  is the connectivity for the  $(m+1)$ -th repeat unit of a polymer chain after  $m$  repeat units have

been placed on the lattice in the infinite dilution limit so that the placing of each polymer chain is isolated from other repeat units already placed on the lattice. For  $m = 1$ , the quantity  $z(m) = z$  because there are  $z$  possible ways to place the second repeat unit, and for  $m \geq 2$ , the quantity  $z(m) = (z - 1)$ . The quantities,  $1/2^N$ ,  $1/M!$ ,  $M(j)$ ,  $z(m)$ , and the terms in curly brackets of Eq. (3.1) have essentially the same values as those in the Flory (1956), Gibbs-DiMarzio (1958) and Milchev (1983) models, but have been expressed in general terms with a single set of notations by Wittmann (1991).

To discuss the meaning of the term  $[\gamma(j, m)]$  and examine it critically, we consider as follows: The number of ways in which the second repeat unit of the first chain can be placed is equal to the coordination number of the lattice,  $z$ . There are two conditions for  $[\gamma(j, m)]$  when  $m \geq 2$  and/or  $j \geq 1$ . First we consider whether or not  $[\gamma(j, m)]$  may be equal to 1. This is the simplest situation of the lattice occupancy, in which none of the nearest neighbors of the site of the  $m$ -th repeat unit of the  $j$ -th chain are occupied by any of the  $(j - 1)$  chains or  $(m-2)$  repeat units of the  $j$ -th chain. Here  $z$  is also the number of ways in which the second repeat unit of the  $j$ -th chain can be placed. In this simplest occupancy situation but for a realistic value of  $m \geq 2$ , none of the nearest neighbors of the site of the  $m$ -th repeat unit of the  $j$ -th chain are occupied by any of the  $(j - 1)$  chains or  $(m-2)$  repeat units of the  $j$ -th chain. Here  $(z - 1)$  becomes the number of ways for placing the  $(m + 1)$ -th repeat unit of  $j$ -th chain. As more and more repeat units are placed on the lattice, the probability of encountering the simplest situation of  $z(m)$  number of ways for placing the repeat unit becomes progressively less. For the second and general situation of lattice occupancy,  $[\gamma(j, m)] \neq 1$ , for both values of  $m$ ,  $m = 1$  (when  $j \geq 1$ ) or  $m \geq 2$ .

Therefore, the quantity  $[y(j, m)]$ , which may be seen as a scaling factor for determining  $z(j, m)$  in the equation,  $z(j, m) = z(m)[y(j, m)]$ , needs to be ascertained. Because  $[y(j, m)]$  can not be obtained explicitly, approximations have been used. These approximations differ in the formalisms developed by Flory (1956), Gibbs and DiMarzio (1958), and Milchev (1983) for the lattice hole models. In particular, Flory's model had used  $[y(j, m)]$  as the ratio of number of available sites to the number of total sites:

$$[y(j, m)]_{\text{Flory}} = \frac{xN + N_0 - [(j-1)x + m]}{xN + N_0} \quad (3.2)$$

In view of the already noted decrease in  $S_{\text{conf}}$  in the Gibbs-DiMarzio formalism (1958), which makes  $S_{\text{conf}}$  unrealistically negative at  $T > 0$  K, a further mathematical consideration of this model is unnecessary, and we do not pursue their formalism.

Milchev (1983) introduced the concept of an average chain volume in Flory's model. He argued that, on average, there is a volume equal to  $[(xN + N_0)/N]$  for each chain. Now if  $(j-1)$  chains have already been embedded on the lattice, then an average  $(j-1)[(xN + N_0)/N]$  sites are already occupied. The effective remaining number of sites on which the  $j$ -th chain can be placed would no longer be  $(xN + N_0)$ , but only  $[(xN + N_0) - (j-1)(xN + N_0)/N]$ . This leads to,

$$[y(j, m)]_{\text{Milchev}} = \frac{(xN + N_0) - [(j-1)x + m]}{(xN + N_0) - (j-1)(xN + N_0)/N} = \left[ \frac{N}{N - (j-1)} \right] \frac{(xN + N_0) - [(j-1)x + m]}{(xN + N_0)} \quad (3.3)$$

Thus Milchev's (1983) and Flory's (1956) approximation are related by,

$$[y(j, m)]_{\text{Milchev}} = \left[ \frac{N}{N - (j-1)} \right] [y(j, m)]_{\text{Flory}} \quad (3.4)$$

The configurational entropy is calculated from  $S_{\text{conf}} = k_B \ln \Omega$  where  $k_B$  is the Boltzmann constant and  $\Omega$  is calculated from Eq. (3.1). For a system with one mole of total repeat units, i.e.,  $xN = N_A$  (Avogadro's number), there are four contributions to the molar configurational entropy in Flory's model. With the limiting condition of  $N \rightarrow \infty$ , the configurational entropy in Flory's model has been written by Milchev (1983) in the form,

$$\begin{aligned} \frac{S}{R} = & -\frac{(1-\theta)\ln(1-\theta)}{\theta} - \frac{\ln\theta}{x} + \frac{1}{x}\ln\left(\frac{z}{2}\right) + \frac{1}{x}\ln(x) + \left(\frac{1}{x}-1\right) \\ & + \left(1 - \frac{2}{x}\right) \left[-f \ln f - (1-f)\ln(1-f) + f \ln(z-2)\right] \end{aligned} \quad (3.5)$$

We separate these contributions as follows:

$$\frac{S^{(\theta, x)}}{R} = -\frac{(1-\theta)\ln(1-\theta)}{\theta} - \frac{\ln\theta}{x} \quad (3.6)$$

$$\frac{S^{(z, x)}}{R} = \frac{1}{x}\ln\left(\frac{z}{2}\right) \quad (3.7)$$

$$\frac{S^{(x)}}{R} = \frac{1}{x}\ln(x) + \left(\frac{1}{x}-1\right) \quad (3.8)$$

$$\frac{S^{(f, x, z)}}{R} = \left(1 - \frac{2}{x}\right) \left[-f \ln f - (1-f)\ln(1-f) + f \ln(z-2)\right] \quad (3.9)$$

where the subscript "conf" from  $S_{\text{conf}}$  has been dropped for simplicity,  $R = k_B N_A$  is the gas constant, and the quantity,  $\theta = xN / (xN + N_0)$  is the ratio of the number of sites occupied by polymer's repeat units to the total number of sites available. This is the fractional

lattice occupancy, which has also been called the dimensionless effective density of the lattice. Equations (3.7) and (3.9) are only applicable for  $x \geq 2$ , i.e., for a dimer or a multimer system.

In Flory's approximation of  $[y(j, m)]$  according to Eq. (3.2), the term  $[(1/x) - 1]$  has a negative value, and as  $x$  increases this negative value increases. Since  $(1/x)\ln(x)$  is a small positive number,  $S^{(x)}/R$  becomes negative for all values of  $x$ . But in Milchev's approximation of  $[y(j, m)]$  according to Eq. (3.3), the negative term  $[(1/x) - 1]$  vanishes in the limit of  $N \rightarrow \infty$ , and therefore [Milchev (1983)],

$$\frac{S^{(x)}}{R} = \frac{1}{x} \ln(x) \quad (3.10)$$

Accordingly,  $S_{\text{conf}}$  approaches zero with  $x$  approaching infinity at  $T$  approaching zero.

We consider that the modification of the average volume be instead made on the basis of the occupancy of each repeat unit, and not of each chain as in Milchev's formalism (1983). To elaborate, the effective remaining number of available sites on which  $(m + 1)$ -th repeat unit of  $j$ -th chain can be placed depends not only on the embedded  $(j - 1)$  chains but also on the  $m$  repeat units of the  $j$ -th chain itself. For each repeat unit, there is an effective volume of  $[(xN + N_0)/xN]$  sites. When  $(j - 1)$  chains and  $m$  repeat units of  $j$ -th chain have already embedded on the lattice, then on average  $[(j - 1)x + m][(xN + N_0)/xN]$  sites have been occupied. The effective remaining number of available sites on which  $(m + 1)$ -th repeat units of the  $j$ -th chain may be placed is therefore,

$$[y(j, m)] = \frac{(xN + N_0) - [(j - 1)x + m]}{(xN + N_0) - [(j - 1)x + m]} \frac{xN\{(xN + N_0) - [(j - 1)x + m]\}}{\{xN - [(j - 1)x + m]\}(xN + N_0)} \quad (3.11)$$

Our approximation for  $[y(j, m)]$  is related to Milchev's and Flory's approximations by,

$$[y(j, m)] = \frac{xN - [(j-1)x]}{xN - [(j-1)x + m]} [y(j, m)]_{\text{Milchev}} = \frac{xN}{xN - [(j-1)x + m]} [y(j, m)]_{\text{Flory}} \quad (3.12)$$

It should be noted that our conclusion from the value of  $[y(j, m)]$  in Eq. (3.11) yields the same results as Eqs. (3.6), (3.7), (3.9) and (3.10), without requiring the limiting condition of  $N \rightarrow \infty$ . (Details are provided in Appendix A). It is also worth noting that Eq. (3.3) leads to  $\Omega_{\text{Milchev}} = (N^N/N!)^{x-1} \Omega_{\text{Flory}}$ , and our Eq. (3.11) leads to  $\Omega = [(xN)^{xN} N! / N^N (xN)!] \Omega_{\text{Flory}}$ , as described in Appendix A.

### 3.3.2 Formalism for a polydispersed linear chain system

Since the growth of polymer chains during the addition polymerization produces a polydispersed system, we need to consider  $S_{\text{conf}}$  of a polydispersed system but within the constraint that its value does not become negative at any temperature. For example, one configuration of a polydispersed system is shown in Fig. 3.2 on a  $8 \times 8$  square lattice.

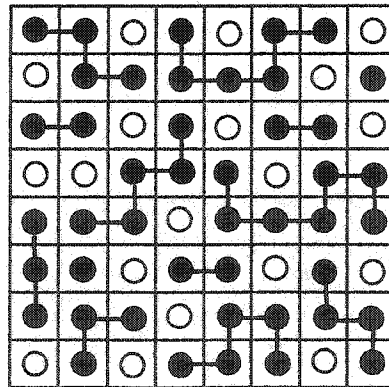


Fig. 3.2. Illustration of one configuration of a mono-dispersed polymer system on a two dimension  $8 \times 8$  square lattice with  $z = 4$  and  $N_0 = 19$ .

Gibbs and DiMarzio (1958) have provided a brief description also of a polydispersed system in terms of the lattice-hole model, and the Huggins approximation. They showed that except for the contribution from the entropy of mixing term, the entropy of the polydispersed state depends upon  $f$ ,  $z$ ,  $\theta$ ,  $x$  and  $T$  in a manner identical to that of a monodispersed system. Therefore, they replaced only the term  $x$  of a monodispersed system by the number average molecular weight,  $\bar{x}$  of the polydispersed system.

After discussing the limitations of Gibbs and DiMarzio's (1958) treatment in detail, Milchev and Gutzow (1982) formulated the number of configurations available for varying degree of polymerization, expressed it in terms of the fractal occupancy of the lattice, length and number of polymer chains. They calculated the value of  $S_{\text{conf}}$  for a fixed  $\theta$ ,  $\bar{x}$ ,  $z$  and  $f$  by using the principle of equal molecular reactivity or molecular agglomeration, as given by Flory (1936) in his description of polydispersity.

However, we find that Milchev and Gutzow's (1982) formalism for polydispersed system can not be used for the purpose of irreversible growth of a polymer in a polymerization reaction because of the reversibility of  $\bar{x}$ . In the second part of Milchev and Gutzow's formalism (1982), they allowed  $\bar{x}$  to vary with  $T$  reversibly, i.e., the polymer chains agglomerated on cooling and deagglomerated on heating maintaining a chemical equilibrium at each temperature. In this case, as  $T \rightarrow 0$  K,  $\bar{x} \rightarrow \infty$  and the polymer chain becomes infinitely long. On that basis, they calculated the configurational entropy of a polydispersed system whose average molecular weight increased with

decrease in  $T$ . This treatment is valid for a system containing different species at a thermodynamic equilibrium, i.e., an equilibrium state of polymerization exists at each temperature and that the concentration of monomers and multimers are at a thermally reversible equilibrium. In their formalism  $\bar{x}$  changes reversibly with  $T$ , and this is similar to a reversible intermolecular association, when the intermolecularly H-bonded chains in alcohols and amides increase in length [Johari and Dannhauser (1969)]. Moreover, this manner of calculating the configurational entropy with increase in the intermolecular association is not specific to the manner in which that association occurs. All that it requires is that the molecular association varies with  $T$ . In our treatment, chemical reactions lead to an irreversible growth of a macromolecule at a fixed  $T$ , which lead to volume contraction, and therefore the number of holes on the lattice decreases at a fixed  $T$  as a result of chemical reactions.

In deriving this formalism, we also find that in the limit of monodispersity, Milchev and Gutzow's (1982) procedure for calculating the number of configurations available leads to the original formula that had been obtained for a monodispersed system by Flory (1956) at all temperatures. The detail of our deduction is given in Appendix B. Since Flory's formalism for a monodispersed system had originally led to a negative value for the configurational entropy at  $T > 0$  K, and is therefore seen as inappropriate, Milchev and Gutzow's (1982) formalism also seems inappropriate for a polydispersed system in that respect. It should be noted that in the Milchev formalism (1983) for a monodisperse system, the configurational entropy does not become negative at  $T > 0$  K.

We use Eqs. (3.6), (3.7), (3.9) and (3.10) for a monodispersed system and consider that a polydispersed system is a mixture of many monodispersed sub-systems with certain distribution of molecular weights or chain lengths. Hence we calculate the configurational entropy of a polydispersed system by using the weighted sum of the individual entropy of each monodispersed polymer sub-system plus the entropy of mixing, as follows:

During the spontaneous polymerization process, both the polydispersity and the number average molecular weight of a polydispersed linear chain polymer are in non-equilibrium conditions, and  $\bar{x}$  increase *irreversibly* with time as the extent of polymerization,  $\alpha$ , increases at a fixed  $T$ . Therefore, we need to describe how  $\alpha$  and  $\bar{x}$  are related. For a system with total number of repeat units given by  $N_A$ ,  $\bar{x}$  is given by,

$$\bar{x} = \frac{\sum_{x=1}^{N_A} xN_x}{\sum_{x=1}^{N_A} N_x} = \frac{N_A}{N} \quad (3.13)$$

where  $N_x$  is the number of polymer chains each chain containing  $x$  number of repeat

units. Hence, the total number of polymer chains is given by,  $N = \sum_{x=1}^{N_A} N_x$ .

There are two limiting conditions: (i) When there are no covalent bonds, i.e., each repeat unit is a molecular species. In this case,  $N_1 = N_A$  and  $N_x = 0$  for the condition  $x > 1$ . (ii) When all molecules become covalently bonded to form one linear chain of -A-A-A-

type, with  $N_A$  repeat units of A or and  $N_A$  covalent bonds. In this case,  $N_{N_A} = 1$ ,  $N_x = 0$  for the condition  $x < N_A$ . For any condition in between these two limits, the ratio of the number of covalent bonds formed to the quantity  $N_A$  is equal to the extent of polymerization,  $\alpha$ . This  $\alpha$  is related to  $\bar{x}$  by,

$$\alpha = \frac{\sum_{x=1}^{N_A} (x-1)N_x}{N_A} = 1 - \frac{1}{\bar{x}} \quad (3.14)$$

Equation (3.14) is the familiar Carother's equation [Carother (1936)], which is valid for a linear chain polymer system irrespective of the molecular weight or chain length distribution. For the special case of a monodispersed system,  $\bar{x} = x$ .

In a polydispersed system, the number of polymer chains with repeat unit  $x$ ,  $N_x$ , is given by:

$$N_x = NP_x \quad (3.15)$$

where  $P_x$  is the probability of occurrence of a polymer chain with repeat unit  $x$  and  $N$  is the total number of polymer chains with different numbers of repeat units. The

normalization constrain requires that  $\sum_{x=1}^{N_A} P_x = 1$ . But since  $N_A$  is already a very large number, the limit  $N_A \rightarrow \infty$  may be justifiably used, and  $N_A$  be replaced by  $\infty$  for summation.

In the equal reactivity approximation, as given by Flory (1936), the polymer chains produced have a distribution which gives  $P_x$ , as,

$$P_x = (1-\alpha)\alpha^{(x-1)} \quad (3.16)$$

In our consideration given above, the configurational entropy of a polydispersed system is given by the weighted sum of the individual entropy of each monodispersed polymer sub-system plus the entropy of mixing,

$$S = \langle S_{\text{mono}} \rangle + S^{\text{mix}} = \sum_{x=1}^{\infty} \left( \frac{xN_x}{N_A} S_x \right) + \sum_{x=1}^{\infty} (-Nk_B P_x \ln P_x) \quad (3.17)$$

where  $\langle S_{\text{mono}} \rangle$  is the weighted entropy of all monodispersed sub-systems and  $S_x$  is the entropy of a polymer chain of length  $x$ , as described by Eqs. (3.6), (3.7), (3.9) and (3.10).

The first term on RHS of Eq. (3.17) represents the sum for all the monodispersed sub-systems. It may be written as,

$$\begin{aligned} \frac{\langle S_{\text{mono}} \rangle}{R} &= \sum_{x=1}^{\infty} \left( \frac{xN_x}{N_A} \frac{S_x}{R} \right) = \sum_{x=1}^{\infty} \left\{ \frac{xN_x}{N_A} \left[ -\frac{(1-\theta)\ln(1-\theta)}{\theta} - \frac{\ln \theta}{x} + \frac{1}{x} \ln x \right] \right\} \\ &+ \sum_{x=2}^{\infty} \frac{xN_x}{N_A} \left\{ \frac{1}{x} \ln \left( \frac{z}{2} \right) + \left( 1 - \frac{2}{x} \right) \left[ -f \ln f - (1-f) \ln(1-f) + f \ln(z-2) \right] \right\} \end{aligned} \quad (3.18)$$

### 3.3.3 Configurational entropy and the extent of polymerization

The total configurational entropy at any instant during the course of polymerization is the sum of five separate contributions, which are associated with the terms  $\theta$ ,  $z$ ,  $f$ ,  $\alpha$  and the entropy of mixing. These contributions may be obtained by separating the RHS of Eq. (3.17) into five terms, as follows:

#### (i) The fractional occupancy contribution.

$$\frac{S^{(\theta, \alpha)}}{R} = \sum_{x=1}^{\infty} \left\{ \frac{xN_x}{N_A} \left[ -\frac{(1-\theta)\ln(1-\theta)}{\theta} - \frac{\ln \theta}{x} \right] \right\} = -\frac{(1-\theta)\ln(1-\theta)}{\theta} - (1-\alpha)\ln \theta \quad (3.19)$$

The fractional occupancy of the lattice,  $\theta$ , as defined by  $\theta = N_A / (N_A + N_0)$ , depends on both  $\alpha$  and  $T$  because  $N_0$  itself depends on both  $\alpha$  and  $T$ . According to Eyring's (1936) hole theory of liquids,

$$\theta = 1 - \delta \exp\left(-\frac{U_h}{RT}\right) = 1 - \frac{v_1}{v_0} \exp\left(-\frac{U_h}{RT}\right) \quad (3.20)$$

where  $U_h$  is the energy for formation of one mole of holes in the system (or energy for the formation of one hole multiplied by the Avogadro number),  $v_1$  is the molar volume of a repeat unit and  $v_0$  the "molar volume" of a hole, and  $\delta = v_1/v_0$ . It has been found that for  $U_h = 2 - 20$  kJ/mol, and  $\delta = v_1/v_0 = 5 - 7$  [Eyring (1936)]. Choi and Plazek (1986) have found that in a polymerization process, there is less than 10% volume contraction of the system from  $\alpha = 0$  to  $\alpha = 1$ . Thus, as the net volume decreases, the quantity  $\delta$  also decreases with the increase of  $\alpha$  and tends to saturate when  $\alpha \rightarrow 1$ . To incorporate this observation empirically in Eq. (3.20), we propose that,

$$\delta = \frac{v_1}{v_0} \left[1 + \exp(-x)\right] = \frac{v_1}{v_0} \left[1 + \exp\left(-\frac{1}{1-\alpha}\right)\right] \quad (3.21)$$

By using Eq. (3.21) we obtain  $\delta$  as a function of  $\alpha$ , and then by using Eq. (3.20) we calculate  $\theta$  as a function of  $\alpha$ . By using Eq. (3.19) we finally calculate  $S^{(\theta,\alpha)}/R$  for the parameter  $U_h = 1500 R$ , and  $v_1/v_0 = 6.85$ . Its value is plotted against  $\alpha$  also in Fig. 3.3(A). It decreases monotonically with increase in  $\alpha$ , with a decreasing slope of the curve of  $S^{(\theta,\alpha)}/R$  against  $\alpha$ .

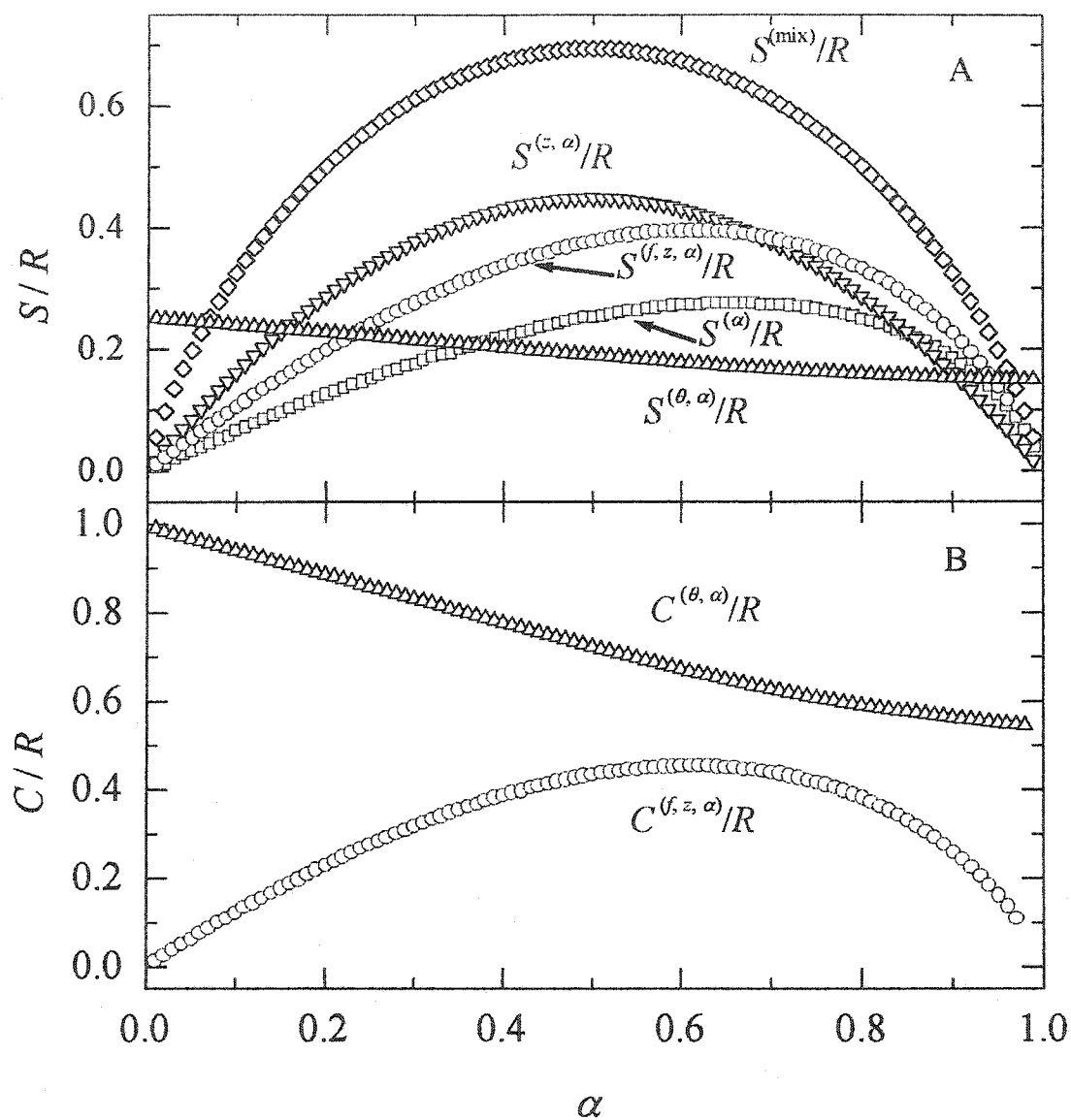


Fig. 3.3. (A). The five contributions to the configurational entropy of a polymerizing system scaled by the gas constant are plotted against the extent of polymerization at 300 K. The various contributions are indicated by their notations. (B). The corresponding contributions to the configurational heat capacity are plotted against  $\alpha$ .

**(ii) The co-ordination number contribution**

$$\frac{S^{(z,\alpha)}}{R} = \sum_{x=2}^{\infty} \frac{xN_x}{N_A} \left\{ \frac{1}{x} \ln\left(\frac{z}{2}\right) \right\} = (1-\alpha) \sum_{x=2}^{\infty} (P_x \ln \frac{z}{2}) = \alpha(1-\alpha) \ln\left(\frac{z}{2}\right) \quad (3.22)$$

We use  $z = 12$  ( i.e., for a fcc lattice), and calculate  $S^{(z,\alpha)}/R$  for different values of  $\alpha$ . It is plotted against  $\alpha$  in Fig. 3.3(A). The curve is parabolic in shape since  $\ln(z/2)$  is a constant, with a maximum at  $\alpha = 0.5$ .

**(iii) The extent of reaction contribution**

$$\frac{S^{(\alpha)}}{R} = \sum_{x=1}^{\infty} \frac{xN_x}{N_A} \frac{1}{x} \ln(x) = (1-\alpha) \sum_{x=1}^{\infty} (P_x \ln x) = (1-\alpha)^2 \sum_{x=1}^{\infty} \alpha^{x-1} \ln x \quad (3.23)$$

The summation term in Eq. (3.23) could not be solved analytically. Therefore, the entire term  $S^{(\alpha)}/R$  was calculated numerically for different values of  $\alpha$  and plotted against  $\alpha$  in Fig. 3.3(A). This curve appears like a skewed arc. Since  $S^{(\alpha)}/R$  is independent of  $T$ , an empirical equation was fitted to this curve for convenience. A fit of this curve by the least square method gave,

$$\frac{S^{(\alpha)}}{R} = (1-\alpha)^2 \sum_{x=1}^{\infty} \alpha^{x-1} \ln x \approx -(1-\alpha) \ln(1-\alpha) - 0.3495\alpha^{1.062} (1-\alpha)^{0.8483} \quad (3.24)$$

It should be stressed that this dependence of  $S^{(\alpha)}/R$  on  $\alpha$  differs from that used by Milchev and Gutzow (1982), as described here in Appendix B.

## (iv) The chain flexibility contribution

$$\begin{aligned} \frac{S^{(f,\alpha,z)}}{R} &= \sum_{x=2}^{\infty} \frac{xN_x}{N_A} \left\{ \left(1 - \frac{2}{x}\right) [-f \ln f - (1-f) \ln(1-f) + f \ln(z-2)] \right\} \\ &= (1-\alpha) \sum_{x=2}^{\infty} xP_x \left\{ \left(1 - \frac{2}{x}\right) [-f \ln f - (1-f) \ln(1-f) + f \ln(z-2)] \right\} \end{aligned} \quad (3.25)$$

When  $f$  is *not* a function of  $x$ , then the net term in the square brackets on RHS of Eq. (3.25) remains constant with changing  $x$ . Thus, on substitution Eq. (3.16), in Eq. (3.25),

$$\frac{S^{(f,\alpha,z)}}{R} = \alpha^2 [-f \ln f - (1-f) \ln(1-f) + f \ln(z-2)] \quad (3.26)$$

This result is the same as that obtained by Milchev and Gutzow (1982), but it has been obtained by using a different approach here.

For polymer chains in a solvent, the flexibility  $f$ , which has been considered to be independent of  $x$ , varies with  $T$  according to Flory (1956),

$$f = \frac{(z-2) \exp\left(-\frac{U_f}{RT}\right)}{1 + (z-2) \exp\left(-\frac{U_f}{RT}\right)} \quad (3.27)$$

where  $U_f$  is the energy needed to excite one mole of flexible bonds from ground state to their flexible state.

Contrary to the above-mentioned independence of  $f$  on  $x$ , we consider that the flexibility of covalent bond would vary with  $x$ . It is known that during the course of polymerization, the viscosity increases and volume decreases. Since a polymer chain folds on itself, the flexibility,  $f$ , of its segments is affected by its intermolecular or interchain environment and is not entirely determined by the intramolecular barriers.

Thus  $f$  is expected to decrease with increase in the number of covalent bonds formed, i.e., with increase in the number of repeat units in the bonded structure. This increase may be related to  $x$ , the number of the repeat units in a polymer chain in several ways. Out of these the two simplest ways are, (i)  $U_f$  may be a progressively increasing function of  $x$ , as has been found from the rapid increase in the activation energy for segmental orientation with increase in the chain length in several cases [Johari (1994), Parthun and Johari (1995)], and (ii)  $f \propto 1/x$ . As a first approximation, we use the latter dependence of  $f$  on  $x$ , multiply Eq. (3.29) by a factor  $1/x$ ,

$$f = \frac{(z-2) \exp\left(-\frac{U_f}{RT}\right)}{x \left[1 + (z-2) \exp\left(-\frac{U_f}{RT}\right)\right]}, \quad \text{or, } f \propto 1/x \quad (3.28)$$

when  $U_f$ ,  $z$  and  $T$  are constants. We calculate  $f$  as a function of  $x$  from Eq. (3.28) by using  $U_f = 700 R$ , and  $z = 12$ , and by substituting  $f$  in Eq. (3.28), and then we calculate  $S^{(f,\alpha,z)}/R$ . The quantity  $S^{(f,\alpha,z)}/R$  is plotted in Fig. 3.3(A). The curve obtained looks like a skewed arc, and both its magnitude and shape are temperature dependent.

#### (v) The entropy of mixing contribution

The second term on RHS of Eq. (3.17) is the entropy of mixing of all the sub-systems. According to the distribution given in Eq. (3.16), this term divided by  $R$  is given by,

$$\frac{S^{(\text{mix})}}{R} = \sum_{x=1}^{\infty} \left( \frac{-Nk_B P_x \ln P_x}{R} \right) = (1-\alpha) \sum_{x=1}^{\infty} (-P_x \ln P_x) = -\alpha \ln \alpha - (1-\alpha) \ln(1-\alpha) \quad (3.29)$$

This contribution is entirely statistical with a maximum of  $R\ln 2$  at  $\alpha = 0.5$ . The values of  $S^{(\text{mix})}/R$  is also plotted against  $\alpha$  in Fig. 3.3(A).

The net configurational entropy is the sum of the five above-given contributions. Its total value at 300 K is expressed as  $S/R$  and is plotted against  $\alpha$  in Fig. 3.4(A). The values  $S/R$  calculated for 275 K and 325 K are also plotted in Fig. 3.4(A). These plots show that the configurational entropy initially increases, reaches a maximum and then decreases as  $\alpha$  increases. The curve shifts downwards as  $T$  is decreased, its shape changes, and the local maximum in the curve shifts to higher values of  $\alpha$ .

It should be stressed that our calculations are for isothermal vitrification of a liquid in which polymer chains spontaneously grow and ultimately cause the liquid to vitrify under normal conditions and the state becomes kinetically frozen on the time scale of one's observations. But when the polymerization temperature is high, the ultimately polymerized liquid may remain in a highly viscous equilibrium state at that temperature.

Although we extend our calculations to different temperatures and show that  $S_{\text{conf}}$  for a polydispersed system of a fixed chemical structure would not become negative at  $T > 0$  K, our calculations differ from those of others who had also determined the variation in free energy and  $S_{\text{conf}}$  with temperature in a reversible manner. Briefly, we fix the temperature and describe the thermodynamics of the changing structure on a lattice in which the number of empty sites irreversibly decrease, which decreases the free volume, and the effective flexibility is gradually reduced as linear chains form at different sites and grow in length as a result of chemical reactions. Also there are four adjustable parameters,  $U_b$ ,  $U_h$ ,  $z$  and the ratio  $v_1/v_0$ , which were needed for the calculations of the

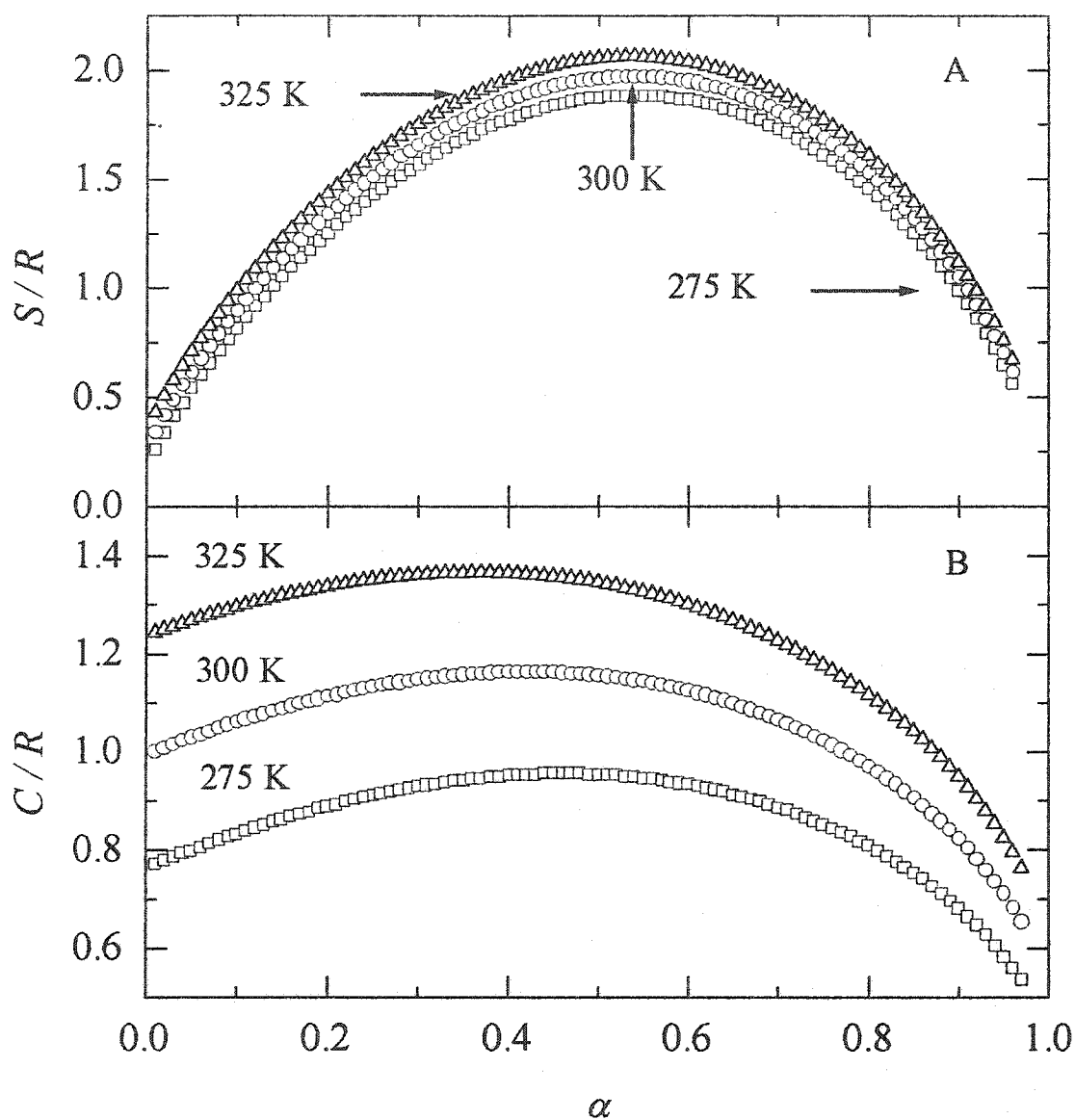


Fig. 3.4. (A). The net configurational entropy of a polymerizing system divided by the gas constant at three temperatures is plotted against the extent of polymerization. (B). The corresponding net configurational heat capacity is plotted against  $\alpha$ .

configurational entropy at temperatures far below the boiling point of the liquid. The values of the parameters used here are plausible, but not quantitatively verifiable.

### 3.3.4 Configurational heat capacity change during polymerization

We now consider how the configurational contribution to the equilibrium heat capacity,  $C$ , would change as polymerization occurs at a fixed temperature. For a polydispersed system,  $C$  may be calculated from,

$$\frac{C}{R} = \frac{T}{R} \frac{\partial S}{\partial T} = \frac{T}{R} \left( \frac{\partial S^{(\theta, \alpha)}}{\partial \theta} \frac{\partial \theta}{\partial T} + \frac{\partial S^{(f, \alpha, z)}}{\partial f} \frac{\partial f}{\partial T} \right) = \frac{C^{(\theta, \alpha)}}{R} + \frac{C^{(f, \alpha, z)}}{R} \quad (3.30)$$

$$\text{where, } \frac{C^{(\theta, \alpha)}}{R} = \frac{T}{R} \left( \frac{\partial S^{(\theta, \alpha)}}{\partial \theta} \frac{\partial \theta}{\partial T} \right) = \frac{-(1-\theta)[\ln(1-\theta) + \alpha\theta] U_h}{\theta^2 RT} \quad (3.31)$$

$$\begin{aligned} \frac{C^{(f, \alpha, z)}}{R} &= \frac{T}{R} \frac{\partial S^{(f, \alpha, z)}}{\partial f} \frac{\partial f}{\partial T} = (1-\alpha) \sum_{x=2}^{\infty} x P_x \left\{ \left( 1 - \frac{2}{x} \right) [-\ln f + \ln(1-f) + \ln(z-2)] \right\} \frac{\partial f}{\partial T} \\ &= \frac{(1-\alpha)}{RT} \sum_{x=2}^{\infty} \frac{P_x U_f (x-2)}{[1 + (z-2) \exp(-\frac{U_f}{RT})]} [-f \ln f + f \ln(1-f) + f \ln(z-2)] \quad (3.32) \end{aligned}$$

The other three contributions,  $C^{(\alpha)}/R$ ,  $C^{(z, \alpha)}/R$  and  $C^{(\text{mix})}/R$ , are formally zero. Equation (3.32) was calculated numerically for the condition that  $f$  is a function of  $x$  and Eq. (3.28) was used. For the same condition as used for obtaining curves in Fig. 3.3(A), values of  $C^{(\theta, \alpha)}/R$  and  $C^{(f, \alpha, z)}/R$  were calculated and plotted against  $\alpha$  in Fig. 3.3(B). The quantity  $C^{(\theta, \alpha)}/R$  decreases with increase in  $\alpha$ , because the effective density of the lattice,  $\theta$  decrease with increase in  $\alpha$ . In contrast,  $C^{(f, \alpha, z)}/R$  first increases with  $\alpha$ , reaches a

maximum value and then rapidly decreases. The initial increase in  $C^{(f,\alpha,z)}$  is a consequence of the increase in the number of bonds formed, and the concurrent decrease is a consequence of the decrease in the flexibility  $f$  which leads to an increase in viscosity and ultimately to vitrification as  $\alpha$  increases. The combination of the two shows a maximum. The net values of  $C/R$  were determined at 275 K, 300 K and 325 K, and are plotted against  $\alpha$  in Fig. 3.4(B). Here the heat capacity initially increases, reaches a maximum value, and then decreases as  $\alpha$  increases. The curve shifts downwards as  $T$  is decreased, its shape changes, and the maximum shifts to higher values of  $\alpha$ .

The five contributions to the configurational entropy and the two contributions to the heat capacity were also calculated as a function of temperature for a fixed value of  $\alpha = 0.80$ . Each of these contributions is plotted against  $T$  in Figs. 3.5(A) and 3.5(B), respectively. Here  $S^{(\theta, \alpha)}/R$  and  $S^{(f,\alpha,z)}/R$  decrease with  $T$  and approach zero at 0 K. Also the two contributions to the configurational heat capacity decrease towards zero at 0 K. If the polydispersity persisted on cooling to 0 K, the terms  $S^{(\theta, \alpha)}/R$ ,  $S^{(\alpha)}/R$  and  $S^{(\text{mix})}/R$  would remain constant on cooling and their magnitudes will persist at 0 K. But if the state of the polymerizing mixture was maintained at a chemical equilibrium at all temperatures, the polydispersity would ultimately decrease and an infinitely long chain would form at 0 K. In that case the three terms,  $S^{(z,\alpha)}/R$ ,  $S^{(\alpha)}/R$  and  $S^{(\text{mix})}/R$  would also approach zero at 0 K. This requires that the equilibrium constants for the various polymerization reactions, and the multiplicity of equilibrium constants for the before and after covalent bonded species all increase with decrease in  $T$ , and loop of a single chain

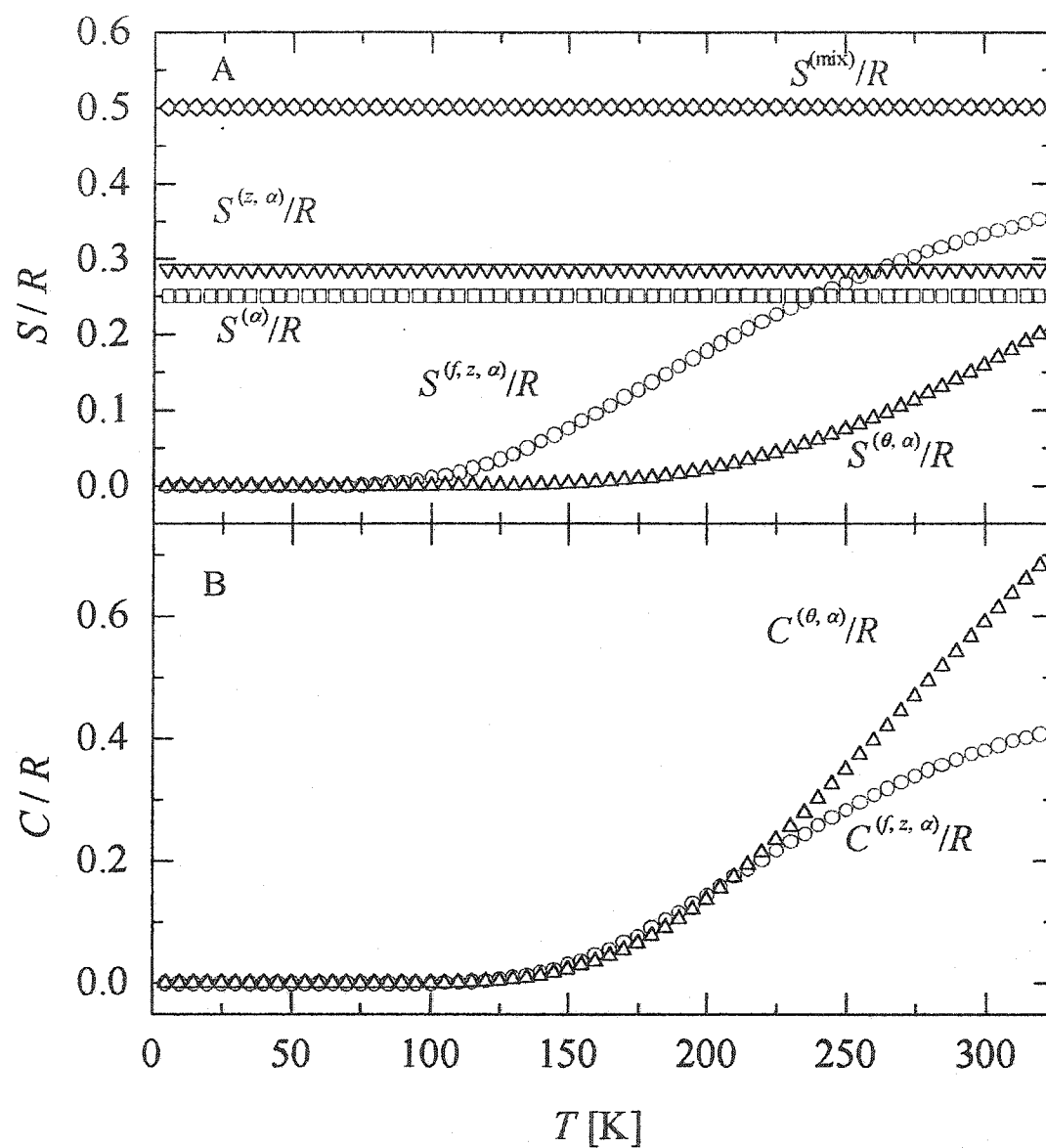


Fig. 3.5. (A). The five contributions to the configurational entropy for a fixed value of  $\alpha$  ( $= 0.8$ ) in a polymerizing system scaled by the gas constant are plotted against the temperature. The various contributions are indicated by their notations. (B). The corresponding contributions to the configurational heat capacity are plotted against the temperature.

would form at infinite time at 0 K [Johari (1994)]. This requires not only the attainment of a configurational thermodynamic equilibrium, but also that of a chemical equilibrium.

Figure 3.6(A) shows the variation of the total entropy with temperature and Fig. 3.6(B) that of the configurational heat capacity for three values of  $\alpha$ , 0.20, 0.50 and 0.80. In the absence of knowledge of the variation of equilibrium constant for polymerization with  $T$ , which would ultimately cause the polydispersity to vanish at 0 K in the system of our interest here, the net configurational entropy is shown to have a finite value at 0 K. This value has a maximum for that  $\alpha$  at which the sum of the terms,  $S^{(z,\alpha)}/R$ ,  $S^{(\alpha)}/R$  and  $S^{(\text{mix})}/R$  reaches a maximum value. If the system was not a *living polymerization* system, or if the reaction stopped as a result of attachment of the molecules to the walls of a container, or to the extraneous particles or dissolved impurities in the liquid, then this entropy will persist as a state entropy at 0 K. This is analogous to the situation of an isotopic mixture of elements or compounds. In the case of living polymerization, it would decrease to zero as poly-dispersity is expected to vanish once the equilibrium constant in favor of the covalent bond formation has approached infinity at 0 K, and the chemical equilibrium has been reached at all temperatures on cooling to 0 K. This requires that both the chemical and internal equilibrium be attained before the entropy of the system would reach zero at 0 K. If the chemical equilibrium is not attained, the temperature-independent entropy of mixing would persist.

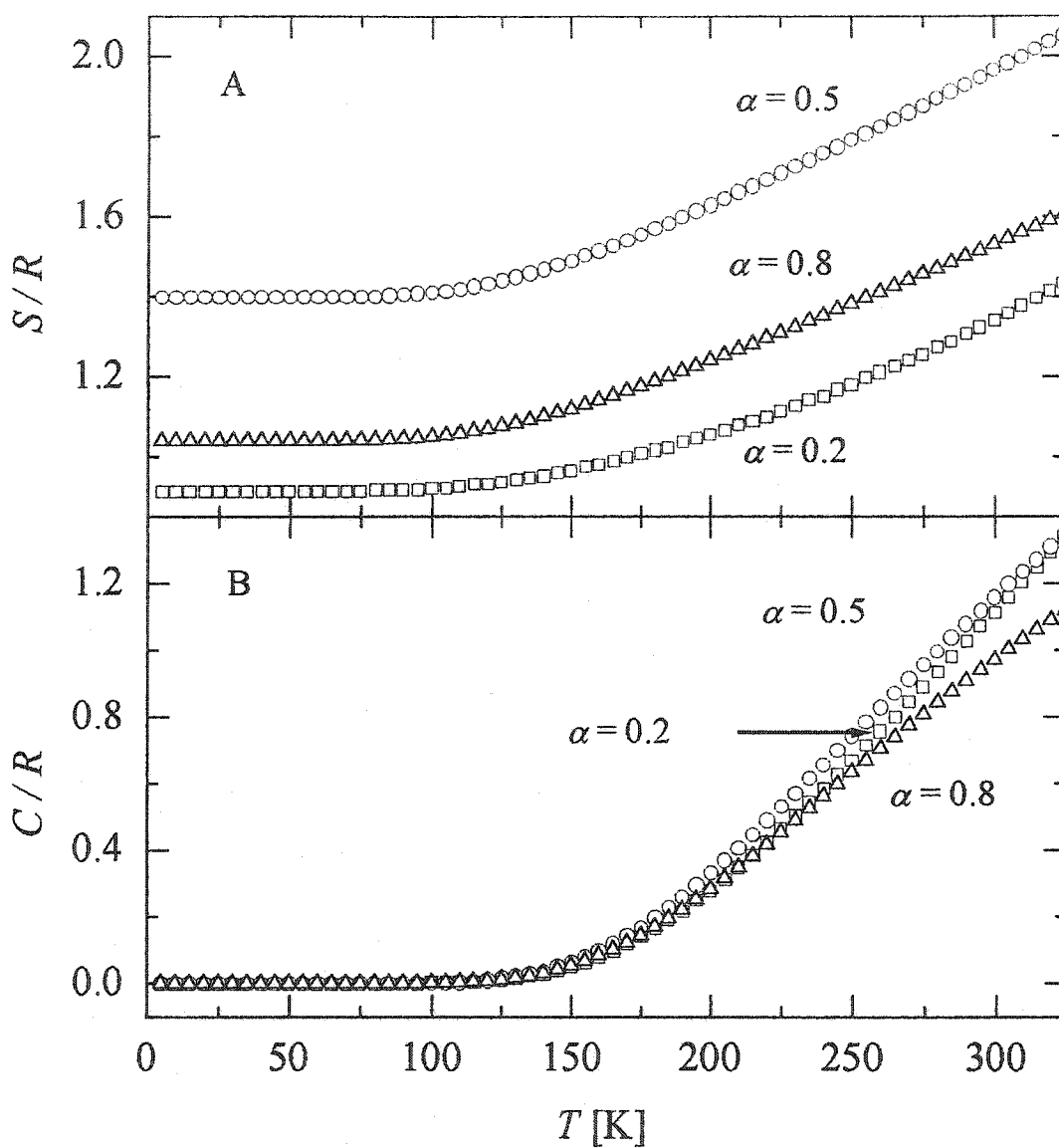


Fig. 3.6. (A). The net configurational entropy for a fixed value of  $\alpha$  in a polymerizing system scaled by the gas constant are plotted against the temperature. The various contributions are indicated by their notations. (B). The corresponding net configurational heat capacity is plotted against the temperature.

### 3.4 Pressure Effects on the lattice chain statistics

Properties of a polymer system and the kinetics of polymerization also vary with pressure at a fixed temperature. In our calculations in Sections 3.3, a stable polymer and a polymerizing system were kept at a fixed pressure of 1 bar. In this section, we calculate the effects of pressure on the lattice chain statistics, in particular on the number of available configuration of a polymer chain and the consequent thermodynamics. We further calculate the effects of temperature on the chain statistics at different fixed pressures.

#### 3.4.1 Formalism for the effects of pressure on the lattice chain statistics

It is known from Eyring's theory [1936] that increase in pressure raises the energy for hole formation, because the density increases. According to the hole theory of a liquid [Eyring (1936), Hirai and Eyring (1959)], the energy needed to create a hole in the structure of a liquid at a pressure  $P$  is then given by,

$$U_h(P) = U_h + P v_0 \quad (3.33)$$

where  $U_h$  is the energy required to create a hole at zero pressure taken as 1 bar here,  $P$  is the pressure and  $v_0$  is the "molar volume of holes", as already mentioned. For polymers at 0.1 MPa pressure, it has been found that  $U_h = 2 - 20$  kJ/mol, and  $v_0 = 15 - 150$  cm<sup>3</sup>/mol. [Eyring (1936), Hirai and Eyring (1959)]. Here, we use,  $U_h = 1500R$  (in units of K)  $\approx 12.5$  kJ/mol. For determining the term  $P v_0$ , we use  $v_0 = 83.14 \times 10^{-6}$  m<sup>3</sup>/mol, which yields,  $P v_0 = 8.314$  J/mol at 0.1 MPa. Hence,

$$U_h(P) = 12500 + 8.314 P \text{ (in unit of J/mol)}$$

$$= (1500 + 1 \times 10^{-5} P)R \text{ (in units of K).} \quad (3.34)$$

The magnitude of  $S^{(\theta, \alpha)}/R$  therefore varies with  $P$  through the variation of  $\theta$  according to Eqs. (3.20) and (3.22).

### 3.4.2 The effects of pressure on configurational entropy

Amongst the five above-listed contributions, which are written in the terms of Eqs. (3.19), (3.22), (3.23), (3.25) and (3.29),  $S^{(\theta, \alpha)}/R$  of Eq. (3.19) contains the  $U_h$  term. Therefore  $S^{(\theta, \alpha)}/R$  varies with both  $T$  and  $P$ , and  $S^{(f, \alpha z)}/R$  of Eq. (3.25), varies only with  $T$ , as long as the chemical structure or  $\alpha$  does not change. For three selected values of  $\alpha$  of 0.2, 0.5 and 0.8, we calculate the magnitude of  $S^{(\theta, \alpha)}/R$  as a function of pressure up to 100 MPa at 300 K. This quantity is plotted against  $P$  in Figs. 3.7(A), (B) and (C). In these figures, the listed magnitudes of the terms,  $S^{(\text{mix})}/R$ ,  $S^{(z, \alpha)}/R$  and  $S^{(\alpha)}/R$  do not depend upon  $T$  and  $P$ , and the listed magnitude of the term  $S^{(f, \alpha z)}/R$  depends upon  $T$ .

The plots in Fig. 3.7 show that for all values of  $\alpha$  at 300 K,  $S^{(\theta, \alpha)}/R$  monotonically decreases nonlinearly with increase in  $P$ . Increase in pressure decreases the  $S^{(\theta, \alpha)}/R$  at a fixed  $\alpha$  more at low pressures than it does at high pressures, i. e., the derivative,  $dS^{(\theta, \alpha)}/dT$ , decreases with increase in  $P$ . For a fixed  $P$  and  $T$ ,  $S^{(\theta, \alpha)}/R$  decreases when  $\alpha$  increases from 0.2 to 0.8.

The total of the above described five contributions to the entropy,  $S/R$ , was calculated for  $\alpha = 0.2, 0.5$  and  $0.8$  at three temperatures, 275 K, 300 K and 325 K. For each temperature it was also calculated as a function of pressure from 0.1 MPa to 100

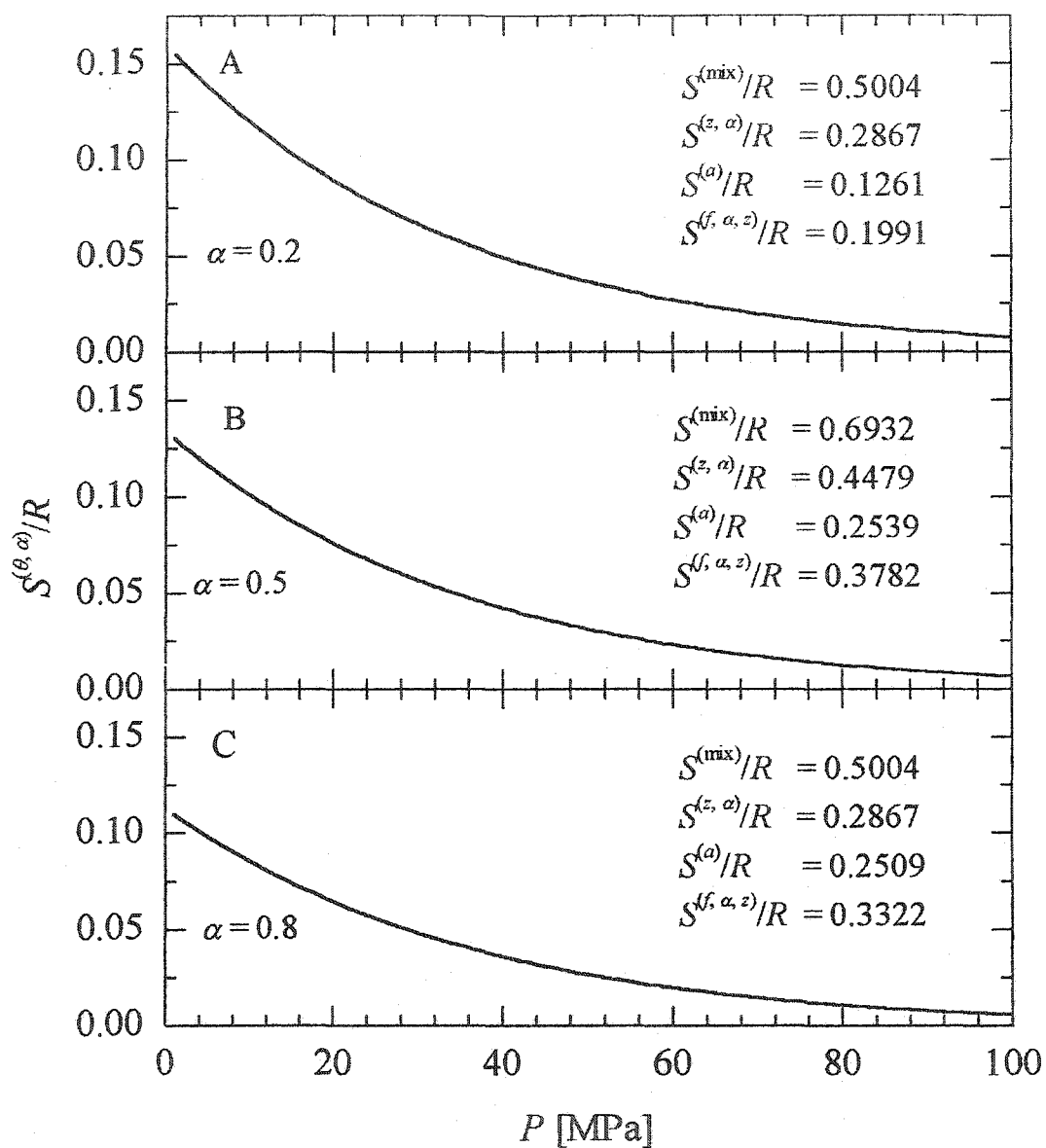


Fig. 3.7. The contribution to the configurational entropy,  $S^{(\theta, \alpha)}/R$  is plotted against the pressure at a temperature of 300 K. The plots in panels A, B, and C are for the extent of polymerization 0.2, 0.5 and 0.8, respectively. For a fixed  $z$ , the magnitudes of the other three contributions,  $S^{(\text{mix})}/R$ ,  $S^{(z, \alpha)}/R$ ,  $S^{(\alpha)}/R$  which depend only on  $\alpha$ , and the magnitude of  $S^{(f, \alpha, z)}/R$ , which depends on both  $T$  and  $\alpha$  but not on  $P$ , are noted in each panel.

MPa. The calculated value of  $S/R$  is plotted against  $P$  in Figs. 3.8(A), (B) and (C), where the  $T$  and  $\alpha$  values are indicated. The plots show that for a fixed value of  $P$  and  $\alpha$ ,  $S/R$  increases as  $T$  is increased from 275 K to 325 K. This is due to increase in both  $S^{(\theta,\alpha)}/R$  and  $S^{(f,\alpha,z)}/R$  with increase in  $T$ . The rate of increase in  $S/R$  with  $T$ , i.e., the derivative  $d[S^{(\theta,\alpha)} + S^{(f,\alpha,z)}]/dT$  has a higher magnitude at low pressures than at high pressures.

For the sake of completeness, two more constructions of the entropy related data are provided here. In the first construction, we describe the compensation effects of changes in pressure and temperature on the net entropy. To do so,  $P$  and  $T$  were calculated for isentropic conditions, i.e., for fixed values of  $S/R$  of a polymer. The calculations were done for  $\alpha = 0.2, 0.5$  and  $0.8$  and several (fixed) values of  $S/R$  at 0.1 interval. These plots are shown in Figs. 3.9(A), (B) and (C), respectively, where the  $S/R$  values are indicated.

In the second construction, the change in the entropy with change in both  $P$  and  $T$  are considered. For this purpose, the surfaces of  $S/R$  for  $\alpha = 0.2, 0.5$  and  $0.8$  are constructed in the  $T, P$  plane. These are shown in Fig. 3.10. The surfaces show the variation of the various quantities and the changes in  $S/R$  that would occur when for a given  $\alpha$ , either  $T$  or  $P$ , or both, are varied. A change in  $\alpha$  in this construction shifts  $S/R$  to another surface. The surfaces can be used to determine how  $S/R$  would change when polymerization occurs with either fixed  $T$  or fixed  $P$ , or with varying  $T$  and  $P$ .

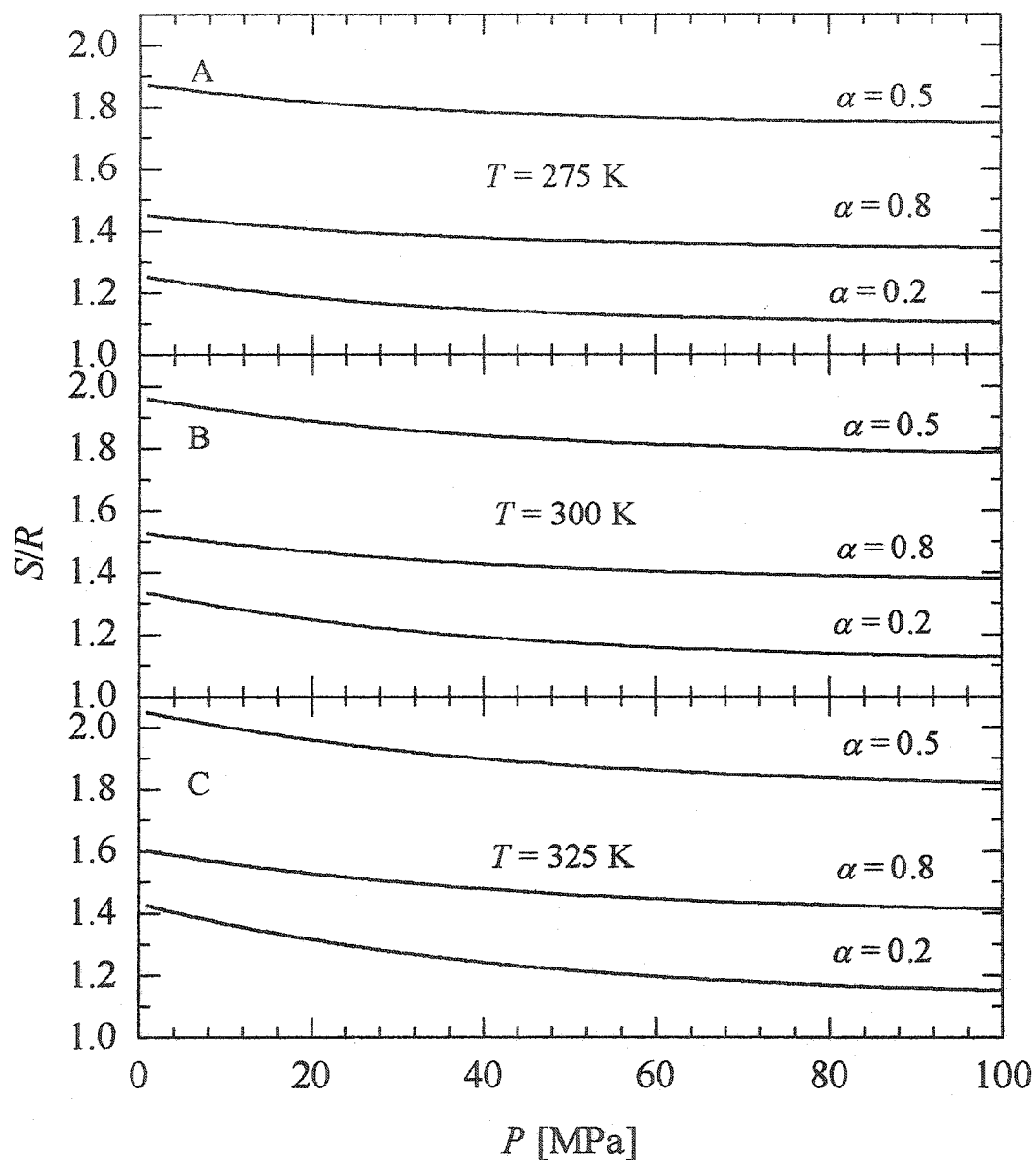


Fig. 3.8. The net configurational entropy ( $S/R = S^{(\text{mix})}/R + S^{(z,\alpha)}/R + S^{(\alpha)}/R + S^{(f,\alpha z)}/R + S^{(\theta,\alpha)}/R$ ), as calculated here is plotted against the pressure. The curves are for the extent of polymerization, 0.2, 0.5 and 0.8. The plots in panels A, B, and C, were calculated at temperatures of 275 K, 300 K and 325 K, respectively.

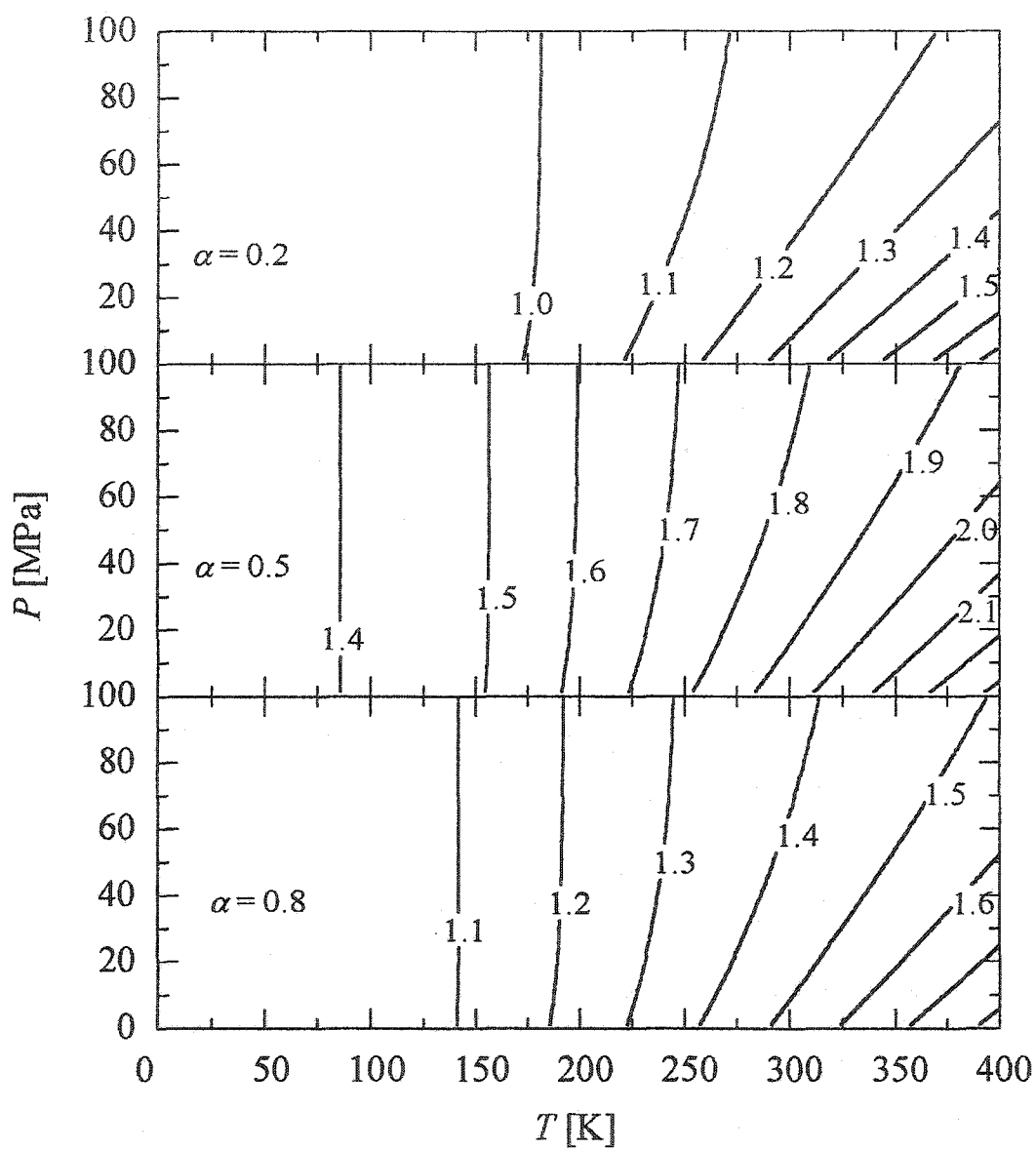


Fig. 3.9. The plots of pressure against temperature for different fixed configurational entropy. The entropy values are indicated. The plots in panels A, B and C are for the extent of polymerization, 0.2, 0.5 and 0.8, respectively.

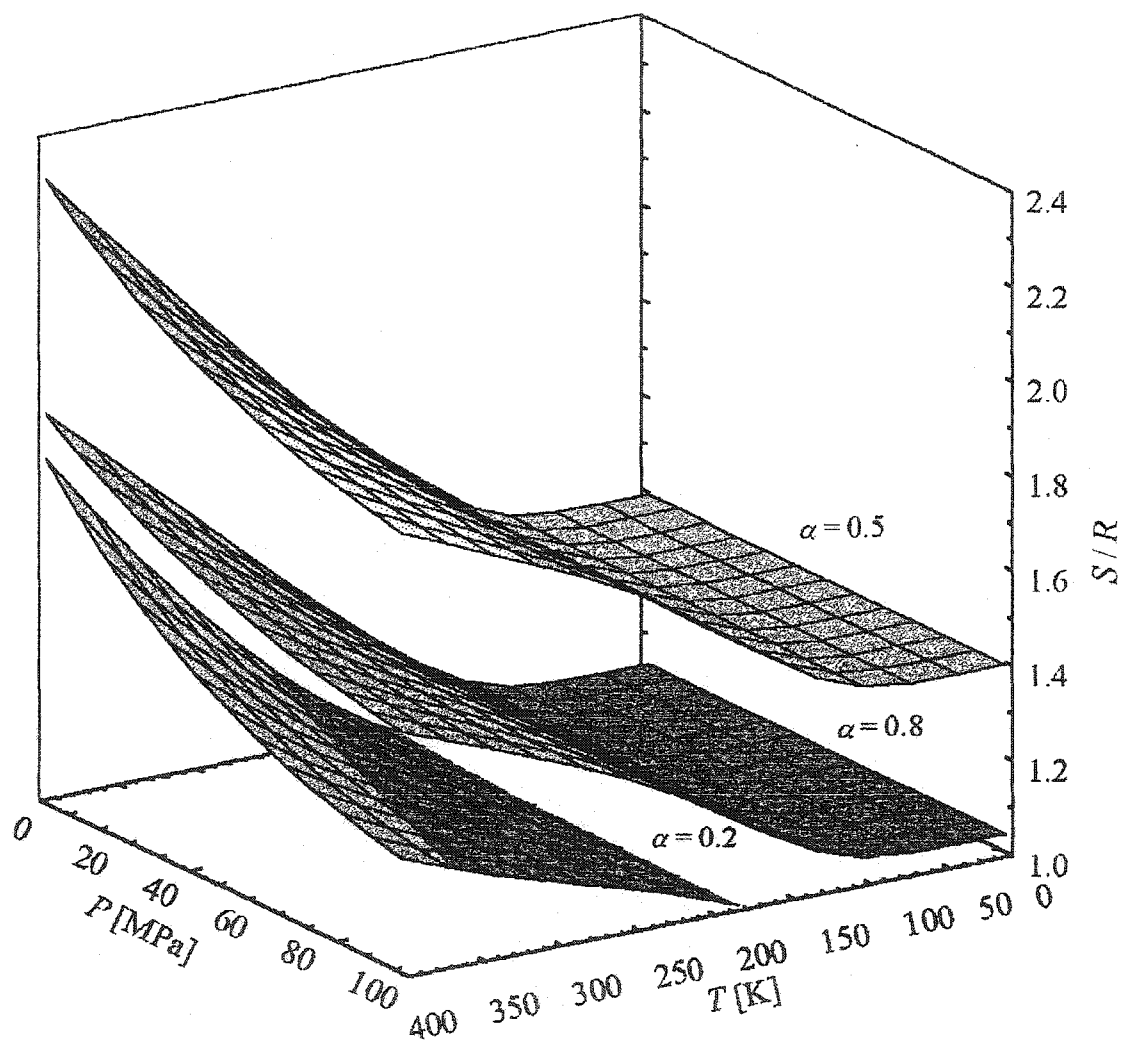


Fig. 3.10. The net configurational entropy ( $S/R = S^{(\text{mix})}/R + S^{(z,\alpha)}/R + S^{(\alpha)}/R + S^{(f,\alpha,z)}/R + S^{(\theta,\alpha)}/R$ ) surface in the temperature and pressure plane, as calculated for the extent of polymerization, 0.2, 0.5 and 0.8, as indicated.

### 3.4.3 The effects of pressure on configurational heat capacity

The configurational contribution to the equilibrium heat capacity,  $C$ , also changes with  $T$ ,  $P$  and  $\alpha$ . We calculate  $[C^{(f,z,\alpha)}/R]$  from Eq.(3.32) numerically for the condition that  $f$  is a function of  $x$ , as given by Eq. (3.28). We also calculate  $C^{(\theta,\alpha)}/R$  from Eq. (3.31) for which  $\theta$  is calculated from Eqs. (3.20), (3.22) and (3.34).

For the same  $\alpha$  values as used here for calculating  $S^{(\theta,\alpha)}/R$  and  $S^{(f,z,\alpha)}/R$ , we calculate  $C^{(\theta,\alpha)}/R$  and  $C^{(f,z,\alpha)}/R$  as a function of pressure at 275 K, 300 K and 325 K. Since the  $S^{(\text{mix})}/R$ ,  $S^{(\alpha)}/R$  and  $S^{(z,\alpha)}/R$  terms do not vary with  $T$ , they do not contribute to the heat capacity and therefore the net  $C/R$  is only the sum of  $C^{(\theta,\alpha)}/R$  and  $C^{(f,z,\alpha)}/R$  terms. This net  $C/R$ , is plotted against  $P$  in Figs. 3.11(A), (B) and (C) at 275 K, 300 K and 325 K, respectively, each for  $\alpha$  values of 0.2, 0.5 and 0.8. Variation of  $C/R$  ( $= C^{(\theta,\alpha)}/R + C^{(f,z,\alpha)}/R$ ) as a function of  $\alpha$  at 300 K at 0.1 MPa is already shown in Fig. 3.3(B). Since this is the only structural contribution to the heat capacity, the plots of  $C/R$  against  $P$  in Fig. 3.11 represent the configurational heat capacity. The vibrational contribution is not considered here.

The plots in Fig. 3.11 show that, like the quantity  $[S^{(\theta,\alpha)}/R + S^{(f,z,\alpha)}/R]$ , the quantity  $C/R[C^{(\theta,\alpha)}/R + C^{(f,z,\alpha)}/R]$  is also a decreasing function of  $T$  and  $P$  for all values of  $\alpha$ , and that its variation with  $P$  is non-linear. Increase in pressure decreases  $C/R$  more at a high temperature and low pressures than it does at a low temperatures and high pressures, i. e., the derivative,  $dC/dT$ , decreases with decrease in  $T$  at a fixed  $P$ , and the derivative,  $dC/dP$ , decreases with increase in  $P$  at a fixed  $T$ . Inter-comparison of the plots in Fig.

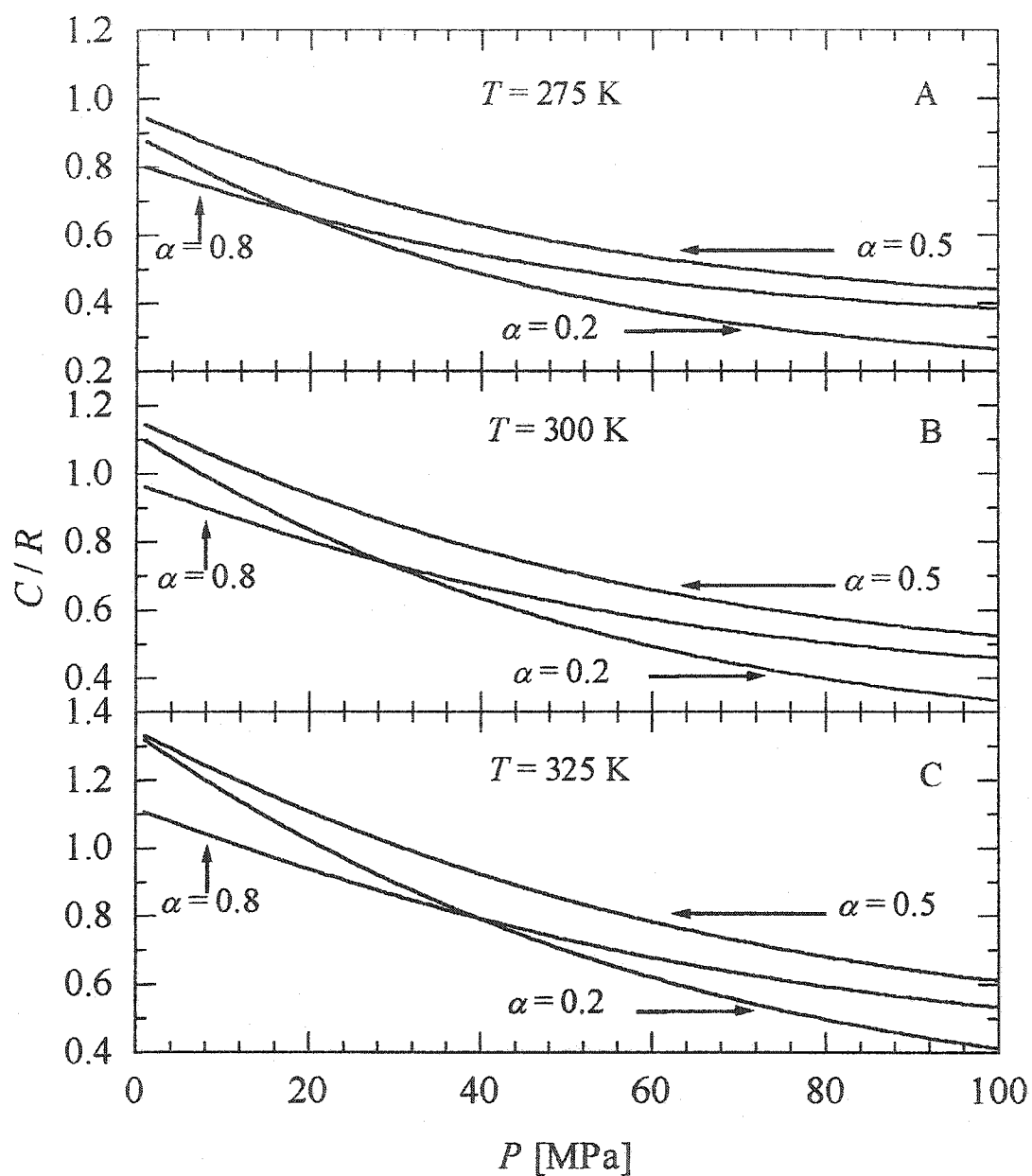


Fig. 3.11. The configurational heat capacity ( $= C^{(f,\alpha,2)}/R + C^{(0,\alpha)}/R$ ), is plotted against the pressure. The curves are for different extents of polymerization, 0.2, 0.5 and 0.8. The plots in Panels A, B, and C were calculated at temperatures of 275 K, 300 K and 325 K, respectively.

3.11 also shows that for a fixed  $P$  and  $T$ ,  $C/R$  initially increases when  $\alpha$  increases from 0.2 to 0.5 and then decreases to a certain value when  $\alpha = 0.8$ , i. e., the derivative  $dC/d\alpha$ , for a fixed  $P$  and  $T$  initially has a positive value, which becomes zero as  $\alpha$  increases toward a certain value, and then finally becomes negative.

#### 3.4.4 Entropy and heat capacity changes with pressure

We first consider the various entropy contributions and their variations with  $\alpha$  and  $P$  at 300 K, as described in Fig. 3.7. Since the population of holes for fixed values of  $\alpha$  varies with both  $T$  and  $P$  and the flexibility varies only with  $T$ , the magnitude of the term  $S^{(\theta,\alpha)}/R$  depends upon  $\alpha$  and also upon both  $P$  and  $T$ , while that of  $S^{(f,z,\alpha)}/R$  depends upon  $\alpha$  and not upon  $T$ . (Note that the magnitudes of  $S^{(\alpha)}/R$  and  $S^{(\text{mix})}/R$  vary with  $\alpha$  only,  $S^{(z,\alpha)}/R$  varies with  $\alpha$  and  $z$  only, and remains constant with changing  $T$  and  $P$ , as indicated in Figs. 3.10). Comparison of the curves in Figs. 3.7(A), (B) and (C) shows that for all pressures, the magnitude of  $S^{(\theta,\alpha)}/R$  decreases with increase in  $\alpha$  and increases with increase in  $T$ . At a fixed  $T$ ,  $S^{(\theta,\alpha)}$  decreases monotonically with increase in  $P$ , as if it is approaching its limiting value of zero. The slope of the plots, or  $(dS^{(\theta,\alpha)}/dP)_T$ , decreases with increase in  $P$ , tending towards zero in the high pressure limit. For all pressures,  $(dS^{(\theta,\alpha)}/dP)_T$ , decreases when  $\alpha$  is increased.

There is an additional variation of the entropy contribution with  $\alpha$  and  $T$  that comes from the flexibility term,  $S^{(f,z,\alpha)}/R$ . As has been shown in Fig. 3.3(B), when  $\alpha$  increases, the  $S^{(f,z,\alpha)}/R$  term first increases, reaches a maximum value and then decreases as  $\alpha$  approaches 1. But the  $S^{(\theta,\alpha)}/R$  term which varies with both  $T$  and  $P$ , decreases

monotonically with increase in  $\alpha$ . It crosses the maximum, or hump in the plot of  $S^{(f,z,\alpha)}/R$ . Also, as shown in Fig. 3.5(A), the magnitude of the  $S^{(f,z,\alpha)}/R$  term for a fixed pressure of 0.1 MPa increases with  $T$  in a sigmoid shape manner. The net effect of temperature on the entropy therefore is obtained from the sum of  $S^{(\theta,\alpha)}/R$  and  $S^{(f,z,\alpha)}/R$  terms.

In Fig. 3.8, the net entropy ( $S/R = S^{(\text{mix})}/R + S^{(z,\alpha)}/R + S^{(\alpha)}/R + S^{(f,\alpha z)}/R + S^{(\theta,\alpha)}/R$ ) is plotted against  $P$  at 275 K, 300 K and 325 K for  $\alpha = 0.2, 0.5$  and  $0.8$  at each  $T$ . It is evident that the net entropy decreases with increase in  $P$  for a fixed  $T$  and  $\alpha$ , and that is increases with increase in  $T$  at a fixed  $P$  and  $\alpha$ . Moreover the slope of the plots,  $(dS/dP)$ , varies with all the three variables  $P, T$  and  $\alpha$ . These plots show a combination of the effects of increase in  $\alpha$  and in  $T$ . As  $\alpha$  increases, the term  $S^{(\theta,\alpha)}/R$  decreases and a maximum appears in the values of  $S^{(f,z,\alpha)}/R, S^{(\text{mix})}/R, S^{(z,\alpha)}/R$  and  $S^{(\alpha)}/R$  in the  $\alpha$ -plane, as has been shown in Fig. 3.3(A). As  $T$  increases, both the  $S^{(\theta,\alpha)}/R$  and  $S^{(f,z,\alpha)}/R$  terms increase in their characteristic manners, as discussed in the preceding paragraph.

We now consider the plots of pressure against the temperature for fixed values of the net entropy,  $S/R$ , as seen in Fig. 3.9. These show that for a fixed value of  $S/R$ , the plot shifts to lower  $T$  as  $\alpha$  increases from 0.2 to  $\sim 0.5$  and thereafter the plot shifts to higher  $T$  as  $\alpha$  increases to 0.8. The plots also show that for  $P = 0.1$  MPa. The slopes for a fixed  $\alpha$  value,  $(dP/dT)_\alpha$ , rapidly decreases as  $S/R$  increases, and for fixed  $\alpha$  and  $S/R$  values,  $(dP/dT)_\alpha$  increases as  $T$  increases, i.e, to maintain  $S/R$  at a constant value, the pressure needed at a higher  $T$  is more than the pressure needed at a lower  $T$ . Since  $S^{(\text{mix})}/R, S^{(z,\alpha)}/R$

and  $S^{(\alpha)}/R$  do not depend upon  $T$ , and both  $S^{(f,\alpha,z)}/R$  and  $S^{(\theta,\alpha)}/R$  do, it appears that, as  $T$  increases, the pressure-dependent term  $S^{(\theta,\alpha)}/R$  becomes relatively less prominent than the temperature sensitive term,  $[S^{(f,\alpha,z)}/R + S^{(\theta,\alpha)}/R]$ . This indicates that the effect of a decrease in the hole occupancy with increase in  $P$  is less than the combined effects of increase in the hole occupancy and flexibility with increase in  $T$ .

By comparison of the curves in the three panels of Fig. 3.11, it becomes evident that for  $\alpha$  of 0.2, 0.5 and 0.8,  $C/R$  decreases with increase in  $P$  and increases with increase in  $T$ . The rate of decrease with increase in  $P$  is highest for  $\alpha = 0.2$  and lowest for  $\alpha = 0.8$  and consequently their respective curves cross over. This means that, although the  $C^{(\theta,\alpha)}/R$  term varies with  $P$  in different ways for different values of  $\alpha$ , the net effect is such that  $C^{(\theta,\alpha)}/R$  approach the same value at a certain  $P$ . A comparison of the plots in Fig. 3.11(A) against Fig. 3.11(C) indicates that the cross-over pressure for  $\alpha = 0.2$  and  $\alpha = 0.8$  curves increases with increase in  $T$ . The higher value of  $C/R$  for  $\alpha = 0.5$  also implies that there is a maximum in  $C/R$  against  $\alpha$  plot at a fixed pressure.

We now consider the observation in terms of the configurational states of a polymer. In terms of the energy landscape [Goldstein (1969)] or inherent structure model [Debenedetti and Stillinger (2001)], as a system's  $T$  is raised at a fixed volume, the probability that its configurations will occupy states corresponding to the higher energy minima of potential energy increases. Consequently, the probability of finding the system's configurations in a multiplicity of different higher energy minima increases, and the system's  $S_{\text{conf}}$ , which is here equal to the sum,  $[S^{(\theta,\alpha)}/R + S^{(f,z,\alpha)}/R]$ , increases. But

increase in  $P$  decreases the volume, which changes the potential energy landscape of the system, for a fixed  $\alpha$  value or a fixed chemical constitution in our study. For different  $\alpha$  values at a fixed volume, the chemical structures differ and therefore the potential landscapes will differ. By varying  $P$  and  $T$  together at a fixed  $\alpha$ , one may maintain a fixed volume and examine whether  $S_{\text{conf}}$  of the system at different  $P$  and  $T$  but fixed volume and fixed  $\alpha$  conditions remain constant. Alternatively, one may determine a variety of  $P$ ,  $T$  conditions for a system of a given  $\alpha$  (fixed chemical structure) and fixed  $S_{\text{conf}}/R$ . These  $P$ ,  $T$  values are plotted in Fig. 3.9. The plots are for  $S/R$  values of 1.0 to 1.5 when  $\alpha = 0.2$ , 1.4 to 2.1 when  $\alpha = 0.5$  and 1.1 to 1.6 when  $\alpha = 0.8$ . It is clear in Fig. 3.9 that the plots of  $P$  in a temperature plane fan-out as  $T$  is increased.

There is little doubt that the decrease in the entropy, enthalpy and volume on polymerization irreversibly (and on decrease in  $T$  and increase in  $P$ , reversibly) are related to the increase in viscosity,  $\eta$ , which ultimately vitrifies a polymerizing liquid as long as the liquid's temperature is lower than the glass softening temperature,  $T_g$  of the fully polymerized state. In terms of the entropy theory [Adam and Gibbs (1958)], as  $S_{\text{conf}}$  decreases,  $\eta$  increases at a fixed  $T$ . Since the temperature-, and pressure-independent terms in the entropy contributions have no role in determining  $\eta$ , and further that  $S^{(\theta,\alpha)}/R$  alone is sensitive to pressure at a fixed polymerization temperature,  $T_{\text{polym}}$ , it alone is equivalent to  $S_{\text{conf}}$ . As any increase in pressure decreases  $S^{(\theta,\alpha)}/R$ , the application of pressure would raise  $\eta$  to above  $10^{13.6}$  Poise at  $T_{\text{polym}}$ , and thus vitrify the liquid. This is equivalent to raising the liquid's  $T_g$  by application of pressure. Thus the vitrification

temperature increases with increase in pressure at a fixed  $T$  and  $\alpha$ . This is consistent with the well-known observation that application of pressure increases  $T_g$  of polymers and of all liquids. Since an increase in  $\alpha$  at a fixed  $T$  and  $P$  also vitrifies a liquid, there is an equivalence between  $P$  and  $\alpha$  at a fixed  $T$ . This equivalence may be determined by making fixed temperature cuts through the various  $S_{\text{conf}}$  surfaces in a  $T, P$  plane, each surface for a different value of  $\alpha$ , as given in Fig. 3.10.

### 3.4.5 The maximum in the entropy and heat capacity

A comparison of the plots for different  $\alpha$  values in Figs. 3.8 shows that there would be a local maximum in the net entropy,  $S/R$ , at a certain value of  $\alpha$ . Similarly the plots of the net heat capacity,  $C/R$ , in Fig. 3.11 show that there would be a maximum in its plot against  $\alpha$ . For a fixed temperature of 300 K, the  $S/R$  and  $C/R$  values were calculated at 0.1 MPa, 10 MPa and 100 MPa at different values of  $\alpha$ . The  $S/R$  are plotted against  $\alpha$  in Fig. 3.12(A). The plots show a broad maximum whose position shifts slightly to higher  $\alpha$  as  $P$  is increased. The corresponding plots of  $C/R$  also show a maximum in Fig. 3.12(B). This maximum shifts to a higher  $\alpha$  values with increase in  $P$ .

We now consider why  $C/R$  shows a maximum in its plot against  $\alpha$ . To do so we return to the manner in which the polymerization process has been considered here. As the polymer chain grows by formation of one C-C bond, the structure of the liquid changes and its configurational state enters a new potential energy landscape [Goldstein (1969), Debenedetti and Stillinger (2001)] with different number of energy minima of different depths and shape. This would also occur if the number of covalent bonds

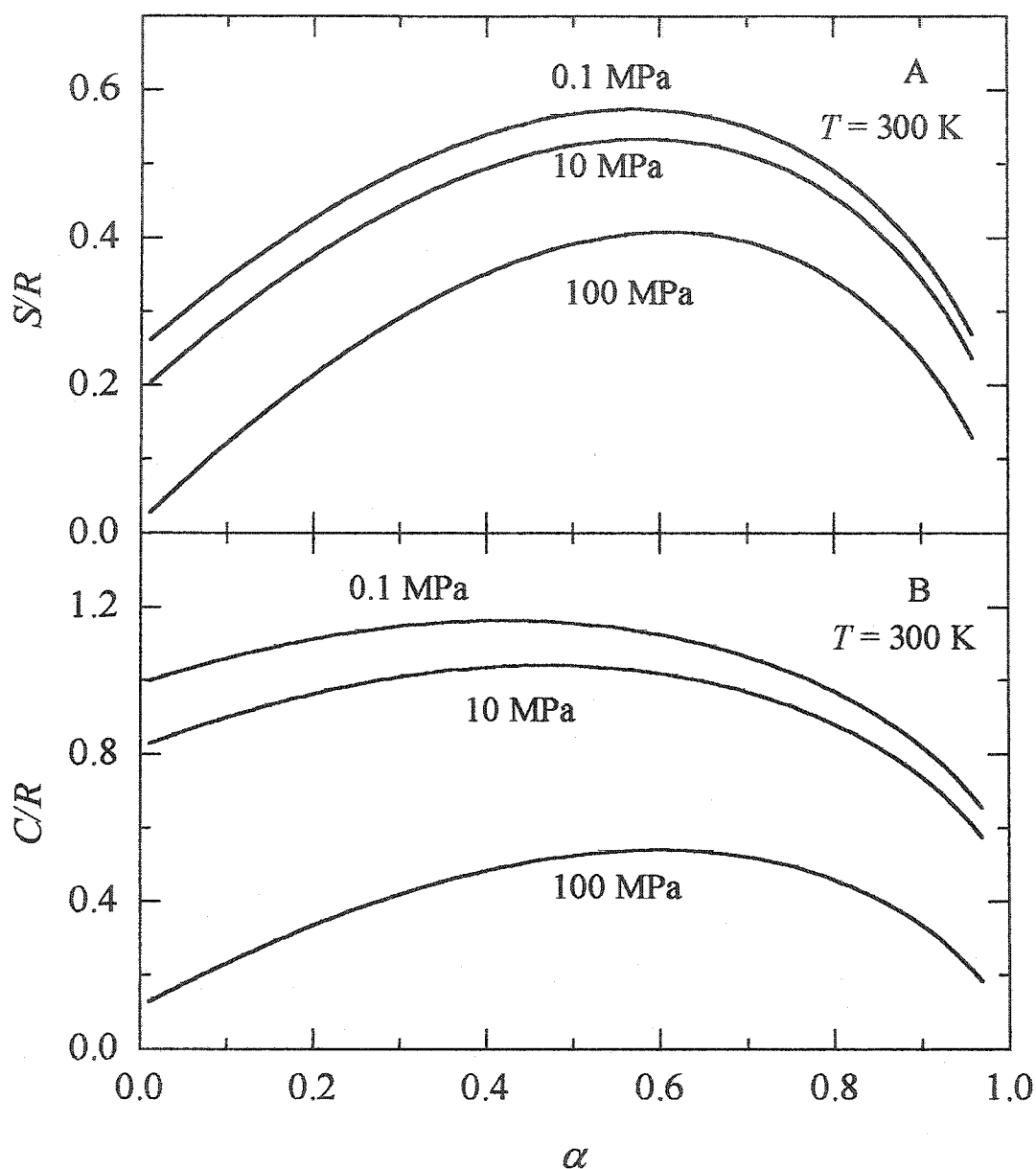


Fig. 3.12. (A). The net configurational entropy,  $S/R$  ( $= S^{(\text{mix})}/R + S^{(z,\alpha)}/R + S^{(\alpha)}/R + S^{(f,\alpha z)}/R + S^{(\theta,\alpha)}/R$ ) is plotted against the extent of polymerization occurring at three pressures, 0.1 MPa, 10 MPa and 100 MPa, and at a fixed temperature of 300 K, as indicated. (B). The configurational heat capacity ( $= C^{(f,\alpha z)}/R + C^{(\theta,\alpha)}/R$ ) is plotted against the extent of polymerization for the corresponding  $P$  and  $T$  conditions.

remained the same in the polydisperse system but the molecular weight distribution changed by one less C-C bond on one chain and one more C-C bond in another chain. It is not possible to describe such a new energy landscape quantitatively, but some idea may be gained in qualitative terms. Since  $\eta$  of the equilibrium liquid increases as  $\alpha$  increases at a fixed value of  $T$  and  $P$ , this means that the number of available minima in the energy landscape for that thermal energy decreases. For fixed  $T$  and  $P$  conditions, a decrease in the number of available minima is possible only if the new potential energy surface of an  $\alpha$  with one more C-C bond were to contain a greater population of deeper energy minima than the potential energy surface of the initial state of one less C-C bond.

#### 3.4.6 The Viscosity of a Polymer System at Different Pressures and Temperatures

According to Adam and Gibbs' (1958) configurational entropy theory, the viscosity of a liquid can be related to its configurational entropy by:

$$\eta = \eta_0 \exp(C / TS_c) \quad (3.35)$$

where  $\eta_0$  is the pre-exponential factor,  $C$  is a constant and its dependence on temperature is neglected, and  $S_c$  is the configurational entropy of the liquid. From Eq. (3.35) we obtain:

$$\ln \frac{\eta}{\eta_0} \propto 1 / TS_c \quad (3.36)$$

For a polymer system with fixed  $\alpha$ ,  $S^{(mix)}/R$ ,  $S^{(z,\alpha)}/R$  and  $S^{(\alpha)}/R$  are independent of the temperature and pressure,  $S^{(f,\alpha z)}/R$  depends on temperature but not on pressure. Since only  $S^{(\theta,\alpha)}/R$  changes with pressure and temperature, only this part of the configurational

entropy will contribute to the change of viscosity when the pressure and temperature are varied.

For convenience, we calculate  $R/[TS^{(\theta,\alpha)}]$ , which is proportional to  $\ln \frac{\eta}{\eta_0}$ , as a function of both the temperature and pressure for fixed values of  $\alpha = 0.2, 0.5$  and  $0.8$ . The plots of  $R/[TS^{(\theta,\alpha)}]$  against  $1000/T$  for  $P = 500, 400, 300, 200, 100, 50$  MPa are shown in Fig. 3.13. The plots of  $R/[TS^{(\theta,\alpha)}]$  against  $P$  for  $T = 550, 500, 450, 400, 350, 300, 250$  K are shown in Fig. 3.14. From Fig. 3.13, we have already found that the curves of  $R/[TS^{(\theta,\alpha)}]$  against  $1000/T$  at different values of fixed pressure are concave upward, and diverge from each other with the increase of  $1000/T$ , i.e., the curves are fanning-out. From Fig. 3.14, we found that the curves of  $R/[TS^{(\theta,\alpha)}]$  against  $P$  at different values of fixed temperature are also concave upward and fanning-out. But the separation between the curves of  $R/[TS^{(\theta,\alpha)}]$  against  $P$  at different fixed  $T$  in Fig. 3.14 is much less than the separation between the curves of  $R/[TS^{(\theta,\alpha)}]$  against  $1000/T$  at different fixed  $P$  in Fig. 3.13. Such “fanning-out” behavior had been observed experimentally in the plots of  $\log(\eta)$  against  $1000/T$  at different densities, which is equivalent to different pressure, for triphenyl phosphite [Ferrer *et al.* (1998)], in the plots of  $\log(\eta)$  against  $P$  at different fixed  $T$  for ortho-terphenyl and salol [Schug *et al.* (1998)], in the plots of  $\log(\tau)$  against  $P$  at different fixed  $T$  obtained from light scattering of poly(bisphenol A-co-epichlorohydrin), glycidyl end capped [Paluch *et al.* (2000)], and in the plots of  $\log(\tau)$  against  $P$  at different fixed  $T$  obtained from dielectric relaxation spectroscopy of triphenylmethane triglycidyl ether [Paluch (2001)].

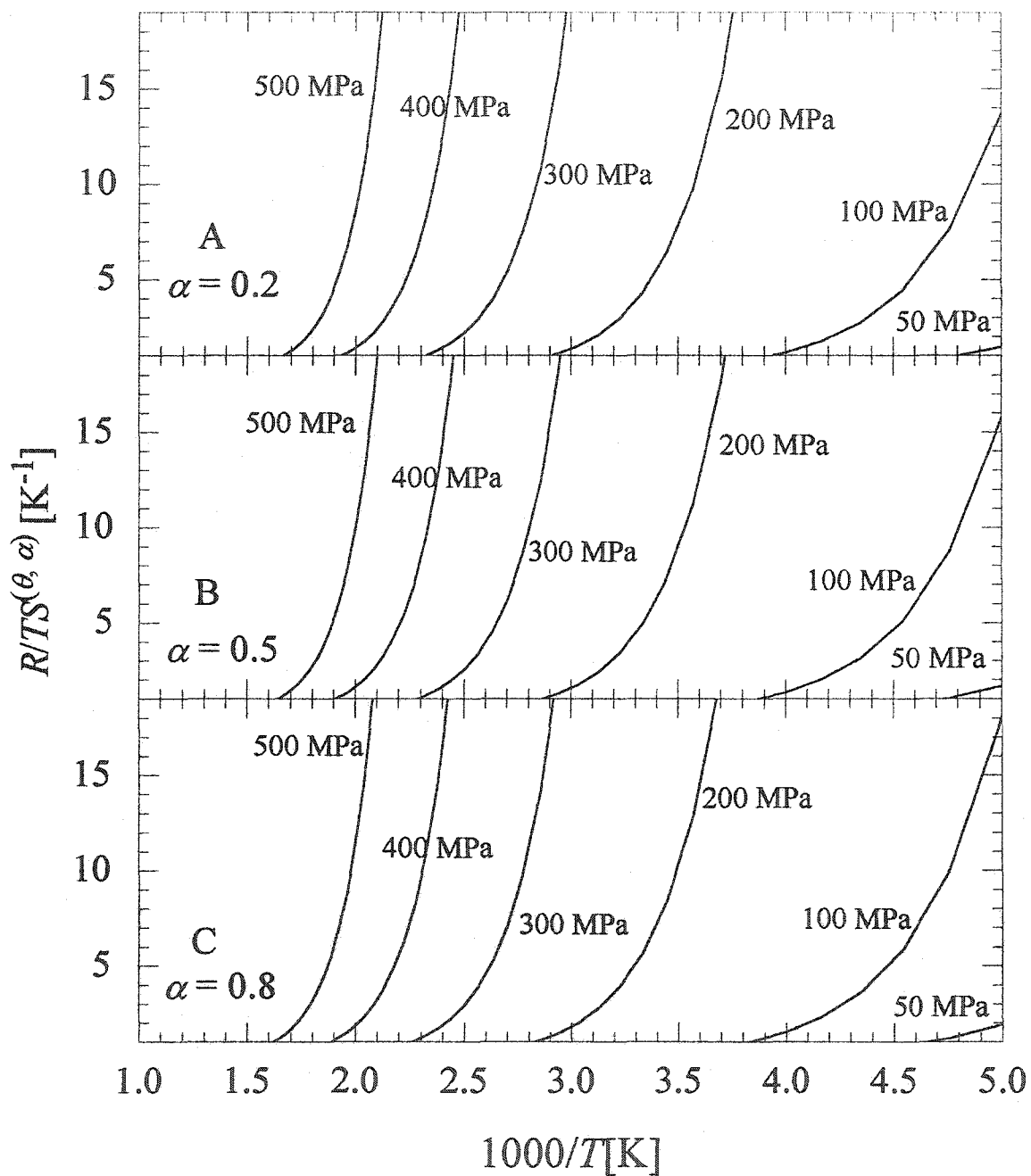


Fig. 3.13. The calculated  $R/[TS^{(\theta, \alpha)}]$  which is proportional to  $\ln(\eta/\eta_0)$ , is plotted against  $1000/T$ . The curves are for  $P = 500, 400, 300, 200, 100, 50$  MPa. The plots in Panels A, B, and C were calculated for different extents of polymerization, 0.2, 0.5 and 0.8, respectively.

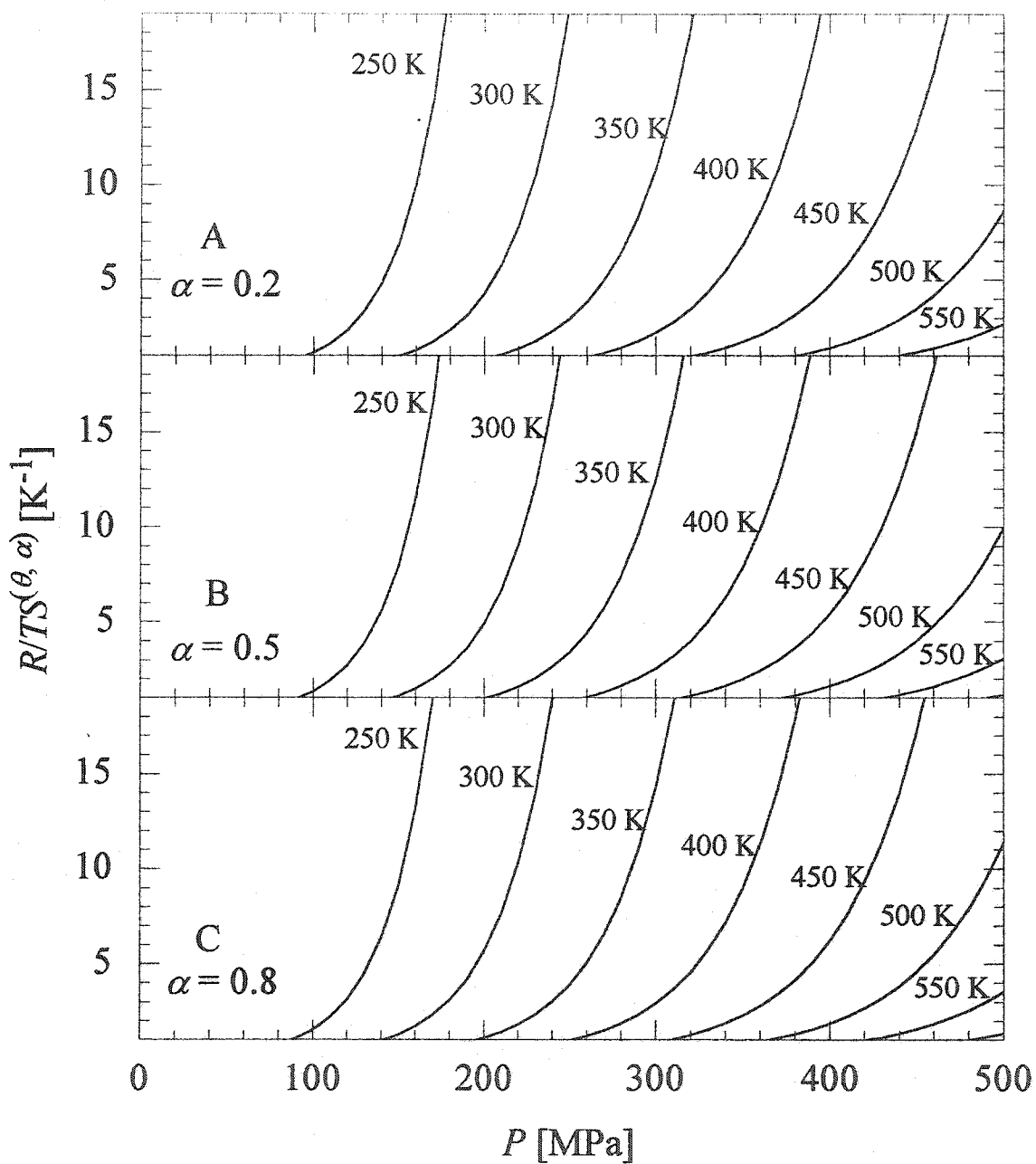


Fig. 3.14. The calculated  $R/[TS^{(\theta, \alpha)}]$  which is proportional to  $\ln(\eta/\eta_0)$ , is plotted against pressure. The curves are for  $T = 550, 500, 450, 400, 350, 300, 250$  K. The plots in Panels A, B, and C were calculated for different extents of polymerization, 0.2, 0.5 and 0.8, respectively.

We also calculated  $R/[TS_c]$  at different fixed  $P$  and  $R/[T(S^{(f,\alpha z)} + S^{(\theta,\alpha)})]$  at different fixed  $T$  (plots not shown here). Neither the plots of  $R/[TS_c]$  against  $1000/T$  at different fixed  $P$  nor the plots of  $R/[T(S^{(f,\alpha z)} + S^{(\theta,\alpha)})]$  against  $P$  at different fixed  $T$  show fanning-out. This may imply that only the contribution from the hole occupancy to the configurational entropy of a polymer system,  $S^{(\theta,\alpha)}$  is responsible for the entropy in Adam and Gibbs's theory (1958). We conclude that the use of  $S^{(\theta,\alpha)}$  in Eq. (3.35) for Adam and Gibbs' entropy theory should be valid also for a molecular system. Johari's (2003) inclusion of the  $P\Delta V$  term in their equation extends this analysis.

### 3.5 Summary

Computations of the contributions to the configurational entropy done within the precepts of the lattice-hole model, but with different and more realistic mean field approximation, show that the configurational heat capacity and entropy of an equilibrium liquid undergoing polymerization isothermally would first increase as the extent of polymerization increases and then decrease, thus showing a broad maximum in a plot against the extent of polymerization. The position of this maximum varies with the temperature of polymerization. Of the five contributions to the configurational entropy, four show a maximum in their plots against the extent of polymerization, but only one of these four contributes to the configurational heat capacity. It is shown that if the polydispersity in the frozen-in liquid structure or that developing during a liquid's polymerization was deliberately inhibited by the interaction of molecules with the container and impurities in the liquid, the configurational entropy would not reach zero at

0 K. Rather, it will remain finite at values that are equal to the temperature-independent entropy of mixing of the entities in a polydispersed system, even when the number of holes in the system has reached zero. This is analogous to the finite entropy of an isotopic mixture of elements or compounds in the crystal state. Only if the polydispersity was lost and a single chain was formed at 0 K, then the entropy would tend to zero.

The finding of the maximum in the heat capacity as polymerization occurs is consistent with the experimental observations that have showed that the heat capacity of the equilibrium state of a polymerizing mixture reaches a maximum before decreasing according to an inverted sigmoid shape when the liquid vitrifies. In the equilibrium state the heat capacity plot against the extent of polymerization shows only the broad maximum and no inverted sigmoid shape [Johari et. al. (1999)]. Only this broad maximum would be found experimentally if polymerization temperature is high enough that the completely polymerized state remains a liquid.

Independent experiments on polymerization in systems that do not vitrify on complete polymerization have more recently been performed with the aim of determining whether this maximum can be observed. In this study [Johari, et. al. (2002)], the heat capacity has been measured during the course of polymerization of diglycidyl ether of bisphenol-A (DGEBA), and Cyclohexylamine (CHA) by a new technique of temperature modulated calorimetry, as described in Chapter 2. The measured data provided the net heat capacity, i.e., the sum of configurational, vibrational and anharmonic force contributions, which showed a maximum. But the maximum was found to shift toward higher  $\alpha$  values when the polymerization temperature was decreased. The difference

between the shift observed from calculations and that found experimentally is attributable to the extra contributions from phonons and anharmonic forces which change with  $\alpha$ .

The calculations also show that the temperature-dependent entropy would become zero for all distributions of chain lengths when no holes are left at 0 K. For a pure monodispersed polymer, *i.e.*, without the entropy of mixing, the total configurational entropy of the system containing (theoretically) infinitely long chains, would approach zero at 0 K. This formalism removes the problem of a hypothetical second order transition at an (unobservable) temperature below  $T_g$ , which had been deduced in the original chain statistics model by Gibbs and DiMarzio (1958). The calculations given here seem reasonably general, although we have ignored any local correlation of molecular orientations, which may also play a role. This is done in favor of a self-consistent approach to polymer chain statistics during an irreversible process of a macromolecule's growth.

The mean field approximation used here has made the temperature dependence of the configurational entropy of polymer chains to agree with the third law of thermodynamics, *i.e.*, that the entropy should approach zero only at 0 K. In addition, the statistical model with a new mean field approximation developed here has provided us an approach to the study of the kinetics of polymerization and relations between the thermodynamic properties and the extent of polymerization. This statistics may be used in reverse for degradation of polymers in which a polymer chain length is decreased at random sites by ultraviolet or other high-energy irradiation.

In this formalism, a liquid with a structure chosen from a multiplicity of its partially polymerized states may be vitrified by cooling both experimentally and theoretically and can be mutually compared. In this case, each state would follow a different path of the heat capacity, and entropy, which provides structural information on the polymer, as proposed by others earlier [Petroff *et. al.* (1996)] by using more approximate models.

Finally, it is worth considering the implications of these observations for the use of the potential energy landscape or inherent structure models currently used for computer simulation of the configurational entropy of liquids [Goldstein (1969), Debenedetti and Stillinger (2001)]. During melt polymerization at a constant temperature, the potential energy landscape does not remain fixed. As covalent bonds form, the number of configurations changes, and the system's state belongs to a new configurational space in new energy landscape, i.e., the system continuously shifts into a different energy landscape with increase in the extent of polymerization. For a polymer system with  $N_A$  number of monomers, supposing the extent of polymerization is 0.1, i.e., 0.1  $N_A$  number of bonds have been formed, there would be at least 0.1  $N_A$  number of new energy landscapes, and much more if the distribution of chain lengths is considered. The current capability at computer simulation, which allows use of a limited number of atoms ( $10^3$ - $10^6$ ) in an ensemble, may show the features deduced from our mean field approximation, but would require inclusion of additional terms for the entropy of mixing.

## **Chapter 4**

# **Structure and Thermodynamics of a New Orientational Glass, CuCN**

### **4.1 Introduction**

We have so far considered the dynamics of a polymer chain whose segments are oriented at random. There are also crystals in which linear chains formed by atoms or ions, can exist and occupy the lattice sites. These chains can exist in conditions of partial disorder. Such chains, which are usually in one dimension along a crystal lattice, provide a simpler model for the chain statistics. The majority of such crystals have an orientational disorder of atoms or molecules, and their kinetically frozen disordered state has been called an orientational glass. Most such crystals consist of non-spherical molecules that occupy the lattice sites of a crystal. At high temperatures these molecules undergo hindered rotations, in a manner similar to those of molecules in a liquid, in which translational diffusion also occurs. Molecules in such crystals have an orientational degree of freedom at high temperatures, which kinetically freezes at low temperatures just as the molecular motions in liquids kinetically freeze at their vitrification temperature. As the temperature is

lowered, the material can bypass its first-order transition to a perfectly-ordered crystal, and supercool. On supercooling, the rotational motions become progressively slower and the time scale of their motions becomes comparable to the experimental time scale. At this temperature, the structure kinetically freezes into what is called an orientational glass [Höchli *et. al.* (1990)]. Because molecules in these solids occupy crystal lattice sites, the kinetic freezing, which is phenomenologically equivalent to a glass transition, can also be modeled. Such modeling is less complicated because of the absence of the translation diffusion of molecules.

Configurational excitations of the non-spherical rigid groups confined to lattice sites, which have also been called the “configurons”, are seen as useful for understanding the manner in which slowing of molecular diffusion vitrifies a liquid. In the 1980s, different compositions of mixed KCN - KBr crystals were seen as an “orientational glass”. (In contrast, an archetype of canonically disordered solids is SiO<sub>2</sub>). This is mainly because freezing-in of the orientations of their ellipsoid-shaped CN group produced unusual features in their electrical, mechanical and vibrational properties, as reviewed by Höchli *et. al.* (1990). At that time, it had seemed that only mixed crystals could be used for this study, even though three entities in such crystals, two anions and one cation, had complicated interpretations of their data.

Since our interest is in disordered crystals with linear chains, we searched for such crystals and found that AgCN forms linear chains along the c-axis of its crystal structure in the R3m space group by neutron scattering study [Browmaker *et. al.* (1998)], but there has been no indication whether or not the arrangement of the CN group in such

structures is disordered. We considered copper cyanides containing the cation of the same periodic table group (group IB), that may show the behavior of an orientational glass with linear chains in one dimension. In this chapter we describe experimental studies of even simpler “orientational glasses”, namely, CuCN. We also provide a thermodynamic approach to the configurational entropy and heat capacity changes in the CuCN crystal, based on the chain statistics similar to the lattice model studied in Chapter 3. A multi-nuclear magnetic and quadrupole Resonance study has shown that CuCN molecular structure is composed of linear chains -Cu-C-N- [Kroeker *et. al.* (1999)]. Part of this study has been published in: J. Wang, M. F. Collins and G. P. Johari, *Phys. Rev. B.*, **65**, 180103(2002).

## 4.2 Experimental Methods

CuCN (99.99 % purity) was purchased from Aldrich Chemicals. The as-received sample is of off-white color and its density is 2.92 g/cm<sup>3</sup>. It had been prepared by flocculation of CuCN precipitate from an aqueous solution as described by Barber (1943). The particle size of the as-received CuCN was 1 - 5 μm, which became air-borne easily. On heating to 593 K in an Argon atmosphere and cooling back to 298 K, its color changed from white to beige. After such heat treatment, its particles appeared to repel each other when attempts were made to grind it in an agate mortar and pestle.

The powder was mounted on a glass plate, and x-ray diffraction spectra were obtained at 298 K using three instruments. (i) Nicolet diffractometer, which uses the Cu-K<sub>α</sub> radiation to obtain the diffraction pattern in the range 10 ° < 2θ < 50 ° in steps of 0.04

°, (ii) Guinier camera, which uses only the Cu-K<sub>α1</sub> line and (iii) Bruker D8 Advance diffractometer, which also uses the Cu-K<sub>α</sub> radiation in order to obtain the diffraction pattern in the range  $20^\circ < 2\theta < 130^\circ$  in steps of  $0.03^\circ$ .

A differential scanning calorimeter (Perkin-Elmer Corp. model DSC 4) was used for calorimetric studies. The instrument was calibrated with indium for both the temperature and the heat effects. Open and sealed aluminum and copper pans were used to contain the sample and argon was used as the purge gas. The baseline was determined for the empty pans prior to the experiment, and this base line was subtracted from the measured DSC signal. The temperature was corrected for the thermal lag. From repeat measurements, accuracy of the heat of transformation is 2 %.

### 4.3 Structural studies by x-ray diffraction

Powder x-ray diffraction of the as-received CuCN measured at 298 K and of that heated to 533 K and thereafter cooled to 298 K showed no change in the diffraction peaks. The spectra of the latter CuCN sample is shown in Fig. 4.1(A). Standard powder x-ray diffraction data in the literature provides two structures of CuCN, (i) monoclinic (JCPDS 1-492) without unit cell parameters [Norberg and Jacobson (1957)] and (ii) orthorhombic (JCPDS 9-152) in a unit cell with  $a = 1.279$  nm,  $b = 18.14$  nm,  $c = 7.82$  nm,  $Z = 36$ ,  $D_x = 2.951$  g/cm<sup>3</sup> and  $D_m = 2.97$  g/cm<sup>3</sup> but no atomic positions [Cromer *et al.* (1957)]. The peaks observed in Fig. 4.1(A) are attributable to the suggested monoclinic (JCPDS-ICCD 1-492) [Norberg and Jacobson (1957)] and orthorhombic structure (JCPDS-ICCD 9-152) [Cromer *et al.* (1957)], whose lines are shown in Figs. 4.1(B) and 4.1(C),

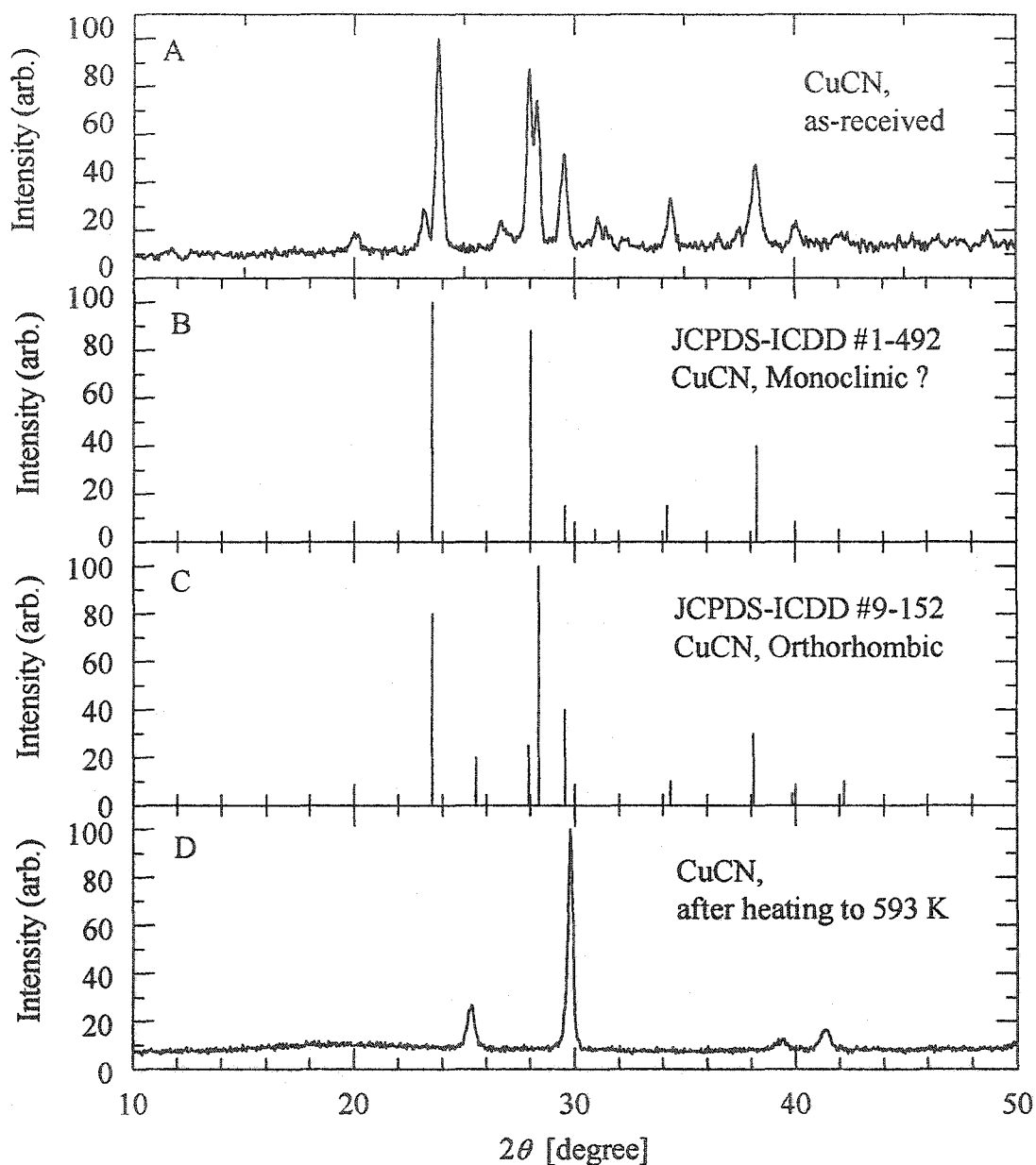


Fig. 4.1. Powder x-ray diffraction patterns of, (A) the as-received CuCN measured at  $\sim 298$  K, (B) the lines and their relative intensities for the reputed structure in the orthorhombic unit cell for suggested monoclinic structure from JCPDS 1- 492, (C) the lines and their relative intensities for the orthorhombic structure from JCPDS 9- 152 and (D) the new phase of CuCN obtained after heating to 593 K in an argon environment and thereafter cooling to 298 K.

respectively. Because of the lack of information about these structures, it was not possible to determine the relative amounts of the two phases in the as-received CuCN.

Powder x-ray diffraction of the CuCN solid, which had been obtained by heating the as-received sample to 593 K in argon atmosphere, is shown at 298 K in Fig. 4.1(D). The peak positions and intensities in the diffraction pattern obtained by using the Guinier camera in the range of  $10^\circ < 2\theta < 90^\circ$  were fitted by Gaussian function, and 11 peaks were identified. The data were input into *CrysFire* program which integrates eight different programs for indexing the powder diffraction data. The several solutions obtained from *TRIOR90* program for possible unit cells were input to another program *CheckCell* and were compared against the entire Guinier diffraction pattern. "Systematic absences" suggested that the space group should be among the  $R3$ ,  $R\bar{3}$ ,  $R3m$ ,  $R\bar{3}m$ , and  $R32$  set. For  $Z = 3$ , i.e., three molecules in the unit cell, this set of rhombohedral unit cells predicts a theoretical density  $D_x$  of  $2.94 \text{ g/cm}^3$ . The  $R3m$  space group was found to fit well and for that group Rietveld refinement of the data obtained from D8 diffractometer was done by using *FullProf* program. This refinement gave satisfactory results.

The Rietveld refinement was then done by choosing C and N positions in the lattice. The best fit for one set of positions for C and N atoms was found to be:  $a = b = 0.6028 \text{ nm}$ ,  $c = 0.4823 \text{ nm}$ ,  $\alpha = \beta = 90^\circ$ , and  $\gamma = 120^\circ$ . Further refinement gave two different, but equally probable, positions of C and N atoms. The final fitting parameters are:  $a = b = 0.6035 \text{ nm}$ ,  $c = 0.4829 \text{ nm}$ , with residual  $R = 5.91 \%$  and  $\chi^2 = 3.25 \%$ . This refinement is compared against the measured diffraction spectra of the CuCN phase in Fig. 4.2, and the atomic positions and occupancies in the unit cell are shown in the insert

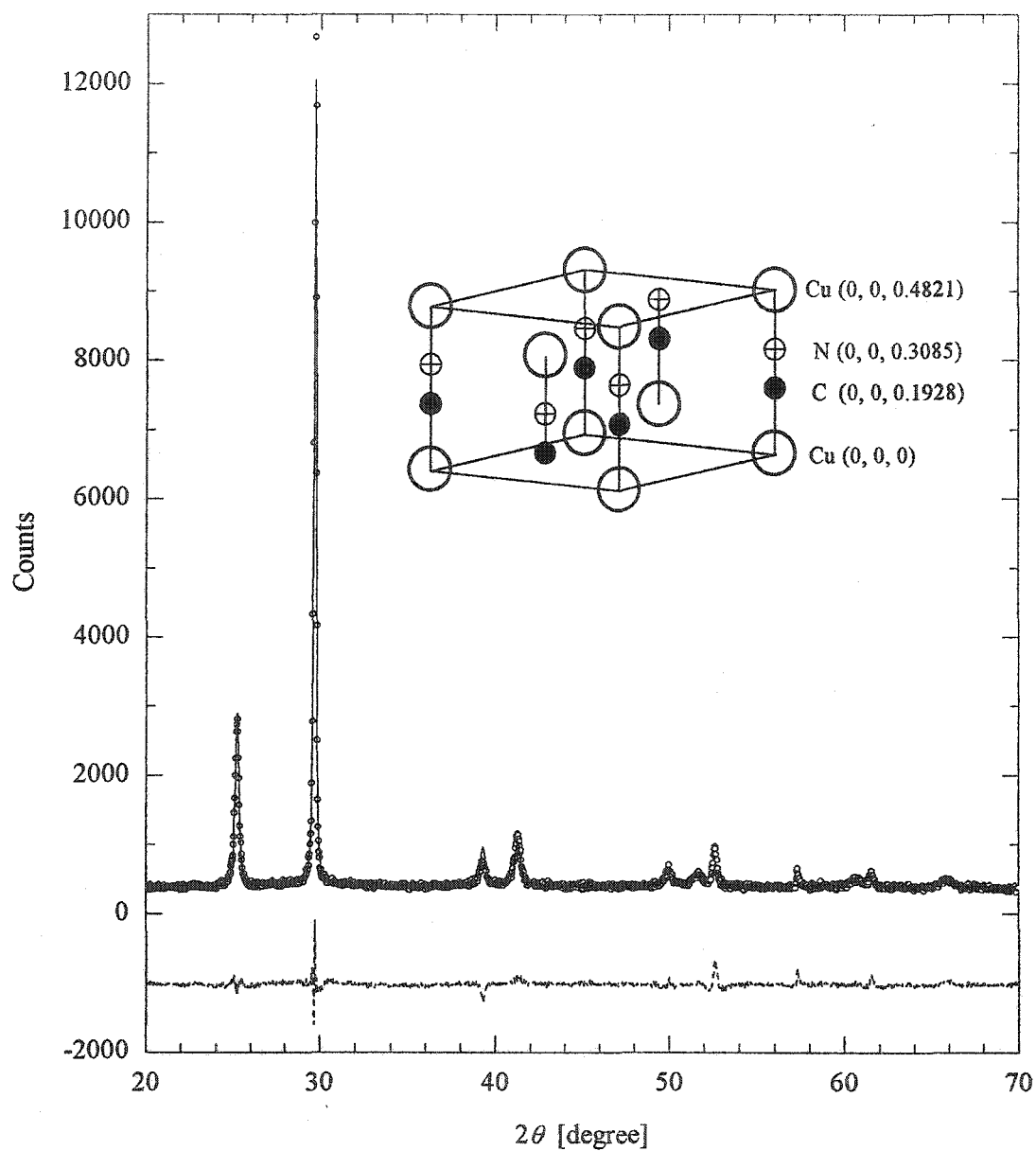


Fig. 4.2. Results of the Rietveld analysis of the powder x-ray diffraction of CuCN after heating to 593 K in an argon environment and thereafter cooling to 298 K. The circle symbols represent the powder x-ray diffraction data and the solid line going through the symbols represents the Rietveld fitting results. The dashed line is the difference between the diffraction data and the fitting results. The dashed line was shifted vertically by -1000 for better illustration. Insert is the unit cell of CuCN structure, with the positions of Cu indicated by large circles, those of C by small filled circles and those of N by small empty circles.

of Fig. 4.2. The final values are:  $x = 0$ ,  $y = 0$ ,  $z = 0$ , and occupancy 1.0 for Cu. The respective values for other atoms are: 0, 0, 0.400 and 0.5 for C(1); 0, 0, 0.648 and 0.5 for N(1); 0, 0, 0.627 and 0.5, for C(2); and: 0, 0, 0.390 and 0.5, for N(2). Inclusion of the anisotropic effect did not lead to further refinement. Because the low atomic scattering factors of C (0.017) and N (0.029) in comparison with Cu (2.0) in x-ray diffraction, it was difficult to resolve the positions of C and N atoms in the CuCN structure from only x-ray diffraction, not even after considering the randomness of the CN orientational groups. Thus according to the structural analysis using the x-ray diffraction, the new CuCN phase has chains of  $(\text{N-Cu-C})_n$  in the crystal, which appear to be confined to one-dimension with a distortion caused by inter-chain interactions.

#### 4.4 Calorimetric studies

The rate of heat release,  $(dH/dt)_q$ , which is equivalent to the specific heat,  $C_p = (dH/dt)_q/q$ , measured on heating the as-received CuCN at  $q = 30$  K/min is shown by curve (1) in Fig. 4.3(A). Since this  $C_p$  is both time and temperature dependent, strictly speaking, it is the "apparent  $C_p$ ", whose magnitude contains the effects of heat released or absorbed by the sample during its structural relaxation. We will use the term  $C_p$  here with the preceding meaning. It shows a broad sigmoid shape rise in the 330 - 380 K range and a large endothermic peak due to the phase transformation in the 550 - 580 K range, as determined from x-ray diffraction and described in Section 4.3. The total heat absorbed in this transformation is 850 J/mol and the transition temperature determined from the slopes of the peak is 563 K. This corresponds to an entropy increase,  $\Delta S$ , by 1.5 J/(mol K) on structural transformation of CuCN. According to the Born-von Karman relation

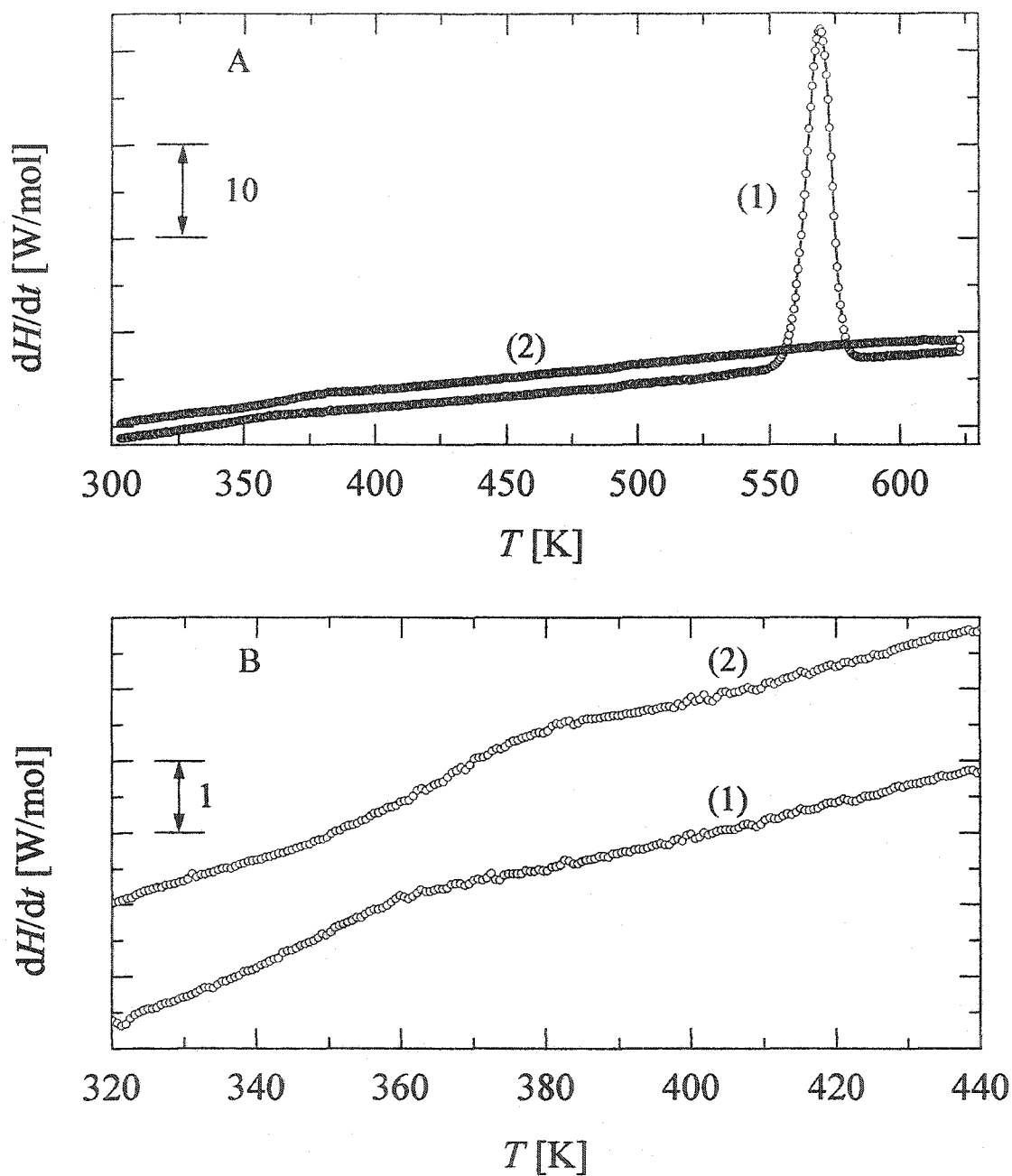


Fig. 4. 3. (A). The differential scanning calorimetry thermogram of CuCN obtained by heating at 30 K/min heating rate is shown by curve (1), and that of the structurally transformed sample which had been cooled to 77 K and then heated is shown by curve (2). (B). The enlarged parts of curves (1) and (2) in Fig. 4.3(A) show the sigmoid shape  $C_p$ -increase for the original CuCN and of its new phase.

(1912),  $\Delta S = S_2 - S_1 = R \ln(\nu_2/\nu_1)$ , where  $R$  is the gas constant,  $S_2$  is the entropy of phase 2,  $S_1$  is the entropy of phase 1, and  $\nu_2$  is the characteristic phonon frequency of phase 2, and  $\nu_1$  is the characteristic phonon frequency of phase 1. Assuming that there is no other contribution related to configurations, the increase in the entropy on the phase transformation indicates a 20 % increase in the phonon frequency on transformation of the original mixed crystals made from flocculation process.

The new phase was cooled to 77 K and reheated. Its thermogram is provided in Fig. 4.3(A). It shows no endothermic peak in the 550 - 580 K range. Therefore, the structural transformation is irreversible. But the new phase still shows the sigmoid-shape increase in  $C_p$  which has shifted to a somewhat higher temperature range of 350 - 380 K. These sigmoid shape curves are clearly seen by comparison of curves (1) and (2) on an enlarged scale in Fig. 4.3(B). The  $C_p$  increase at the end of the sigmoid-shape curve is estimated as 1.2 J/(mol K) from curve (2) in Fig. 4.3 (B).

The samples were then annealed at  $T = 318.2$  K, 323.2 K and 328.3 K for 1.8 ks. The  $C_p$  of these annealed samples plotted against the temperature is shown in Fig. 4.4. These sigmoid-shape  $C_p$  curves are sharper than for the unannealed samples and become even sharper as the annealing temperature is increased. This is a characteristic feature of enthalpy relaxation and is well known for glasses [Ritland (1956), Kovacs (1963), Goldstein (1964), Hodge and Huvad, (1983), Hodge (1983), (1987), (1994), (1995) and (1997)]. We therefore conclude that the  $C_p$  change observed for CuCN is due to the onset of reorientational motions, indicating kinetic unfreezing of orientational disorder.

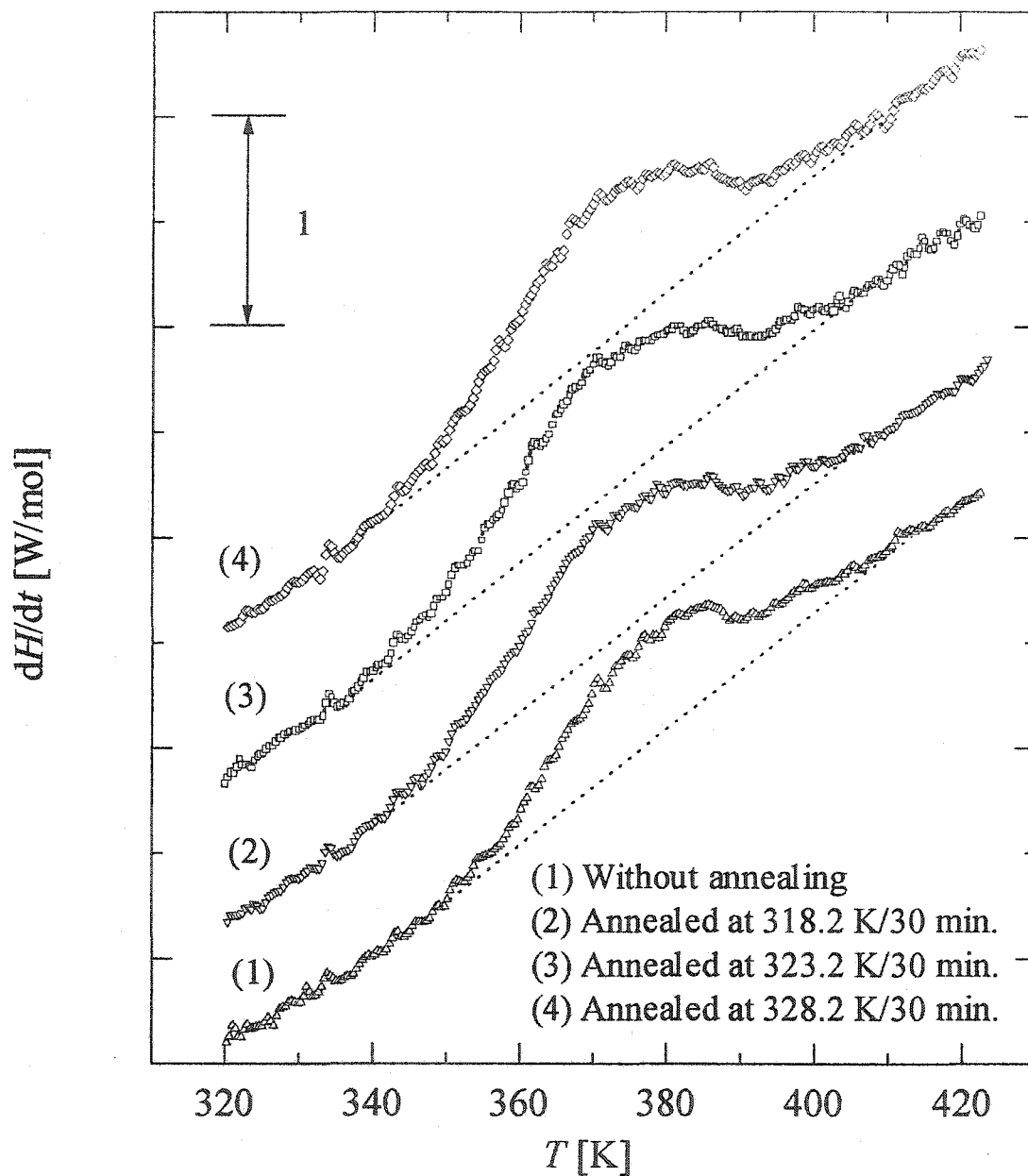


Fig. 4. 4. The differential scanning calorimetry thermogram of CuCN sample obtained by heating at a rate of 30 K/min. is shown by curves for the conditions of, (1) without annealing, (2). annealed at 318.2 K for 30 min. (3). annealed at 323.2 K for 30 min. (4). annealed at 328.2 K for 30 min. The dotted line for each curve indicates the baseline for each scan if there is no glass transition.

The  $C_p$  values of curve (2) in Fig.4.3(B) was normalized and the data was fitted by using the procedure described in Chapter 2 section 2.2.4 and Eqs.(2.24 - 2.29). Fitting was done by an algorithm described earlier [Hodge and Huvard (1983), Hodge (1983), (1987), (1994), (1995) and (1997)] and the calculations were confirmed by new algorithm written in Pascal program, as described in Charter 2. The parameters obtained are:  $\ln A = -28.35$ ,  $x = 1.0$ ,  $\beta = 0.74$ , and  $\Delta h^* = 95$  kJ/mol. The normalized  $C_p$  both for the experimental and the fitting results are plotted against temperature in Fig. 4.5. The calculated relaxation time  $\tau$  and fictive temperature  $T_f$  are plotted against temperature in Fig 4.6(A) and (B).

#### **4.5 Chain statistics of a linear chain in the CuCN orientational glass**

Here we adapt the idea of the lattice-hole model developed in Chapter 3, and calculate the configurational entropy change with increase in temperature. We consider that the number of holes or vacancies in the CuCN crystal per mole at these temperatures is on the order of  $10^{-17}$ , or the fractional population of  $10^{-6}$ , which is much less than that on the order of  $10^{-1}$  used for polymers. Because of the low population of vacancies, their contribution to the configurational entropy can be ignored, as is usually done for crystals.

In structural terms, the Cu atoms in the CuCN crystal are exactly located on the lattice sites, but the C and N can lie either on or off these sites, as in Fig. 4.7(A). Thus the orientational group CN may lie along c axis or at an angle to it. We treat each CN group as "rigid" when its orientation is along the c-axis, and as "flexible" when its orientation is not along c axis direction. From a consideration of the symmetry of the lattice, we deduce

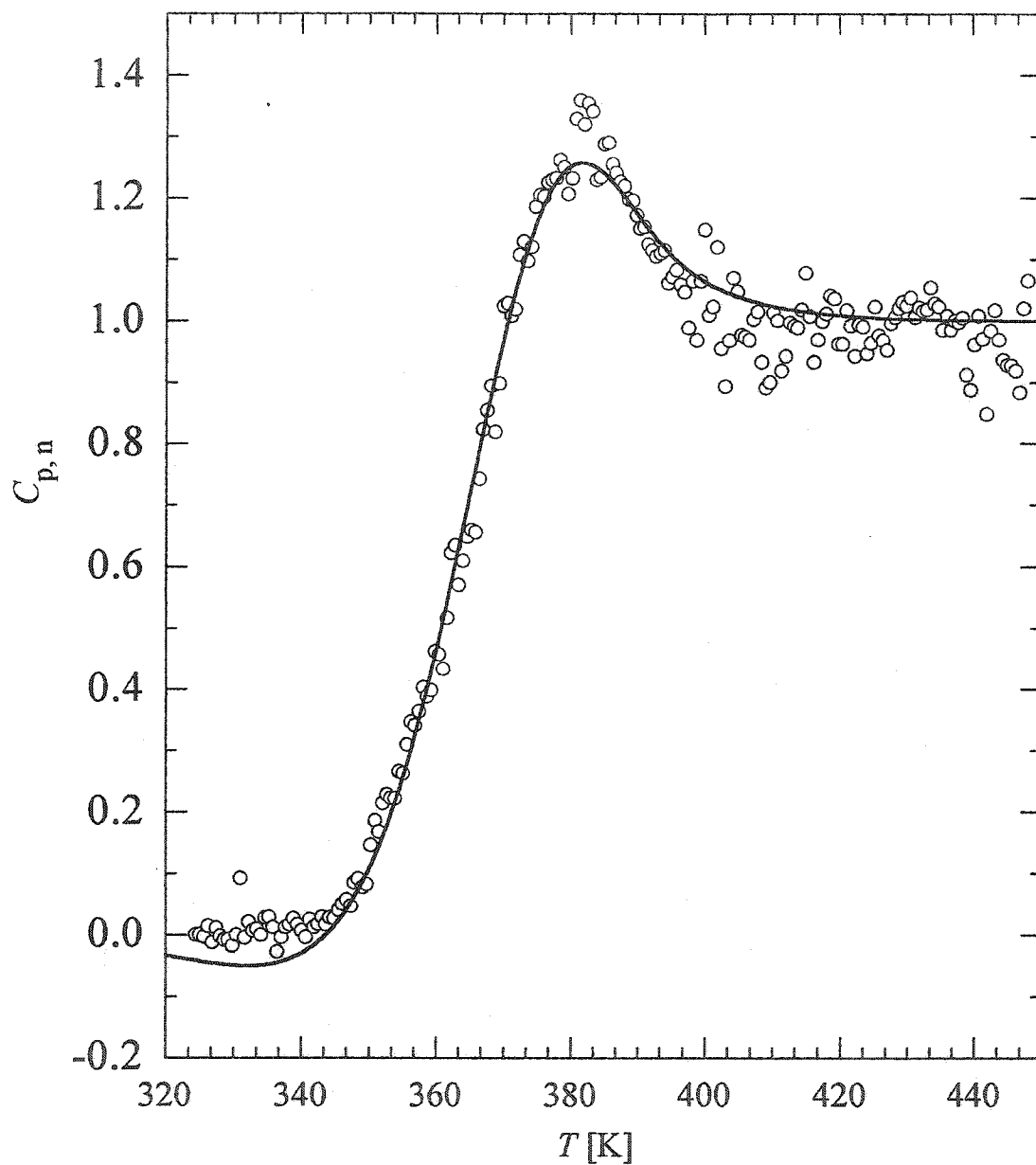


Fig. 4.5. The normalized heat capacity  $C_{p,n}$  plotted against the temperature. The circles denote the data from the DSC measurement and the solid line is the best fit to the data obtained by using Eqs.(2.26) - (2.29).

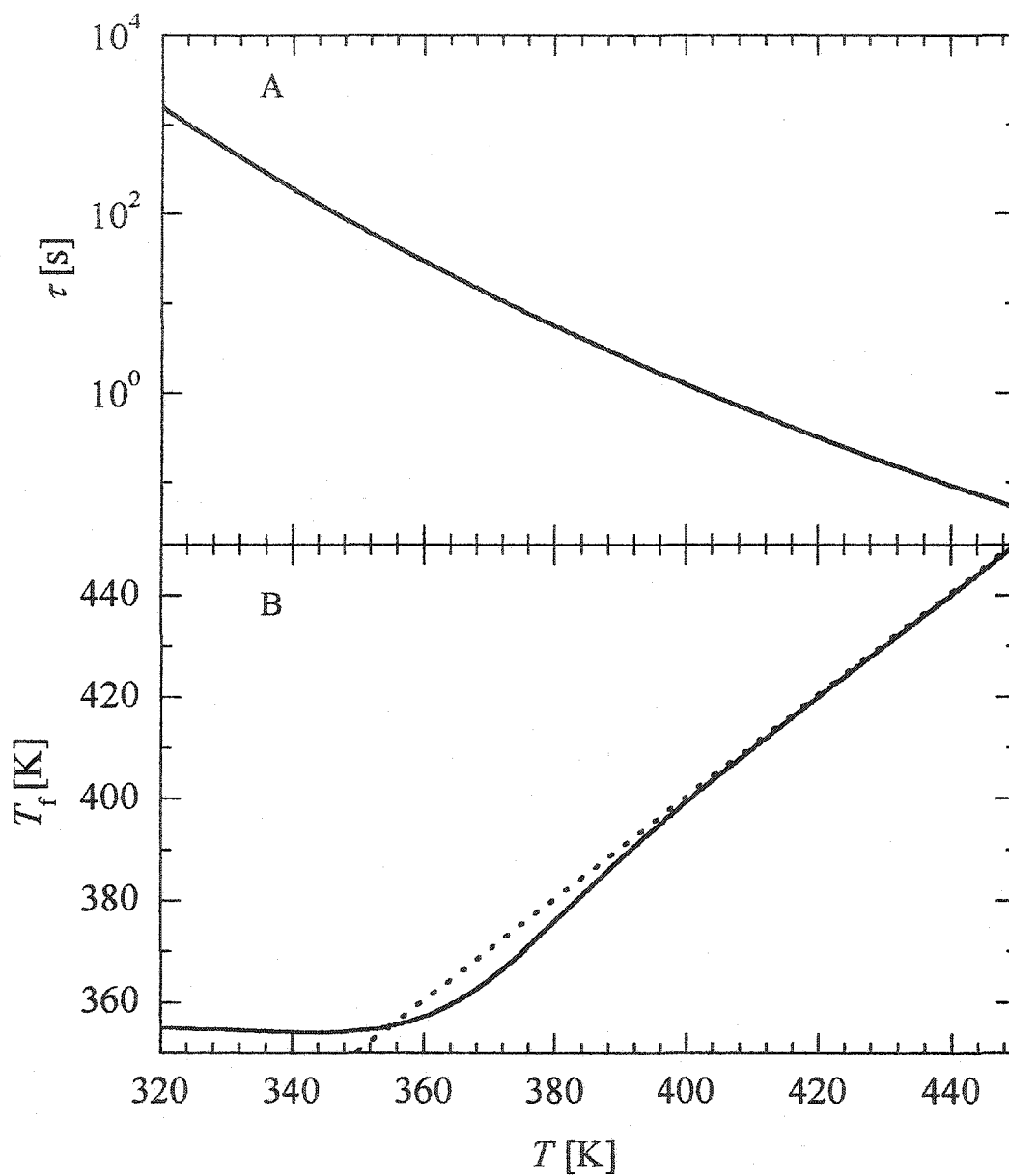


Fig. 4.6. (A). The calculated relaxation time  $\tau(t)$  plotted against temperature during the heating at 30 K/min. (B). The calculated fictive temperature  $T_f$  is plotted against the temperature during the heating at 30 K/min. The solid line is for the calculated  $T_f$  and the dashed straight line for  $T_f = T$ .

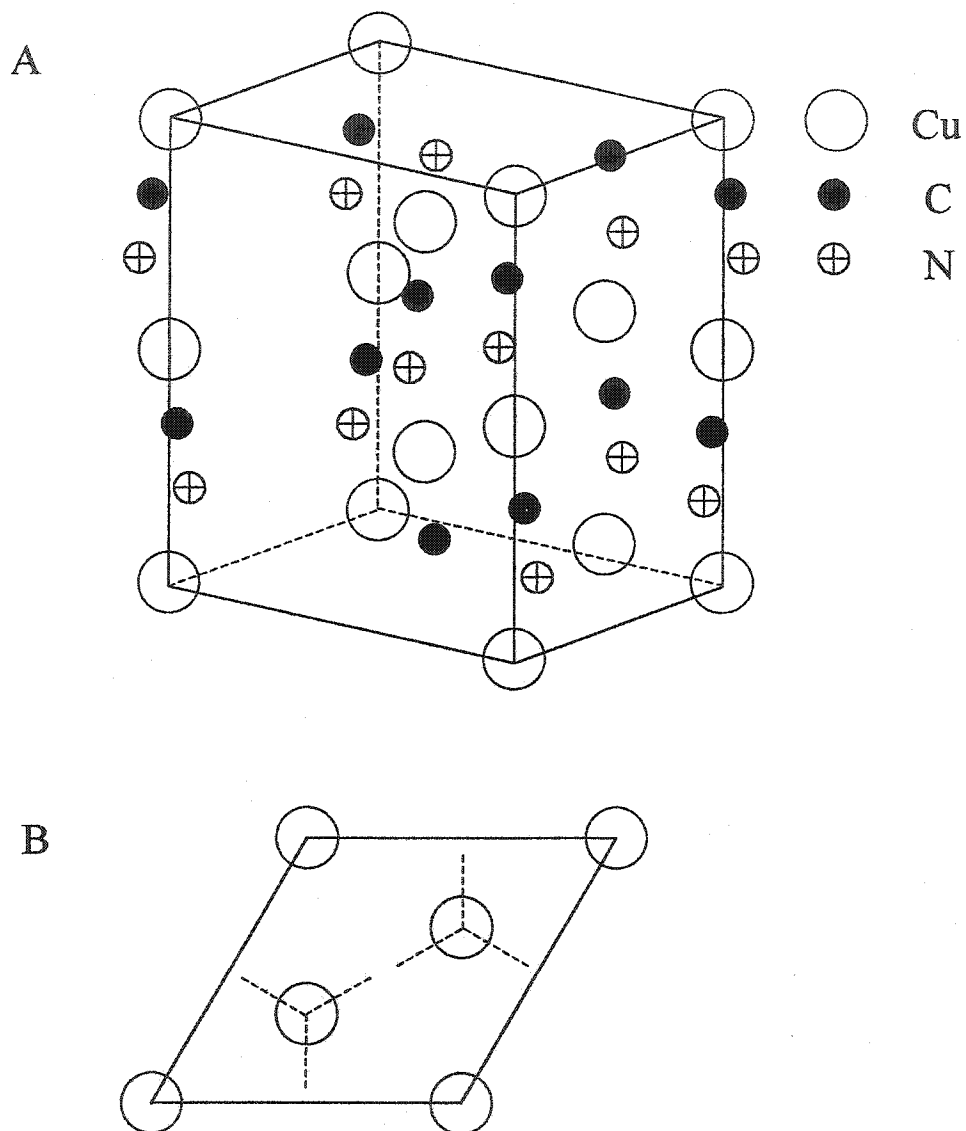


Fig. 4.7. (A). The illustration of orientations of CN groups in the cell structure with  $R3m$  space group of the new CuCN phase. (B). The projection of the Cu atoms on a-b plane. The dashed line indicate the projections of the three possible orientation directions of the CN groups departing from each axis along c direction.

that the number of possible directions for different orientations direction is three, i.e., there are three equivalent orientation directions of the CN group, as shown in Fig. 4.7(B). This corresponds to  $z = 4$  in the lattice model, as described already in Chapter 3. Since every CN group in a chain is capable of reorientation, which is unlike the linear polymer chains in which one of the two end covalent bonds is rigid in flexibility, the corresponding entropy from orientational contribution from CN chains would be different from that in a polymer. Specifically, for CN chains, this contribution has the term  $f \ln(z)$  instead of the term  $f \ln(z - 2)$  in Eq. (3.26), and therefore,

$$\frac{S(f, z)}{R} = -f \ln f - (1 - f) \ln(1 - f) + f \ln(z), \quad (4.1)$$

where  $z$ , which has been defined as the co-ordination number in the case of polymers is equivalent here to the orientation degeneracy. The reason is the equivalence of the three orientations, and  $f$  being a measure of the ability of orientation instead of the flexibility in the case of polymers. The quantity  $f$ , is therefore a measure of the probability that a CN group is not along the  $c$ -axis direction. We use an equation corresponding to Eq. (3.27), and calculate  $f$ , from,

$$f = \frac{z \exp\left(-\frac{U_o}{RT}\right)}{1 + z \exp\left(-\frac{U_o}{RT}\right)} \quad (4.2)$$

where  $U_o$  is the excitation energy for one CN group to change its position from that in which it is orientated in the  $c$ -axis direction to a position in which it is inclined to the  $c$ -axis. From the derivative of Eq. (4.1), the configurational heat capacity is given by,

$$\frac{C^{(f,z)}}{R} = \frac{T}{R} \frac{\partial S^{(f,z)}}{\partial f} \frac{\partial f}{\partial T} = \left(\frac{U_o}{RT}\right)^2 \frac{z \exp\left(-\frac{U_o}{RT}\right)}{\left[1 + z \exp\left(-\frac{U_o}{RT}\right)\right]^2} = \left(\frac{U_o}{RT}\right)^2 \frac{f}{1 + z \exp\left(-\frac{U_o}{RT}\right)} \quad (4.3)$$

The configurational entropy and heat capacity were calculated according to Eqs. (4.1 - 4.3) with  $U_o = 11.5$  kJ/mol. The calculated  $S^{(f,z)}/R$  and  $C^{(f,z)}/R$  are plotted in Fig. 4.8(A) and (B). At 400 K, the configurational entropy is about  $0.52 R \approx 4.3$  J/(mol K) and the configurational heat capacity is about  $0.15 R \approx 1.2$  J/(mol K), which is approximately the same as the  $C_p$  increase occurring sigmoidally in Fig. 4.3(B). This justifies our use of  $U_o = 11.5$  kJ/mol.

The above given calculation shows that on cooling from 400 K to 350 K, the kinetic freezing-in of the number of configurational states corresponds to  $\Delta S_{\text{conf}} = 0.52 R$  and  $\Delta C_p = 0.15 R$ , i.e., these states do not contribute at the time scale of 1 s for 0.5 K temperature change during the DSC scan obtained at a heating rate of 0.5 K/s (30 K/min.). This is also seen from the magnitude of the relaxation time in Fig. 4.6(A) in which  $\tau$  changes from 1s at 400 K to 73 s at 350 K.

It is well known that the sigmoid-shape increase in  $C_p$  is a characteristic feature of the onset of molecular diffusion in the glass-softening range in canonical glasses. The new metastable rhombohedral form of CuCN is certainly in the orientationally disordered state, and at least one of the low-energy forms of CuCN crystals present in the as-received CuCN, which was prepared by the flocculation process, is in an orientationally disordered state at 298 K. But the onset of their configurational contribution occurs at different temperatures, 350 K for the new form and 338 K for the as-received form.

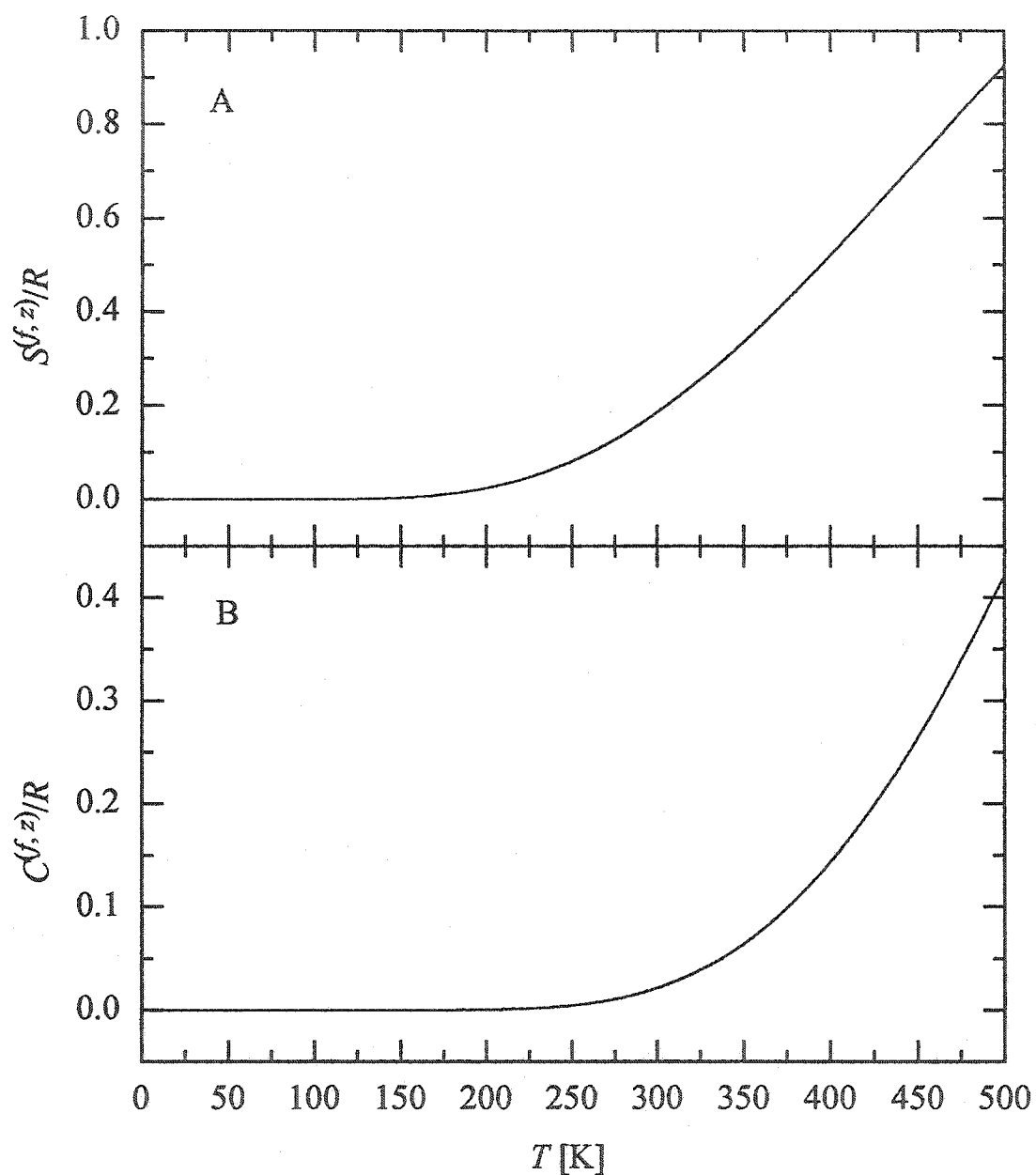


Fig. 4.8 (A). The calculated orientational contribution to the configurational entropy divided by gas constant for the orientational disorder in the linear chains modeled for the arrangement of CN group is plotted against the temperature. (B). The corresponding contribution to the configurational heat capacity divided by gas constant is plotted against the temperature.

It is also conceivable that the  $C_p$  increase in the 340 - 375 K range in all the three forms of CuCN is due to the increase of anharmonic force contributions in the librational motions of CN on their lattice sites. In this theory, which has been justified for another orientational glass TiNO<sub>2</sub> [Johari *et. al.* (2000)], a vacancy defect randomly diffuses to the neighboring site of the CN group. The proximity of the vacancy and CN group distorts, asymmetrically, the shape of the potential energy well and thus increases the anharmonic force contribution from librations of the CN group. Therefore the  $C_p$  increases on orientational unfreezing. This increase is small and is spread over a broader range due to the low activation energy for vacancy diffusion. In as much as vacancy diffusion leads to a change in the configuration of a crystal, this  $C_p$  -increase may be seen also as configurational, but its contribution to  $C_p$  is much less. According to this mechanism, slowing of the vacancy diffusion rate and decrease in the vacancy population would cause a loss in the number of configurations on cooling leading to the formation of an orientational glass. Conversely, increase in the vacancy diffusion rate and population on heating would cause gain of configurations and thus a rise in  $C_p$ , as has been observed for TiNO<sub>2</sub> [Johari *et. al.* (2000)]. Our model calculations can not be performed for TiNO<sub>2</sub>, because its crystal do not contain chain structures. The success of the model calculations in this case nevertheless shows that the orientational glass of CuCN consisting of chain structure in one dimension can be thermodynamically treated in the same manner as polymer chains of a canonical glass.

#### 4.6 Summary

The observations on the CuCN crystals enable us to examine the behavior of configurons in orientational glasses more simply than has been possible from a study of KCN-KBr and related mixed crystals, where quadrupole interactions appear to dominate [Höchli *et al.* (1990)]. Although their excess entropy over an ordered crystal phase can not be determined, the study of CuCN crystals would provide a simpler approach to understand the merit of configurational and vibrational contributions to  $C_p$  and entropy of canonical glasses. The thermodynamic and kinetic behaviors of these glasses are currently being computer-simulated in terms of the potential energy landscape or inherent structure models of a condensed phase, but within the precepts of statistical mechanics and harmonic approximation [Debenedetti and Stillinger (2001)]. In one such approach, the structure of the CuCN crystal as an orientational glass can be seen to belong to a deep configurational minimum from which escape to a neighboring minimum of a lower-energy, ordered crystal structure is thermally improbable, i.e., the high-temperature form is metastable with respect to the low-temperature form. This deep minimum for the crystal may be seen to have a corrugated bottom rather than a round one, with corrugations of different depths representing configurations of lower energy. These configurations are achievable by the diffusion of vacancies but still in the disordered arrangement of the high-temperature crystal phase. Asymmetry of the potential energy corresponding to each corrugation represents the anharmonic forces, which change when the vacancy appears next to a non-spherical CN group. In this case, the  $C_p$  rise on the onset of configurational changes is a reflection of the accessibility of the local minima envisaged as corrugations in a deep potential minimum of a potential landscape.

## Chapter 5

# The Polymerization Reaction kinetics

### 5.1 Introduction

In most liquid state chemical reactions, the liquid's viscosity,  $\eta$ , is low and the reaction product does not significantly raise  $\eta$ , or lower the diffusion coefficient of the reactants,  $D$ . Since the rate of such reactions is determined by the molar concentration of the reacting entities, the reactions are called mass-controlled. They follow the classical laws of reaction kinetics, *i.e.*, (i) the reaction rate coefficient,  $k$ , remains constant with increase in the extent of reaction,  $\alpha$ , or with the reaction time  $t$ , and, (ii)  $k$  varies with the temperature,  $T$ , according to the Arrhenius equation,  $k = k_0 \exp(-E/RT)$ , where  $k_0$  is the  $k$  value at formally infinite  $T$ ,  $E$  is the activation energy and  $R$  the gas constant.

In contrast, when a chemical reaction occurs in liquids of high  $\eta$  or low  $D$ , the probability of reaction depends upon the probability of encounter between the reacting pair, and not only upon the concentration of the reactants. Such probability of encounter between the reacting entities depends on their diffusion coefficients. These chemical reactions are called diffusion-controlled. Several reviews on the subject of diffusion-control in reaction kinetics have appeared, written by Wilemski and Fixman (1973, 1974a, 1974b), Doi (1975), Calef and Deutch (1983), Zumofen *et al.* (1985), Keizer

(1987), Zwanzig (1990), Plonka (1986, 2001)]. Also, comprehensive experiments and mathematical descriptions of the diffusion-controlled kinetics of the ligand binding have been provided by Calef and Deutch (1983), and by Zwanzig (1990). These are of significant biological interest. Wilemski and Fixman (1973, 1974a, 1974b) and Doi (1975) have described the diffusion control in the segmental motions of polymer chains, and the intra-chain reaction of ring closure in a flexible-chain polymer.

Polymerization by addition reactions in a liquid is an example of a case in which  $\eta$  is low and  $D$  is high at the initial stages. As polymerization progresses,  $\eta$  gradually increases and  $D$  decreases. Hence the reaction kinetics, which is initially mass-controlled, becomes ultimately diffusion-controlled. Also, as the reacting entities becoming bigger in size,  $D$  decreases. This in turn decreases the reaction rate. The resulting negative feedback between the physical process of diffusion and the chemical process of polymerization brings both diffusion and polymerization to a virtual halt, and the liquid vitrifies before polymerization has reached its full extent [Johari (1994)]. Thus the extent of polymerization does not reach its maximum value of one. In an exceptional case of polymerization occurring at a high  $T$ , the fully polymerized state remains a low-viscosity liquid and the reaction kinetics may remain mass-controlled. Despite the many studies available on the reaction kinetics of both types [Calef and Deutch (1983), Zumofen *et al.* (1985), Keizer (1987)], little is known on either the experimental manifestation of the gradual transition from mass-controlled kinetics at the initial stage of polymerization to diffusion-controlled kinetics at later stage in real time, or about the criteria that could be used for investigating it. In the following, we provided a method for determining the

onset of transition from mass-controlled to diffusion-controlled kinetics and an experimental study of a polymerization reaction as an example of the procedure and its use. Part of the study has been published in: J. Wang and G. P. Johari, *J. Chem. Phys.*, 117, 9897(2002).

## 5.2 Experimental Methods

For this study we chose a stoichiometric mixture of 4, 4' diaminodicyclohexyl methane, also known as *p*-aminodicyclohexyl methane and diglycidyl ether of bisphenol-A, because changes in the dielectric properties and kinetics of polymerization of this mixture have been studied several times by Tombari *et. al.* (1999), (2000) and Cardelli *et. al.* (2002), and these could be used for comparison with our studies. Para-aminodicyclohexyl methane (PACM) of 99.5% purity was purchased from Fluka, and electronic grade diglycidyl ether of bisphenol-A (DGEBA) was purchased from Shell Chemicals. The molecule weight of PACM is 210.4 and its functionality is 4. The molecule weight of DGEBA is 380 and its functionality is 2. Both PACM and DGEBA were used without further purification. These were weighed in appropriate amounts to prepare a stoichiometric mixture and immediately transferred to the aluminum pan of a Perkin-Elmer differential scanning calorimeter, Model 4. The rate of heat evolved,  $(dH/dt)_r$ , at a fixed polymerizing temperature  $T_{poly}$  was measured with time,  $t$ , up to  $\sim 9$  ks. Thereafter the sample was then cooled from the  $T_{poly}$  to 313.2 K and heated at  $q = 10$  K/min and  $(dH/dt)_q$  was measured at different  $T$  during the heating from to 313.2 K to 548.2 K.

In the general chemical reaction mechanism of a diamine with a diepoxide, one epoxide group of the linear molecule diepoxide opens to accept one H atom of one of the  $\text{NH}_2$  group of the diamine. Thus a covalent bond forms between the terminal C atom of the diepoxide molecule and N atom of the amine, and the O atom of the epoxy group becomes an OH group. The second H atom of the now secondary amine similarly forms a covalent bond with another diepoxide molecule. Since PACM is tetrafunctional, i.e., contains four reacting H atoms in the two  $\text{NH}_2$  groups, it connects with four (difunctional) DGEBA molecules and hence the polymerization of a stoichiometric mixture of 1 mole of PACM and 2 moles of DGEBA produces a three dimensional random network structure on complete polymerization. In this random network rings of different sizes exist. The chemical structures of PACM and DGEBA and the reaction are shown in Fig. 5.1.

### 5.3 Results

The extent of polymerization of the liquid at a certain time,  $t$ , and at constant temperature  $T_{\text{poly}}$ , was determined as follows: The total heat evolved,  $\Delta H^0$ , on polymerization at  $T$ , was determined by adding two quantities: (i) the total heat evolved during isothermal polymerization at  $T_{\text{poly}}$ , and (ii) the heat evolved during heating the partially polymerized sample at 10 K/min from  $T_{\text{poly}}$  to a temperature  $T_{\text{max}}$ , at which the rate of heat evolution becomes negligible. For the first,  $(dH/dt)_T$  against  $t$  obtained from the isothermal measurements at  $T_{\text{poly}}$  was integrated as:

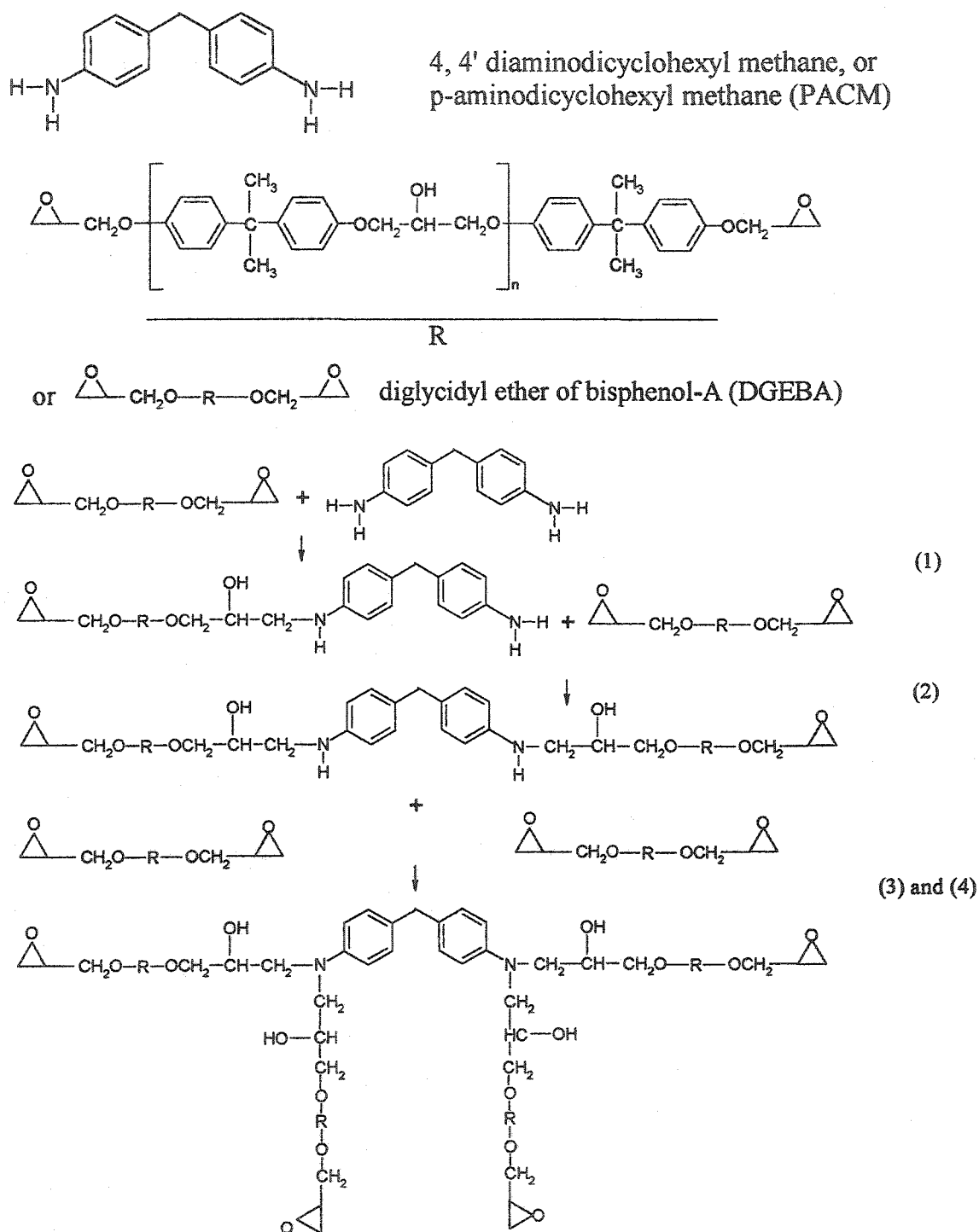


Fig. 5.1. The chemical structures of *p*-aminodicyclohexyl methane (PACM) and diglycidyl ether of bisphenol-A(DGEBA), and the four steps of polymerization reactions which forms polymer network in the 1:2 ratio PACM and DGEBA mixture.

$$\Delta H_1 = \int_0^{t_{\text{poly}}} \left( \frac{dH}{dt} \right)_T dt \quad (5.1)$$

For the second, the  $(dH/dt)_q$  against  $T$  obtained from the heating measurements was integrated as:

$$\Delta H_2 = \int_{T_{\text{poly}}}^{T_{\text{max}}} \frac{1}{q} \left( \frac{dH}{dt} \right)_q dT \quad (5.2)$$

The total heat evolved of polymerization,  $\Delta H^0$  is the sum of  $\Delta H_1$  and  $\Delta H_2$ .

$$\Delta H^0 = \Delta H_1 + \Delta H_2 \quad (5.3)$$

The heat of polymerization, was determined from Eqs. (5.1-5.3). It was found to be  $188 \pm 9$  kJ/mol(DGEBA) for the PACM-DGEBA stoichiometric mixture.

For the isothermal polymerization starting at  $t = 0$ , the total heat evolved until the time  $t$  is:

$$\Delta H(t) = \int_0^t \left( \frac{dH}{dt} \right)_T dt \quad (5.4)$$

The extent or the degree of polymerization,  $\alpha$ , at time  $t$  was calculated from:

$$\alpha(t) = \frac{\Delta H(t)}{\Delta H^0} = \frac{1}{\Delta H^0} \int_0^t \left( \frac{dH}{dt} \right)_T dt \quad (5.5)$$

By using  $\Delta H^0$  of 188 kJ/mol obtained above,  $\alpha(t)$  was determined from Eq. (5.5) for the polymerization of several PACM-DGEBA samples at different fixed temperatures. The rate of heat released,  $(dH/dt)_T$ , as a function of the polymerizing time,  $t$ , for the PACM-DGEBA mixture kept at five different polymerizing temperatures, 333.2 K, 338.2 K, 343.2 K, 348.2 K and 353.2 K, is plotted against  $t$  in Fig.5.2(A). These plots show the

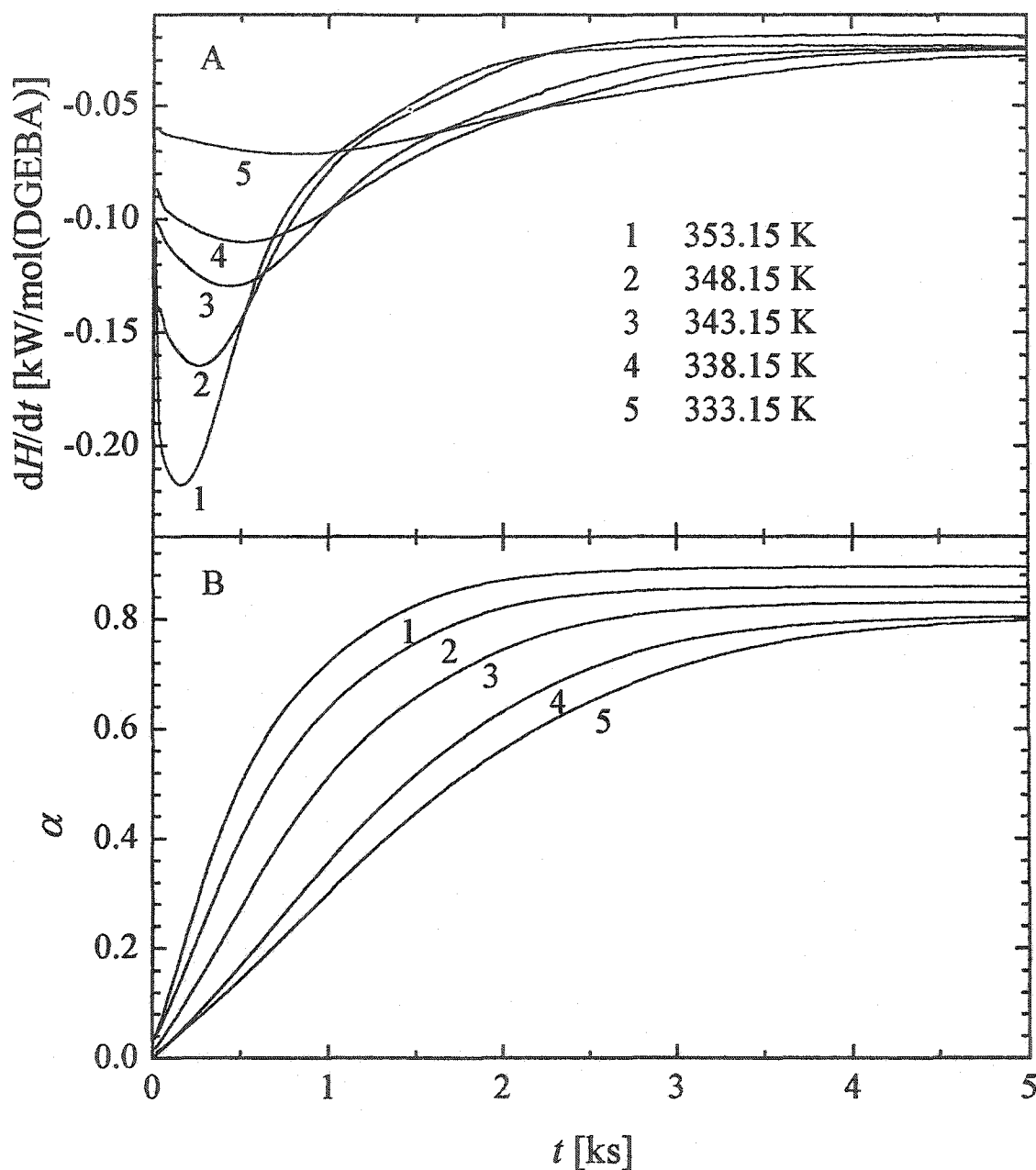


Fig. 5.2. (A) The rate of enthalpy release measured during polymerization of the stoichiometric PACM-DGEBA mixture at five fixed temperatures, as indicated, is plotted against the polymerization time. (B) The extent of polymerization,  $\alpha$ , of the stoichiometric PACM-DGEBA mixture at the indicated temperatures is plotted against the polymerization time.

minimum as a result of the heat released, which is a characteristic of an exothermic process. Fig. 5.2(B) shows the plots of  $\alpha$  against the polymerization time at the same temperatures. The glass softening temperature of the almost fully polymerized PACM-DGEBA mixture was measured. It was  $\sim 439$  K. Therefore in this study at a fixed  $T_{\text{poly}}$ , the liquid vitrified before reaching complete polymerization.

## 5.4 Discussion

Because of the different experimental and theoretical aspects, the results of this study are discussed in several sections each covering a different aspect of the polymerization, as follows:

### 5.4.1 Effects of the extent of polymerization at a fixed temperature

As mentioned earlier, when the reaction rate coefficient,  $k$ , does not change with  $\alpha$  or the reaction time, the reaction kinetics is mass-controlled. Conversely, if  $k$  is found to change with  $\alpha$  or the reaction time, the reaction kinetics is no longer mass-controlled. Therefore, in our studies of the polymerization kinetics, we first need to determine  $k$ . Its value can be determined only from relevant equations for the overall order of the polymerization reaction. This overall order of reaction is obtained by fitting various equations for different orders of reactions to the experimental data and then determining which one of the simplest equation for the overall reaction fits the data.

Studies of polymerization kinetics of DGEBA and amines by differential scanning calorimetry have shown that for the network polymerization reactions of DGEBA with a variety of diamines, the rate of polymerization is initially given by [Horie *et. al.* (1970)],

$$\left(\frac{d\alpha}{dt}\right) = (k_1 + k_2\alpha^m)(1-\alpha)^n \quad (5.6)$$

where  $k_1$  and  $k_2$  are related to the rate coefficients for the primary and secondary amine reactions provided they have equal reactivity, and  $m$  and  $n$  are empirical parameters. But after a certain time for polymerization when  $\alpha$  has reached a certain value, polymerization occurs according to first order rate equation,

$$\left(\frac{d\alpha}{dt}\right) = k(1-\alpha) \quad (5.7)$$

This has been interpreted in terms of the secondary amine reaction dominating the polymerization kinetics of the diamine-diepoxy mixtures at long times or at high  $\alpha$  values. Thus the order of the overall polymerization reaction becomes reduced to a first order rate process. Therefore, we calculate  $k$  from Eq. (5.7) and the data in Fig. 5.1(B). The logarithmic plots of the quantity  $k (= [(d\alpha/dt)/(1-\alpha)]_T$ ) against  $\alpha$  at polymerization temperatures of 333.2 K, 338.2 K, 343.2 K, 348.2 K and 353.2 K are shown in Fig. 5.3. Here the plots beginning at  $\alpha = 0.4$  show that there are two regions of  $\alpha$  in terms of the variation of  $\ln[(d\alpha/dt)/(1-\alpha)]_T$  at each temperature. In the first region,  $\ln(k)$  appears to decrease towards a plateau-value with increase in  $\alpha$  and in the second region, it decreases progressively more rapidly with increase in  $\alpha$ . The region of constant  $k$  is an indication that the first order reaction rate is being approached or else it has already been reached.

In the second region of the plots in Fig. 5.3, the quantity  $\ln[(d\alpha/dt)/(1-\alpha)]_T$  decreases progressively more rapidly as  $\alpha$  increases. To relate this observation to the transport properties, we recall that independent studies of polymerization of the diamine-

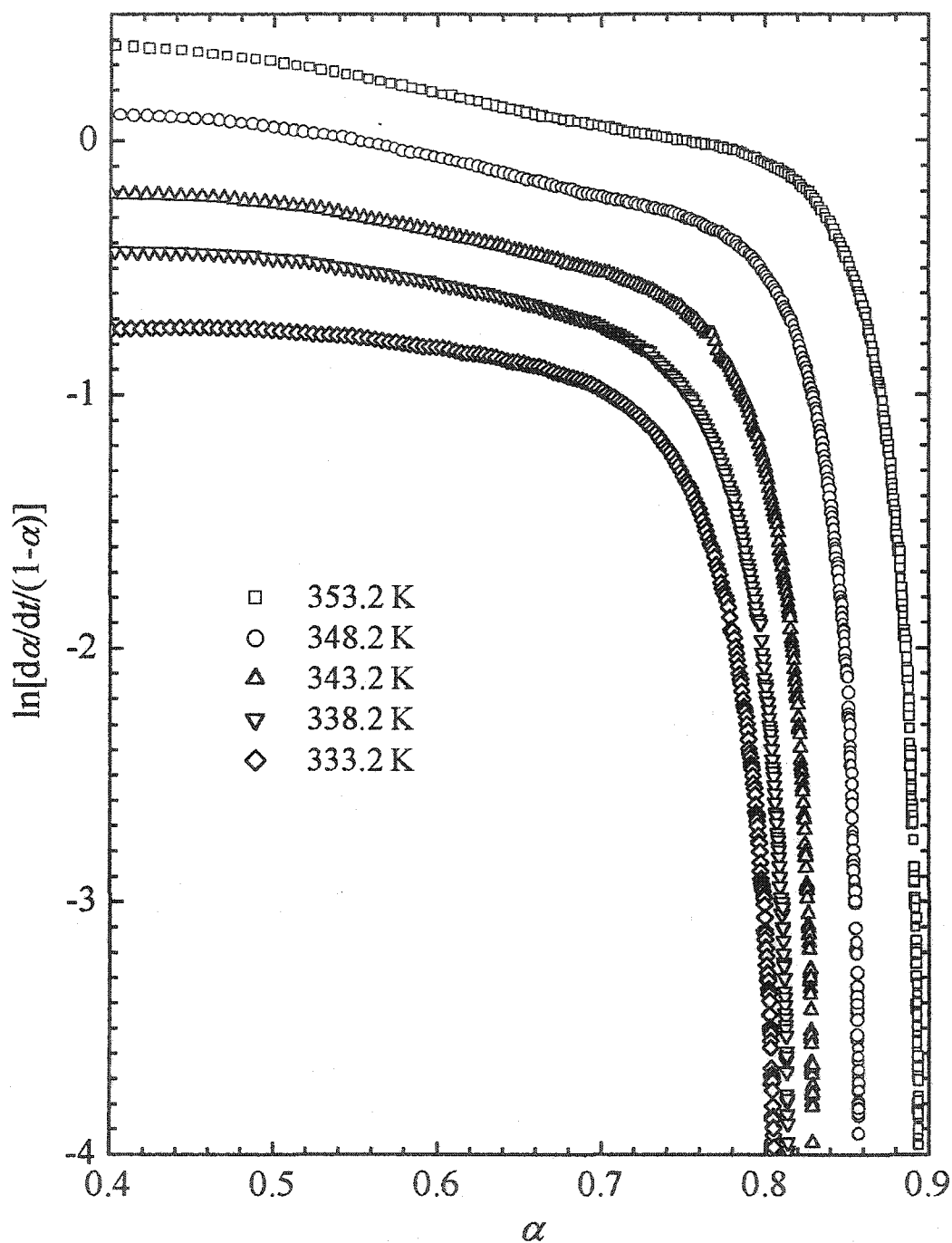


Fig. 5.3. The logarithmic value of  $[d\alpha/dt/(1-\alpha)]$  for the stoichiometric PACM-DGEBA mixture is plotted against the extent of polymerization  $\alpha$  at five fixed temperatures, as indicated.

diepoxide mixtures have shown that  $\eta$  [Alig *et. al.* (1989), Malkin and Kulichikhin (1991)], dielectric relaxation time ( $\tau_{\text{diel}}$ ) [Parthun and Johari (1995), Wasylyshyn and Johari (1997), Tombari *et.al.* (1997), (1999)] and ultrasonic relaxation time ( $\tau_{\text{ulson}}$ ) [Alig *et. al.* (1992), Parthun and Johari (1995)] increase progressively more rapidly as  $\alpha$  increases at a fixed  $T$ . Alternatively stated, their  $\ln(1/\eta)$ ,  $\ln(1/\tau_{\text{diel}})$  and  $\ln(1/\tau_{\text{ulson}})$  decrease progressively more rapidly as  $\alpha$  increases. This is the same manner in which  $\ln[(d\alpha/dt)/(1-\alpha)]_T$  decreases in the second region of the plots in Fig. 5.3. This shows that  $k$  may be approximately proportional to the inverse of  $\eta$ ,  $\tau_{\text{diel}}$  and  $\tau_{\text{ulson}}$ .

The plots in Fig. 5.3 also show that as  $T_{\text{poly}}$  is decreased, the onset of the rapid decrease in  $\ln(k)$  shifts to lower value of  $\alpha$ . An analogous shift has also been observed in the plots of  $\ln(1/\eta)$  against  $\alpha$  by Alig *et. al.* (1989), and Malkin and Kulichikhin (1991), and in the plots of  $\ln(1/\tau_{\text{diel}})$  against  $\alpha$  by Parthun and Johari (1995), Wasylyshyn and Johari (1997), and by Tombari *et.al.* (1997, 1999). Similar behavior has also been found in the plots of  $\ln(1/\tau_{\text{ulson}})$  against  $\alpha$  by Alig *et. al.* (1992), and Parthun and Johari (1995). These observations show that the progressively rapid decrease in  $\ln(k)$  with increase in  $\alpha$  is a consequence of the increase in  $\eta$  during the course of polymerization, and therefore it is an indication of the onset of diffusion-controlled reaction kinetics. The lower the polymerizing temperature, the lower is the  $\alpha$  value for this onset.

#### 5.4.2 Effects of the polymerization temperature at a fixed extent of polymerization

It is also well known that at high temperatures where  $\eta$  of a liquid (of a fixed structure or fixed  $\alpha$ ) is in the centiPoise to Poise range, and where  $D$  is correspondingly high, the temperature dependence of  $D$  and  $\eta^{-1}$  follows the Arrhenius equation [Andrade (1930)],

$$D \text{ (or } \eta^{-1}) = A \exp[-E_A/RT] \quad (5.8)$$

Where  $E_A$  is the Arrhenius energy,  $A$  is the preexponential term and  $R$  is the gas constant. At low temperatures where  $D$  is low and  $\eta$  is high, the temperature dependence of the two quantities deviates from the Arrhenius equation and tends toward an equation of the type provided by Vogel (1921), Fulcher(1925), and Tammann(1926),

$$D \text{ (or } \eta^{-1}) = A \exp[-B/(T-T_0)] \quad (5.9)$$

where  $A$ ,  $B$  and  $T_0$  are a material's constant. In graphical terms, this means that the plot of  $\ln(D \text{ or } \eta^{-1})$  against  $1/T$  is close to a straight line at high  $T$  where  $D$  is high and  $\eta$  is low and that the plot bends downward at low  $T$  where  $D$  is low and  $\eta$  is high.

In the simplest approximation for a diffusion-controlled kinetics in liquids, it is expected that  $k$  would vary with  $T$  in the same manner as  $\eta^{-1}$  and  $D$  vary with  $T$ , i. e.,  $k$  would also follow the Vogel-Fulcher-Tammann equation. Thus, as a mass-controlled polymerization kinetics changes gradually to diffusion-controlled kinetics, the  $\ln(k)$  against  $1/T_{\text{poly}}$  plot for a fixed value of  $\alpha$  would be a straight line initially at high  $T_{\text{poly}}$  and then bend downwards progressively more rapidly as  $T_{\text{poly}}$  decreases. Thus the bending of the  $\ln(k)$  against  $1/T_{\text{poly}}$  plots would serve as another indication of the onset of diffusion-control kinetics. This would also be the case if  $\eta$  of the liquid in the colloidal aggregations is increased by decreasing  $T$ , allowing thereby the use of Smoluchowki's

formalism (1917) for such aggregation, and of its later modification by Waite (1958) for bimolecular chemical reactions.

To examine the effect of temperature on  $k$  through the change in  $D$  and  $\eta$  with  $T$ , and not through the change in the reacting entities' size, values of  $\ln(k)$  for several fixed values of  $\alpha$  were read from Fig. 5.3 and is plotted against  $1/T_{\text{poly}}$  in Fig. 5.4. (Note that a fixed structure at a fixed  $\alpha$  value is an approximation here, because a multitude of distributions of molecular weights in the partially polymerized liquid can be consistent with a given  $\alpha$  value.) For polymerization of the DGEBA-PACM mixture up to a time when  $\alpha < 0.75$ , the  $\ln(k)$  plots in Fig. 5.4 are linear over the temperature range of 333.2 – 348.2 K, and follow the Arrhenius equation,  $k = k_0 \exp(-E_A/RT_{\text{poly}})$ .

For these plots, (i)  $\ln(k_0) = 17.3 \pm 0.6$  and  $E = 48.8 \pm 1.7$  kJ/mol when  $\alpha = 0.55$ , (ii)  $\ln(k_0) = 16.8 \pm 0.7$  and  $E = 48.2 \pm 2.1$  kJ/mol when  $\alpha = 0.6$ , (iii)  $\ln(k_0) = 16.5 \pm 0.7$  and  $E = 50.7 \pm 1.9$  kJ/mol when  $\alpha = 0.65$ , (iv)  $\ln(k_0) = 16.5 \pm 0.7$  and  $E = 50.7 \pm 1.9$  kJ/mol when  $\alpha = 0.7$ , and, (v)  $\ln(k_0) = 22.2 \pm 0.4$  and  $E = 65.2 \pm 1.1$  kJ/mol when  $\alpha = 0.75$ .

Over the temperature range covered in Fig. 5.4, the plots for  $\alpha > 0.75$  begin to curve downwards, thus indicating a deviation from the Arrhenius behavior towards the Vogel-Fulcher-Tammann type behavior. Although the data provided here are insufficient for fitting the curves to the equation of the type,  $k$  ( $D$  and  $\eta^{-1}$ )  $\propto \exp[-B/(T-T_0)]$ , it is clearly evident that for a fixed high values of  $\alpha$ ,  $\ln(k)$  becomes progressively more sensitive as  $1/T_{\text{poly}}$  increases in the temperature range studied. More accurate data

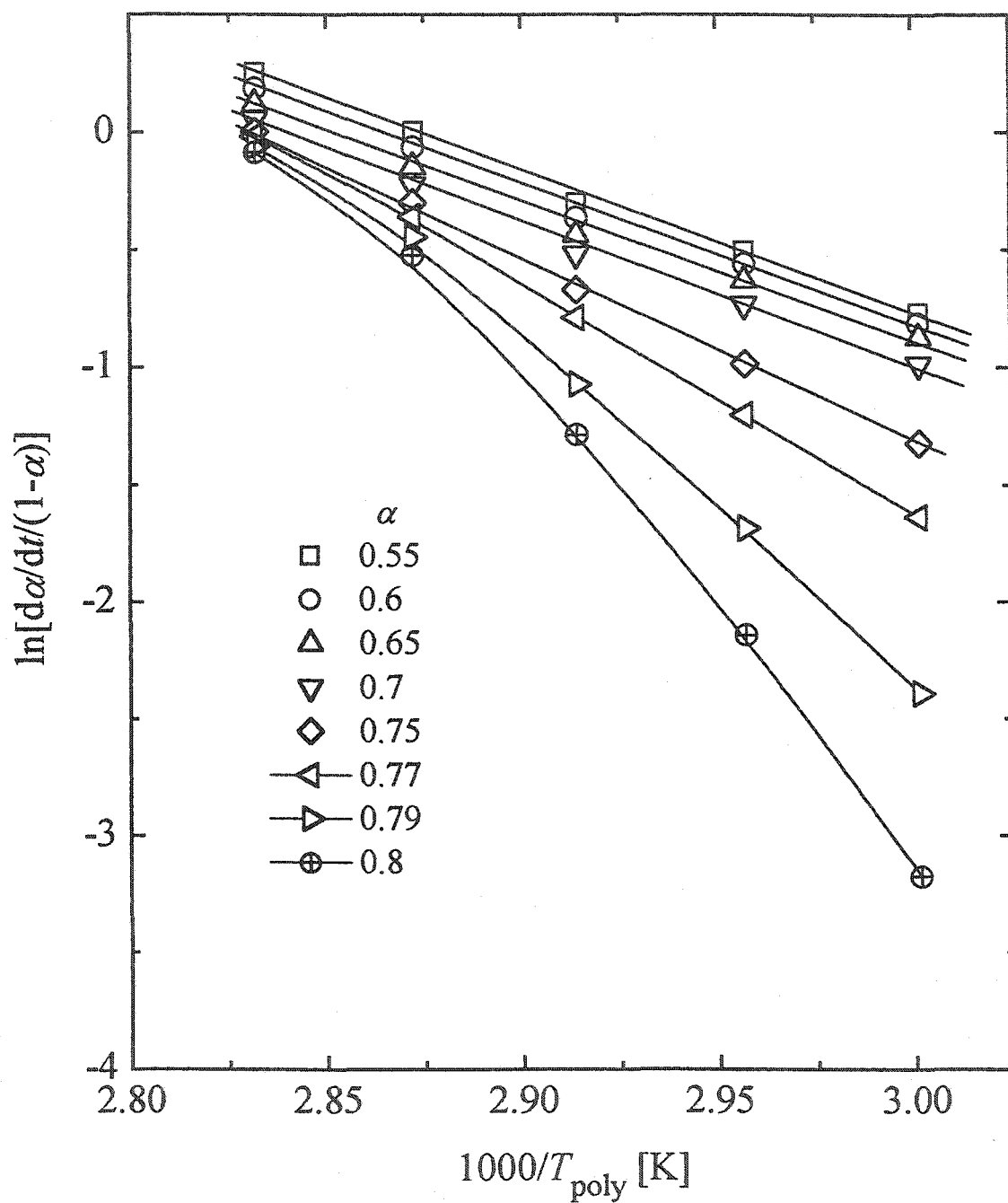


Fig. 5.4. The logarithmic value of the reaction rate coefficient,  $k$ , for the stoichiometric PACM-DGEBA mixture at different extents of polymerization,  $\alpha$ , is plotted against the reciprocal polymerization temperature. The value of  $\alpha$  for each plot is indicated by the symbols.

perhaps obtained from other measurement techniques are needed to determine the parameters  $A$ ,  $B$  and  $T_0$  of this equation. Here, we conclude that the onset of the downward curvature indicates a change from mass-controlled to diffusion-controlled kinetics.

A comparison of the plots for different values of  $\alpha$  in Fig. 5.4 also shows that the onset of diffusion-control shifts towards higher temperatures as  $\alpha$  increases. However, there is a difficulty in determining the onset of the curvature in the plots in Fig. 5.4, and that prevents us from obtaining a precise value of  $T$  or  $\alpha$  for the onset of diffusion control.

The plots may also be interpreted in terms of the polymerization time,  $t$  instead of  $\alpha$ . For a given polymerization temperature, say 353.2 K, the onset of diffusion control would be in the  $t$  range where  $\alpha$  is between 0.8 and 0.85. Similarly, for 343.2 K, the onset of diffusion-control is in the  $t$  range where  $\alpha$  is between 0.75 and 0.8. On the basis of these plots, we also deduce that a polymerization reaction can be brought from its mass-controlled kinetics to diffusion-controlled kinetics by decreasing  $T_{\text{poly}}$  for a fixed  $\alpha$ , or by increasing  $\alpha$  at a fixed  $T_{\text{poly}}$ , or else by a combination of both changes.

We propose that a simple polymerization reaction may be maintained in the mass-controlled domain by raising the liquid's temperature which decreases  $\eta$  while  $\alpha$  continues to increase. In this procedure, the polymerizing liquid may be heated at a rate, which would raise  $k$  and maintain a low viscosity of the polymerized state. An aspect of this method has been described earlier [Tombari *et al.* (1999)] without reference to diffusion control kinetics. In that study [Tombari *et al.* (1999)], dielectric measurements

finding the temperature-time conditions so that full polymerization could be achieved in the shortest time.

The calorimetric procedure described here seems more direct than the procedure of step-pressure application [Wasylyshyn and Johari (1998), (1999)] or of dielectric data analysis [Johari and Wasylyshyn (1999), McAnanama *et. al.* (2000)], as used earlier for detecting the onset of diffusion control in polymerization kinetics.

#### 5.4.3 Distinction between the simulated reaction rates for mass- and diffusion-controlled reactions

We now consider how the measured reaction rate data can be used to distinguish between the mass-controlled kinetics and diffusion-controlled kinetics of a polymerization process. In general, the rate of a bimolecular reaction is related to  $\alpha$  by,

$$(d\alpha/dt)_r = k[1 - \alpha]^2. \quad (5.10)$$

When one reacting entity is in excess of the second or if one entity diffuses toward a substrate and reacts with it, the reaction rate is given by the first order rate equation,

$$(d\alpha/dt)_r = k[1 - \alpha]. \quad (5.11)$$

The rate coefficient of the mass-controlled kinetics,  $k_{\text{mass}}$ , which is independent of  $\alpha$ , in this case is,

$$k_{\text{mass}} = \left[ \frac{(d\alpha / dt)}{(1 - \alpha)} \right]. \quad (5.12)$$

In contrast, the rate coefficient of a diffusion-controlled kinetics,  $k_{\text{diff}}$ , varies with  $\alpha$  in the same manner as  $D$  of the least mobile reacting entity varies with  $\alpha$ . Therefore, to

relate  $k_{\text{diff}}$  with  $\alpha$ , one needs the relation between  $D$  and  $\alpha$ . This relation is not known, but the dielectric relaxation time,  $\tau_{\text{diel}}$ , which is inversely proportional to  $D$ , has been related to  $\alpha$  in the studies of the diamine-diepoxy polymerization reactions [Tombari and Johari (1992), Wasylyshyn and Johari (1997), Tombari *et. al.* (1997)], and it has been found that,

$$\tau_{\text{diel}} = \tau_{\text{diel}}(0)\exp[S\alpha^p], \quad (5.13)$$

where  $\tau_{\text{diel}}(0)$  is a constant pre-factor and refers to  $\tau_{\text{diel}}$  at the beginning of the polymerization at  $t = 0$  when  $\alpha = 0$ . The parameter  $S$  is a function of  $T$ , but not a function of  $\alpha$ , and  $p$  ( $p \approx 1 - 4$ ) is a dimensionless parameter which varies with  $T_{\text{poly}}$ . On replacing  $\tau_{\text{diel}}$  in Eq. (13) by  $k_{\text{diff}}^{-1}$ ,

$$k_{\text{diff}} = k_{\text{diff}}(0)\exp[-S\alpha^p], \quad (5.14)$$

where  $k_{\text{diff}}(0)$ , a constant pre-factor, refers to  $k_{\text{diff}}$  when the polymerization time,  $t = 0$ , or  $\alpha = 0$ .

For convenience of description in terms of the polymerization time domain, we consider that starting from  $t = 0$ , the extent of reaction for a mass-controlled kinetics,  $\alpha_{\text{mass}}$ , is equal to extent of reaction for a diffusion-controlled kinetics,  $\alpha_{\text{diff}}$ , i.e.,  $\alpha(0) = \alpha_{\text{mass}}(0) = \alpha_{\text{diff}}(0)$ , and further that,  $(d\alpha_{\text{mass}}/dt)_{t=0} = (d\alpha_{\text{diff}}/dt)_{t=0}$ . With these conditions,

$$k_{\text{mass}}(0)[1 - \alpha_{\text{mass}}(0)] = k_{\text{diff}}(0)[1 - \alpha_{\text{diff}}(0)]\exp[-S\alpha(0)^p] \quad (5.15)$$

Since,  $\alpha_{\text{mass}}(0) = \alpha_{\text{diff}}(0) = \alpha(0)$ ,

$$\left( \frac{k_{\text{mass}}(0)}{k_{\text{diff}}(0)} \right) = \exp[-S\alpha(0)^p] \quad (5.16)$$

The quantities,  $S$ ,  $\alpha(0)$  and  $p$  are positive. Therefore,  $\exp[-S\alpha(0)^p] < 1$ . This means that,  $k_{\text{diff}}(0) > k_{\text{mass}}(0)$ .

By replacing  $k$  in Eq. (5.12) by  $k_{\text{mass}}$  and on rearranging, we obtain,

$$\left( \frac{d\alpha_{\text{mass}}}{1 - \alpha_{\text{mass}}} \right) = k_{\text{mass}}(0) dt \quad (5.17)$$

By integrating Eq. (5.17) on both side we obtain,

$$\ln[1 - \alpha_{\text{mass}}(t)] = -k_{\text{mass}}(0)t + C_1 \quad (5.18)$$

where  $C_1$  is an integration constant. For the condition of  $\alpha_{\text{mass}}(t) = \alpha(0)$  when  $t = 0$ , we find  $C_1 = \ln[1 - \alpha(0)]$  and Eq. (5.18) leads to,

$$\alpha_{\text{mass}}(t) = 1 - [1 - \alpha(0)] \exp[-k_{\text{mass}}(0)t], \quad (5.19)$$

and 
$$\left( \frac{d\alpha_{\text{mass}}}{dt} \right) = k_{\text{mass}}(0)[1 - \alpha(0)] \exp[-k_{\text{mass}}(0)t] \quad (5.20)$$

By substituting  $k_{\text{diff}}$  from Eq. (5.14) for  $k$  in Eq. (5.11) and denoting  $\alpha(t)$  by  $\alpha_{\text{diff}}(t)$ ,

$$\left( \frac{d\alpha_{\text{diff}}}{dt} \right) = k_{\text{diff}}(0)[(1 - \alpha_{\text{diff}}(t)] \exp[-S\alpha_{\text{diff}}(t)^p] \quad (5.21)$$

By rearranging Eq. (5.21), 
$$\left( \frac{d\alpha_{\text{diff}}}{(1 - \alpha_{\text{diff}}) \exp(-S\alpha_{\text{diff}}^p)} \right) = k_{\text{diff}}(0) dt \quad (5.22)$$

and on integrating, 
$$\int_{\alpha(0)}^{\alpha_{\text{diff}}(t)} \frac{d\alpha_{\text{diff}}}{(1 - \alpha_{\text{diff}}) \exp(-S\alpha_{\text{diff}}^p)} = k_{\text{diff}}(0)t + C_2, \quad (5.23)$$

where  $C_2$  is an integration constant which is equal to zero because the integration is from the polymerization time,  $t = 0$ .

The LHS of Eq. (5.23) can not be expressed by elemental functions even for the simplest case of  $p = 1$ . Nevertheless,  $\alpha_{\text{diff}}(t)$  can be calculated by numerical integration for each value of  $\alpha$  from  $\alpha = \alpha(0)$  to  $\alpha = \alpha(\infty) = 1$ . For this purpose, we use values for  $\alpha_{\text{mass}}(0)$  and  $\alpha_{\text{diff}}(0)$  as 0.5,  $k_{\text{diff}}(0) = 1 \times 10^6 \text{ s}^{-1}$ ,  $S = 130.254$ ,  $p = 2.5$ , and calculate  $\alpha_{\text{mass}}(t)$  and  $\alpha_{\text{diff}}(t)$ . The calculated plots are shown in Fig. 5.5(A). The relevant derivatives,  $(d\alpha_{\text{mass}}/dt)$  and  $(d\alpha_{\text{diff}}/dt)$ , are plotted against the polymerization time  $t$  in Fig. 5.5(B) and the ratio  $(d\alpha_{\text{mass}}/dt)/(d\alpha_{\text{diff}}/dt)$ , against  $t$  in Fig. 5.5(C). The relevant derivatives,  $(d\alpha_{\text{mass}}/d\alpha)$  and  $(d\alpha_{\text{diff}}/d\alpha)$ , are also calculated in the  $\alpha$ -domain and plotted against  $\alpha$  in Fig. 5.6(A) and the ratio  $[(d\alpha_{\text{mass}}/d\alpha)/(d\alpha_{\text{diff}}/d\alpha)]_{\text{T}}$ , against  $\alpha$  is plotted in Fig. 5.6(B).

Since the ratio,

$$\left( \frac{(d\alpha_{\text{diff}}/dt)}{(d\alpha_{\text{mass}}/dt)} \right) = \left( \frac{1 - \alpha_{\text{diff}}(t)}{1 - \alpha_{\text{mass}}(t)} \right) \exp[S\alpha(0)^p - S\alpha_{\text{diff}}(t)^p] \quad (5.24)$$

The ratio in the pre-exponential term in Eq. (5.24) increases as  $t$  increases, because  $\alpha_{\text{mass}}$  initially increases more rapidly with  $t$  than  $\alpha_{\text{diff}}$ . The exponential term in Eq. (5.24) decreases with  $t$ , because  $S\alpha_{\text{diff}}(t)^p$  increases with  $t$  and  $S\alpha(0)^p$  is a constant. Since the increase in the pre-exponential term with  $t$  is much slower initially than the decrease in the exponential term, the ratio  $[(d\alpha_{\text{diff}}/dt)/(d\alpha_{\text{mass}}/dt)]$  in Eq. (5.24) decreases initially with  $t$ . At longer times, as  $\alpha_{\text{mass}} \rightarrow 1$ , the pre-exponential term in Eq. (5.24) increases more rapidly and compensates for the decreasing exponential term. Consequently, the plot of the ratio  $[(d\alpha_{\text{diff}}/dt)/(d\alpha_{\text{mass}}/dt)]$  against  $t$  shows a local minimum. Also, there are two points in Fig. 5.5(B) at which this ratio is equal to 1, one point is at the (assumed)  $t = 0$ ,

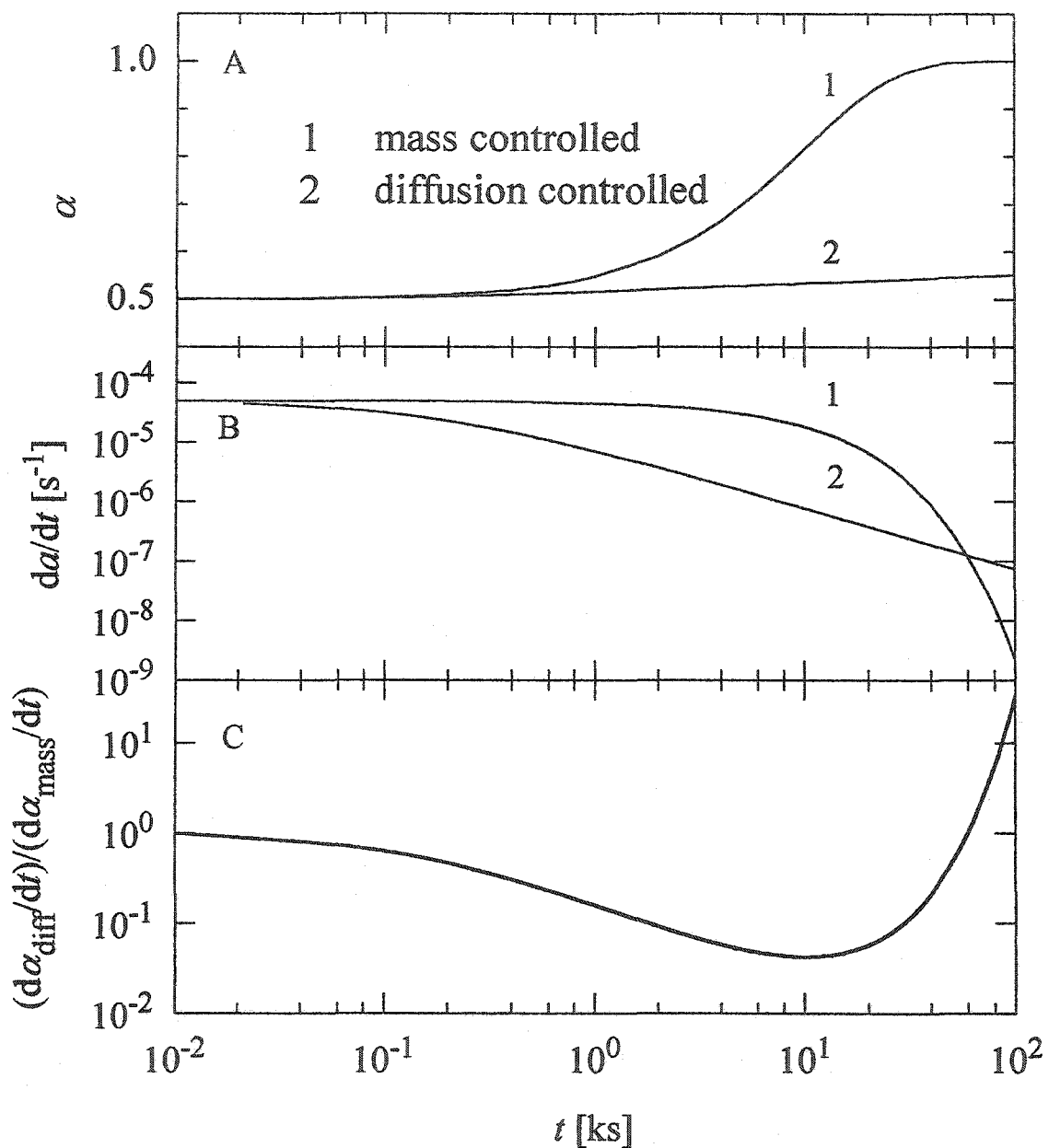


Fig. 5.5. (A). The calculated  $\alpha$  for mass-controlled and diffusion-controlled reactions is plotted against the logarithmic reaction time. (B). The corresponding  $d\alpha/dt$  values for a mass controlled and diffusion controlled reaction are plotted against the logarithmic reaction time. (C). The ratio of corresponding calculated  $(d\alpha_{\text{diff}}/dt)/(d\alpha_{\text{mass}}/dt)$  values are plotted against the logarithmic reaction time. In (A) and (B), curve 1 refers to the mass-controlled, and curve 2 to the diffusion-controlled reaction kinetics.

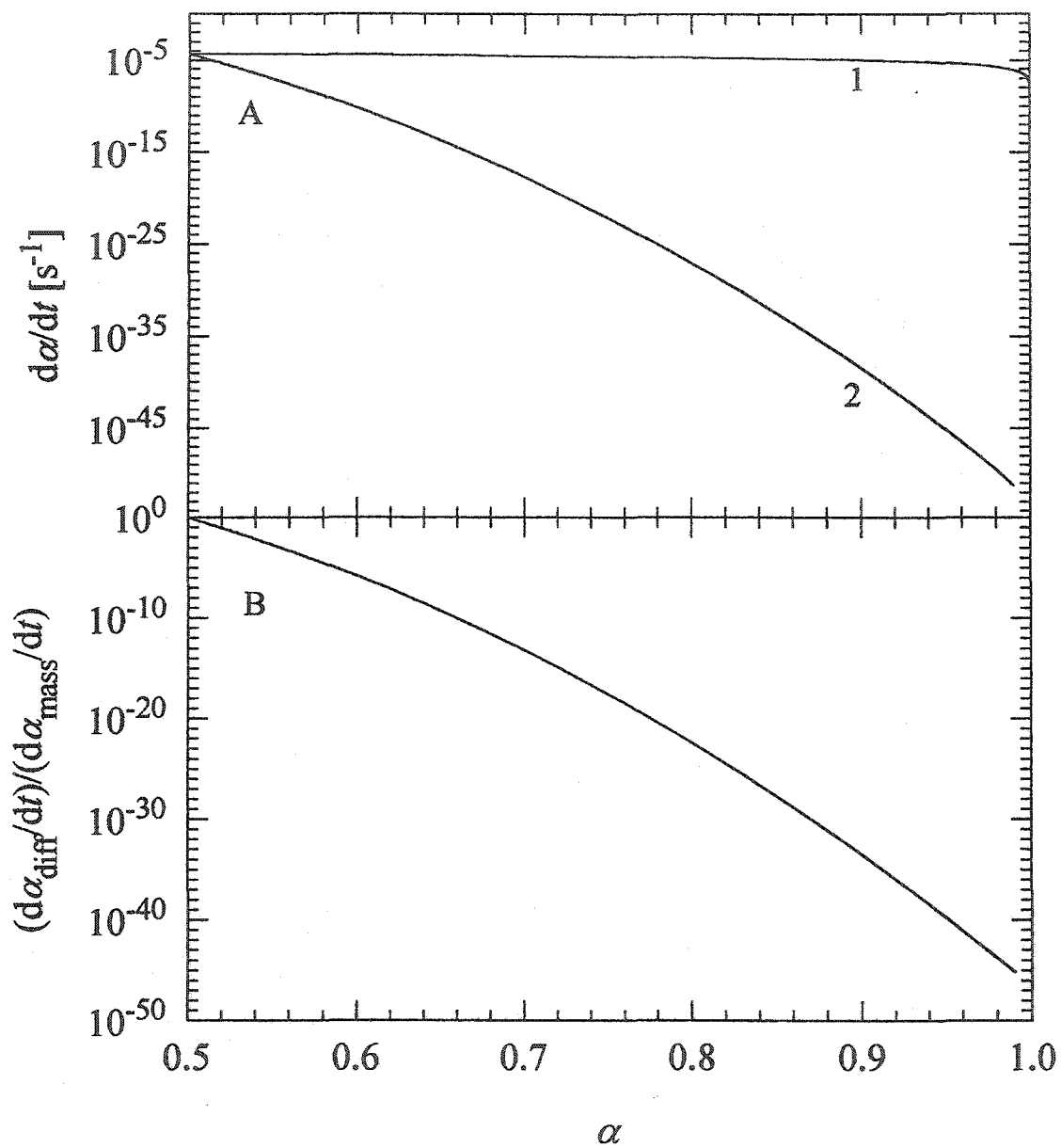


Fig. 5.6. (A). The calculated  $d\alpha/dt$  for mass-controlled and diffusion-controlled reactions is plotted against the extent of polymerization  $\alpha$ . Curve 1 refers to the mass-controlled, and 2 to the diffusion-controlled reaction kinetics. (B). The ratio of corresponding calculated  $(d\alpha_{diff}/dt)/(d\alpha_{mass}/dt)$  values is plotted against the extent of polymerization  $\alpha$ .

and the second at  $t_x = 60$  ks, where curve 1 crosses curve 2, and  $(d\alpha_{\text{diff}}/dt) = (d\alpha_{\text{mass}}/dt)$ . Before  $t_x$ ,  $(d\alpha_{\text{diff}}/dt) < (d\alpha_{\text{mass}}/dt)$ , and after  $t_x$ ,  $(d\alpha_{\text{diff}}/dt) > (d\alpha_{\text{mass}}/dt)$ .

We now compare the shape of the plots of  $(d\alpha_{\text{diff}}/dt)$  and  $(d\alpha_{\text{mass}}/dt)$  in the  $\alpha$ -domain, i. e., irrespective of the difference in polymerization time. Since  $\alpha_{\text{diff}} = \alpha_{\text{mass}}$  and  $\alpha(0) < \alpha_{\text{diff}}(t)$ , the quantity  $(d\alpha_{\text{diff}}/dt)$  in Eq. (5.24) will be less than  $(d\alpha_{\text{mass}}/dt)$ . Except at  $t = 0$ , where  $(d\alpha_{\text{diff}}/dt)$  and  $(d\alpha_{\text{mass}}/dt)$  are assumed to be equal, there is no condition in the  $\alpha$ -domain for which  $(d\alpha_{\text{diff}}/dt)$  would be equal to  $(d\alpha_{\text{mass}}/dt)$ , as is seen in Fig. 5.6(A) and (B). The distinction between the mass-controlled and diffusion-controlled kinetics therefore appears in the plots of  $(d\alpha_{\text{mass}}/dt)$  and  $(d\alpha_{\text{diff}}/dt)$ , at high  $\alpha$  values. We conclude that changes in the shape of such plots with  $\alpha$  may be used as an indication of the change in the reaction kinetics from mass-controlled to diffusion-controlled.

## 5.5 Summary

As the extent of polymerization increases at a fixed temperature, the increase in the liquid's viscosity causes a decrease in the reaction rate coefficient, as the mass-controlled polymerization kinetics changes gradually to diffusion-controlled polymerization kinetics. This change is indicated by a progressively more rapid increase in the negative slope of the plot of logarithmic rate coefficient against the extent of polymerization. The onset of diffusion-control may be determined from such plots. This onset shifts to a lower extent of reaction when the polymerization temperature is decreased.

For a fixed extent of polymerization after the viscosity has reduced to a relatively high value, the reaction rate coefficient decrease with decrease in the polymerization

temperature in the same manner as the reciprocal of the liquid's viscosity. This would indicate that the polymerization kinetics has become diffusion-controlled. The temperature for the onset of diffusion control at a certain extent of reaction may be determined from the plots of logarithmic rate coefficient against the reciprocal polymerization temperature. For higher extents of polymerization, the onset temperature is higher.

The simulated plots of the reaction rates for the mass-controlled kinetics are distinguished from those for the diffusion-controlled kinetics. For all extents of polymerization, the rate for the former kinetics remains higher than the rate for the latter kinetics. In the polymerization time domain, the rate for mass-controlled kinetics is higher than that of the diffusion-controlled kinetics up to a certain time, and then becomes lower. The ratio of the two rates goes through a maximum at a certain time of polymerization.

## Chapter 6

# Dielectric Properties and Polymerization Conditions

### 6.1 Introduction

Dielectric spectroscopy has recently been developed as a technique for studying the physical property changes that occur during the course of polymerization of a molecular liquid [Johari (1993, 1994)]. The technique is also seen to be useful for studying polymer degradation. Experiments may also be conducted either isothermally or with decreasing or increasing temperature or a combination of the three [Tombari *et. al.* (1997)]. In this spectroscopic technique, the real and imaginary components of the dielectric permittivity,  $\epsilon'$  and  $\epsilon''$ , respectively, are measured as function of frequency over a wide range from 0.1 Hz to 12 GHz. This also leads to determination of the dc conductivity,  $\sigma_0$ , at different times during the course of polymerization or of polymer degradation. The shape of the  $\epsilon'$  and  $\epsilon''$  spectra changes as polymerization progresses and the position of the spectra shifts along the frequency scale [Johari (1993, 1994), Tombari *et. al.* (1997)]. In addition, the equilibrium dielectric permittivity, the infrared polarizability and the optical refractive

index change because the density increases on polymerization or on polymer's degradation [Tombari *et. al.* (1997), Johari *et. al.* (1999), Wasylshyn *et. al.*(1997, 1999)].

Polymerization performed at a fixed temperature does not reach completion when the temperature is low. But a low temperature is necessary for performing polymerization when the molecular liquids are volatile or have a low boiling point or else decompose at high temperature. Once polymerization has occurred to a limited extent the vapor pressure decreases and boiling point increases. Thereafter, the partially polymerized mixture may be heated to a higher temperature to allow further polymerization until the maximum limit of polymerization is reached. This process is known as post-polymerization.

During the course of polymerization chemical structure of the liquid changes as much as new covalent bonds form although the entities in the polymer structure remain the same as in the molecular liquid state if polymerization is additive. Thus dielectric spectroscopy has been used to study the effects of these chemical structure changes on the physical state of a polymerizing mixture or of a polymer degrading to its oligomer structure.

Here, we provide results of an experimental study of typical polymerizing mixture, aniline and resorcinol diglycidyl ether, and its analysis in terms of its physical state as observed by dielectric spectroscopy performed during the course of polymerization. In order to familiarize a reader with the subject of dielectric spectroscopy, we first provide a brief background to the dielectric phenomenon.

## 6.2 The Dielectric Polarization and Relaxation Formalism

When a constant external electric field  $E_0$  is applied at time  $t = 0$ , to a homogeneous, isotropic and linear dielectric medium containing electric dipoles under constant temperature and pressure, the polarization  $P$  changes with time according to,

$$P(t) = P_U + (P_R - P_U)[1 - \phi(t)], \quad (6.1)$$

where  $P_U$  is the instantaneous polarization which includes both the infrared and the electronic polarization,  $P_R$  is the equilibrium or long-time limit of the polarization and  $\phi(t)$  is a relaxation function of the material. The term  $(P_R - P_U)[1 - \phi(t)]$  is a measure of the time-dependent polarization. The value of  $\phi(t)$  is 1 when  $t = 0$ , and 0 when  $t \rightarrow \infty$ . Thus,  $P(t = 0) = P_U$ , and  $P(t = \infty) = P_R$ . The electrical displacement,  $D$ , is defined by,

$$D(t) = \epsilon_0 E(t) + P(t) = \epsilon_0 \epsilon(t) E(t), \quad (6.2)$$

where  $\epsilon_0$  is the permittivity of vacuum ( $= 8.8542 \text{ pF/m}$ ), and  $\epsilon(t)$  is called the relative permittivity of the dielectric material. Its magnitude is given by

$$\epsilon(t) = \epsilon_\infty + (\epsilon_s - \epsilon_\infty)[1 - \phi(t)] = \epsilon_\infty + \Delta\epsilon[1 - \phi(t)], \quad (6.3)$$

where  $\epsilon_\infty$  is the limiting high-frequency relative permittivity approximated at  $t = 0$  or at a frequency in the low limit of the infrared spectra, and  $\epsilon_s$  is the limiting low-frequency relative permittivity approximated for the condition when  $t \rightarrow \infty$ . The latter is also called the equilibrium permittivity. The difference  $\Delta\epsilon \equiv (\epsilon_s - \epsilon_\infty)$  is known as the magnitude or strength of the dielectric relaxation and it is a measure of the orientation polarization.

When the applied electric field is sinusoidal in time, it is expressed as a complex function as:

$$E^*(t) = E_0 \exp(i\omega t), \quad (6.4)$$

where,  $E_0$  is the amplitude of the electrical field,  $\omega$  is the angular frequency ( $\omega = 2\pi f$ , where  $f$  is the frequency) and  $i = \sqrt{-1}$ . The complex electric displacement is given by:

$$D^*(t) = \varepsilon^* E^*, \quad (6.5)$$

where  $\varepsilon^*$  is now the complex dielectric function.

According to the Boltzmann superposition principle [Boltzmann (1876), Hopkinson (1877), Curie (1888)],  $\varepsilon^*$  in the frequency domain may be written as,

$$\varepsilon^*(\omega) = \varepsilon_\infty + \Delta\varepsilon \int_0^\infty \exp(-i\omega t) \left[ -\frac{\partial\phi(t)}{\partial t} \right] dt, \quad (6.6)$$

where the integral term is the Laplace transformation of the function  $(-d\phi/dt)$ . Equation (6.6) therefore describes the frequency dependence of  $\varepsilon^*(\omega)$  according to the relaxation function  $\phi(t)$ . By separating the real and imaginary parts of  $\varepsilon^* \equiv \varepsilon' - i\varepsilon''$  in Eq. (6.6),

$$\frac{\varepsilon'(\omega) - \varepsilon_\infty}{\Delta\varepsilon} = \text{Re} \left\{ \int_0^\infty \exp(-i\omega t) \left[ -\frac{\partial\phi(t)}{\partial t} \right] dt \right\}, \quad (6.7)$$

$$\text{and, } \frac{\varepsilon''(\omega)}{\Delta\varepsilon} = \text{Im} \left\{ \int_0^\infty \exp(-i\omega t) \left[ -\frac{\partial\phi(t)}{\partial t} \right] dt \right\}, \quad (6.8)$$

where  $\varepsilon'$  is called the dielectric permittivity,  $\varepsilon''$  the dielectric loss. These two quantities define the loss tangent or the loss factor as,  $\tan\delta \equiv \varepsilon''/\varepsilon'$ . For our convenience here, the normalized complex dielectric function  $N^*(\omega)$ , normalized dielectric permittivity  $N(\omega)$  and normalized dielectric loss  $N''(\omega)$  are defined as:

$$N^*(\omega) \equiv \frac{\varepsilon^*(\omega) - \varepsilon_\infty}{\Delta\varepsilon}, \quad (6.9)$$

$$N'(\omega) \equiv \frac{\varepsilon'(\omega) - \varepsilon_\infty}{\Delta\varepsilon}, \quad (6.10)$$

$$N''(\omega) \equiv \frac{\varepsilon''(\omega)}{\Delta\varepsilon}. \quad (6.11)$$

Debye (1929) had shown that for dielectric relaxation of most liquids at high temperatures, the relaxation function in the time domain is given by,

$$\phi(t) = \exp\left(-\frac{t}{\tau_0}\right), \quad (6.12)$$

where  $\tau_0$ , is the relaxation time. In the frequency domain, therefore, Eqs.(6.6) - (6.8) for Debye relaxation function become,

$$\frac{\varepsilon^* - \varepsilon_\infty}{\Delta\varepsilon} = N^*(\omega) = \frac{1}{1 + i\omega\tau_0}, \quad (6.13)$$

$$\frac{\varepsilon' - \varepsilon_\infty}{\Delta\varepsilon} = N'(\omega) = \frac{1}{1 + \omega^2\tau_0^2}, \quad (6.14)$$

$$\frac{\varepsilon''}{\Delta\varepsilon} = N''(\omega) = \frac{\omega\tau_0}{1 + \omega^2\tau_0^2}, \quad (6.15)$$

$$\tan \delta = \frac{\Delta\varepsilon\omega\tau_0}{\Delta\varepsilon + \varepsilon_\infty(1 + \omega^2\tau_0^2)}. \quad (6.16)$$

The Debye relaxation function of Eq. (6.12) has been found to be an approximation for the dielectric behavior of liquids or of dilute solutions containing simple polar molecules and at not too low temperatures, or too viscous a state. In reality, for a variety of molecular liquids, ceramics, glasses, polymers, and polymer solutions, the relaxation function is more complex, and has been described by empirical equations obtained by fitting to the data. In dielectric studies performed in the frequency domain, the empirical functions have been

known as, Cole-Cole (1941, 1942), Fuoss-Kirkwood (1941), Davidson-Cole (1950), Havriliak-Negami (1966, 1967), Johnscher (1975) and Hill (1978).

An empirical function most widely used since 1980 is the stretched exponential relaxation function. It was first introduced by Kohlrausch (1847), for mechanical deformation of fibers in the time domain. Williams and Watts (1970) adapted the stretched exponential relaxation function for dielectric studies in the frequency domain. The stretched exponential relaxation function is thus generally referred as KWW function. It is written as:

$$\phi(t) = \exp\left(-\frac{t}{\tau_0}\right)^\beta, \quad (6.17)$$

where  $\beta$  is the stretched exponential parameter whose value is between 0 and 1, and  $\tau_0$  is the characteristic relaxation time. Although its form in the time domain, *i.e.*, Eq. (6.17), is mathematically simple, its corresponding frequency domain form is mathematically somewhat complex and has to be calculated numerically. Accordingly, for  $0 < \beta < 1$ ,  $N'$  and  $N''$  have been written as [Moynihan *et al.* (1973), Lindsey and Patterson (1980), Dishon *et al.* (1985) and Muzeau *et al.* (1991)],

$$N'(z) = 1 - \pi z V(\beta, z), \quad (6.18)$$

$$N''(z) = \pi z Q(\beta, z), \quad (6.19)$$

where  $z = \omega\tau_0$ , and  $V(\beta, z)$  and  $Q(\beta, z)$  are integral terms, as defined below,

$$V(\beta, z) = \frac{1}{\pi} \int_0^\infty \exp(-u^\beta) \sin(zu) du, \quad (6.20)$$

$$Q(\beta, z) = \frac{1}{\pi} \int_0^\infty \exp(-u^\beta) \cos(zu) du, \quad (6.21)$$

where  $u$  is a variable for integration. Equations (6.20) and (6.21) have been calculated numerically by Moynihan *et al.* (1973), Lindsey and Patterson (1980), Dishon *et al.* (1985) and Muzeau *et al.* (1991) for  $\beta$  between 0.1 and 0.7 and for  $z (= \omega\tau_0)$  between  $10^{-3}$  to  $10^4$ .

The stretched exponential function has also been mathematically expressed as a superposition of exponential relaxation functions with a relaxation time distribution function  $g(\tau)$  as,

$$\phi(t) = \int_0^{\infty} g(\tau) \exp(-t/\tau) d\tau, \quad (6.22)$$

within the normalization condition,

$$\int_0^{\infty} g(\tau) d\tau = 1. \quad (6.23)$$

Therefore, the average relaxation time,  $\langle \tau \rangle$  is given by

$$\langle \tau \rangle \equiv \int_0^{\infty} \tau g(\tau) d\tau = \int_0^{\infty} \phi(t) dt. \quad (6.24)$$

Moynihan *et al.* (1973) have combined Eqs. (6.17) and (6.24) to express  $\langle \tau \rangle$  in terms of  $\tau_0$  and  $\beta$  through a gamma function of  $1/\beta$ .

$$\langle \tau \rangle = \frac{\tau_0}{\beta} \Gamma\left(\frac{1}{\beta}\right). \quad (6.25)$$

### 6.3 Experimental Methods

The chemicals used as the precursors were, Aniline (AN) and Resorcinol diglycidyl ether (RDGE). Aniline of better than 99.0% purity was purchased from Anachemia, and

Resorcinol diglycidyl ether of better than 99% purity was purchased from Aldrich Chemicals. These chemicals were liquids at ambient temperature. Their molecular structures and polymerization reactions are shown in Fig. 6.1. Stoichiometric mixtures of AN and RDGE in molar ratio of 1:1 were prepared by weighing in a total amount of about 2 grams, thoroughly mixed mechanically and transferred to a glass vial of diameter 10 mm and length 35 mm. A miniature capacitor with 18 parallel plates was immersed in the liquid mixture contained inside the vial. The capacitor's electrical capacitance ( $\approx 16$  pF) was measured precisely in air before it was inserted to the vial. A copper-constantan thermocouple was also immersed in the liquid, the electrical connections were made and the vial was sealed. It was then inserted into the hole drilled thermostat block already maintained at a predetermined temperature. The temperature of the thermostat block was controlled during both heating and cooling cycles at a constant rate, or else it was kept at predetermined temperature for performing experiments under isothermal conditions. The detailed method has been described earlier [Wasylyshyn *et. al.* (1997)]

The dielectric permittivity and loss spectra was measured over the frequency range 10 Hz - 500 MHz by using QuadTech Model 7400 Precision LCR Meter. The accuracy of QuadTech 7400 was set at  $\pm 0.25\%$ . A Labview program run on a PC computer was used to record the data automatically. The data acquisition program allowed us to collect a complete set of spectra containing 48 frequency data points equally spaced on a logarithmic frequency scale, in 30 – 45 s. The data files thus obtained contained the permittivity  $\epsilon'$ , the dielectric loss  $\epsilon''$ , and the ac conductivity

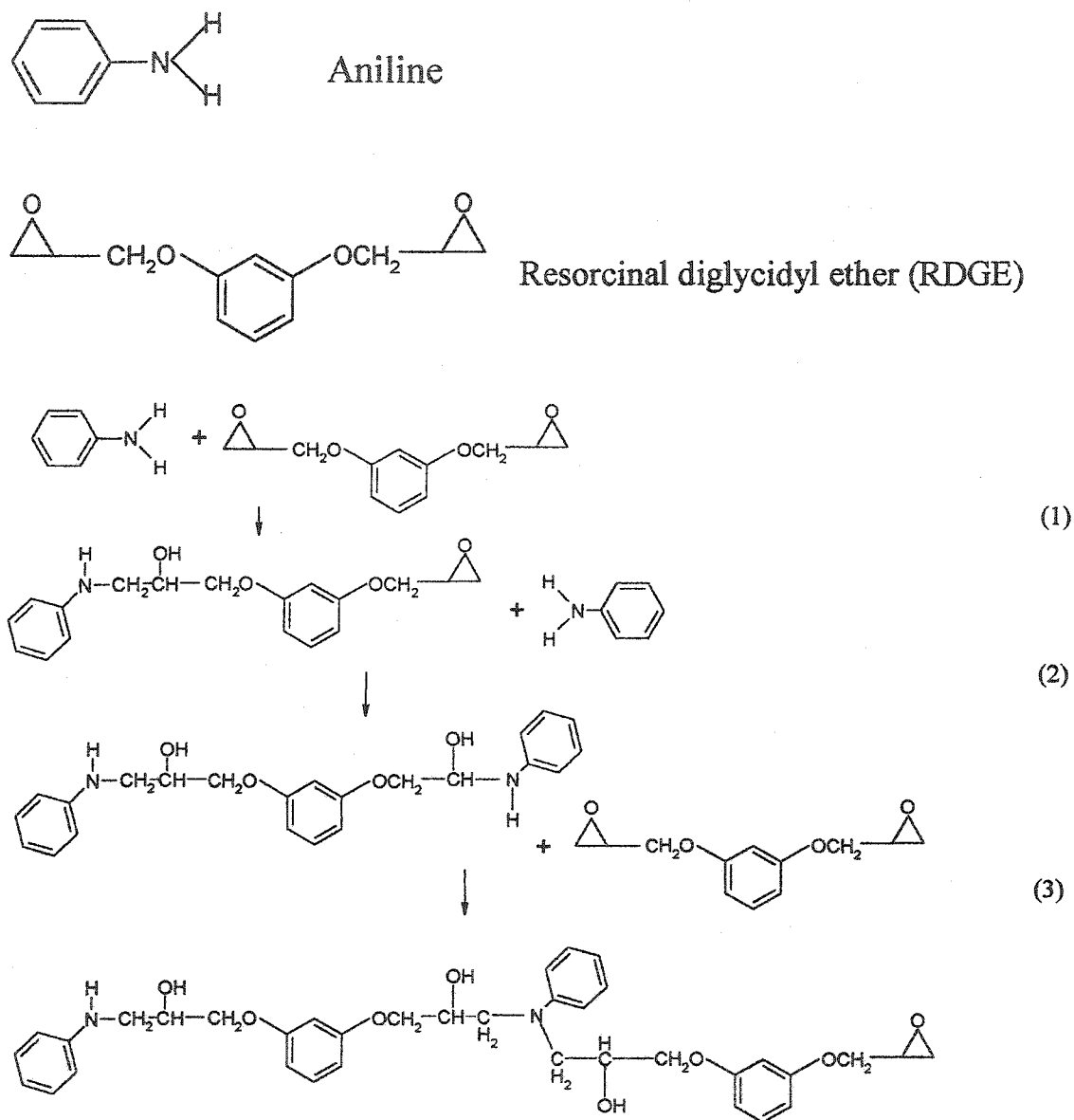


Fig. 6.1. The chemical structures of aniline (AN) and Resorcinol diglycidyl ether (RDGE), and the first three steps of polymerization reaction which forms linear polymer chain in the 1:1 AN and RDGE mixture.

measured at the time of polymerization,  $t_{\text{poly}}$  and the temperature  $T_{\text{poly}}$ . The data were continuously measured at a time interval of 1 - 5 minutes, depending upon the time elapsed since the polymerization began. For a typical dielectric permittivity of  $\epsilon' \sim 4.0$  and loss factor of  $\epsilon'' \sim 0.1$ , the accuracy of  $\epsilon$  are  $\Delta\epsilon' \sim \pm 0.01$  and  $\Delta\epsilon'' \sim \pm 0.00025$ . The absolute accuracy of the temperature measurement is less than 0.5 K and the relative accuracy of the time measurement is less than 0.05%.

The glass transition temperature,  $T_g$  of the completely polymerized AN and RDGE mixture was determined by using the method described in Section 2.3.2 on the differential scanning calorimetry data measured as described in Section 5.2. It was found to be about  $333 \pm 1$  K. Five samples of the mixture were polymerized by keeping isothermally at different temperatures,  $T_{\text{poly}}$  for different times,  $t_{\text{poly}}$ . These were: 303.2 K for 260 ks, 313.2 K for 86 ks, 323.2 K for 60 ks, 333.2 K for 60 ks, 343.2 K for 54 ks.

After polymerization of each sample at the above mentioned temperatures and time periods, the sample was cooled to 298 K, heated at a rate of  $q_h = 0.3$  K/min to a post-polymerization temperature,  $T_{\text{post}}$ , which is well above  $T_g$ . The isothermal post-polymerization time,  $t_{\text{post}}$ , was 60 ks. For the samples with  $T_{\text{poly}}$  at 303.2, 313.2 and 333.2 K,  $T_{\text{post}}$  was set at 400 K and for samples with  $T_{\text{poly}}$  at 323.2, and 343.2 K,  $T_{\text{post}}$  was set at 373 K. Details of the thermal history of each sample during polymerization and post-polymerization are provided in Table 6.1.

Table 6.1. The polymerization conditions for AN-RDGE mixture.

$T_{\text{poly}}$ [K]	$t_{\text{poly}}$ [ks]	$q_{\text{h}}$ [K/min]	$T_{\text{post}}$ [K]	$t_{\text{post}}$ [ks]
303.2	260	0.3	400.2	60
313.2	86	0.3	400.2	60
323.2	60	0.3	373.2	60
333.2	60	0.3	400.2	60
343.2	60	0.3	373.0	60

## 6.4 Results and Data Analysis

The equipment had been designed to collect spectra at two minute intervals during the period of polymerization. Therefore, in a typical polymerization period, more than one hundred  $\epsilon'$  and  $\epsilon''$  spectra of a polymerizing mixture at each of the preselected polymerization temperature were collected. Here, the spectra obtained only at selected time,  $t_{\text{poly}}$ , during the progress of polymerization are included. These spectra are shown in Figs. 6.2 - 6.6, where the polymerization time has been indicated. The spectra correspond to the polymer structure formed at time  $t_{\text{poly}}$  during the isothermal polymerization.

In Figs. 6.2-6.6, when the  $\epsilon''$  peak was in the frequency range from 10 Hz to 500 MHz, the measurement range of QuadTech Model 7400 Precision LCR Meter, the spectra of both  $\epsilon'$  and  $\epsilon''$  can be analyzed by fitting to KWW relaxation function and using Eqs. (6.10 - 6.11, 6.18 - 21). Over this frequency window, the contribution to measured  $\epsilon''$  and  $\epsilon'$  from the electrode polarization effect were calculated in the manner given earlier [Wasylyshyn *et al.* (1997)]. It was found to be at most 2%, and was neglected. Therefore, the measured  $\epsilon'$  value is only from the mixture's dipolar

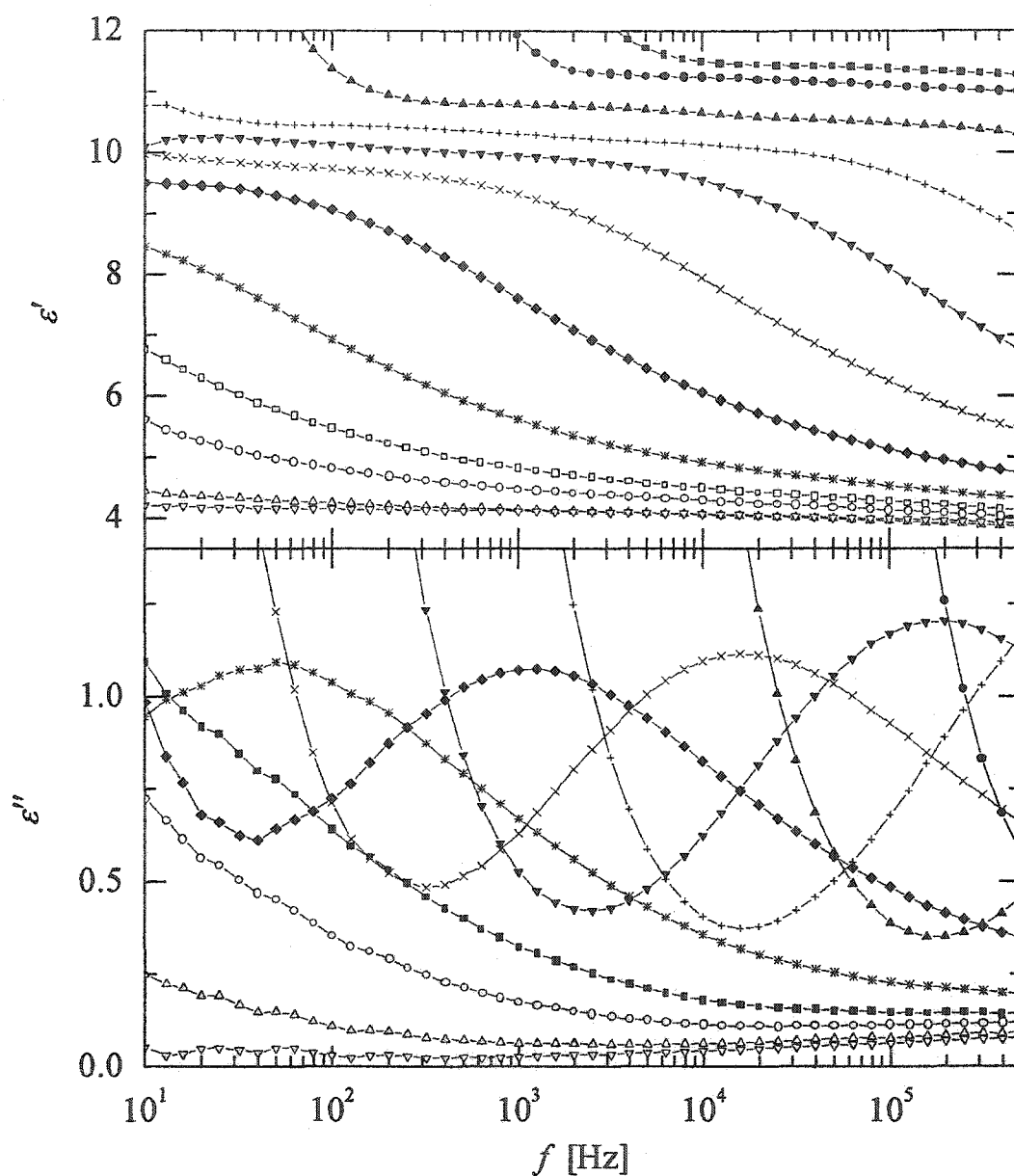


Fig. 6.2. The spectra of  $\epsilon'$  and  $\epsilon''$  measured during the course of polymerization for AN-RDGE mixture at 303.2 K. The symbols correspond to different  $t_{\text{poly}}$  (ks) as: (■) 0.20, (●) 24.3, (▲) 50.3, (+) 65.2, (▼) 75.2, (×) 85.2, (◆) 95.1, (\*) 105.2, (□) 115.1, (○) 125.0, (△) 150.1, (▽) 260.3.

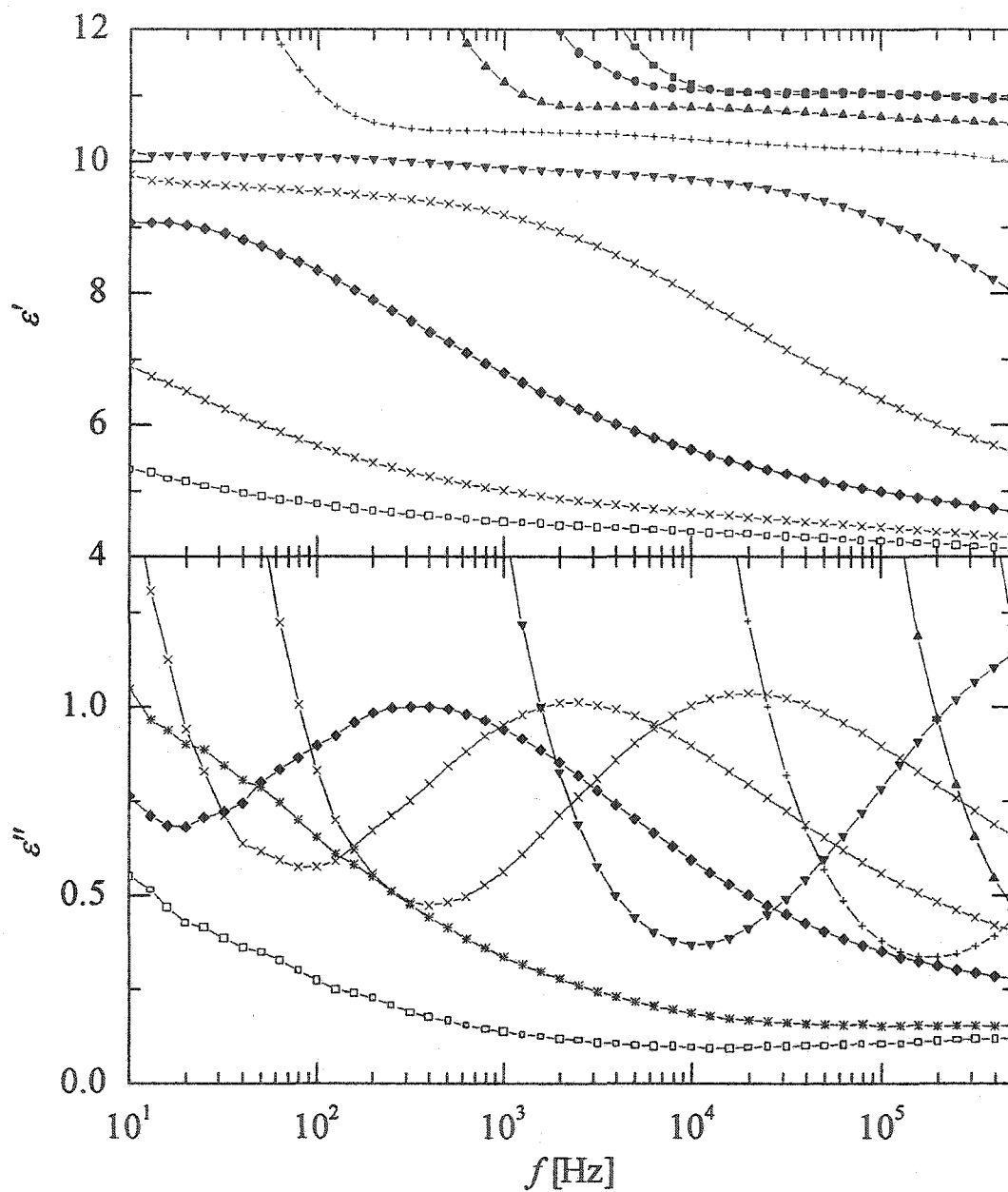


Fig. 6.3. The spectra of  $\epsilon'$  and  $\epsilon''$  measured during the course of polymerization for AN-RDGE mixture at 313.2 K. The symbols correspond to different  $t_{\text{poly}}$  (ks) as: (■) 1.0, (●) 10.0, (▲) 20.0, (+) 30.0, (▼) 39.9, (×) 49.9, (◆) 59.9, (\*) 72.9, (□) 85.7.

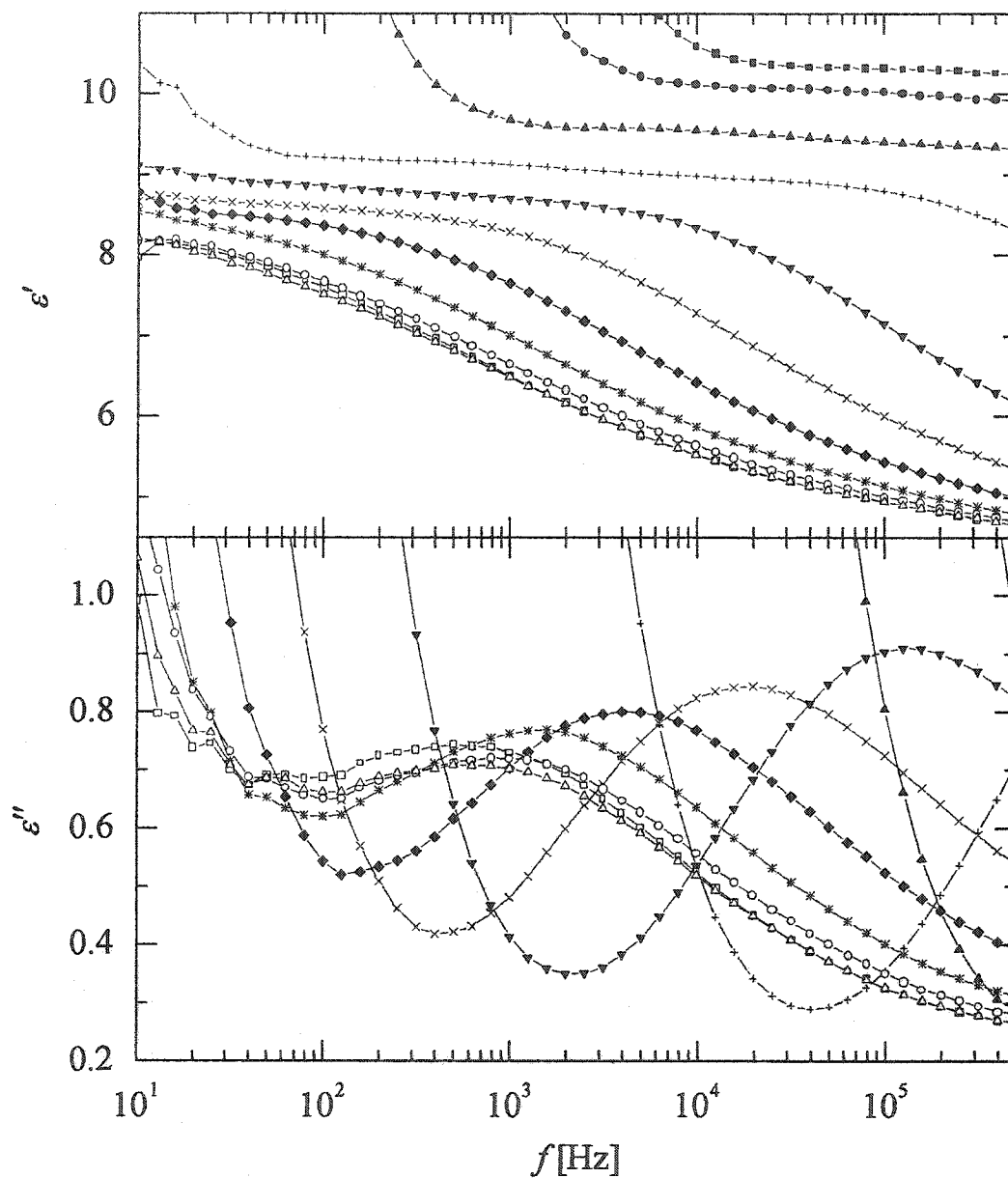
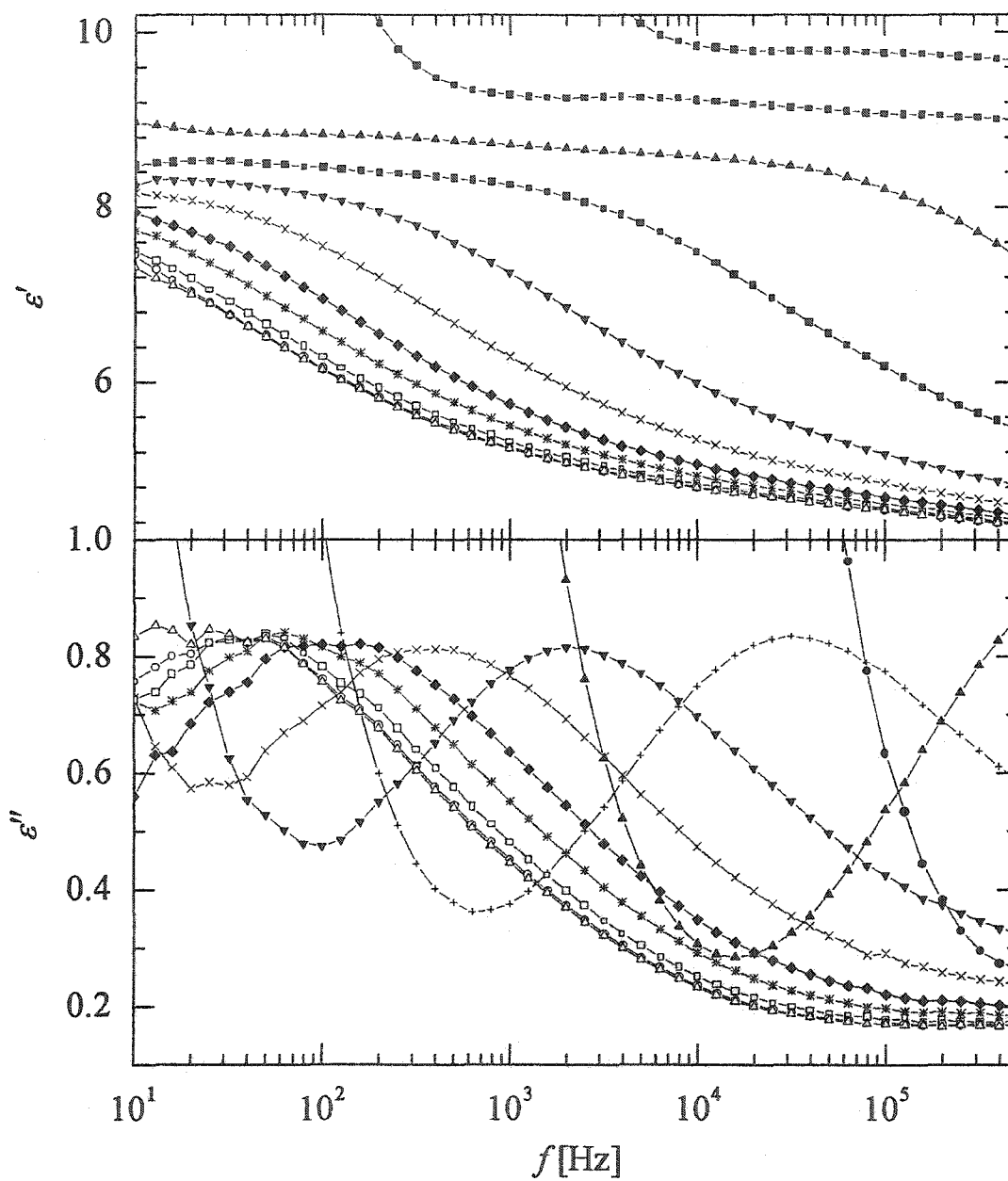


Fig. 6.4. The spectra of  $\varepsilon'$  and  $\varepsilon''$  measured during the course of polymerization for AN-RDGE mixture at 323.2 K. The symbols correspond to different  $t_{\text{poly}}$  (ks) as: (■) 5.0, (●) 10.0, (▲) 15.0, (+) 20.0, (▼) 25.0, (×) 30.0, (◆) 35.0, (\*) 40.0, (□) 45.0, (○) 50.0, (Δ) 55.0.



6.5. The spectra of  $\epsilon'$  and  $\epsilon''$  measured during the course of polymerization for AN-RDGE mixture at 333.2 K. The symbols correspond to different  $t_{\text{poly}}$  (ks) as: (■) 5.0, (●) 10.0, (▲) 15.0, (+) 20.0, (▼) 25.0, (×) 29.9, (◆) 35.1, (\*) 40.0, (□) 48.0, (○) 57.9, (Δ) 66.9.

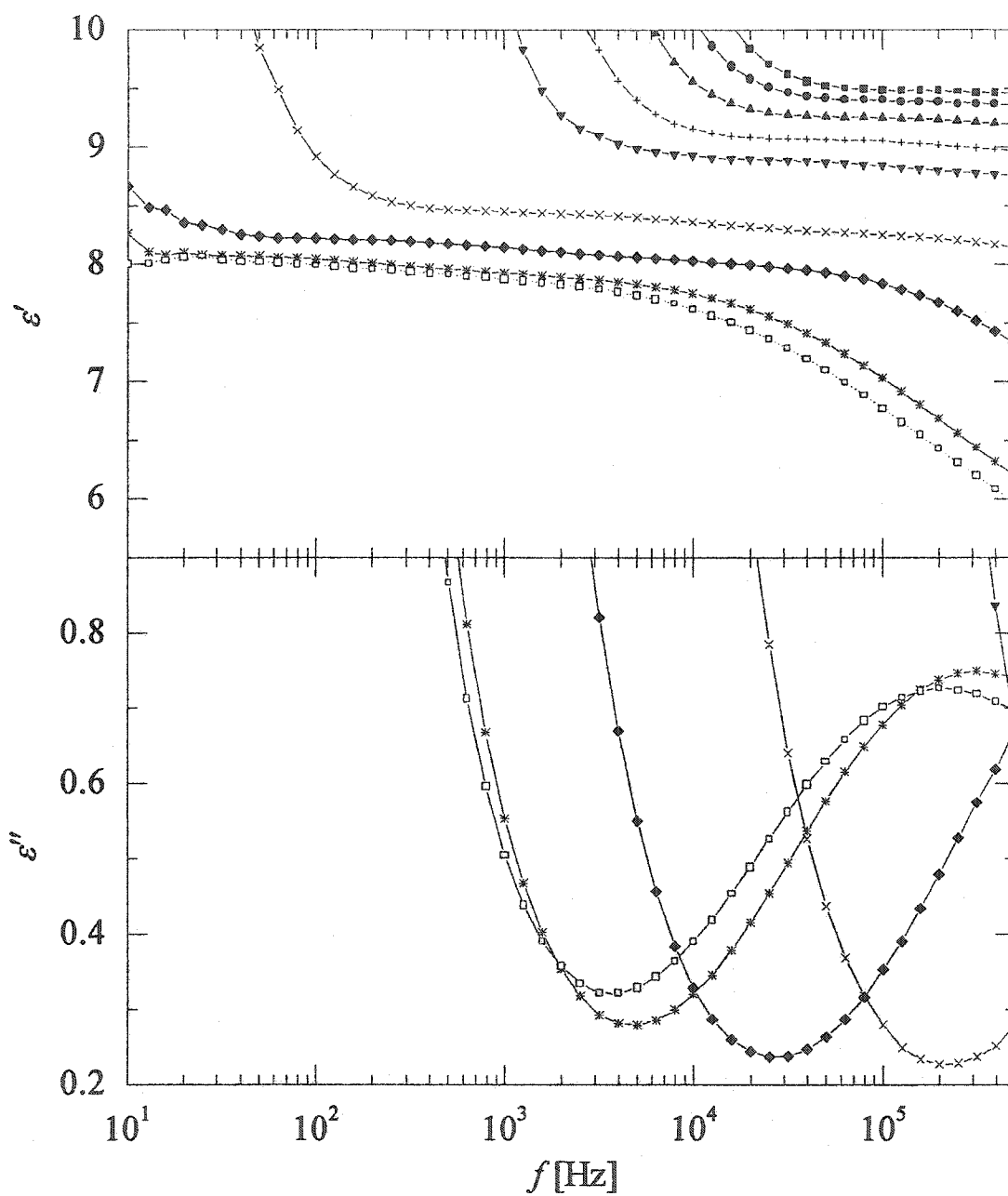


Fig. 6.6. The spectra of  $\varepsilon'$  and  $\varepsilon''$  measured during the course of polymerization for AN-RDGE mixture at 343.2 K. The symbols correspond to different  $t_{\text{poly}}$  (ks) as: (■) 1.01, (●) 2.03, (▲) 3.05, (+) 4.07, (▼) 4.94, (×) 7.55, (◆) 10.0, (\*) 15.1, (□) 57.8.

orientation, i.e.,  $\varepsilon' = \varepsilon'_{\text{dip}}$ . When the mixture's viscosity is low, as at the early stage of polymerization, or at a high temperature above its  $T_g$ , the ionic impurities have a high mobility and since these ions transport the electrical charge, the dc conductivity is high. This increases the dc conductivity contribution to  $\varepsilon''$  according to the equation [von Schweidler (1907), Manning and Bell (1940)]:

$$\varepsilon''_{\text{dip}}(f) = \varepsilon''(f) - \frac{\sigma_0}{2\pi\varepsilon_0 f} \quad (6.26)$$

where  $\sigma_0$  is the dc conductivity, or  $\sigma(f \rightarrow 0)$ ,  $\varepsilon_0$  is the permittivity of vacuum ( $= 8.8542$  pF/m) and  $f$  is the frequency in Hz. Since,  $\varepsilon''_{\text{dip}} \rightarrow 0$  as  $f \rightarrow 0$ , Eq. (6.26) in the low frequency limit becomes,  $\log[\varepsilon''(f)] = \log[\sigma_0/(2\pi\varepsilon_0)] - \log(f)$ , and a plot of  $\log[\varepsilon''(f)]$  against  $\log(f)$  is a straight line with a slope of 1, and intercept  $\log[\sigma_0/(2\pi\varepsilon_0)]$ . The value of  $\sigma_0$  at different  $t_{\text{poly}}$  was determined from such plots.

The  $\log(\sigma_0)$  for mixture polymerizing at 303.2, 313.2, 323.2, 333.2 and 343.2 K is plotted against the  $\log(t_{\text{poly}})$  in Fig. 6.7. In this figure the magnitude of  $\log(\sigma_0)$  decreases rapidly with increase in  $t_{\text{poly}}$  with a progressively increasing negative slope for polymerization performed at 303.2K and 313.2 K. In contrast, the slope of the plot for polymerization performed at 323.2 K and 333.2 K tends to decrease at high value of  $t_{\text{poly}}$ . For polymerization performed at 343.2 K, the plot remains horizontal with a near zero slope.

We should note here that in our measured frequency range of 10 Hz - 500 MHz, only the  $\alpha$ -relaxation, i.e., the primary relaxation at temperature around and above  $T_g$ , could be observed. Thus in all the equations given in Section 6.2,  $\varepsilon_s$  should be

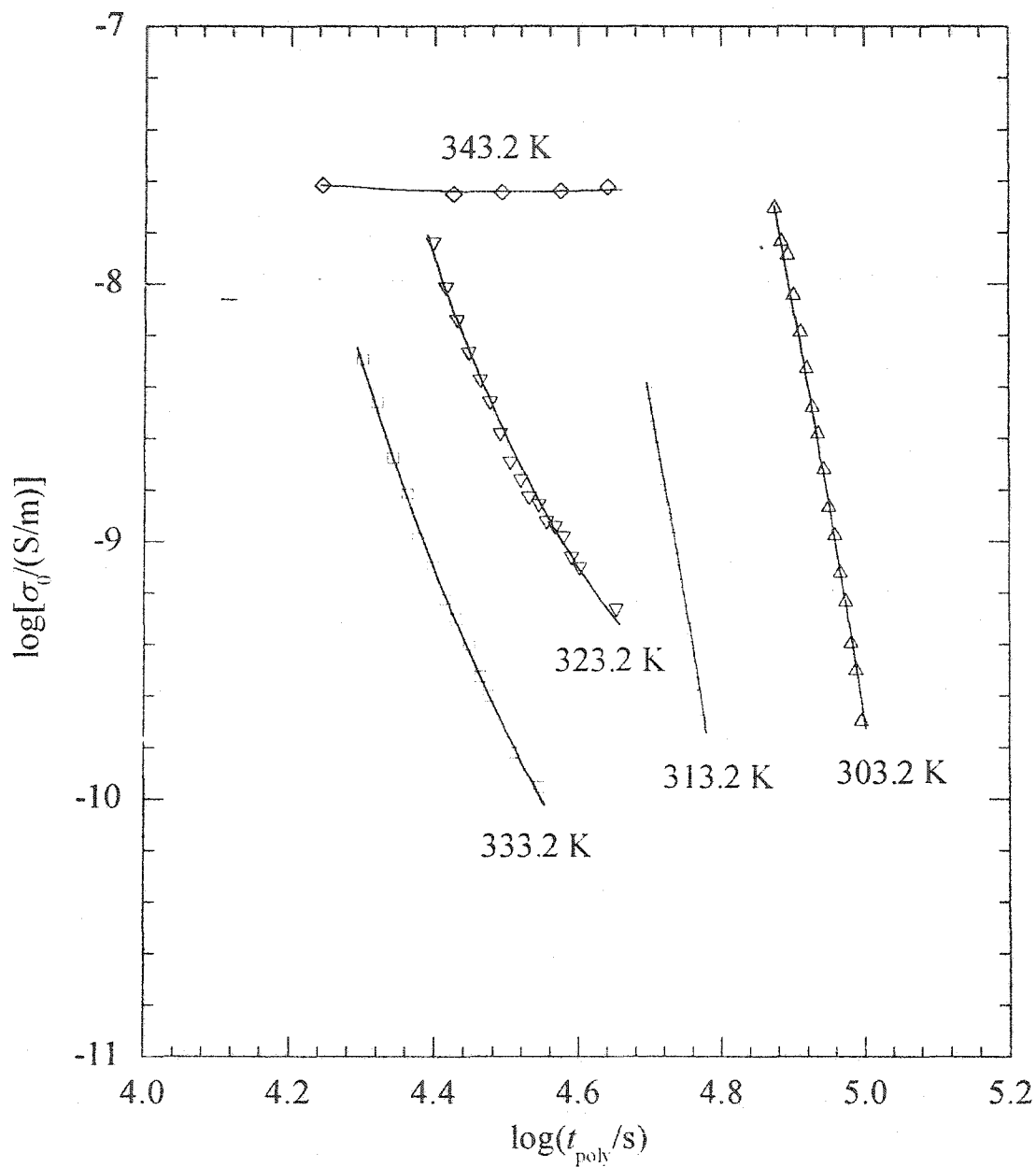


Fig. 6.7. The logarithmic dc conductivity  $\log(\sigma_0)$  is plotted against  $\log(t_{poly})$  during the polymerization of AN-RDGE mixture. The symbols correspond to different  $T_{poly}$  (K) as: ( $\Delta$ ) 303.2, ( $\circ$ ) 313.2, ( $\nabla$ ) 323.2, ( $\square$ ) 333.2, ( $\diamond$ ) 343.2.

corresponding to  $\varepsilon_{\alpha, s}$  and  $\varepsilon_{\infty}$  should be corresponding to  $\varepsilon_{\alpha, \infty}$ . The difference  $\Delta\varepsilon$  should thus correspond to  $\Delta\varepsilon_{\alpha} = (\varepsilon_{\alpha, s} - \varepsilon_{\alpha, \infty})$ , the magnitude of the  $\alpha$ -relaxation. Since we do not deal with other relaxation processes, the subscript  $\alpha$  will henceforth be dropped.

The parameters of  $\Delta\varepsilon$ ,  $\varepsilon_{\infty}$ ,  $\beta$  and  $\tau_0$  were obtained by fitting with the KWW relaxation function according to Eqs. (6.10 - 6.11, 6.18 - 21) to both  $\varepsilon'_{\text{dip}}$  and  $\varepsilon''_{\text{dip}}$  spectra simultaneously. The tabulated forms of  $N'(\omega\tau_0)$  and  $N''(\omega\tau_0)$  for this function were taken from calculations by Moynihan *et al.* (1973), Lindsey and Patterson (1980), Dishon *et al.* (1985) and Muzeau *et al.* (1991). In the fitting procedures using Eqs. (6.10 - 6.11, 6.18 - 21),  $\Delta\varepsilon$ ,  $\varepsilon_{\infty}$ ,  $\beta$  and  $\tau_0$  were input as adjustable parameters. The  $\varepsilon'_{\text{dip}}$  and  $\varepsilon''_{\text{dip}}$  spectra and the curves calculated from KWW relaxation function by Eqs. (6.10 - 6.11, 6.18 - 21) were plotted in three graphs simultaneously, two of which were  $\varepsilon'$  and  $\varepsilon''$  spectra and the third was the complex plane plots or the Cole-Cole plot of  $\varepsilon'$  against  $\varepsilon''$ . The four parameters  $\Delta\varepsilon$ ,  $\varepsilon_{\infty}$ ,  $\beta$  and  $\tau_0$  were adjusted manually until all the three calculated curves fitted the corresponding experimental data in each graph window. The fitting parameters  $\Delta\varepsilon$ ,  $\varepsilon_{\infty}$ ,  $\beta$  and  $\tau_0$  were obtained for one set of  $\varepsilon'_{\text{dip}}$  and  $\varepsilon''_{\text{dip}}$ . An example of a typical fit of the  $\varepsilon'_{\text{dip}}$  and  $\varepsilon''_{\text{dip}}$  spectra and the Cole-Cole plot is shown in Fig. 6.8(A), (B) and (C) for the AN-RDGE mixture polymerized at 303.2 K and at  $t_{\text{poly}}$  94.3 ks. The absolute fitting precision is 0.01 for  $\Delta\varepsilon$  and  $\varepsilon_{\infty}$ , and  $\beta$ . The relative fitting precision for  $\tau_0$  is 1%. The fittings were done for the selected spectra at different polymerization time for AN-RDGE mixture polymerized at different temperatures. The value of  $\langle\tau\rangle$  was then calculated from Eq. (6.25) from the known values  $\beta$  and  $\tau_0$ . The obtained parameters  $\beta$  and  $\log\langle\tau\rangle$  for all the

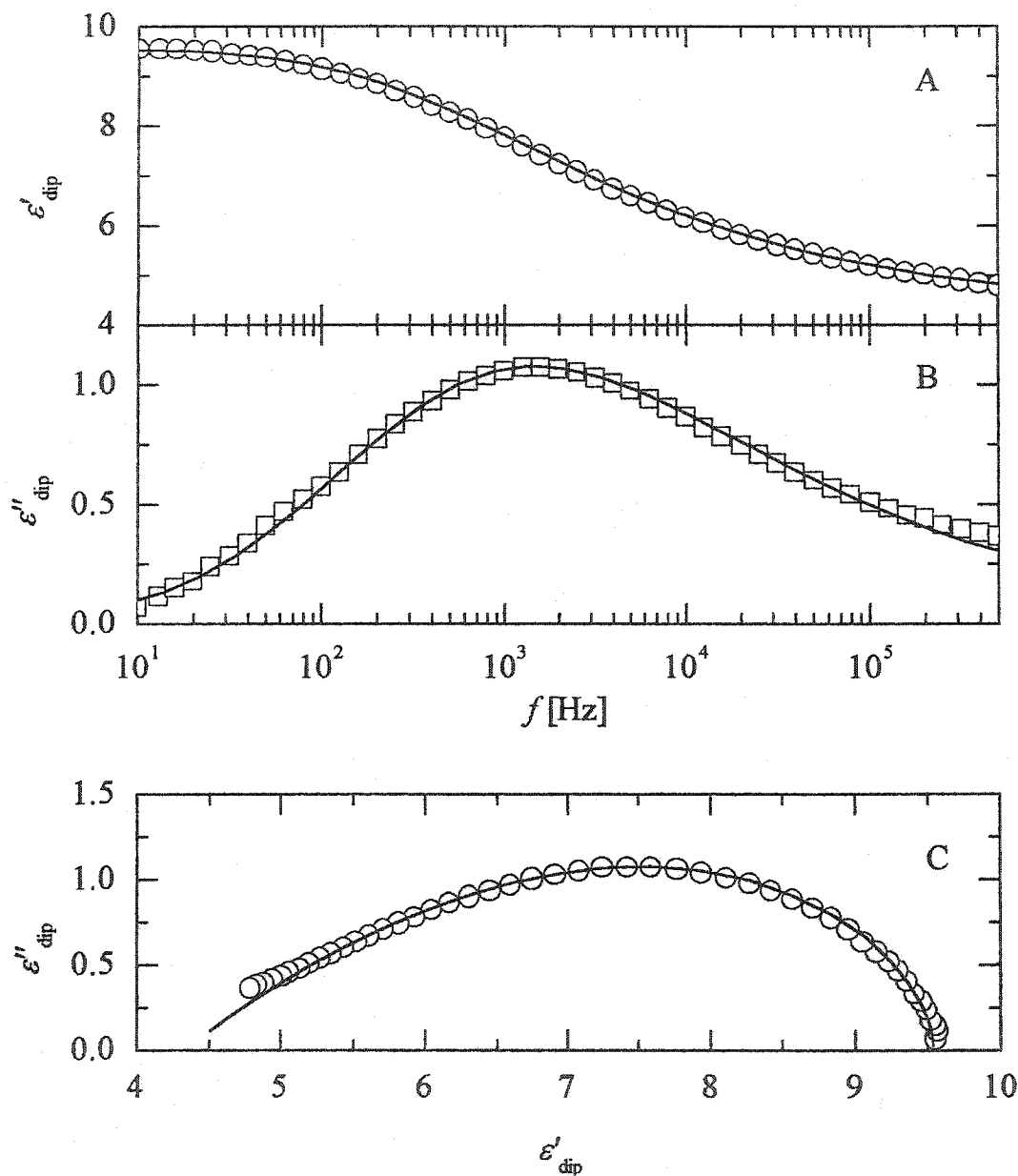


Fig. 6.8. A typical fitting of dielectric spectra  $\epsilon'_{\text{dip}}$  and  $\epsilon''_{\text{dip}}$  with KWW model for AN-RDGE mixture polymerizing at 303.2 K and at  $t_{\text{poly}}$  of 94.3 ks: (A).  $\epsilon'_{\text{dip}}$  and (B).  $\epsilon''_{\text{dip}}$ . They are plotted against frequency  $f$  in logarithmic scale. (C). the Cole-Cole plot of  $\epsilon''_{\text{dip}}$  against  $\epsilon'_{\text{dip}}$ . The symbols correspond to data obtained and the solid lines are the fitting results with KWW relaxation function.

five polymerization temperatures are plotted against  $\log(t_{\text{poly}})$  in Fig. 6.9(A) and (B). The values of  $\varepsilon_s (= \varepsilon_\infty + \Delta\varepsilon)$ ,  $\varepsilon_\infty$  and  $\Delta\varepsilon$  obtained from this analysis are plotted against  $\log(t_{\text{poly}})$  in Fig. 6.10.

The samples polymerized at different temperature were then cooled to 300 K and heated at 0.3 K/min to a post-polymerization temperature  $T_{\text{post}}$  and allowed to further polymerize for 60 ks to ensure complete polymerization if it may not have already occurred. The post-polymerization temperature,  $T_{\text{post}}$  was 373 K or 400 K, which is 40 K and 67 K, respectively, higher than the  $T_g$  of 333 K of the fully polymerized polymer, as measured here. Thus we consider that polymerization was completed after the post-polymerization within 60 ks at 373 K and at 400 K. Following the post-polymerization, the samples were cooled from the post-polymerization temperature at 0.3 K/min to 300 K and the dielectric measurement were performed during the cooling. The  $\varepsilon'$  and  $\varepsilon''$  spectra were measured during the cooling from post-polymerization temperatures to room temperature. An example of a typical  $\varepsilon'$  and  $\varepsilon''$  spectra at different temperatures during cooling from 400 K to 300 K is shown in Fig. 6.11 for the sample polymerized at 333.2 K for 60 ks and post-polymerized at 400.2 K for 60 ks. The above-described methods were used for obtaining  $\sigma_0$ ,  $\Delta\varepsilon$ ,  $\varepsilon_\infty$ ,  $\beta$  and  $\tau_0$  for each spectrum thus obtained for all the five samples which had been polymerized at selected temperatures. The  $\log(\sigma_0)$  is plotted against  $1000/T$  in Fig. 6.12 for all the five samples. The obtained parameters  $\beta$  and  $\log\langle\tau\rangle$  for all five samples of AN-RDGE mixture are plotted against  $1000/T$  in Fig. 6.13, and  $\varepsilon_s$ ,  $\varepsilon_\infty$  and  $\Delta\varepsilon$  are plotted against  $1000/T$  in Fig. 6.14.

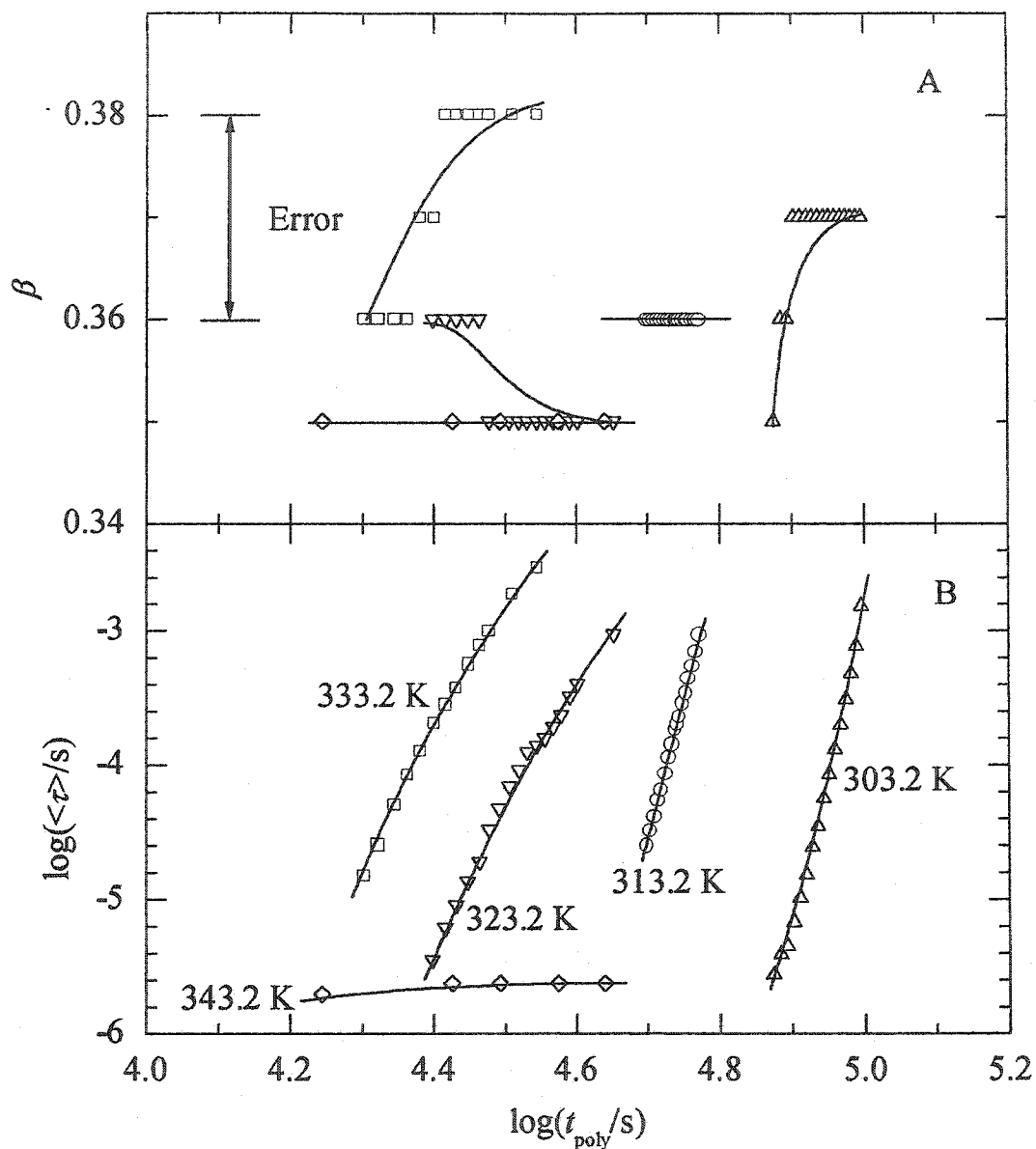


Fig. 6.9. The parameters obtained by fitting the dielectric spectra  $\varepsilon'_{\text{dip}}$  and  $\varepsilon''_{\text{dip}}$  with KWW relaxation function for AN-RDGE mixture during polymerization: (A). non-exponential parameter  $\beta$ , (B). logarithmic average relaxation time  $\log\langle\tau\rangle$ . These are plotted against  $\log(t_{\text{poly}})$  during polymerization for AN-RDGE mixture. The symbols correspond to different  $T_{\text{poly}}$  (K) as: ( $\Delta$ ) 303.2, ( $\circ$ ) 313.2, ( $\nabla$ ) 323.2, ( $\square$ ) 333.2, ( $\diamond$ ) 343.2.

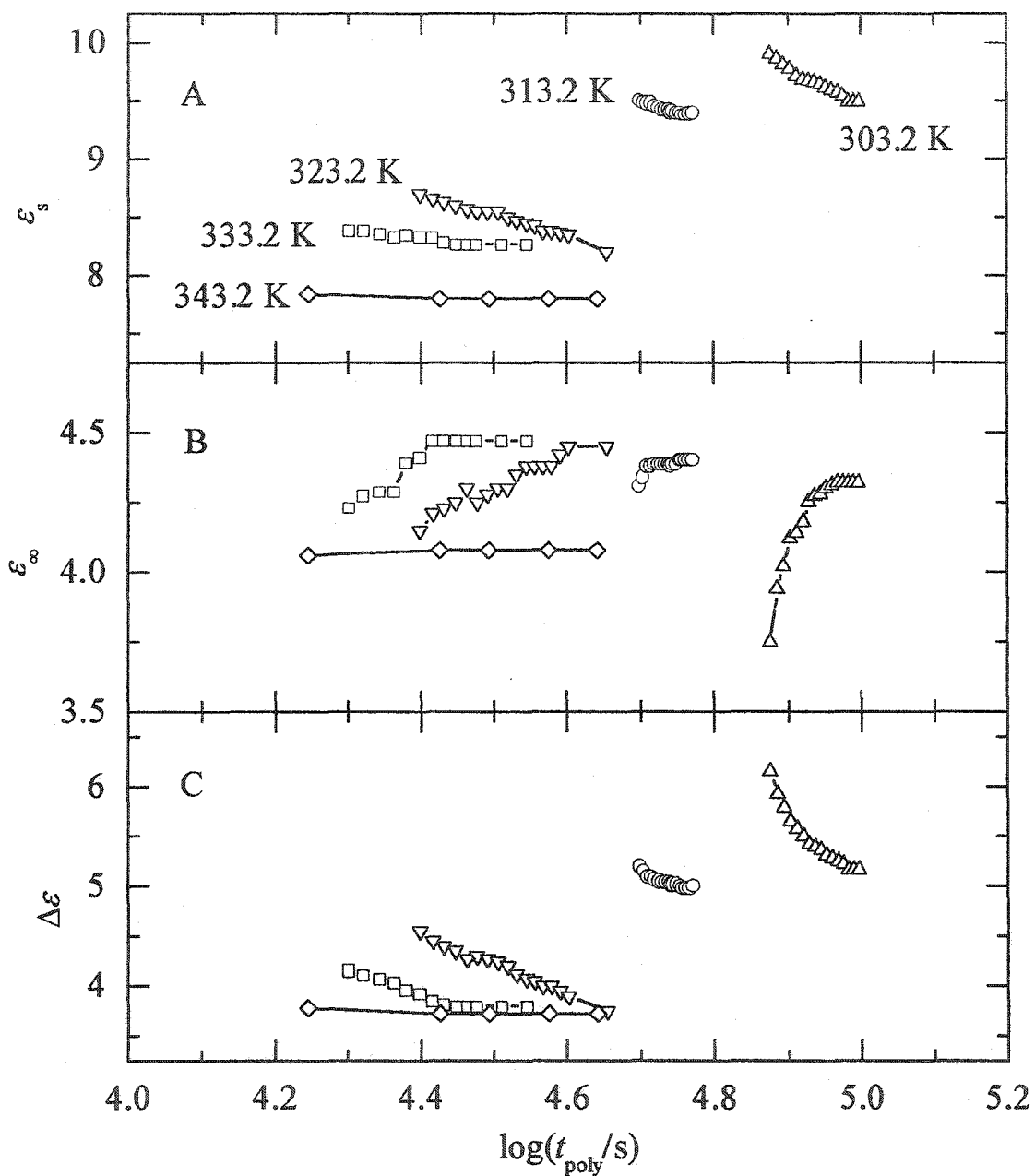


Fig. 6.10. The parameters obtained by fitting the dielectric spectra  $\epsilon'_{\text{dip}}$  and  $\epsilon''_{\text{dip}}$  with KWW relaxation function for AN-RDGE mixture measured during polymerization: A.  $\epsilon_s$ , B.  $\epsilon_\infty$  and C.  $\Delta\epsilon$ . They are plotted against  $\log(t_{\text{poly}})$  during polymerization for AN-RDGE mixture. The symbols correspond to different  $T_{\text{poly}}$  (K) as: ( $\Delta$ ) 303.2, ( $\circ$ ) 313.2, ( $\nabla$ ) 323.2, ( $\square$ ) 333.2, ( $\diamond$ ) 343.2.

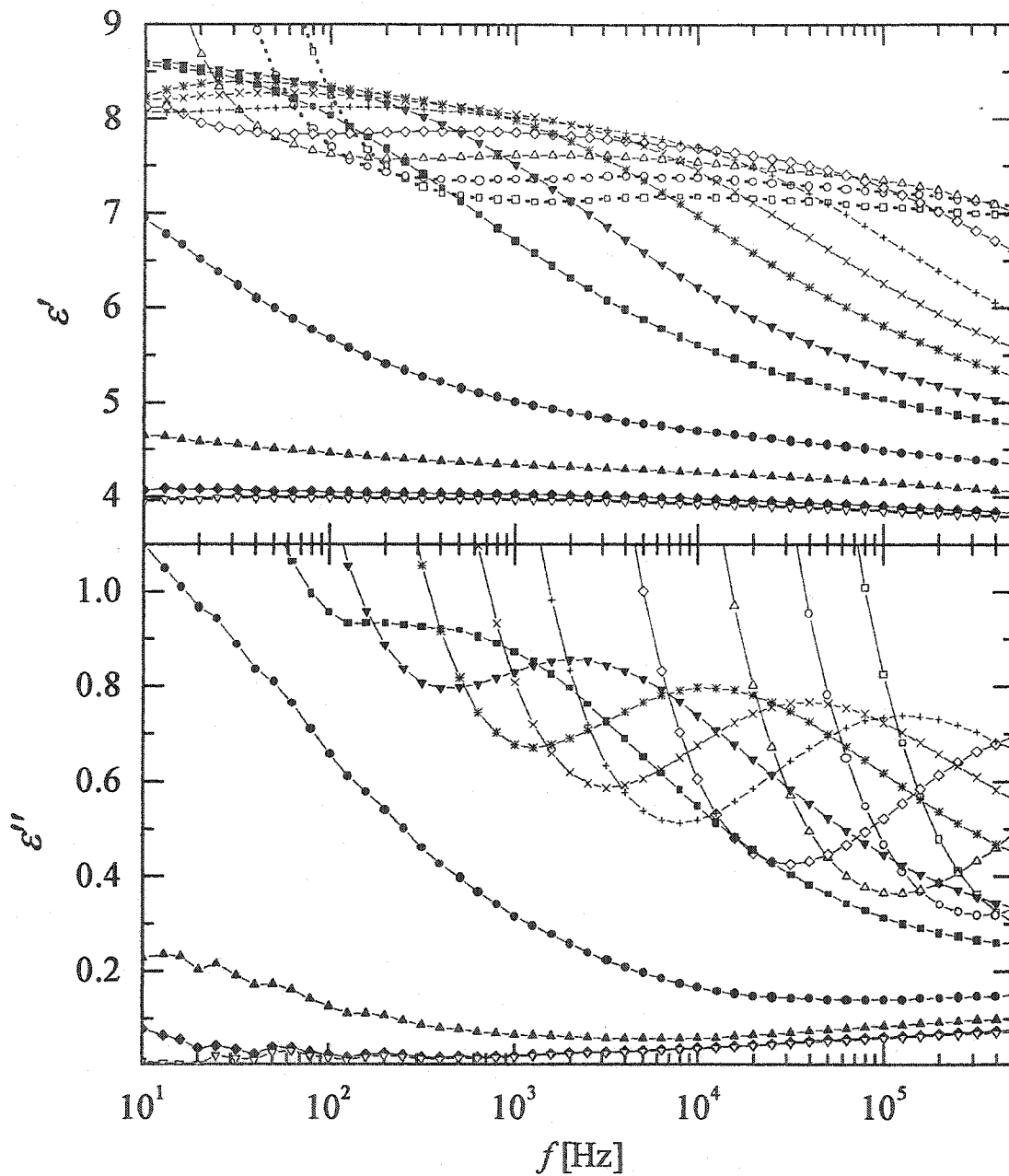


Fig.6.11. The spectra of  $\epsilon'$  and  $\epsilon''$  measured during cooling from 400 K to 300 K for AN-RDGE mixture polymerized at 333.2 K for 60 ks and post-polymerized at 400.2 K for 60 ks. The symbols correspond to different temperature (K) as: ( $\square$ )399.7, ( $\circ$ )389.3, ( $\Delta$ )379.6, ( $\diamond$ )369.3, (+)360.1, ( $\times$ )355.5, (\*)350.5, ( $\nabla$ )345.1, ( $\blacksquare$ )340.5, ( $\bullet$ )329.9, ( $\blacktriangle$ )320.1, ( $\blacklozenge$ )310.0, ( $\nabla$ )306.7.

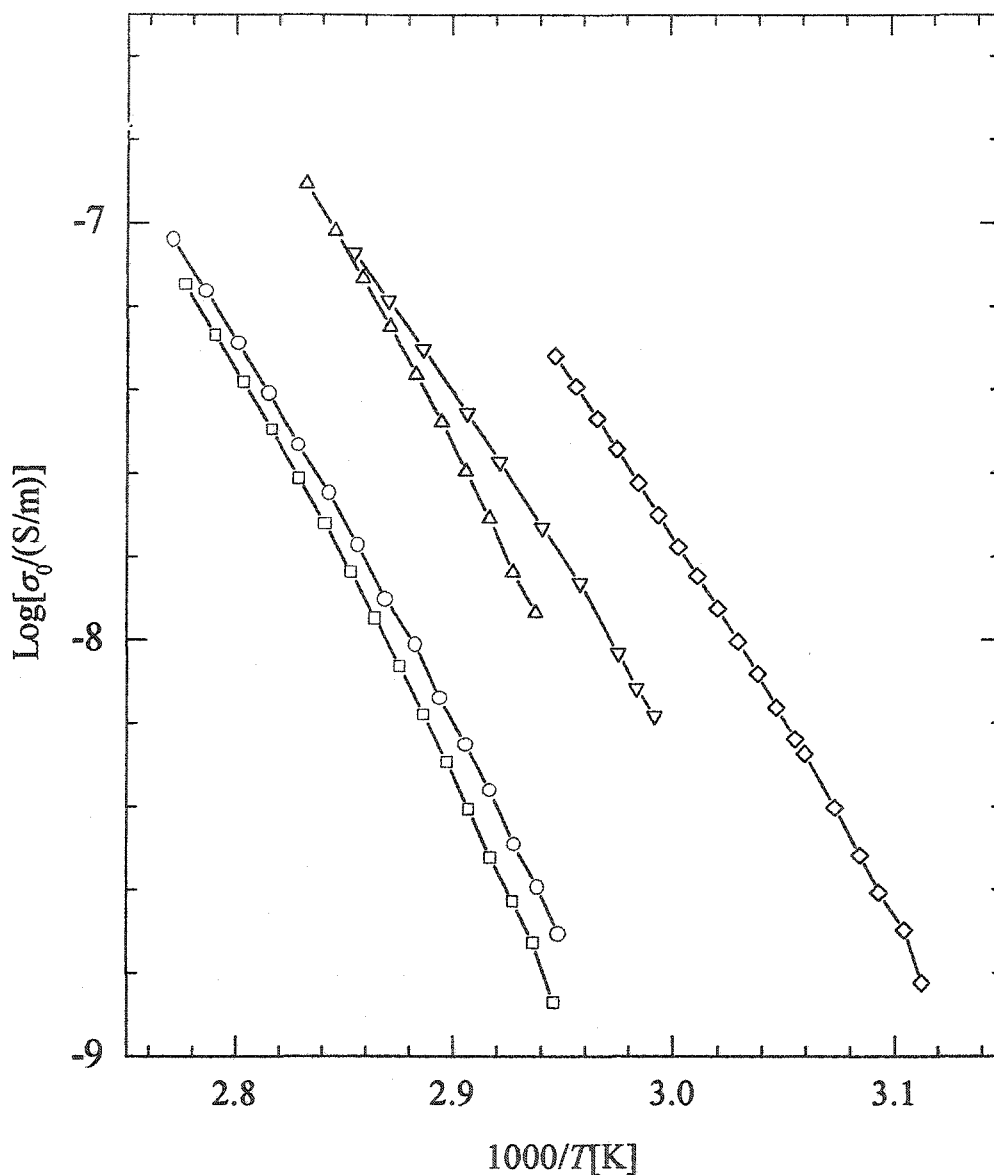


Fig. 6.12. The logarithmic dc conductivity  $\log(\sigma_0)$  plotted against  $1000/T$  for AN-RDGE mixture measured during cooling from post polymerization temperature to 300 K. The symbols correspond to different polymerization history as: ( $\Delta$ )  $T_{\text{poly}} = 303.2$  K,  $t_{\text{poly}} = 260$  ks,  $T_{\text{post}} = 400.2$  K,  $t_{\text{post}} = 60$  ks, ( $\circ$ )  $T_{\text{poly}} = 313.2$  K,  $t_{\text{poly}} = 86$  ks,  $T_{\text{post}} = 400.2$  K,  $t_{\text{post}} = 60$  ks, ( $\nabla$ )  $T_{\text{poly}} = 323.2$  K,  $t_{\text{poly}} = 60$  ks,  $T_{\text{post}} = 373.2$  K,  $t_{\text{post}} = 60$  ks, ( $\square$ )  $T_{\text{poly}} = 333.2$  K,  $t_{\text{poly}} = 60$  ks,  $T_{\text{post}} = 400.2$  K,  $t_{\text{post}} = 60$  ks, ( $\diamond$ )  $T_{\text{poly}} = 343.2$  K,  $t_{\text{poly}} = 60$  ks,  $T_{\text{post}} = 373.2$  K,  $t_{\text{post}} = 60$  ks.

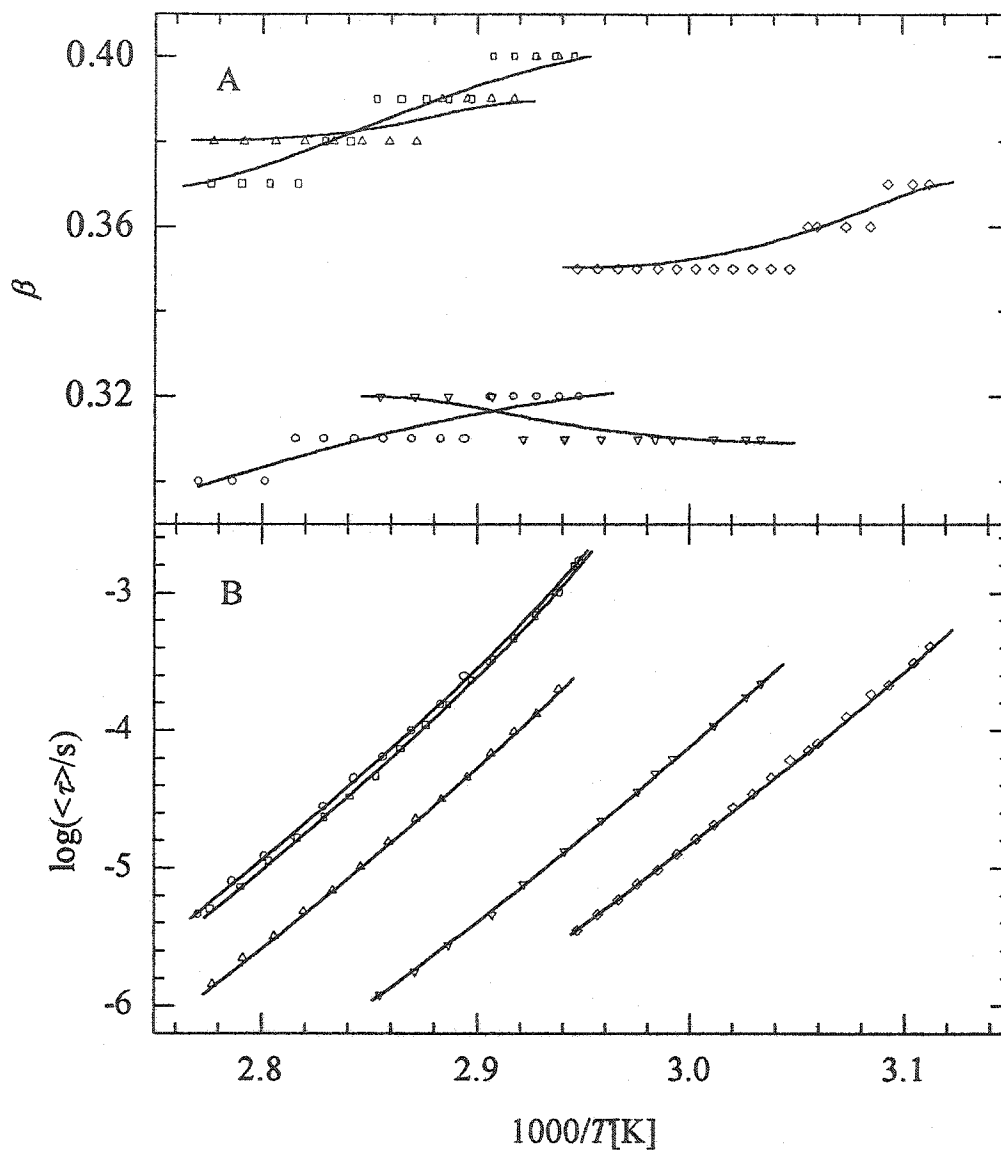


Fig. 6.13. The parameters obtained by fitting the dielectric spectra  $\epsilon'_{\text{dip}}$  and  $\epsilon''_{\text{dip}}$  with KWW relaxation for AN-RDGE mixture measured during cooling from post polymerization temperature to 300 K: A. non-exponential parameter  $\beta$ , B. logarithmic average relaxation time  $\log\langle\tau\rangle$ . They are plotted against  $1000/T$ . The symbols correspond to different polymerization history as: ( $\Delta$ )  $T_{\text{poly}} = 303.2$  K,  $t_{\text{poly}} = 260$  ks,  $T_{\text{post}} = 400.2$  K,  $t_{\text{post}} = 60$  ks, ( $\circ$ )  $T_{\text{poly}} = 313.2$  K,  $t_{\text{poly}} = 86$  ks,  $T_{\text{post}} = 400.2$  K,  $t_{\text{post}} = 60$  ks, ( $\nabla$ )  $T_{\text{poly}} = 323.2$  K,  $t_{\text{poly}} = 60$  ks,  $T_{\text{post}} = 373.2$  K,  $t_{\text{post}} = 60$  ks, ( $\square$ )  $T_{\text{poly}} = 333.2$  K,  $t_{\text{poly}} = 60$  ks,  $T_{\text{post}} = 400.2$  K,  $t_{\text{post}} = 60$  ks, ( $\diamond$ )  $T_{\text{poly}} = 343.2$  K,  $t_{\text{poly}} = 60$  ks,  $T_{\text{post}} = 373.2$  K,  $t_{\text{post}} = 60$  ks.

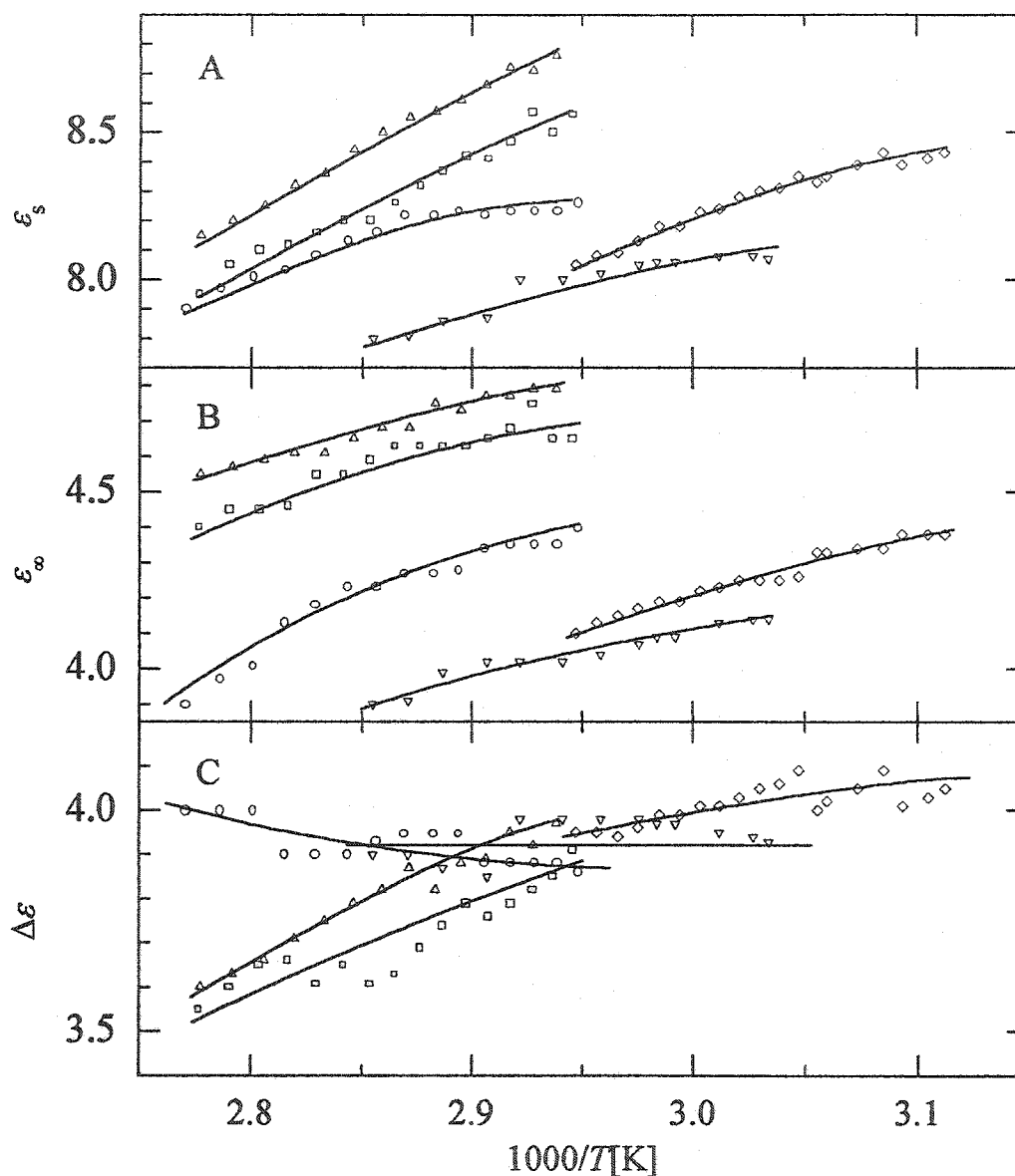


Fig. 6.14. The parameters obtained by fitting the dielectric spectra  $\epsilon'_{\text{dip}}$  and  $\epsilon''_{\text{dip}}$  with KWW relaxation function for AN-RDGE mixture measured during cooling from post polymerization temperature to 300 K: A.  $\epsilon_s$ , B.  $\epsilon_\infty$  and C.  $\Delta\epsilon$ . They are plotted against  $1000/T$ . The symbols correspond to different polymerization history as: ( $\Delta$ )  $T_{\text{poly}} = 303.2$  K,  $t_{\text{poly}} = 260$  ks,  $T_{\text{post}} = 400.2$  K,  $t_{\text{post}} = 60$  ks, ( $\circ$ )  $T_{\text{poly}} = 313.2$  K,  $t_{\text{poly}} = 86$  ks,  $T_{\text{post}} = 400.2$  K,  $t_{\text{post}} = 60$  ks, ( $\nabla$ )  $T_{\text{poly}} = 323.2$  K,  $t_{\text{poly}} = 60$  ks,  $T_{\text{post}} = 373.2$  K,  $t_{\text{post}} = 60$  ks, ( $\square$ )  $T_{\text{poly}} = 333.2$  K,  $t_{\text{poly}} = 60$  ks,  $T_{\text{post}} = 400.2$  K,  $t_{\text{post}} = 60$  ks, ( $\diamond$ )  $T_{\text{poly}} = 343.2$  K,  $t_{\text{poly}} = 60$  ks,  $T_{\text{post}} = 373.2$  K,  $t_{\text{post}} = 60$  ks.

## 6.5 Discussion

### 6.5.1 Dielectric changes during the polymerization process

The rapid decrease in  $\log(\sigma_0)$  with the increase of  $t_{\text{poly}}$  during polymerization at 303.2 K and 313.2 K in Fig. 6.7 indicates that the mobility of the ionic impurities in the mixture decreases very rapidly during the course of polymerization. But for the sample being polymerized at 343.2 K,  $\sigma_0$  tends to approach a high limiting value of  $\sigma_0 \approx 2.37 \times 10^{-6}$  S/m. The reason is that the polymerization temperature of 343 K is 10 K above the glass transition temperature of 333 K for the completely polymerized AN-RDGE mixture. Thus the AN-RDGE mixture polymerized at 343 K did not further polymerize and therefore its viscosity, although low, did not increase. In this condition, the polymerization temperature is higher than the vitrification temperature of its fully polymerized state, and the already high mobility of the ionic impurities also does not decrease with polymerization time at a fixed temperature.

In Fig. 6.9(A), the value  $\beta$  is in the range 0.35 to 0.38 for the five polymerization temperatures. Considering the fitting error of 0.01 for  $\beta$ , its value either slightly increases with the polymerization time or remains constant. Also it remains constant with change in the polymerization temperature. This seems to be consistent with Tombari *et. al.*'s results (1997) for the isothermal polymerization of another linear chain structure of cyclohexylamine(CHA)-DGEBA mixture at 314.2 K. In their report,  $\beta$  remains constant at 0.39.

In Fig. 6.9(B), the values of  $\log\langle\tau\rangle$  increase very rapidly with polymerization time for the mixture polymerized at 303.2, 313.2, 323.2 and 333.2 K. This rapid increase

of  $\log\langle\tau\rangle$  with the increase of polymerization time is caused by the rapid increase of viscosity of the mixtures during the course of polymerization. For the mixture polymerizing at 343.2 K, the  $\log\langle\tau\rangle$  increases very slowly and tends to approach a constant value of  $-5.626$  ( $\langle\tau\rangle \approx 2.37 \times 10^{-6}$  s). Such an approach to the upper  $\langle\tau\rangle$  limit with polymerization occurs when the viscosity of a polymerizing mixture remains constant, and the state remains a liquid at the condition when the polymerization temperature is above the glass transition temperature of the fully polymerized product. In this case,  $T_{\text{poly}}$  of 343.2 K is 10 K above the  $T_g$ .

We now consider the change in the magnitude of orientation polarization,  $\Delta\varepsilon$ , during the course of polymerization. Onsager (1939), Kirkwood (1939) and Fröhlich (1958) had developed a general statistical theory of the static dielectric constant for a dipolar molecule system, according to which,

$$\Delta\varepsilon \equiv \varepsilon_s - \varepsilon_\infty = \left[ \left( \frac{\varepsilon_\infty + 2}{3} \right)^2 \left( \frac{\varepsilon_s}{2\varepsilon_s + \varepsilon_\infty} \right) \right] \frac{4\pi N_d g \mu_0^2}{k_B T} \quad (6.27)$$

where  $N_d$  is the number density of the dipoles,  $g$  is the dipolar orientational correlation factor,  $\mu_0$  is the vapor-phase dipole moment, and all other terms have the same meaning as before.

At a fixed temperature during polymerization, the volume of the polymer mixture decreases during the polymerization by as much as 10% [Choi and Plazek (1986)]. If there is no other change in the dipolar orientational correlation factor  $g$  and in the vapour-phase dipole moment  $\mu_0$ , both  $\varepsilon_s$  and  $\varepsilon_\infty$  should increase with increase in the extent of polymerization, because the number density of the dipoles  $N_d$  increases. The decreases of

$\varepsilon_s$  with the increase of  $\log(t_{\text{poly}})$  seen in Fig. 6.10(A) should therefore be attributed to the decrease of the  $g\mu_0^2$  during polymerization, when the epoxide ring of RDGE opens, reacts with N-H group of aniline to form a covalent bond. This process eliminates the dipoles of one N-H group and of one epoxide ring, and produces a new dipole of O-H group and a new N-C covalent bond. The increase in  $\varepsilon_\infty$  with the polymerization time in Fig. 6.10(B) is therefore the net effect of the increase in  $N_d$  and the decrease of the  $\mu_0^2$  during the course of polymerization. The decrease of  $\varepsilon_s$  and the increase of  $\varepsilon_\infty$  on polymerization therefore decrease  $\Delta\varepsilon (\equiv \varepsilon_s - \varepsilon_\infty)$ , as seen in Fig. 6.10(C). We calculate the term  $[(\varepsilon_\infty+2)/3]^2[\varepsilon_s/(2\varepsilon_s + \varepsilon_\infty)]$  in Eq. (6.27) and find that it increases with the increase in  $t_{\text{poly}}$ . For example, it decreases from 1207 to 867 with the increase of  $t_{\text{poly}}$  from 4.87 ks to 4.98 ks for the sample polymerized at 303.2 K. Thus we conclude that the decrease of  $\Delta\varepsilon$  with the increase of  $\log(t_{\text{poly}})$  is due to the effect of decrease of the  $g\mu_0^2$  during the polymerization.

Tombari *et al.* (1997) have reported that the value of  $\varepsilon_\infty$  decreases gradually from 4.2 to 4.1 and the value of  $\varepsilon_s$  decreases gradually from 7.0 to 6.8 during the polymerization of the CHA-DGEBA mixture at 314.2 K. Johari *et al.* (1999) also reported that the value of  $\varepsilon_\infty$  decreases gradually from 4.2 to 4.1 and the value of  $\varepsilon_s$  decreases gradually from 7.5 to 7.0 for CHA-DGEBA mixture polymerized at 300.2 K. We find that the value of  $\varepsilon_\infty$  instead increases gradually from 4.3 to 4.4 and the value of  $\varepsilon_s$  decreases gradually from 9.5 to 9.4 during the polymerization of the AN-RDGE mixture at 313.2 K. For our AN-RDGE mixture being polymerized at 303.2 K, we also find that

the value of  $\epsilon_\infty$  increases gradually from 3.8 to 4.3 and the value of  $\epsilon_s$  decreases gradually from 9.9 to 9.5. Our observation that  $\epsilon_s$  decreases with the increase of polymerization time is consistent with the results obtained by Tombari *et al.* (1997) and by Johari *et al.* (1999), but our observation of  $\epsilon_\infty$  increasing with the increase of  $t_{\text{poly}}$  is inconsistent with their results. This difference could come from the difference in the respective polymerization mixtures' characteristics such as  $N_d$ ,  $g$  and  $\mu_0$  and the structure formed. We also find that the lower the polymerization temperature, the higher is the amount of net changes in  $\epsilon_s$  and  $\epsilon_\infty$  during the same polymerization time.

### 6.5.2 Dielectric properties of the polymerized state

We now consider the dielectric properties of the polymerized state. In Fig. 6.12, the values of  $\log(\sigma_0)$  generally decreases. The plot bends downward with the decrease in  $T$ , as expected and observed generally. The curves of  $\log(\sigma_0)$  against  $1000/T$  for the two samples with different  $T_{\text{poly}}$  of 313.2 K and 333.2 K but same  $T_{\text{post}}$  of 400 K are parallel to each other. The curves of  $\log(\sigma_0)$  for the two samples with  $T_{\text{poly}}$  of 303.2 K and  $T_{\text{post}}$  of 400 K,  $T_{\text{poly}}$  of 323.2 K and  $T_{\text{post}}$  of 373 K seem to merge with the decreases of  $1000/T$ , and separate with the increase of  $1000/T$ . The curve of  $\log(\sigma_0)$  for the sample with  $T_{\text{poly}}$  of 343.2 K and  $T_{\text{post}}$  of 373 K is separated from the curves of  $\log(\sigma_0)$  of the other four samples. The slopes of these five curves are closely similar. By fitting the Arrhenius equation to these data, we obtain an activation energy of  $175 \pm 20$  kJ/mol.

In Fig. 6.13(A), the values of the non-exponential parameter  $\beta$  range from 0.30 to 0.40 for five samples and the changes are between 0.01 - 0.03 for each sample. Considering the fitting error of 0.01 for  $\beta$ , we conclude that the  $\beta$  value remains unchanged or increases very slightly for each sample with decrease in  $T$ . The  $\beta$  values are obviously different for different samples. This difference could come from the structural difference, which will be discussed in the last paragraph of this section. In Fig. 6.13(B), although the  $\log\langle\tau\rangle$  curves are separated from each other, their slopes are almost the same. By fitting the Arrhenius equation to these data, we obtain an activation energy of  $260 \pm 40$  kJ/mol, which is higher than the activation energy for dc conductivity. This means that the diffusion of the ionic impurities have a lower activation barrier than the dipolar relaxation process. The first process involves a random translational diffusion of relatively small, spherical ions, but the second process involves both the hindered translational and rotational motions of polymer chains that may have already been entangled.

In Fig. 6.14(A) and 6.14(B), the values of  $\varepsilon_s$  and  $\varepsilon_\infty$  for all five samples increase monotonically with the decrease in  $T$ . The values of  $\Delta\varepsilon$  ( $\equiv\varepsilon_s-\varepsilon_\infty$ ) for different sample show different types of changes. The values of  $\Delta\varepsilon$  increases with decrease in  $T$  for three samples, and remains unchanged for one sample. Since  $\Delta\varepsilon$  is determined by six variables in the Onsager-Kirkwood-Fröhlich equation, namely,  $\varepsilon_s$ ,  $\varepsilon_\infty$ ,  $N_d$ ,  $g$ ,  $\mu_0$  and  $T$  in Eq. (6.27), the temperature dependence of  $\Delta\varepsilon$  would reflect the net effect of changes in all these six variables. The variation of  $\Delta\varepsilon$  on  $1000/T$  can be predicted only when the temperature

dependence of all the five variables  $\epsilon_s$ ,  $\epsilon_\infty$ ,  $N_d$ ,  $g$  and  $\mu_0$  is known. In our study these are not known.

If the five samples, whose polymerization at different temperatures has been studied here, were to have been completely polymerized, the difference between the curves in Figs. 6.12 - 6.14 would come from their different polymer structures resulting from their different thermal histories. Although all aniline and RDGE completely react or fully polymerize, they do not necessarily form long linear chains. Ideally, the completely polymerized linear chain polymer will only form one loop of a single chain. In practice, they tend to form smaller loops (as opposed to smaller chains which would react ultimately to form longer chains or loops) with varying numbers of repeat units. The molecular weight of the loops, and the distribution of the molecular weights of the loops, might be different in each sample. Such difference will result in different diffusion coefficients of ionic impurities and different viscosity of the system and hence different dc conductivities. A difference in polymer structure would also result in different distributions of dipoles and dipolar orientational correlation, which are evident from the variations of the parameters  $\beta$ ,  $\tau_0$ ,  $\epsilon_s$ ,  $\epsilon_\infty$  and  $\Delta\epsilon$  for different samples, as is seen in Figs. 6.12 - 6.14. Tombari *et. al.* (1998) have found a similar effect in the CHA-DGEBA mixture. However, they had found that for a fixed temperature and extent of polymerization  $\alpha$ , only the values of  $\epsilon_s$  and  $\tau_0$  differ significantly when the thermal history of polymerization differs.

## 6.6 Summary

The real time dielectric spectroscopy of a linear chain polymerizing system, 1:1 ratio of aniline and resorcinol diglycidyl ether mixture, were measured during polymerization at different fixed temperatures. The dielectric spectra during the isothermal polymerization were found to develop differently with polymerization time. For polymerization of the liquid at a temperature below the vitrification temperature of the fully polymerized state, the peak position of the dielectric loss against frequency decreases monotonically from high frequency to low frequency and move out the lower frequency limit of 10 Hz, and the dc conductivity and the relaxation time decrease monotonically, with time. For polymerization of the liquid at a temperature above the vitrification temperature of the fully polymerized state, the peak position of the dielectric loss spectrum decreases slightly and then ceases to decrease below 200 kHz, and the dc conductivity and the relaxation time approach their respective constant values with time, as polymerization reaches completion. The stretched-exponential parameter for the spectra remain constant for the mixture polymerized for different times and at different temperatures. Other dielectric properties change monotonically with polymerization time with different rates at different polymerization temperatures.

Dielectric spectra of samples post-polymerized at high temperatures were also measured at different temperatures. The spectra showed that the dielectric properties of the fully polymerized state depend upon the polymerization history. A difference in the distribution and the molecular weights of the chains and loops formed appear to determine the dielectric properties of the polymer.

The activation energy obtained for dc conductivity for the fully polymerized state is found to be 174 kJ/mol and independent of the polymerization history. This is 85 kJ/mol less than the activation energy obtained for dielectric relaxation time. This means that the ions have a lower energy barrier for translational diffusion than the dipolar vectors in the entangled polymer chains and loops in the fully polymerized state have for angular diffusion.

## Chapter 7

### Conclusions

Because of the discrete nature of the studies, it is appropriate to provide separate conclusions in order of the study described in this thesis.

(1). Mathematical considerations of the modulation effects on a physical property of an amorphous material held at a fixed mean temperature but under sinusoidal modulation of temperature with time, have shown that the second derivative of the magnitude of the property with respect to temperature determines the changes observed in the average magnitude of a property relative to those observed in the unmodulated condition. Sinusoidal modulation of pressure on an amorphous material at a fixed mean pressure has a qualitatively similar effect on the average physical property.

When the temperature of a material is sinusoidally modulated and it is also heated at a constant rate, the average normalized heat capacity against temperature shows extra features relative to the unmodulated conditions. These features depend on, (i) the extent of non-linearity of the relaxation time with real time, expressed in terms of the non-exponential decrease of the fictive temperature with time, (ii) the broadness of the distribution of relaxation times, expressed as the stretched exponential parameter, (iii) the nature of modulation (sine wave or square wave), (iv) the modulation amplitude, (v) the modulation frequency, and (vi) the heating rate. These extra features may lead to a

misinterpretation of the sigmoid-shaped endothermic feature of the glass-softening region and an incorrect estimate of the glass transition temperature. Its importance is to be recognized by Perkin-Elmer and TA Instruments which produce instruments for such measurements.

(2). The earlier calculations of the configurational entropy of linear chain polymers, which had implied a negative configurational entropy, has been corrected by providing a new mean field approximation, and calculations performed with this approximation within the precepts of the lattice hole model show that the configurational entropy would approach a positive value at 0 K, in contrast to the current belief that the configurational entropy would approach a negative value at 0 K. This has been verified by others since the publication of our report.

Calculations of the configurational entropy and heat capacity as a function of temperature, pressure and the extent of polymerization performed by using Eyring' hole theory and Flory's flexibility bond concepts, have shown that the configurational heat capacity will reach a maximum value during the course of polymerization and then will decrease, thus showing a local maximum. This prediction has also been verified by others since the publication of our study.

Calculations combined with the configurational entropy theory of viscosity have shown that the normalized viscosity of a polymer would increase progressively more rapidly with increase in pressure at a fixed temperature and such plots against pressure would diverge. This is consistent with the known observations on polymers.

(3). In their thermodynamic behavior, CuCN crystals have shown features of a glass, and an endothermic effect resembling the glass-liquid transition. This crystal is designated as an orientational glass. Its x-ray powder diffraction has shown that a new phase of CuCN forms when the known phase of the crystal is heated to 593 K. The new phase has a higher enthalpy than the original sample and on cooling it remains metastable at 77 K. The structure of the new phase is in the  $R\bar{3}m$  space group, with Cu atoms located at (0, 0, 0) sites of the unit cell. Because of the orientational disorder, the C and N atom positions could not be determined. The CN chains are found to be aligned along the c-axis with frozen-in random orientations of CN at room temperature. This new phase also shows an endothermic feature associated with the glass transition, as well as the effects of structural relaxation during physical aging. Its structural relaxation time determined by fitting of the normalized values of the measured heat capacity to a non-linear and non-exponential relaxation model, has shown an Arrhenius increase with decreasing temperature. The chain statistics of the -Cu-CN-Cu-CN- performed in the same manner as those of the polymer chains in the lattice-hole model led to reasonable values of its configurational entropy and heat capacity due to orientational motions.

(4). A study of diglycidyl ether of bisphenol-A, an epoxy resin, reacting with *p*-aminodicyclohexyl methane, at different fixed temperatures to produce a polymer structure, has allowed us to determine the characteristic feature of the change in polymerization reaction kinetics. In this study, as the extent of polymerization increased, the chemical reaction kinetics changed gradually from the initially mass-controlled process to an ultimately diffusion-controlled process and deviations occurred from the

Arrhenius plot of the reaction rate. A method for studying this change, which is developed here showed that the extent of polymerization at which the change occurs decreases with decrease in the polymerization temperature. This has been supported by the numerical simulations of the two cases of the mass-controlled and diffusion-controlled reactions.

(5). Dielectric spectroscopy study of the isothermal polymerization of aniline and resorcinol diglycidyl ether mixtures which upon chemical reaction form a linear chain polymer has shown that the dipolar part of the dielectric spectra has a distribution of relaxation times which remains constant as polymerization occurs, the dc conductivity and the static permittivity decreases, the relaxation time increases. The rate of these changes varies with the temperature of polymerization and the manner in which the glass transition temperature increases with increase in the extent of polymerization. Further polymerization of the mixture to the fullest extent at higher temperatures has led to a material of different dielectric properties depending upon the polymerization temperature. This demonstrates that the ultimate polymer structure, in terms of the distribution and the molecular weights of linear polymer chain and/or polymer chain loops, varies with the polymerization history.

## Appendix A

### The Number of Configurations Available for the Monodispersed Polymer Chain System

For a monodispersed polymer system, by using Flory's approximation of Eqn. (3.2) in Chapter 3, the quantity in square brackets of Eq. (3.1) can be simplified as:

$$\begin{aligned}
 & \frac{1}{N!} \frac{1}{2^N} \prod_{j=1}^N M(j) \prod_{m=1}^{x-1} [z(j, m)]_{\text{Flory}} \\
 &= \frac{1}{N!} \frac{1}{2^N} \prod_{j=1}^N [xN + N_0 - (j-1)x] \prod_{m=1}^{x-1} z(m) \frac{(xN + N_0) - [(j-1)x + m]}{(xN + N_0)} \\
 &= \frac{1}{N!} \left(\frac{z}{2}\right)^N (z-1)^{N(x-2)} \left(\frac{1}{xN + N_0}\right)^{N(x-1)} \prod_{j=1}^N \frac{[xN + N_0 - (j-1)x]!}{[xN + N_0 - jx]!} \\
 &= \frac{1}{N!} \left(\frac{z}{2}\right)^N (z-1)^{N(x-2)} \left(\frac{1}{xN + N_0}\right)^{N(x-1)} \frac{(xN + N_0)!}{N_0!} \\
 &= \left(\frac{z}{2}\right)^N (z-1)^{N(x-2)} \left(\frac{1}{xN + N_0}\right)^{N(x-1)} \frac{(xN + N_0)!}{N! N_0!} \tag{A1}
 \end{aligned}$$

Therefore, the number of configurations in Flory's model (1957) can be simplified as:

$$\begin{aligned}
 \Omega_{\text{Flory}} &= \left(\frac{z}{2}\right)^N (z-1)^{N(x-2)} \left(\frac{1}{xN + N_0}\right)^{N(x-1)} \frac{(xN + N_0)!}{N! N_0!} \\
 &\times \left\{ \left( \frac{N(x-2)}{fN(x-2)} \right) \left( \frac{1}{z-1} \right)^{(1-f)N(x-2)} \left( \frac{z-2}{z-1} \right)^{fN(x-2)} \right\} \\
 &= \left(\frac{z}{2}\right)^N \left(\frac{1}{xN + N_0}\right)^{N(x-1)} \frac{(xN + N_0)!}{N! N_0!} \left( \frac{N(x-2)}{fN(x-2)} \right) (z-2)^{fN(x-2)} \tag{A2}
 \end{aligned}$$

For Milchev's monodispersed model (1983), using his approximation of Eq. (3.3), the quantity in square brackets of Eq. (3.1) can be simplified as:

$$\begin{aligned}
& \frac{1}{N!} \frac{1}{2^N} \prod_{j=1}^N M(j) \prod_{m=1}^{x-1} [z(j, m)]_{\text{Milchev}} \\
&= \frac{1}{N!} \frac{1}{2^N} \prod_{j=1}^N [xN + N_0 - (j-1)x] \prod_{m=1}^{x-1} z(m) \frac{N\{xN + N_0 - [(j-1)x + m]\}}{[N - (j-1)](xN + N_0)} \\
&= \frac{1}{N!} \left(\frac{z}{2}\right)^N (z-1)^{N(x-2)} \left(\frac{N}{xN + N_0}\right)^{N(x-1)} \prod_{j=1}^N \frac{[xN + N_0 - (j-1)x]!}{[N - (j-1)]^{(x-1)} [xN + N_0 - jx]!} \\
&= \frac{1}{N!} \left(\frac{z}{2}\right)^N (z-1)^{N(x-2)} \left(\frac{N}{xN + N_0}\right)^{N(x-1)} \frac{(xN + N_0)!}{N_0! (N!)^{(x-1)}} \\
&= \left(\frac{z}{2}\right)^N (z-1)^{N(x-2)} \left(\frac{1}{xN + N_0}\right)^{N(x-1)} \frac{(xN + N_0)!}{N! N_0!} \left(\frac{N^N}{N!}\right)^{(x-1)} \tag{A3}
\end{aligned}$$

Since the quantity in the curly brackets of Eq. (3.1) in Chapter 3 is the same for Flory's (1957) and Milchev's (1983) models, the numbers of configurations available in the two models are related by,

$$\Omega_{\text{Milchev}} = \left(\frac{N^N}{N!}\right)^{(x-1)} \Omega_{\text{Flory}} \tag{A4}$$

For the condition that  $N = 1$ ,  $\Omega_{\text{Milchev}} = \Omega_{\text{Flory}}$ , which means that Milchev's model will also yield negative entropy when  $T > 0$  K just as Flory's model. Thus Milchev's model is correct only for  $N \rightarrow \infty$  and should be modified to be valid for other values of  $N \geq 1$ .

For our model, using the approximation for the effective volume of each repeat unit, i.e., Eq. (3.11), the quantity in square brackets of Eq. (3.1) can be simplified as:

$$\begin{aligned}
& \frac{1}{N!} \frac{1}{2^N} \prod_{j=1}^N M(j) \prod_{m=1}^{x-1} z(j, m) \\
&= \frac{1}{N!} \frac{1}{2^N} \prod_{j=1}^N [xN + N_0 - (j-1)x] \prod_{m=1}^{x-1} z(m) \frac{xN \{xN + N_0 - [(j-1)x + m]\}}{\{xN - [(j-1)x + m]\} (xN + N_0)} \\
&= \frac{1}{N!} \left(\frac{z}{2}\right)^N (z-1)^{N(x-2)} \left(\frac{xN}{xN + N_0}\right)^{N(x-1)} \\
&\times \prod_{j=1}^N \frac{[xN + N_0 - (j-1)x][xN + N_0 - (j-1)x - 1][xN - jx]!}{[xN + N_0 - jx]![xN - (j-1)x - 1]!} \\
&= \frac{1}{N!} \left(\frac{z}{2}\right)^N (z-1)^{N(x-2)} \left(\frac{xN}{xN + N_0}\right)^{N(x-1)} \\
&\times \prod_{j=1}^N \frac{[xN + N_0 - (j-1)x][xN - jx]![xN - (j-1)x]}{[xN + N_0 - jx]![xN - (j-1)x]!} \\
&= \frac{1}{N!} \left(\frac{z}{2}\right)^N (z-1)^{N(x-2)} \left(\frac{xN}{xN + N_0}\right)^{N(x-1)} \frac{(xN + N_0)!}{N_0!} \frac{1}{(xN)!} \prod_{j=1}^N \{xN - [(j-1)x]\} \\
&= \left(\frac{z}{2}\right)^N (z-1)^{N(x-2)} \left(\frac{xN}{xN + N_0}\right)^{N(x-1)} \frac{(xN + N_0)!}{(xN)! N_0!} x^N \tag{A5}
\end{aligned}$$

Therefore, the number of configurations available in Eq. (A1) can be simplified

as:

$$\begin{aligned}
\Omega &= \left(\frac{z}{2}\right)^N (z-1)^{N(x-2)} \left(\frac{xN}{xN + N_0}\right)^{N(x-1)} \frac{(xN + N_0)!}{(xN)! N_0!} x^N \\
&\times \left\{ \binom{N(x-2)}{fN(x-2)} \left(\frac{1}{z-1}\right)^{(1-f)N(x-2)} \left(\frac{z-2}{z-1}\right)^{fN(x-2)} \right\} \\
&= \left(\frac{z}{2}\right)^N \left(\frac{Nx}{Nx + N_0}\right)^{N(x-1)} \frac{(Nx + N_0)!}{(Nx)! N_0!} x^N \binom{N(x-2)}{fN(x-2)} (z-2)^{fN(x-2)} \tag{A6}
\end{aligned}$$

Thus the number of configurations available  $\Omega$  can be related to  $\Omega_{\text{Milchev}}$  and  $\Omega_{\text{Flory}}$ :

$$\Omega = \frac{(x^N N!)^x}{(Nx)!} \Omega_{\text{Milchev}} = \frac{(xN)^{xN} N!}{N^N (xN)!} \Omega_{\text{Flory}} \tag{A7}$$

For  $N = 1$ , our model yields  $\Omega = \frac{x^x}{x!} \Omega_{\text{Flory}} = \frac{x^x}{x!} \Omega_{\text{Milchev}}$ , which is different from Milchev's model (1983). In the limit of  $N \rightarrow \infty$ , we use Stirling's approximation,  $N! \cong N^N e^{-N}$ , and find that:  $\Omega = \Omega_{\text{Milchev}} = e^{N(x-1)} \Omega_{\text{Flory}}$ . When  $xN = N_A$ ,  $N(x-2) = N_A(1-2/x) \gg 1$  and  $fN(x-2) = fN_A(1-2/x) \gg 1$ . By using Stirling's approximation  $\ln(A!) \cong A \ln A - A$  for  $A \gg 1$ , it gives,

$$\ln \left( \frac{A}{\beta A} \right) \cong \ln \left( \frac{A!}{(\beta A)! [(1-\beta)A]!} \right) \cong A [-\beta \ln \beta - (1-\beta) \ln(1-\beta)]$$

$$\text{Therefore, } \ln \left( \frac{N(x-2)}{fN(x-2)} \right) \cong N_A \left( 1 - \frac{2}{x} \right) [-f \ln f - (1-f) \ln(1-f)] \quad (\text{A8})$$

Recalling  $xN/(xN + N_0) = \theta$ ,

$$\ln \frac{(xN + N_0)!}{(xN)! N_0!} = \ln \frac{(N_A / \theta)!}{[\theta(N_A / \theta)]! [(1-\theta)(N_A / \theta)]!} \cong \frac{N_A}{\theta} [-\theta \ln \theta - (1-\theta) \ln(1-\theta)] \quad (\text{A9})$$

$$\ln \left( \frac{xN}{xN + N_0} \right)^{N(x-1)} = N(x-1) \ln(\theta) = N_A \left( 1 - \frac{1}{x} \right) \ln(\theta) \quad (\text{A10})$$

According to the Boltzmann equation,  $S_{\text{conf}} = k_B \ln \Omega$ , and therefore,

$$\begin{aligned} \frac{S}{R} &= \frac{k_B \ln \Omega(N, x, N_0, f, z)}{k_B N_A} = -\frac{(1-\theta) \ln(1-\theta)}{\theta} - \frac{\ln \theta}{x} + \frac{1}{x} \ln \left( \frac{z}{2} \right) + \frac{1}{x} \ln x \\ &+ \left( 1 - \frac{2}{x} \right) [-f \ln f - (1-f) \ln(1-f) + f \ln(z-2)] \end{aligned} \quad (\text{A11})$$

Thus Eq. (A11) is the sum of Eqs. (3.6), (3.7), (3.9) and (3.10).

## Appendix B

### The Configurational Entropy for a Polydispersed Polymer Chain System

For a polydispersed system with distribution of Eq. (3.16), Milchev and Gutzow's (1982) equation for the net  $S_{\text{conf}}$  can be separated to obtain the contribution from the fractional occupancy to the configurational entropy as,

$$\frac{S^{(\theta)}}{R} = -\frac{(1-\theta)\ln(1-\theta)}{\theta} - \frac{\ln\theta}{x} - \left(1 - \frac{1}{x}\right) + \left(1 - \frac{1}{x}\right)L \quad (\text{B1})$$

where,

$$L = -\frac{1}{x} \sum_{u=1}^{\infty} u P_{u+1} \ln \left\{ 1 - \frac{\theta}{x} \sum_{k=1}^u k P_k \right\} \quad (\text{B2})$$

$$= -(1-\alpha)^2 \sum_{u=1}^{\infty} u \alpha^u \ln \left\{ 1 - \theta \left[ 1 - (u+1)\alpha^u + u\alpha^{u+1} \right] \right\} \quad (\text{B3})$$

For a monodisperse polymer system, i.e.,  $P_u = 1$  for  $u = x$  and  $P_u = 0$  for  $u \neq x$ , we found that  $L = 0$  from Eq. (B2). Thus Eq. (B1) becomes:

$$\frac{S^{(\theta)}}{R} = -\frac{(1-\theta)\ln(1-\theta)}{\theta} - \frac{\ln\theta}{x} - \left(1 - \frac{1}{x}\right) \quad (\text{B4})$$

which contains the exact negative term,  $-(1 - \frac{1}{x})$  as Flory's model. This means that if

Milchev and Gutzow's (1982) model for a polydispersed system is reduced to a

monodisperse system, the negative entropy term would appear, which is inconsistent with the third law of thermodynamics. This means that Milchev and Gutzow's model (1982) for a polydispersed polymer chain system would still lead to a negative entropy term, which is inappropriate.

For polydisperse system, Milchev and Gutzow (1982) calculated  $L$  numerically and gave the best fitting as,

$$L \approx \theta^{\frac{2}{3}} \left(1 - \frac{1}{x}\right)^{-\frac{1}{2}} \quad (\text{B5})$$

The other contributions to the configurational entropy are,

$$\frac{S(z, \bar{x})}{R} = \frac{1}{x} \left(1 - \frac{1}{x}\right) \ln\left(\frac{z}{2}\right) \quad (\text{B6})$$

$$\frac{S(\text{mix})}{R} = \frac{1}{x} [\bar{x} \ln \bar{x} - (\bar{x} - 1) \ln(\bar{x} - 1)] \quad (\text{B7})$$

$$\frac{S(f, \bar{x}, z)}{R} = -\left(1 - \frac{1}{x}\right)^2 [f \ln f + (1 - f) \ln(1 - f) - f \ln(z - 2)] \quad (\text{B8})$$

Originally, Milchev and Gutzow (1982) used  $f \ln(z-1)$  in Eq. (B8), instead of  $f \ln(z-2)$  which Flory (1957) and Gibbs and DiMarzio (1958) had used and which Milchev (1983) and Wittmann (1991) later used for a monodispersed system. This is also applicable to a polydispersed system.

In order to compare the results of their approach against the results of our approach, Eqs. (B1) and (B5)- (B8) can be written in terms of  $\alpha$ ,

$$\begin{aligned} \frac{S^{(\theta, \alpha)}}{R} &= -\frac{(1-\theta)\ln(1-\theta)}{\theta} - (1-\alpha)\ln\theta - \alpha + L\alpha \\ &\approx \frac{(1-\theta)\ln(1-\theta)}{\theta} - (1-\alpha)\ln\theta - \alpha + \alpha^{\frac{1}{2}}\theta^{\frac{2}{3}} \end{aligned} \quad (\text{B9})$$

$$\frac{S^{(z, \alpha)}}{R} = \alpha(1-\alpha)\ln\left(\frac{z}{2}\right) \quad (\text{B10})$$

$$\frac{S^{(f, \alpha, z)}}{R} = -\alpha^2[f\ln f + (1-f)\ln(1-f) - f\ln(z-2)] \quad (\text{B11})$$

$$\frac{S^{(\text{mix})}}{R} = -\alpha\ln(\alpha) - (1-\alpha)\ln(1-\alpha) \quad (\text{B12})$$

Equation (B9) corresponds to our Eq. (3.19), but with the extra negative term  $-\alpha + \alpha^{\frac{1}{2}}\theta^{\frac{2}{3}}$ . Equations (B10), (B11) and (B12) are exactly the same as our Eqs. (3.22), (3.26) and (3.29), but obtained by our approach. We find that Milchev and Gutzow (1982) had overlooked one contribution to the configurational entropy in their deduction, which we have deduced from their approach to be equal to,

$$\frac{S^{(\alpha)}}{R} = -\alpha(1-\alpha)\ln(1-\alpha) = \frac{\ln \bar{x}}{x} \quad (\text{B13})$$

Equation (B13) corresponds to our Equation (3.23), but it is different in its form.

## Bibliography

- Adam, G. and Gibbs, J. H. (1965), *J. Chem. Phys.*, **43**, 139.
- Alig, A., Häusler, K. G. Nancke, K., Tanzer, W. and Wartewig, S. (1989), *Acta Polym.*, **40**, 590.
- Alig, I., Lellinger, D., and Johari, G.P. (1992), *J. Polym. Sci. B, Polym. Phys.*, **30**, 791.
- Andrade, E. N. (1930), *Nature*, **125**, 309.
- Barber, H. J. (1943), *J. Chem. Soc.* 79.
- Baur, P. and Wunderlich, B. J. (1998), *Therm. Analysis.*, **54**, 437.
- Beiner, M., Korus, J., Lockwenz, K., Schroeter, K. and Donth, E. (1996), *Macromolecules*, **29**, 6589.
- Beiner, M., Kahle, S., Hempel, E., Schroeter, K. and Donth, E. (1998), *Europhys. Lett.*, **44**, 312.
- Bhattacharya, A. K. and Ferrel, J. A. (1981), *Phys. Rev. A*, **24**, 1643.
- Bhattacharya, A. K. and Ferrel, J. A. (1985), *Phys. Rev. A*, **31**, 1788.
- Birge, N. O. (1986), *Phys. Rev. B*, **34**, 1631.
- Birge, N. O., Jeong Y. H. and Nagel, S. R. (1986), *Ann. N. Y. Acad. Sci.* **484**, 101.
- Birge, N. O. and Nagel, S. R. (1985), *Phys. Rev. Lett.*, **54**, 2674.
- Bittmann, E., Alig, I. and Woermann, W. (1994), *Ber. Bunsenges Phys. Chem.*, **98**, 189.
- Boltzmann, L. (1876), *Pogg. Ann. Physik*, **7**, 108.
- Born M. and von Karman Th., (1912), *Phys. Zeit.* **13**, 297.
- Bragg, W. L. and Williams, E. J. (1934), *Proc. Roy. Soc. A (London)*, **145**, 699.

- Browmaker, G. A., Kennedy, B. J. and Reid, J. C. (1998), *Inorg. Chem.* **37**, 3968.
- Calef, D.F., and Deutch, J.M. (1983), *Ann. Rev. Phys. Chem.*, **34**, 493.
- Cardelli, C., Tombari, E. and Johari, G. P. (2002), *J. Phys. Chem. B*, **105**, 11035.
- Carother, (1936), *Trans. Faraday Soc.*, **32**, 39.
- Choi, I.-C. and Plazek, D. J. (1986), *J. Polym. Sci. B, Polym. Phys.*, **24**, 1303.
- Cole, K. S. and Cole, R. H. (1941), *J. Chem. Phys.*, **9**, 341.
- Cole, K. S. and Cole, R. H. (1942), *J. Chem. Phys.*, **10**, 98.
- Cromer, D. T., Douglass, R. M. and Staritzky, E. (1957), *Anal. Chem.* **29**, 316.
- Curie, P. J. (1888), *Ann. Chim. Phys.*, **17**, 385.
- Davidson, D. W. and Cole, R. H. (1950), *J. Chem. Phys.*, **18**, 1950.
- Debye, P. (1929), *Polar Molecules* (New York, Chemical Catalog Co).
- Debenedetti, P. G. and Stillinger, F. H. (2001), *Nature* (London), **410**, 259.
- DiMarzio, E. A. and Gibbs, J. H., (1958), *J. Chem. Phys.*, **28**, 807.
- DiMarzio, E. A. and Gibbs, J. H., (1959), *J. Polym. Sci.*, **40**, 121.
- Dishon, M., Weiss, G.H., and Bendler, J.T. (1985), *J. Res. N.B.S.*, **90**, 27.
- Dixon, P. K. and Nagel, S. R. (1988), *Phys. Rev. Lett.* , **61**, 341.
- Doi, M., (1975), *Chem. Phys.*, **9**, 455.
- Donth, E. (1992), in: *Relaxation and Thermodynamics in Polymer-Glass Transition*, Academic Verlag.
- Eyring, H. (1936), *Chem. Phys.*, **64**, 1052.
- Eyring, H. and Jhon, M. S. (1969), *Significant Liquid Structures*, John Wiley & sons.
- Ferrari, C., Salvetti, G., Tombari, E. and Johari, G. P. (1996), *Phys. Rev. E*, **54**, R1058.
- Flory, P. J. (1936), *J. Am. Chem. Soc.*, **58**, 1877.

- Flory, P. J. (1941), *J. Chem. Phys.* **9**, 660.
- Flory, P. J. (1942), *J. Chem. Phys.*, **10**, 51.
- Flory, P. J. (1943), *Principles of Polymer Chemistry*, Cornell University Press, Ithaca.
- Flory, P. J. (1956), *Proc. Roy. Soc. A* (London), **234**, 60.
- Fröhlich, H. (1958), *Theory of Dielectrics*, 2nd Ed., Oxford University Press, Oxford.
- Fulcher, G. S. (1925), *J. Amer. Ceram. Soc.*, **8**, 339.
- Fuoss, R. M. and Kirkwood, J. G. (1941), *J. Am. Chem. Soc.*, **63**, 385.
- Gardon, R. and Narayanaswamy, O. S. J. (1970), *Am. Ceram. Soc.*, **53**, 380.
- Gibbs, J. H. (1960), in *Modern Aspects of the Vitreous State*, Ed. J. D. MacKenzie (Butterworths, Lond.) vol. 1, p. 152.
- Gibbs, J. H. and DiMarzio, E. A., (1958), *J. Chem. Phys.*, **28**, 373.
- Goldstein, M. (1964), in *Modern Aspects of the Vitreous State*, Ed. J. D. MacKenzie (Butterworths, Lond.) vol. 3, p. 90.
- Goldstein, M. (1969), *J. Chem. Phys.*, **51**, 3728.
- Gordon, M., Kapadia, P. and Malakis, A. (1976), *J. Phys. A. Math. Gen.*, **9**, 751.
- Grest, G. S. and Cohen, M. H. (1981), in: *Advances in Chemical Physics*, Eds. Prigogine, I. and Rice S. A., Wiley, N. Y., vol. 5, p. 455.
- Guggenheim, E. A. (1944), *Proc. Roy. Soc. (London) A*, **183**, 203.
- Gujrati, P. D. (1980), *J. Phys. A*, **13**, L437.
- Gujrati, P. D. and Goldstein, M. (1981), *J. Chem. Phys.*, **74**, 2596.
- Gutzow, I. and Schmelzer, J. (1995), *The Vitreous State, Thermodynamics, Structure, Rheology and Crystallization* (Springer-Verlag), Chap. 5.
- Gutzow, I. Z. (1962), *Phys. Chemie (Leipzig)* **221**, 153.
- Gutzow, I. Z. (1972), in *Amorphous Materials*, Eds. Douglas, R. W. and Ellis, B. (Wiley, London), p. 159.

- Gutzow, I. Z. (1977), *The Physics of Non-Crystalline Materials*, Ed. G. H. Frischat, Trans. Tech Publi. Aedermannsdorff, p. 356.
- Havriliak, S and Negami, S. (1966), *J. Polym. Sci. C*, **14**, 99.
- Havriliak, S and Negami, S. (1967), *Polymer*, **8**, 161.
- Hill, R. M. (1978), *Nature*, **275**, 96.
- Hirai, N. and Eyring, H. (1959), *J. Polym. Sci.*, **37**, 51.
- Höchli, U. T., Knorr, K. and Loidl, A. (1990), *Adv. Phys.*, **39**, 405.
- Hodge, I. M. and Huvard, G. S. (1983), *Macromolecules*, **16**, 371.
- Hodge, I. M. (1983), *Macromolecules*, **16**, 1983.
- Hodge, I. M. (1987), *Macromolecules*, **20**, 2897.
- Hodge, I. M. (1994), *J. Non-Cryst. Solids*, **169**, 211.
- Hodge, I. M. (1995), *Science*, **267**, 1945.
- Hodge, I. M. (1997), *J. Res. Natl. Inst. Stand. Technol.* **102**, 195.
- Hopkinson, J. (1877), *Phil. Trans. Roy. Soc.*, **167**, 599.
- Horie, K., Hiura, H., Sawada, M., Mita, I. and Kambe, H. (1970), *J. Polym. Sci. A-1*, **8**, 1357.
- Huggins, M. L. (1942), *Ann. N. Y. Acad. Sci.*, **43**, 1.
- Jeong, Y. H. and Moon, I. K. (1995), *Phys. Rev. B.*, **52**, 6381.
- Johari, G. P. (1976), *Ann. N. Y. Acad. Sci.*, **279**, 117
- Johari, G. P. (1985), *J. de Physique. C*, **8**, 567.
- Johari, G. P. (1987), in: *Molecular Dynamics and Relaxation Phenomena in Glasses*, eds. Th. Dorfmueller and G. Williams, Springer-Verlag, Berlin Heidelberg, p. 90.
- Johari, G. P. (1993), in *Chemistry and Technology of Epoxy Resins*, eds. B. Ellis, Balckie Academic & Professional, London, p. 175.

- Johari, G. P. (1994), in *Disorder Effects in Relaxational Processes*, eds. R. Richert and A. Blumen, Springer-Verlag, Berlin, p. 627.
- Johari, G. P. (2000), *J. Chem. Phys.*, **113**, 751.
- Johari, G. P. (2001), *Chem. Phys.*, **265**, 217.
- Johari, G. P. (2001a), *J. Non-Cryst. Solids*, **288**, 148.
- Johari, G. P. (2001b), *J. Phys. Chem. B*, **105**, 3600.
- Johari, G. P. (2003), *J. Chem. Phys.*, in press.
- Johari, G. P., and Dannhauser, W. (1969), *J. Phys. Chem. B*, **50**, 1862.
- Johari, G. P., Collins M. F. and Feyerherm, R. (2000), *Phys. Rev. B*, **61**, 5827.
- Johari, G. P., Ferrari, C., Tombari E. and Salvetti, G. J. (1999), *J. Chem. Phys.*, **110**, 11592.
- Johari, G. P., McAnanama, J. A. and Wasylyshyn, D. A (1996), *J. Chem. Phys.*, **105**, 10621.
- Johari, G. P., Tombari, E., Presto, S. and Salvetti, G. (2002), *J. Chem. Phys.*, **117**, 5086.
- Johari, G. P., and Wasylyshyn, D. A (1999), *Chem. Phys.*, **242**, 283.
- Johnscher, A. K. (1975), *Colloid. Polymer Sci.*, **253**, 231.
- Lindsey, C. P., and Patterson, G. D. (1980), *J. Chem. Phys.*, **73**, 3348.
- Kahle, S., Hempel, E., Beiner, M., Unger, R., Schroeter, K. and Donth, E. (1999), *J. Mol. Struct.*, **479**, 149.
- Kasteleyn, P. W. (1962), *Physica*, **29**, 1329.
- Kasteleyn, P. W. (1967), in *Graph Theory and Theoretical Physics*, Ed. F. Harrrary (Academic, Lond.), p. 44.
- Kauzmann, W. (1948), *Chem. Rev.*, **43**, 219.
- Keizer, J. (1987), *Chem. Rev.*, **87**, 167.
- Kirkwood, J.G. (1939), *J. Chem. Phys.*, **7**, 911.

- Kohlrausch, R. (1847), *Ann. Phys. (Leipzig)*, **91**, 179.
- Kovacs, A. J. (1963), *Fortschr. Hochpolym.-Forsch.*, **3**, 394.
- Kovacs, A. J., Hutchinson, J. M. and Aklonis, J. J. (1977), in: *The Structure of Non-Crystalline Materials*, edited by, P. H. Gaskell, Taylor and Francis, London, pp. 153.
- Kroeker, S., Wasylishen, R. E. and Hanna, J. V. (1999), *J. Am. Chem. Soc.*, **121**, 1582.
- Landau, L. D. and Lifshitz, E. M. (1980), in: *Statistical Physics*, vol. 5, Pergamon, Oxford.
- Malkin, A. Y. and Kulichikhin, S. G. (1991), *Adv. Polym. Sci.*, **101**, 217.
- Mangion, M. B., Vanderwell, J. J. Walton, D. and Johari, G. P. (1991), *J. Polym. Sci. B, Polym. Phys.*, **29**, 723.
- Manning, M. F. and Bell, M. E. (1940), *Rev. Mod. Phys.*, **12**, 215.
- Matsuoka, S. (1992), in: *Relaxation Processes in Polymers*, Hanser, N. Y.
- Mayer, J. and Göppert-Mayer, M. (1940), *Statistical Mechanics*, Wiley, N. Y.
- Mayer, W., Hoffmann, S. Meier G. and Alig, I. (1997), *Phys. Rev. E*, **55**, 3102.
- McAnanama, J. G., Wasylyshyn, D. A. and Johari, G. P. (2000), *Chem. Phys.*, **252**, 237.
- Meyer, K. H. (1939), *Z. Phys. Chem. (Leipzig) B*, **44**, 383.
- Milchev, A. and Gutzow, I. (1982), *J. Macromol. Sci.- Physics. B*, **21**, 583.
- Milchev, A. (1983), *C. R. Bulg. Acad. Sci.*, **36**, 1415.
- Moynihan, C. T., Boesch, L. P., and Labarge, N.L. (1973), *Phys. Chem. Glasses*, **14**, 122.
- Moynihan, C. T., Macedo, P. B., Montrose, C. J., Gupta, P. K., DeBolt, M. A., Dill, J. F., Dom, B. E., Drake, P. W., Eastal, A. J., Elterman, P. B., Moeller, R. P., Sasabe, H. and Wilder, (1976), *J. A., Ann. N. Y. Acad. Sci.*, **279**, 15.
- Muzeau, E., Cavaille, J. Y., Vassoille, R., Perez, J., and Johari, G. P. (1992), *Macromolecules*, **25**, 5108.
- Narayanaswamy, O. S. (1971), *J. Am. Ceram.Soc.*, **54**, 491.

- Ngai, K. L., Rendell, R. W., Rajagopal, A. K. and Teitler, S. (1986), *Ann. N. Y. Acad. Sci.*, **484**, 150.
- Norberg, B. and Jacobson, B. (1957), *Acta Chem. Scand.*, **3**, 174.
- Onsager, L. (1936), *J. Amer. Ceram. Soc.*, **58**, 1486.
- Paluch, M, Patkowski, A., and Fischèr, E. W. (2000), *Phys. Rev. Lett.*, **85**, 2140.
- Paluch, M (2001), *J. Chem. Phys.*, **115**, 10029.
- Parthun, M. G. and Johari, G. P. (1995), *J. Chem. Phys.*, **102**, 6301.
- Parthun, M. G. and Johari, G. P. (1995a), *J. Chem. Phys.*, **103**, 7611.
- Pascheto, W., Parthun, M. G., Hallbrucker A. and Johari, G. P. (1994), *J. Non-Cryst. Solids*, **171**, 182.
- Perez, J. (1992), in: *Physique et Mechanique des Polymeres Amorphes*, Lavoisier, Tec & Doc, Paris.
- Petroff, B., Milchev, A. and Gutzow, I. (1996), *J. Macromol. Sci.-Phys. B*, **35**, 763.
- Plonka, A. (1986), in: *Time-dependent Reactivity of Species in Condensed Media*, Springer-Verlag, Berlin Heidelberg.
- Plonka, A. (2001), *Dispersive Kinetics*, Kluwer.
- Ritland, H. N. (1956), *J. Am. Ceram. Soc.*, **39**, 403.
- Schawe, J. E. K. (1995), *Thermochim. Acta*, **261**, 183.
- Schawe, J. E. K. and Theobald, S. (1998), *J. Non-Cryst. Solids*, **235-237**, 496.
- Scherer, G. W. (1986), in: *Relaxation in Glass and Composites*, Wiley-Interscience, N. Y.
- Schneider, U. Brand, R., Lunkenheimer, P. and Loidl, A. (2000), *Phys. Rev. Lett.*, **84**, 5560.
- Simon, S. L. and McKenna, G. B. (1997), *J. Chem. Phys.*, **107**, 8678.
- Simon, S. L. and McKenna, G. B. (2000), *Thermochi. Acta*, **348**, 77.

- Smoluchowski, M. V. (1917), *Z. Physik. Chem.*, (Leipzig), **92**, 192.
- Tammann, G and Hesse, G (1926), *Z. Anorg. Allg. Chem.*, **156**, 245.
- Tombari, E. and Johari, G. P. (1992), *J. Chem. Phys.*, **97**, 6677.
- Tombari, E. Ferrari, C., Salvetti G. and Johari, G. P. (1997), *J. Phys.: Condens. Matter*, **9**, 7017.
- Tombari, E. Ferrari, C., Salvetti G. and Johari, G. P. (1998), *J. Polym. Sci.: Polymer Phys.*, **36**, 303.
- Tombari, E. Ferrari, C., Salvetti G. and Johari, G. P. (1999), *Phys. Chem. Chem. Phys.*, **1**, 1965.
- Tombari, E, Salvetti G. and Johari, G. P. (2000), *J. Chem. Phys.*, **113**, 6957.
- Tool, A. Q. (1946), *J. Am. Ceram. Soc.*, **29**, 240.
- Turnbull, D. and Cohen, M. H. (1961), *J. Chem. Phys.*, **34**, 120.
- Turnbull, D. and Cohen, M. H. (1971), *J. Chem. Phys.*, **52**, 3038.
- Vogel, H. (1921), *Phys. Z.*, **22**, 645.
- von Schweidler, E. (1907), *Ann. Phys.*, **24**, 711.
- Waite, T. R. (1957), *Phys. Rev.*, **107**, 463.
- Waite, T. R. (1958), *J. Chem. Phys.*, **28**, 103.
- Wasylyshyn, D. A. and Johari, G. P. (1997), *J. Polym. Sci.: Polymer Phys.*, **35**, 437.
- Wasylyshyn, D. A. and Johari, G. P. (1998), *Chem. Phys.*, **237**, 345.
- Wasylyshyn, D. A. and Johari, G. P. (1999), *J. Phys. Chem. B*, **103**, 3997.
- Wilemski, G. and Fixman, M. (1973), *J. Chem. Phys.*, **58**, 4009.
- Wilemski, G. and Fixman, M. (1974a), *J. Chem. Phys.*, **60**, 866.
- Wilemski, G. and Fixman, M. (1974b), **60**, 878.
- Williams, G., and Watts, D.C. (1970), *Trans. Faraday Soc.*, **66**, 80.

Wittmann, H.-P. (1991), *J. Chem. Phys.*, **95**, 8449.

Zumofen, G. Blumen, A. and Klafter, J. (1985), *J. Chem. Phys.*, **82**, 3198.

Zwanzig, R. (1990), *Acc. Chem. Res.*, **23**, 148.

## Nomenclature

Variables	Description
$\alpha$	extent of polymerization
$\beta$	non-exponential parameter
$\delta$	volume ratio of a repeat unit (monomer) to a hole
$\epsilon$	dielectric constant
$\epsilon(\omega)$	frequency-dependence of dielectric constant
$\epsilon(t)$	time dependence of dielectric constant
$\epsilon'$	real part of the dielectric constant
$\epsilon''$	imaginary part of the dielectric constant
$\epsilon_s$	limiting low-frequency relative permittivity
$\epsilon_\infty$	limiting high-frequency relative permittivity
$\Delta\epsilon$	magnitude of the dielectric relaxation
$\phi$	normalized relaxation function
$\eta$	viscosity
$\theta$	fractional lattice occupancy, or dimensionless effective density of a lattice
$\rho$	general property
$\sigma$	conductivity
$\tau$	relaxation time
$\omega$	angular frequency
$\Omega$	microcanonical partition function, or the number of microstates
$\xi$	reduced time variable
$\Psi$	relaxation function
$C_P$	heat capacity under constant pressure
$C_{P, \text{conf}}$	configurational heat capacity under constant pressure
$D$	diffusion coefficient
$E$	activation energy
$f$	flexibility of polymer chain
$H$	enthalpy
$\Delta h^*$	activation enthalpy
$k$	relaxation rate
$N$	number of polymer chains in a polymer system
$N_0$	number of holes in a polymer system
$P$	pressure
$P_U$	instantaneous polarization
$P_R$	equilibrium or long-time limit of the polarization
$q$	heating or cooling rate
$S$	entropy
$S_{\text{conf}}, S_c$	configurational entropy

$t$	time
$T$	temperature
$T_f$	fictive temperature
$T_g$	glass transition temperature
$U_f$	activation energy of flexible bonds
$U_h$	activation energy of holes
$U_o$	activation energy of CN group orientated from c-axis
$v_0$	“molar volume” of a hole
$v_1$	molar volume of a repeat unit (monomer)
$V$	volume
$x$	non-linear parameter
$x$	number of monomers on a polymer chain, or chain length
$\bar{x}$	average chain length of a polymer system
$y$	general variable (general force)
$z$	coordination number of lattice

### Constants

### Description

$\epsilon_0$	absolute dielectric constant in vacuum, 8.854 pF/m
$k_B$	Boltzman constant, $1.381 \times 10^{-23}$ J/K
$N_A$	Avogadro number, $6.022 \times 10^{23}$ /mol
$R$	gas constant, 8.314 J/(mol·K)